# Halogen and Pnictogen Bonding in Host-Guest Chemistry




Heike Kuhn

Keble College

University of Oxford

A thesis submitted for the degree of

Doctor of Philosophy

Trinity 2022

# Halogen and Pnictogen Bonding in Host-Guest Chemistry

## Abstract

Heike Kuhn, Keble College, University of Oxford

Abstract of thesis submitted for the degree of D.Phil., Trinity Term 2022

---

This thesis describes the synthesis and characterisation of acyclic and macrocyclic receptors containing halogen- and pnictogen bonding motifs for the study of sigma(σ)-hole interactions for anion recognition, as well as the stabilisation of reactive halonium species through macrocyclic ligands.

**Chapter 1** introduces supramolecular chemistry and the central concepts related to host-guest recognition and self-assembly. Different types of non-covalent interactions are discussed with a focus on sigma(σ)-hole interactions. Relevant literature examples related to anion recognition as well as interlocked host structures are furthermore presented.

**Chapter 2** presents the synthesis of a series of antimony(III) and bismuth(III) based pnictogen bonding acyclic receptors, which were studied to elucidate the strength and selectivity of pnictogen bonding based anion recognition. The synthesis and study of mixed pnictogen- and halogen bonding tripodal receptors as well as mono- and bis-stibanotriazole based receptors is furthermore discussed.

**Chapter 3** describes the synthesis of a series of halogen bonding lariat macrocycles incorporating ambidentate iodotriazole motifs into both the macrocycle and lariat arm. These were used to investigate anion and metal cation template directed synthetic routes for potential pseudo-[1]rotaxane assembly with the goal of constructing a functional [1]rotaxane capable of anion recognition through halogen bonding.

**Chapter 4** details the study of four different bis-pyridine-based macrocycles for the complexation and stabilisation of reactive halonium cations. To this end, the solid-state

structures of bromonium complexes as well as their parent Ag(I) and electronically related $d^{10}$ Au(I) complexes are presented together with solution phase halonium cation $^{1}$H NMR ligand exchange studies, which reveal evidence for a macrocyclic effect for halonium guest species.

**Chapter 5** presents a summary of the major conclusions from the research project and discusses future work.

**Chapter 6** contains synthetic details and full characterisation of all novel compounds, as well as further details regarding $^{1}$H NMR titration experiment protocols and single-crystal XRD experiments.

# Acknowledgements

First and foremost, I would like to thank my supervisor Prof. Paul D. Beer for all his guidance, advise, support, and knowledge throughout my DPhil. I am incredibly thankful for his trust in me and will always cherish having been able to be part of his research group. The members of the Beer Group have been an amazing support during my time at Oxford and I am especially grateful for the mentorship of Dr Andrew Docker and Dr Richard Tse. I would like to thank Andrew in particular for his support during my thesis writing process and would furthermore like to thank Jamie Wilmore for his input and comments.

I would like to thank Prof. Ho Yu Au-Yeung, who took me on as a project student at HKU and allowed me to gain my first research experience in the world of supramolecular chemistry. It has also been an absolute pleasure to work with Prof. Simon Parsons and I am eternally grateful for all his encouragement and advice.

I would like to thank Dr Amber Thompson and Dr Kirsten Christensen for teaching me all things crystallography and enabling me to run my own single crystal XRD experiments, which has truly been one of my favourite parts of my DPhil research. Thank you for always supporting me and answering all my questions!

Moreover, the support staff of the Chemistry Department has been truly amazing and our research would not be possible without them!

I would like to also thank everyone at Keble College for making my time at Oxford truly special and it has been a great pleasure to be part of such a welcoming community.

And I of course would like to express my eternal gratitude to my family and friends for all their love and support!

# Previously Published Work

## Work arising from this thesis

Anion Recognition with Sb(III) and Bi(III) Triaryl-Based Pnictogen Bonding Receptors
H. Kuhn, A. Docker and P. D. Beer, *Chemistry – A European Journal*, 2022, **28**, e202201838.

## Other publications

Anion and pH dependent molecular motion by a halogen bonding [2] rotaxane
H. A. Klein, H. Kuhn and P. D. Beer, *Chemical Communications*, 2019, 55, 9975-9978.

Highly Active Halogen Bonding and Chalcogen Bonding Chloride Transporters with Non-Protonophoric Activity
L. E. Bickerton, A. Docker, A. J. Sterling, H. Kuhn, F. Duarte, P. D. Beer and M. J. Langton, *Chemistry – A European Journal*, 2021, 27, 11738-11745.

Halogen Bonding Tetraphenylethene Anion Receptors: Anion-Induced Emissive Aggregates and Photoswitchable Recognition
A. Docker, X. Shang, D. Yuan, H. Kuhn, Z. Zhang, J. J. Davis, P. D. Beer and M. J. Langton, *Angewandte Chemie International Edition*, 2021, 60, 19442-19450.

Modulating Chalcogen Bonding and Halogen Bonding Sigma-Hole Donor Atom Potency and Selectivity for Halide Anion Recognition
A. Docker, C. H. Guthrie, H. Kuhn and P. D. Beer, *Angewandte Chemie International Edition*, 2021, 60, 21973-21978.

Organotelluroxane molecular clusters assembled *via* Te⋯ X−(X= Cl−, Br−) chalcogen bonding anion template interactions
A. Docker, A. J. Martínez Martínez, H. Kuhn and P. D. Beer, *Chemical Communications*, 2022, 58, 3318-3321.

Selective Potassium Chloride Recognition, Sensing, Extraction, and Transport Using a Chalcogen-Bonding Heteroditopic Receptor
A. Docker, I. Marques, H. Kuhn, Z. Zhang, V. Felix and P. D. Beer, *Journal of the American Chemical Society*, 2022, 144, 14778-14789.

# Abbreviations

| | |
|---|---|
| δ | chemical shift, partial charge |
| Δ | change in (a measurement), heat |
| ε | dielectric constant |
| Σσ | summed Hammett constant |
| σ | sigma, standard deviation |
| λ | wavelength |
| μ | micro, dipole moment |
| ν | frequency |
| ° | degree |
| °C | degrees Celsius |
| A | acceptor |
| Å | Ångstrom |
| $A^-$ | anion |
| abs | absorption |
| Ala | alanine |
| AMT | active metal template |
| aq. | aqueous |
| Ar | aromatic |
| Arg | arginine |
| Asp | aspartate |
| au | arbitrary units |
| $Bar^F$ | tetrakis[3,5-bis(trifluoromethyl)phenyl]borate |
| bipy | 2,2'-bipyridine |
| Boc | di-*tert*-butyl dicarbonate |
| br | broad |
| Bu | butyl |
| cat. | catalytic |
| Ch | chalcogen |
| ChB | chalcogen bonding |
| conc. | concentrated |
| COSY | homonuclear correlation spectroscopy |
| CSD | The Cambridge Structural Database |
| CuAAC | copper(I)-catalysed azide–alkyne cycloaddition |
| D | donor |
| d | doublet |
| *d* | deuterated |
| DBU | 1,8-diazabicyclo[5.4.0]undec-7-ene |
| DCM | dichloromethane |
| dd | doublet of doublets |
| DFT | density functional theory |
| DIPEA | *N,N*-di-iso-propylethylamine |
| DMAP | 4-(dimethylamino)pyridine |

| | |
|---|---|
| DMF | N,N-dimethylformamide |
| DMSO | dimethyl sulfoxide |
| DNA | deoxyribonucleic acid |
| e | electron |
| EDTA | ethylenediaminetetraacetic acid |
| eq., equiv. | equivalent |
| ESI | electrospray ionisation |
| Et | ethyl |
| *et al.* | et alia |
| EtOAc | ethyl acetate |
| E.T. | energy transfer |
| EWG | electron withdrawing groups |
| $F^2$ | square of the structure factor |
| FRET | Förster resonance energy transfer |
| G | Gibbs free energy |
| g | gram |
| Gly | glycine |
| h | Planck's constant, hour |
| HB | hydrogen bonding |
| HOMO | highest occupied molecular orbital |
| HSQC | heteronuclear single quantum coherence |
| Hz | hertz |
| I | intensity |
| *i.e.* | id est |
| ICSD | Inorganic Crystal Structure Database |
| int. | internal |
| J | Joule, coupling constant |
| K | Kelvin |
| k | kilo |
| $K_a$ | association constant |
| L | litre |
| LB | Lewis base |
| LUMO | lowest occupied molecular orbital |
| m | milli, multiplet, meta |
| M | molar, mega |
| m/z | mass-to-charge ratio |
| Me | methyl |
| Mes | 1,3,5-trimethylbenzene |
| MIM | mechanically interlocked molecule |
| min | minute(s) |
| MLCT | metal-to-ligand charge transfer |
| mol | mole |
| MS | mass spectrometry |
| Ms | methane sulfonyl |
| n | nano |

| | |
|---|---|
| NDI | naphthalenediimide |
| NMR | nuclear magnetic resonance |
| NOESY | Nuclear Overhauser Effect Spectroscopy |
| o | *ortho* |
| o/n | overnight |
| OAc | acetate |
| p | *para* |
| PBP | phosphate-binding protein |
| PDB | Protein Data Bank |
| PET | photoinduced electron transfer |
| pH | $-\log_{10}[H^+]$ |
| Ph | phenyl |
| Phe | phenylalanine |
| pKa | −log10Ka |
| Pn | pnictogen |
| PnB | pnictogen bonding |
| pos. | positive |
| ppm | parts per million |
| Pr | propyl |
| Py | pyridinium |
| q | quartet |
| quant. | quantitative |
| quin. | quintet |
| R | chemical substituent |
| R[I > 2σ(*I*)] | R-factor based upon data with I > 2σ(*I*) |
| ROESY | Rotating frame Overhauser Enhancement Spectroscopy |
| rt | room temperature |
| s | second, singlet |
| S | goodness of fit |
| sat. | saturated |
| SBP | sulfate-binding protein |
| sept. | septet |
| Ser | serine |
| *syn* | synperiplanar |
| t | triplet |
| t, *tert* | tertiary |
| TBA | tetrabutyl ammonium |
| TBTA | tris[(1-benzyl-1H-1,2,3-triazol-4-yl)methyl]amine |
| TFA | trifluoroacetic acid |
| THF | tetrahydrofuran |
| Thr | threonine |
| TLC | thin layer chromatography |
| TMA | tetramethylammonium |
| TMS | trimethylsilyl |
| Trp | tryptophan |

| | |
|---|---|
| Ts, tosyl | *para*-toluenesulfuonyl chloride |
| UV | ultra-violet |
| V | volt |
| v/v % | volume/volume percent |
| vis. | visible |
| vs. | versus |
| VT | variable temperature |
| wrt | with respect to |
| $wR(F^2)$ (all) | weighted R factor based upon all data and $F^2$ |
| X | halogen atom |
| XB | halogen bonding |
| XRD | X-ray diffraction |

# Table of Contents

**Abstract** ..... ii

**Acknowledgements** ..... iv

**Previously Published Work** ..... v

**Abbreviations** ..... vi

**1 Introduction** ..... 1

**1.1 Supramolecular Chemistry** ..... 1

**1.2 Non-Covalent Interactions** ..... 3

1.2.1 Electrostatic Interactions ..... 3

1.2.2 Hydrogen Bonding ..... 4

1.2.3 Ion-π Interactions ..... 5

1.2.4 Sigma(σ)-Hole Interactions ..... 6

1.2.4.1 Halogen Bonding ..... 8

1.2.4.2 Chalcogen Bonding ..... 9

1.2.4.3 Pnictogen Bonding ..... 11

**1.3 Anion Binding** ..... 13

1.3.1 Biological Anion Recognition ..... 14

1.3.2 Anion Receptor Design Considerations ..... 15

1.3.3 Synthetic Anion Receptors ..... 17

1.3.3.1 Introduction ..... 17

1.3.3.2 Positively Charged Receptors ..... 18

1.3.3.3 Neutral Receptors ..... 22

1.3.3.4 Sigma-Hole Anion Receptors ..... 25

**1.4 Interlocked Structures** ..... 32

1.4.1 Introduction and Historical Context ..... 32

**1.5 Template Synthesis of MIMs** ..... 34

1.5.1 Metal Templates ..... 34

1.5.2 Active Metal Templates ..... 36

1.5.3 Anion Templation ..... 38

**1.6 Interlocked Structures for Host-Guest Recognition** ..... 41

**1.7 Objectives** ..... 47

**1.8 References ..... 48**

**2 Anion Recognition with Sb(III) and Bi(III)-Based Pnictogen Bonding Receptors .....63**

**2.1 Introduction ..... 63**

**2.2 Project Aims ..... 65**

**2.3 Triaryl Antimony(III) and Bismuth(III) Receptors ..... 66**

2.3.1 Synthesis .....66

2.3.2 Single-Crystal XRD Characterisation .....69

2.3.3 Anion Binding Studies of **1·Pn$^R$** Receptors .....70

2.3.4 Conclusions .....76

**2.4 PnB-HB Tripodal Receptors ..... 76**

2.4.1 Synthesis of mixed PnB-HB Tripodal based Receptors .....76

2.4.2 Anion Binding Studies of **2·Pn$^R$** Receptors .....80

2.4.3 Conclusions .....82

2.4.4 PnB-XB Tripodal Receptors .....83

2.4.4.1 Attempted Synthesis of Mixed XB-PnB Tripods .....83

**2.5 Stibanotriazole Receptors ..... 85**

2.5.1 Synthesis of 5-Stibano-1H-1,2,3-Triazole Receptors .....86

2.5.2 Anion Binding Studies of Stibanotriazole Receptors .....91

2.5.3 Conclusions .....94

**2.6 Conclusions and Further Outlook ..... 95**

**2.7 References ..... 97**

**3 Towards a Functional [1]Rotaxane.....99**

**3.1 Introduction ..... 99**

**3.2 Project Aims ..... 105**

**3.3 Iodotriazole-Lariat Macrocycle for Pseudo [1]Rotaxane Investigation ..... 106**

3.3.1 Pseudo [1]Rotaxane Design Strategy .....107

3.3.2 Synthesis of Lariat Macrocycles .....109

**3.4 $^1$H-NMR Pseudo [1]Rotaxane Assembly Investigation *via* Anion Templation..... 112**

3.4.1 Modified Iodotriazole-Lariat Macrocycle .....115

1.1.1.1 $^1$H-NMR Pseudo [1]Rotaxane Assembly Investigation *via* Anion Templation .....117

3.4.2 Pentafluorophenyl-Lariat Macrocycle .....118

3.4.2.1 $^1$H-NMR Pseudo [1]Rotaxane Assembly Investigation *via* Anion Templation .....120

**3.5 Metal Cation Template Pseudo[1]Rotaxane Assembly Investigation ..... 122**

3.5.1 $^{1}$H-NMR Study of Zinc(II) Complexation ..... 122

3.5.2 Attempts to prepare a [1]Rotaxane *via* Zinc(II) Templation ..... 124

**3.6 Attempted [1]Rotaxane Formation *via* Active Metal Template Methodology ..... 127**

3.6.1 AMT Reaction [1]Rotaxane Synthesis Attempts using a Lariat Macrocycle ..... 128

3.6.2 Synthesis of Pyridyl Modified Lariat Macrocycles for AMT [1]Rotaxane Investigation ..... 130

**3.7 Conclusion and Future Work ..... 138**

**3.8 References ..... 140**

**4 Exploiting the Macrocyclic Effect for the Stabilisation of Halonium Cations ..... 144**

**4.1 Introduction ..... 144**

**4.2 Project Aims ..... 151**

**4.3 Target Macrocycle Designs ..... 152**

**4.4 Synthesis of Macrocyclic Bis-Pyridine Ligands for Halonium Stabilisation ..... 153**

4.4.1 Synthesis of Macrocyclic Ligands **MC1** and **MC2** ..... 153

4.4.2 Synthesis of Macrocyclic Ligand **MC3** ..... 155

4.4.3 Synthesis of Macrocyclic Ligand **MC4** ..... 156

**4.5 Formation of Ag(I) and Au(I) d$^{10}$ Metal Complexes ..... 157**

4.5.1 Ag(I) Complex Formation ..... 157

4.5.2 Ag(I) Complex Solid-State Characterisation ..... 158

4.5.3 Au(I) Complex Formation ..... 162

4.5.4 Au(I) Complex Solid-State Characterisation ..... 163

4.5.5 Conclusions ..... 165

**4.6 Formation of Halonium Complexes ..... 165**

4.6.1 Iodonium ..... 165

4.6.2 Bromonium ..... 166

**4.7 Further Investigation of MC1 as a Macrocyclic Ligand for Br(I) Stabilisation ..... 169**

4.7.1 Solid-State Structures of Protonated Macrocycle Side Products ..... 173

4.7.2 Preliminary Investigation of a Halonium Cation Macrocyclic Effect ..... 175

**4.8 Conclusion and Future Work ..... 178**

**4.9 References ..... 179**

**5 Summary and Conclusions ..... 183**

**6 Experimental.....189**

**6.1 General Considerations..... 189**

6.1.1 Materials, Methods and Instrumentation for Synthesis and Characterisation.....189

6.1.2 Instrumentation and Methods for Single-Crystal XRD .....189

6.1.3 General Procedures for $^{1}$H NMR Studies .....190

6.1.3.1 $^{1}$H NMR Anion Titrations .....190

6.1.3.2 $^{1}$H-NMR Pseudo [1]Rotaxane Assembly Investigations via Anion Templation .....191

**6.2 Experimental Information Related to Chapter 2..... 191**

6.2.1 General Synthetic Procedures .....191

6.2.2 Synthesis and Characterisation.....195

6.2.2.1 Synthesis of Triaryl Pnictogens.....195

6.2.2.2 Synthesis of Pnictogen Tripods .....198

6.2.2.3 Synthesis of Mono Stibanotriazoles .....204

6.2.2.4 Synthesis of Bis Stibanotriazoles .....205

6.2.3 CHN Elemental Analysis for Triaryl Pnictogens.....207

6.2.4 Single Crystal X-Ray Diffraction Data .....208

6.2.5 $^{1}$H NMR Titration Data .....212

6.2.5.1 Bismuth(III) Triaryl Compounds .....212

6.2.5.2 Antimony(III) Triaryl Compounds .....218

6.2.5.3 Pnictogen Tripods.....224

6.2.5.4 Stibanotriazoles.....226

**6.3 Experimental Information Related to Chapter 3..... 227**

6.3.1 General Synthetic Procedures .....227

6.3.2 Synthesis and Characterisations .....229

6.3.2.1 Synthesis of **LM1** and **LM2** .....229

6.3.2.2 Synthesis of **LM-3** .....237

6.3.2.3 Synthesis of **LM-4** .....239

6.3.2.4 Synthesis of **LM-5** and **LM-6**.....243

6.3.2.5 Synthesis of **LM-7** .....248

6.3.2.6 Synthesis of **LM-9** and **LM-10**.....252

**6.4 Experimental Information Related to Chapter 4..... 258**

6.4.1 General Procedures .....258

6.4.2 Synthesis and Characterisation.....260

6.4.2.1 Synthesis of Macrocycle **MC1** .....260

6.4.2.2 Synthesis of Macrocycle **MC2** .....261

6.4.2.3 Synthesis of Macrocycle **MC3** .....263

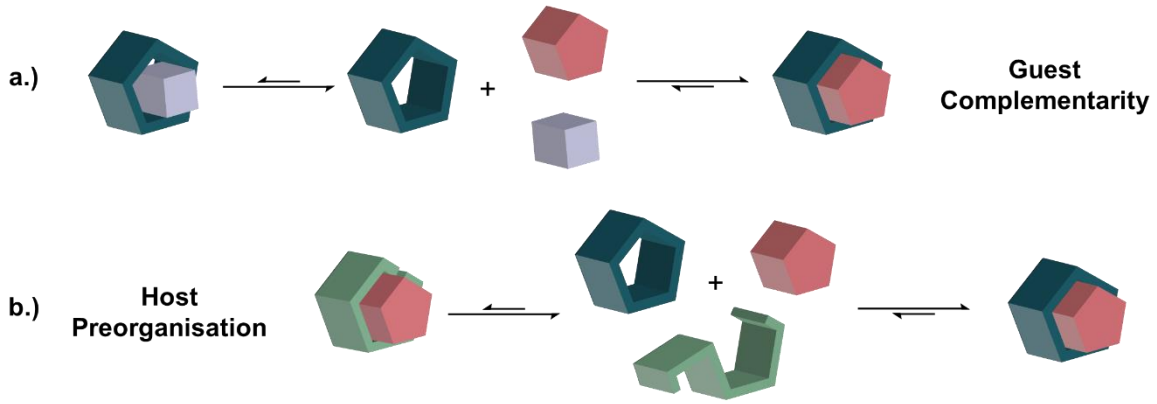
6.4.2.4 Synthesis of Macrocycle **MC4** ....264
6.4.3 Single Crystal X-Ray Diffraction Data ....265
6.4.3.1 **MC1** Complexes....265
6.4.3.2 **MC2** Complexes....269
6.4.3.3 **MC3** Complexes....270
**6.5 References .... 270**

# 1 Introduction

## 1.1 Supramolecular Chemistry

In his 1988 Nobel Lecture, Jean-Marie Lehn described supramolecular chemistry as the "chemistry of the intermolecular bond, covering the structures and functions of the entities formed by association of two or more chemical species".[1] The two key areas of this field are host-guest recognition and self-assembly, both of which are governed by a library of non-covalent interactions, as well as key principles such as complementarity and preorganisation.[1-4]

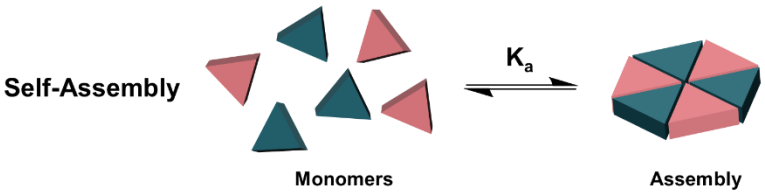
In host-guest recognition, a substrate is bound by a receptor through reversible non-covalent interactions.[3] Strong binding can be achieved through designing a host with a binding site that is complementary in both shape and size to the substrate as to maximise non-covalent interactions between host and guest molecules (Scheme 1.1 a).[2] Furthermore, minimising the conformational change that the host molecule experiences upon guest binding, termed preorganisation, leads to more favourable binding (Scheme 1.1 b).[4]




*Scheme 1.1.Cartoon representation of concepts of a.) host-guest complementarity and b) host preorganisation in host-guest recognition*

In a self-assembly process, monomers come together through non-covalent interactions to form a stable and distinct supramolecular assembly (Scheme 1.2).[5] Biomolecules, such as

proteins, peptides or polysaccharides often form supramolecular assemblies that carry out a particular function within a biotic system.[6] Arguably the most famous example of this is the self-assembly of the DNA double helix strand *via* complementary hydrogen bonding interactions between the nucleotide base building blocks (Figure 1.2 b). Furthermore, enzymes provide an example of the unparalleled ability of supramolecular biotic host systems to recognise substrates strongly and selectively.[7] These impressive biological systems have greatly inspired the development of supramolecular chemistry, which often aims to mimic the functions of these systems using synthetic approaches.[6]




*Scheme 1.2. Cartoon representation of a self-assembly*

Overall, supramolecular chemistry uses an interdisciplinary approach with aspects of organic, inorganic, analytical as well as physical chemistry in order to elucidate a deeper understanding of complex functional systems and the non-covalent interactions that govern them.[8] Modern applications of supramolecular chemistry include the binding of drug molecules by receptors to aid drug delivery, solubility and stability[9-11] and the design of receptors capable of removing pollutants from bodies of water[12, 13]. The field has also seen the emergence of molecular machines,[14-17] as well as a large range of functional materials with unique properties governed by self-assembly.[8] These are just a few examples of the wide range of scope and applications of this vast field of chemistry.

This thesis focuses on the host-guest recognition of anions *via* sigma(σ)-hole interactions as well as the stabilisation of potent halonium σ-hole donors through macrocyclic structures. This introduction will therefore focus on non-covalent interactions (Section 1.2), general aspect of

anion binding (Section 1.3) as well as the synthesis and study of interlocked structures (Section 1.4) and their anion binding abilities (Section 1.5).

## 1.2 Non-Covalent Interactions

The library of non-covalent interactions that govern supramolecular chemistry encompasses a large range of attractive and repulsive forces. The following is a brief survey of the supramolecular chemistry toolbox of non-covalent interactions which are commonly exploited for the purpose of host-guest recognition.

### 1.2.1 Electrostatic Interactions

Attractive electrostatic interactions occur between opposite charges from either ions or dipoles (Figure 1.1).[18]

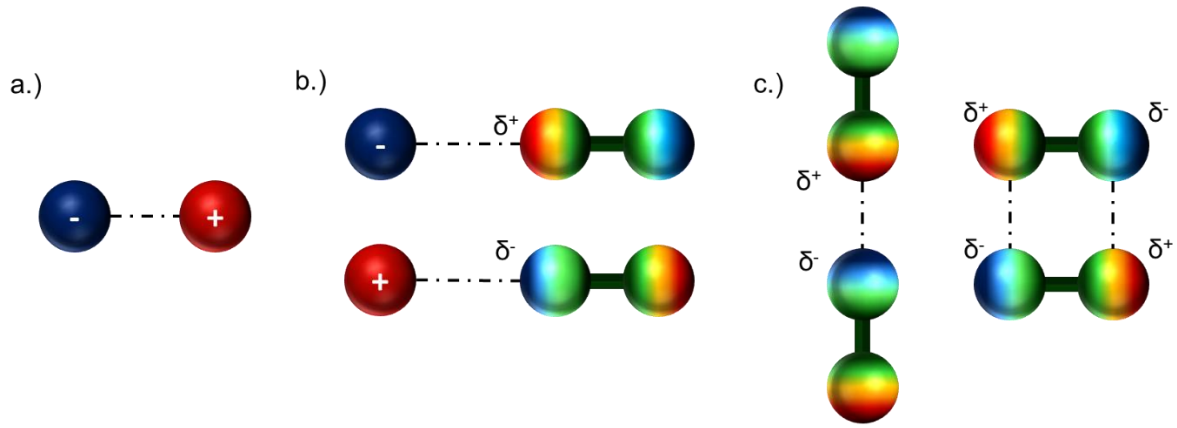



*Figure 1.1. Graphical representation of electrostatic interactions with a.) ion-ion, b.) ion-dipole and c.) dipole-dipole*

While most non-covalent bonds are weaker, ion-ion interactions are comparable in strength to covalent bonding (100 – 300 kJ $mol^{-1}$).[18] Ion-dipole interactions are interactions between an ion and a polar molecule and typically range in strength from 50 to 200 kJ mol (Figure 1.1 b).[18]

Dipole-dipole interactions between two polar molecules are often weaker but their strength can be maximised through alignment of the dipoles (Figure 1.1 c).[18] They typically range in strength from 5 to 50 kJ mol$^{-1}$ and are particularly weak in solution.[18] Both ion-dipole and dipole-dipole interactions show an enhanced directionality over ion-ion interactions.[19, 20]

### 1.2.2 Hydrogen Bonding

Ubiquitous within nature, hydrogen bonding (HB) is a non-covalent interaction arising from a polarised hydrogen atom bearing a partial positive charge, typically covalently linked to an electron withdrawing group (R), which forms an attractive interaction with a Lewis base (LB).[21] Hence, HB can be regarded as a special case of a dipole-dipole or dipole-ion interaction depending on the nature of the LB. The strength of HB interactions generally increases with increasing electronegativity of R, which in turn leads to a shorter H···R' bond.[21]

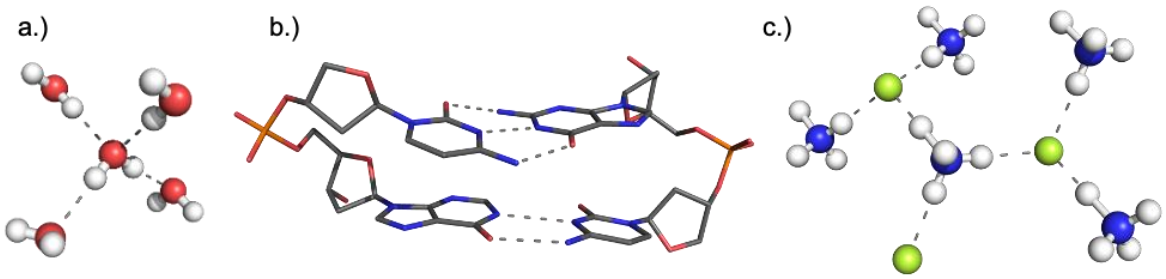



*Figure 1.2. Selected examples of HB networks in the solid state with a.) water (ICSD: 27837)[22], b.) truncated DNA structure showing HB between selected base pairs (PDB: 1BNA)[23] and c.) $NH_4F$ (ICSD: 14294)[24]. HB shown as grey dashes.*

The strength of a hydrogen bond can reach up to 160 kJ mol$^{-1}$ for highly acidic compounds such as $HF_2^-$, however, their strength typically ranges between 4 to 60 kJ mol$^{-1}$.[8, 18] The strongest HBs are displaying bond angles close to 180° but deviation from linearity often occurs and they can also be bent or bifurcated, especially in cases where a HB donor has multiple hydrogens capable of partaking in HB or the acceptor has more than one lone pair (Figure 1.2 a, c).[18, 25]

### 1.2.3 Ion-π Interactions

Aromatic π-systems, as well as other π-bonds, are formed through overlap of p-orbitals.[26] They can be electron rich or electron deficient depending on the aromatic molecule's electronic nature as well as substituents, and are thereby capable of partaking in non-covalent bonding with ions of corresponding opposite charge.[27, 28] Even though the importance of π-interactions is recognised due to their occurrence in many biological systems, the nature and properties of these interactions are still debated.[29-31]

Cation-π interactions typically display the strongest interaction energies among the class of π-interactions.[32] Their binding energies are in the range of 40 – 170 kJ $mol^{-1}$ as determined by computational methods in the gas phase and the nature of the interaction is dominated by electrostatics and polarisation.[32-34] Figure 1.3 a shows an example of a cation-π interaction in which a tetramethylammonium cation is bound by a cyclophane based receptor.[35]

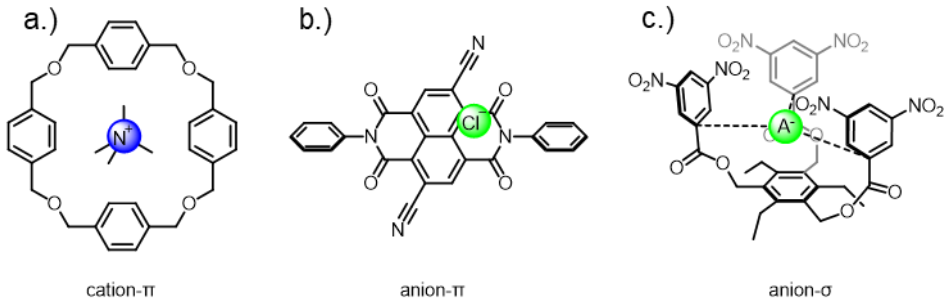



*Figure 1.3. Examples of aromatic-ion interactions in supramolecular chemistry with a.) cation-π[35], b.) anion-π[36] and c.) anion-σ ($A^-$=$Cl^-$,$Br^-$,$I^-$)[37]*

Anion-π interactions are typically weaker and less explored that their cation-π counterparts.[36, 38, 39] Calculations for gas phase complexes have determined the strength of the interaction to be in the range of 40 – 80 kJ $mol^{-1}$.[40] The nature of the anion and π-system dictate the geometric requirement for a stable complex.[40, 41] Models of the interaction between an arene and a halide have revealed that the halide anion resides over the centre of the ring, however, favourable

interactions can also occur when the anion is off-centre with many off-centre complexes occurring in the solid state (Figure 1.3 a, b).[37, 40] Anion-π complexes are typically observed with electron-deficient aromatic units and, similarly to cation-π interactions, are governed by electrostatic as well as polarisation effects.[34]

### 1.2.4 Sigma(σ)-Hole Interactions

While they had not been identified as such at the time, sigma(σ)-hole interactions have been observed since the start of the 19th century.[42] Hassel's seminal study of strong interactions of halogen species with Lewis bases in the solid state (Figure 1.4) allowed for a more structural understanding of these halogen bonding (XB) interactions, and sparked further interest in this type of interaction.[43]

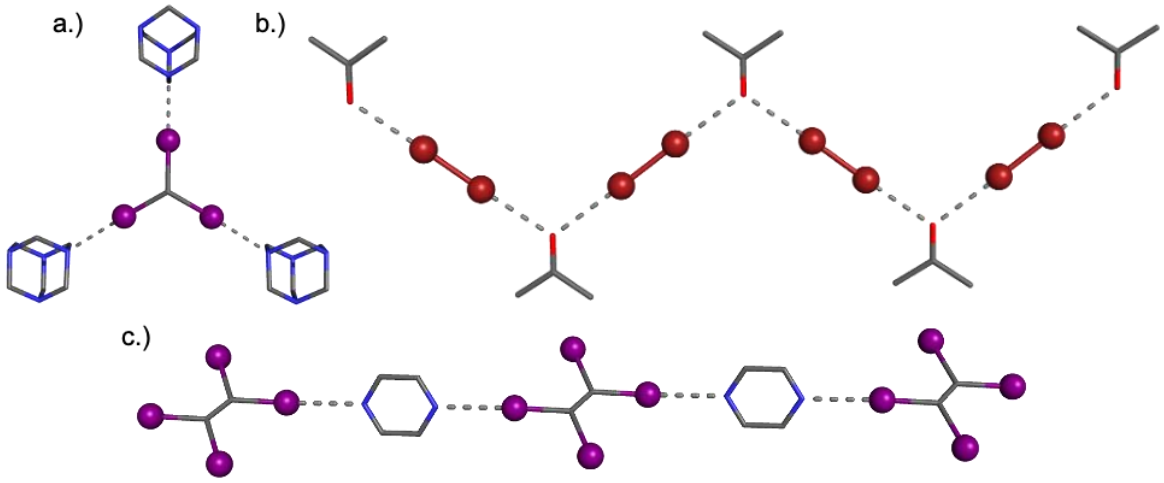



*Figure 1.4. Hassel's XB crystals with a.) cocrystal of hexamethylenetetramine with iodoform (CSD: HEXAIF10), b.) cocrystal of acetone and bromine (CSD: ACETBR) and c.) cocrystal of pyrazine and tetra iodoethylene (CSD: IETPYA10). XB shown as grey dashes.*[42]

While it may initially seem counterintuitive that these highly electronegative atoms can favourably interact with nucleophilic sites, seminal computational work by Politzer *et al.* revealed that the involvement of main group atoms in a covalent bond result in an anisotropic distribution of electron deficiency.[44-46] This region of electron deficiency, coined a sigma(σ)-hole,

is notably enhanced when the main group atom is bonded to a residue more electronegative than itself.[47]

Computed molecular electrostatic potential surfaces allow for visualisation of the localised electron-deficient σ-hole responsible for XB interactions on the extension of the X-R bond (Figure 1.5).[48, 49] This area of low electron density on the halogen is surrounded by an electron-rich equatorial belt (Figure 1.5).[50]

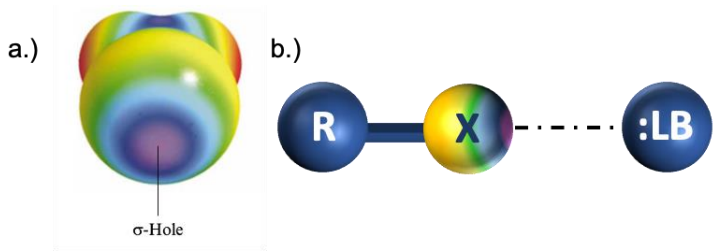



*Figure 1.5. Visualisations of σ-hole on halogens with a.) Computed electrostatic potential on the 0.001 au molecular surface of I-$NO_2$ showing σ-hole in pink (adapted from[48, 49]) and b.) cartoon representation of XB interaction with a Lewis base (X=Cl, Br, I; R=electron withdrawing substituent)*

While initially observed for halogens, σ-hole interactions have since been identified and reported for main group atoms in groups 14 to 18.[49, 51, 52] These interactions, which are named after the group of atoms involved, such as halogen (XB), chalcogen (ChB) or pnictogen (PnB) bonding, are defined as the attractive interaction between a Lewis base (LB) and a σ-hole (Figure 1.6).[51]

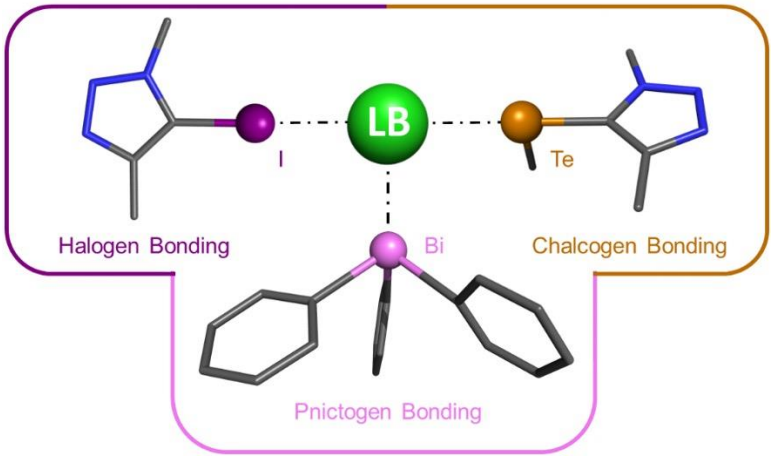



*Figure 1.6. Graphical representation of σ-hole interactions involving group 15-17 atoms*

Because they arise from the very localised region of electron deficiency at the main group atom, their interaction geometries are generally linear with respect to the covalent bonds at the σ-hole donor.[50] Furthermore these interactions are hydrophobic in nature[53] and are most pronounced when the atom is less electronegative, polarisable, and bound to electron withdrawing groups.[51] While tetrel (group 14)[54-56] and aerogen (group 18)[52, 57] bonding have been reported in the literature, the focus here will only be on σ-hole interactions involving group 15-17 elements, which are of particular relevance to the theme of this thesis.

#### 1.2.4.1 Halogen Bonding

Arguably, the most well-known and studied interaction of the σ-hole bonding class is halogen bonding (XB). From a crystallography viewpoint, XB interactions between Lewis acidic halogens and a wide variety of neutral and anionic Lewis bases have been well documented,[43, 58-61] while studies in solution still remain relatively rare.[62, 63] However, recent investigations have focused on organic based XB donors and their interactions with Lewis bases to elucidate the thermodynamics and unique characteristics of this interaction in solution.[64-68]

A notable example of a strong, all neutral XB complex was reported by Huber in 2014, showing high levels of cooperativity between a tridentate XB donor and the neutral tricyclic *ortho*-amine Lewis base.[69] Single crystal X-ray diffraction data revealed a well-defined three-point XB based binding of the substrate. The receptor containing three XB donors bound the LB in a 1:1 stoichiometric fashion (Figure 1.7 a, c), whereas a modified receptor containing six XB donors was capable of binding two LBs, each *via* three XB (Figure 1.7 b, d).[69] For the receptor containing three XB donors, $^{19}$F NMR studies in cyclohexane-$d_{12}$ solution confirmed a strong 1:1 host-guest association ($K_a = 5.8 \times 10^3\ M^{-1}$) with the tricyclic *ortho*-amine. Binding to the monodentate LB guest triethylamine in toluene-$d_8$ was three orders of magnitude lower than

for the tricyclic *ortho*-amine in the same solvent, which highlighted the strength of the complex with the tridentate LB resulted from multidentate XB and complementary geometric host-guest match of XB donors and LB.[69]

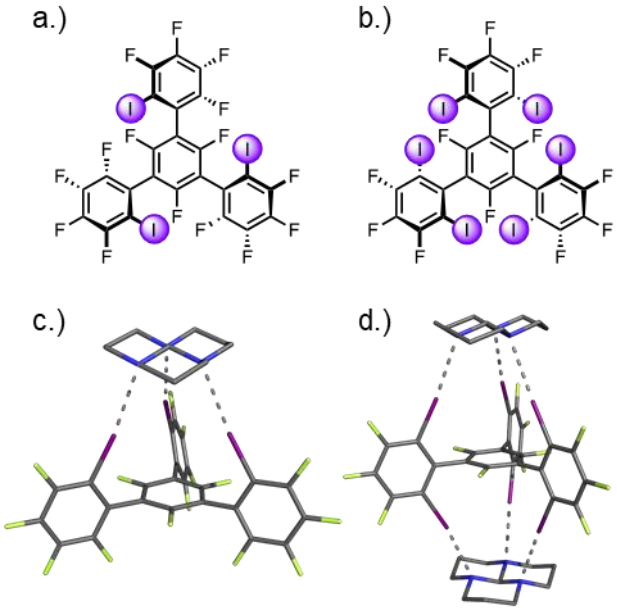



*Figure 1.7. Huber's three-point XB donors with a.) three XB donor, b.) six XB donor, c.) single-crystal X-ray structure of 1:1 complex and d.) single-crystal X-ray structure of 2:1 guest to host complex (CSD: LORQUG). XB shown as grey dashes.*[69]

### 1.2.4.2 Chalcogen Bonding

Chalcogen bonding (ChB), in contrast to XB, has received considerably less attention.[70, 71] Unlike halogens, chalcogens can exhibit up to two electropositive regions along the Ch-R covalent bonds depending on the number of substituents and their oxidation state (Figure 1.8).[50]

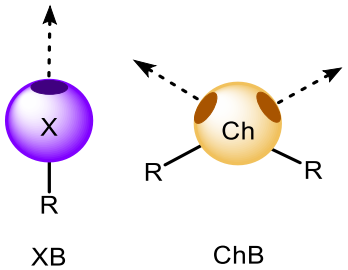



*Figure 1.8. Schematic representation of XB and ChB σ-holes*

Contrasting halogens, chalcogens can also act as Lewis bases due to their lone pairs.[72] As with XB, the σ-hole is the most potent for the less electronegative, heavier chalcogens.[73] In addition, the increased polarisability of the heavier chalcogens results in a relatively smaller energy difference between the σ and σ* orbital, favouring the donation of electron density from the LB into the antibonding orbital.[74] Hence, selenium and tellurium donor atom containing molecules form the strongest chalcogen bonds.[75] However, the weak C-Te bond (ca. 200 kJ $mol^{-1}$) can often be a limiting factor in the design of ChB receptors.[74]

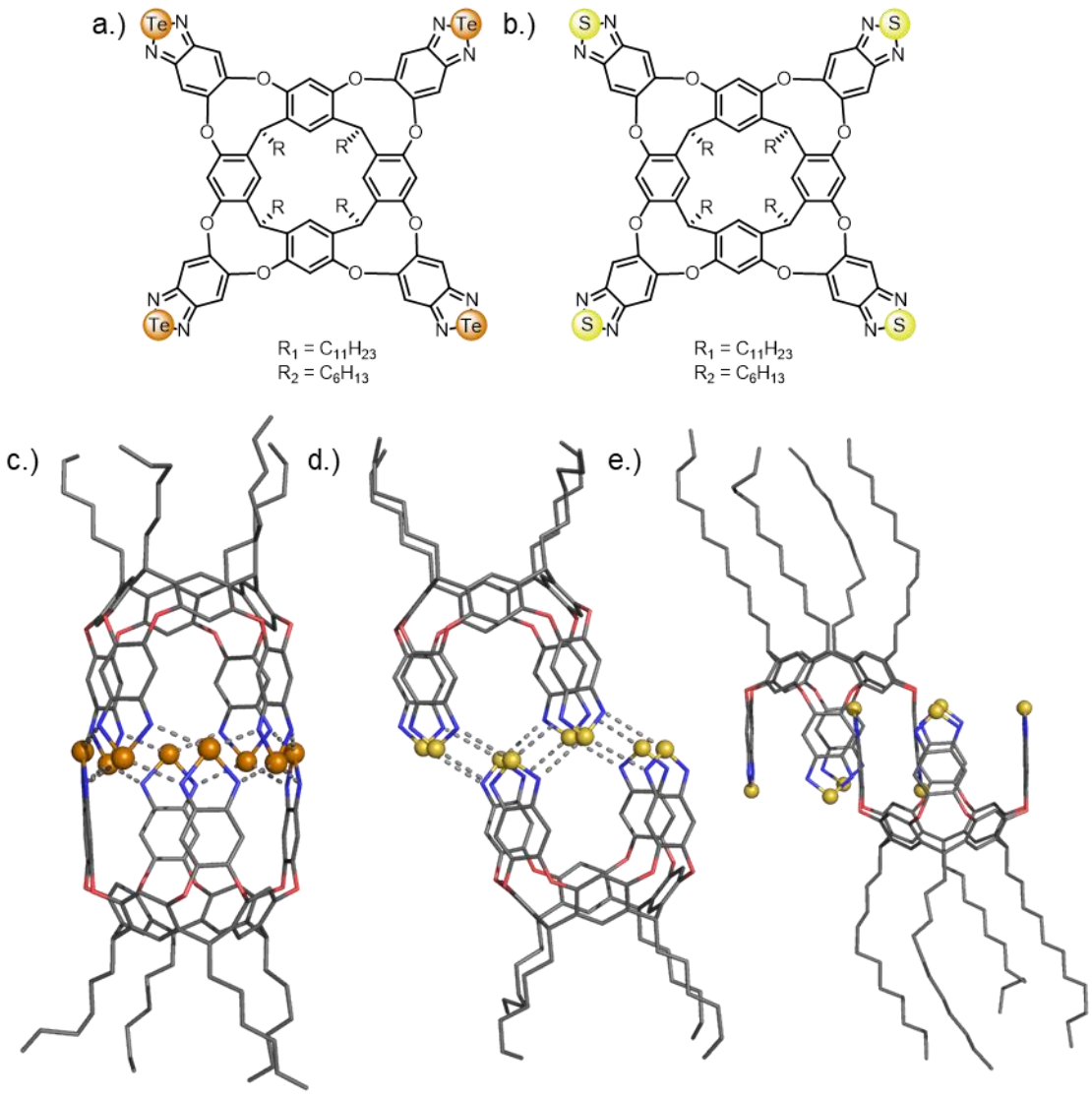



*Figure 1.9. Diederich's ChB supramolecular capsules with a.) Te monomer, b.) S monomer, c.) Te based dimer in 'vase' form (CSD: DIVSOT) with 16 ChB, d.) Se based dimer in 'shifted' form (CSD: DIVZUG) and e.) S 'interlocked' dimer showing π-π stacking (CSD: DIVTIO). ChB shown as grey dashes.*[76]

In 2018, Diederich and co-workers reported a particularly elegant example of the ChB self-assembly of two capsules based on cooperative multidentate S···N and Te···N ChB interactions respectively.[76] 2,1,3-Benzotelluradiazole and 2,1,3-benzothiadiazole motifs were incorporated into resorcin[4]arene structural frameworks and shown to be capable of dimerization both in solution from $^{1}$H NMR investigations and the solid state (Figure 1.9 a, b).[76] Single crystal X-ray data revealed a linear Te based capsule, with each Te centre forming two ChB with adjacent N atoms to give a total of 16 ChB holding the structure together (Figure 1.9 c).[76] In contrast to the Te based capsule, the sulfur dimer ensemble displayed two distinct capsule assemblies dependent upon the nature of the solvent. A 'shifted' capsule made up of 12 ChB bonds was observed for non-polar solvents such as toluene or benzene, however, crystallisation from $CH_2Cl_2$ resulted in no observable ChB bonds but rather a series of π-π stacking arrangements (Figure 1.9 d, e).[76] These observations clearly indicated the difference in ChB strength with Te···N ChB interactions being much stronger than S···N chalcogen bonds.

#### 1.2.4.3 Pnictogen Bonding

Pnictogen bonding (PnB) describes the σ-hole interactions of the group 15 elements.[77] Depending on the oxidation state of the Pn atom, up to three σ-holes can be observed along the axis of the R−Pn covalent bonds.[78] The formation of one pnictogen bond, however, often results in a decreased electrophilicity of the remaining PnB sites.[79] As with the previously discussed XB and ChB interactions, the σ-hole is most pronounced for the heavier more electropositive pnictogens, such as antimony (Sb) and bismuth (Bi).[80] Like chalcogens, pnictogens can also act as Lewis bases due to their lone pair.[80] This lone pair exhibits an increased s-character for the heavier Pn, which enhances the anisotropic distribution of electron density around the atom.[79] In addition, low-lying antibonding orbitals involved in the σ-hole interactions become more energetically accessible down the group.[79] A unique feature of the

heavier main group elements is the ability to access multiple oxidation states.[81] From a σ-hole donor capability it would be anticipated that higher oxidation states would increase element centred electrophilicity.[81] Despite the exciting potential of pnictogen bonding applications, very few examples have appeared in the literature to date.[82]

Cozzolino and co-workers have recently utilised PnB for the self-assembly of supramolecular cages.[83, 84] Antinomy(III) was incorporated into a tris-indole ligand system (Figure 1.10 a, b) and a pyridyl appended arylene ethynylene system was synthesised as a tridentate PnB acceptor (Figure 1.10 c). The cage was characterised by single crystal X-ray diffraction with three PnB interactions observed for each Sb(III) centre (Figure 1.10 d, e).[84]

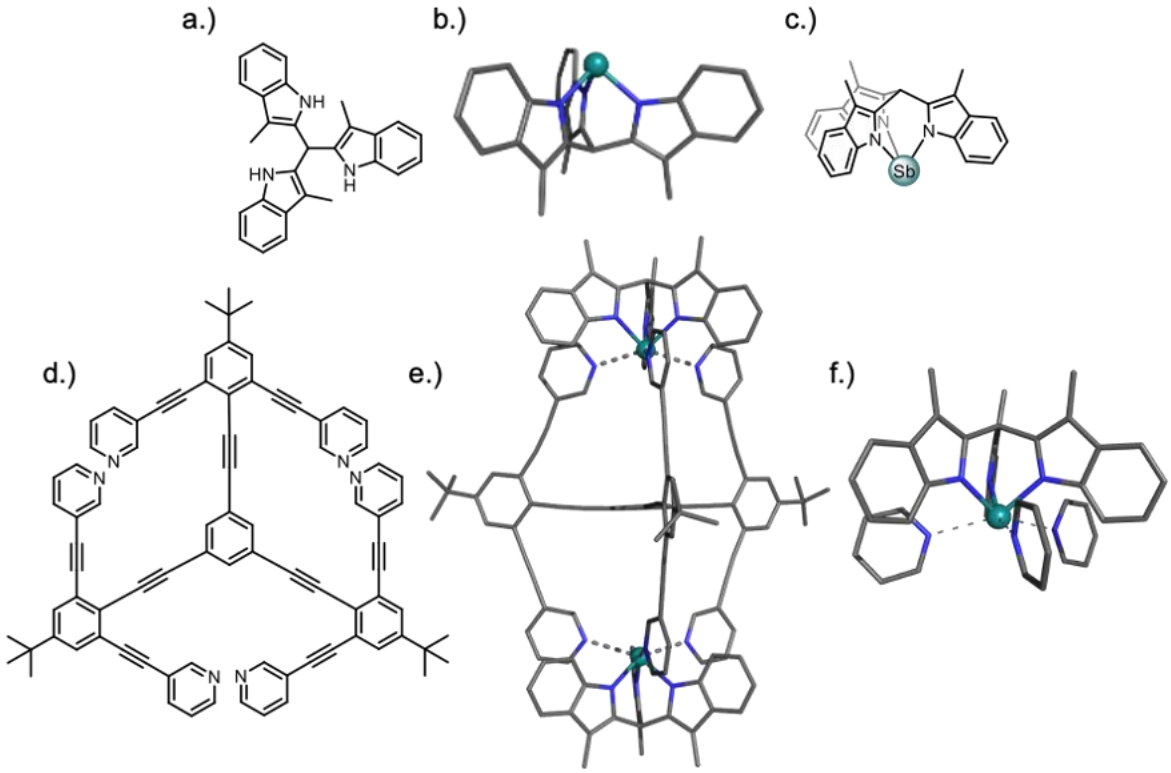



*Figure 1.10. Cozzolino's PnB cage with a.) tris-indole ligand, b.) X-ray single crystal structure of Sb(III) PnB donor (CSD: MOYDUC), c.) tris-indole based Sb(III) donor, d.) pyridyl-based PnB acceptor, e.) X-ray single-crystal structure of PnB cage (CSD: MOYFOY) and f.) truncated X-ray single-crystal structure of PnB cage. PnB bonds shown as dashed lines.*[84]

Gabbaï and Matile have reported significant enhancements in PnB donor ability by oxidation of Sb(III) to Sb(V).[81, 85, 86] This results in an increased σ-hole donor electrophilicity due to the

lowering of the energy of the σ* orbital (LUMO) upon oxidation to Sb(V), as well as a greater partial positive charge at the σ-hole region.[81] Gabbaï's 2018 study compared the Pn donor strength of three tetrachlorocatecholate Sb(V) receptors and their Sb(III) triaryl analogues towards triphenylphosphine oxide (Figure 1.11).[81] All Sb(III) receptors showed no significant interaction with the $Ph_3PO$ in $CDCl_3$ as determined by $^{1}H$, $^{19}F$ and $^{31}P$ NMR. The Sb(V) analogues, however, displayed significant interactions in this solvent system. Binding constants determined *via* $^{31}P$ NMR revealed a moderate $K_a$ of 120 $M^{-1}$ for the non-fluorinated receptor (Figure 1.11 a). The fully fluorinated receptor exhibited an increase of two orders of magnitude with a binding constant of $3\times10^{4}$ $M^{-1}$ (Figure 1.11 b). The strongest receptor contained trifluoromethyl groups at the *ortho*-positions with a Ka of $3\times10^{5}$ $M^{-1}$ (Figure 1.11 c).[81] In addition to the $^{31}P$ NMR studies, the binding of $Ph_3PO$ by the Sb(V) receptors was confirmed by UV/Vis titration studies.

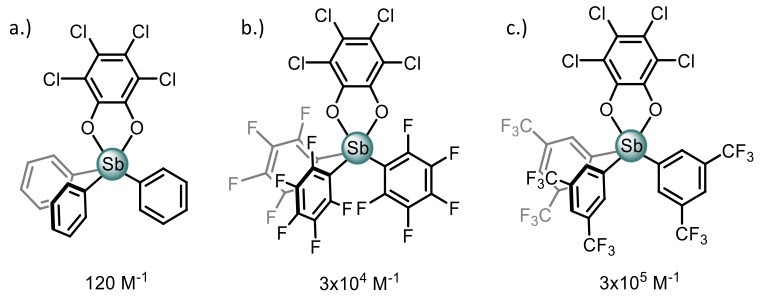



*Figure 1.11. Sb(V) PnB donors with $PhPO_3$ 1:1 host:guest binding constants in $CDCl_3$ determined by a.) $^{31}P$ NMR, b.) and c.) UV/Vis absorbance.*[81]

Further exploiting applications of this exotic σ-hole interaction, Sb(V) PnB donors have also recently been tested as potential organocatalysts.[86-88]

## 1.3 Anion Binding

Anions are essential to many biological as well as industrial processes and anion pollutants are of ever-increasing environmental concern.[89] During the past three decades, this has stimulated

the design and synthesis of a variety of functional receptors capable of binding, sensing, and sequestering anions.[55, 90, 91]

### 1.3.1 Biological Anion Recognition

The inspiration for designing strong and selective synthetic anion receptors comes from nature's biotic systems which are capable of binding even hydrophilic anions with a remarkably high affinity and selectivity in aqueous media. Figure 1.12 depicts the salmonella typhimurium sulfate-binding protein (SBP), the structure of which was first elucidated by Pflugrath and Quiocho in 1985 through X-ray crystallography.[92] The sulfate dianion is completely buried within the binding pocket of the protein and strongly bound through seven concerted hydrogen bonds. It is noteworthy that SBP achieves sulfate recognition in aqueous media with remarkable affinity and selectivity over closely related tetrahedral anionic species through no charge assisted hydrogen bond donor motifs.[93] The hydrogen bond donors are mainly main-chain peptide secondary amine or amide groups in addition to one indole NH donor and hydroxyl group (Figure 1.12 b, c).

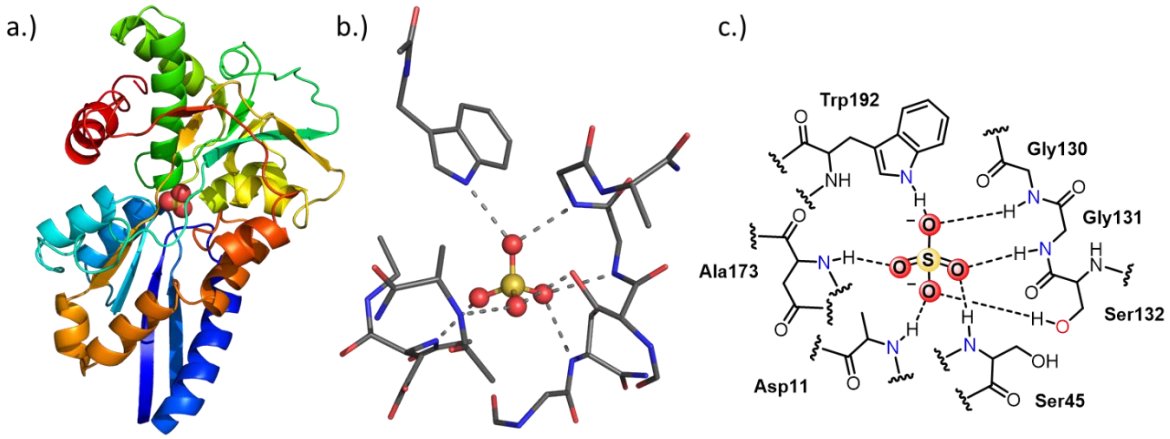



*Figure 1.12. Salmonella typhimurium sulfate-binding protein (SBP), a.) X-ray crystallography structure of the protein (PDB: 1SBP)[93], b.) truncated X-ray crystal structure of binding cavity depicting H-bonding trough dashed lines, c.) two-dimensional projection of binding cavity.*

The solid-state structure of another biological receptor capable of selective anion recognition through hydrogen bonding was reported in 1990 by Lücke and Quiocho (Figure 1.13).[94]

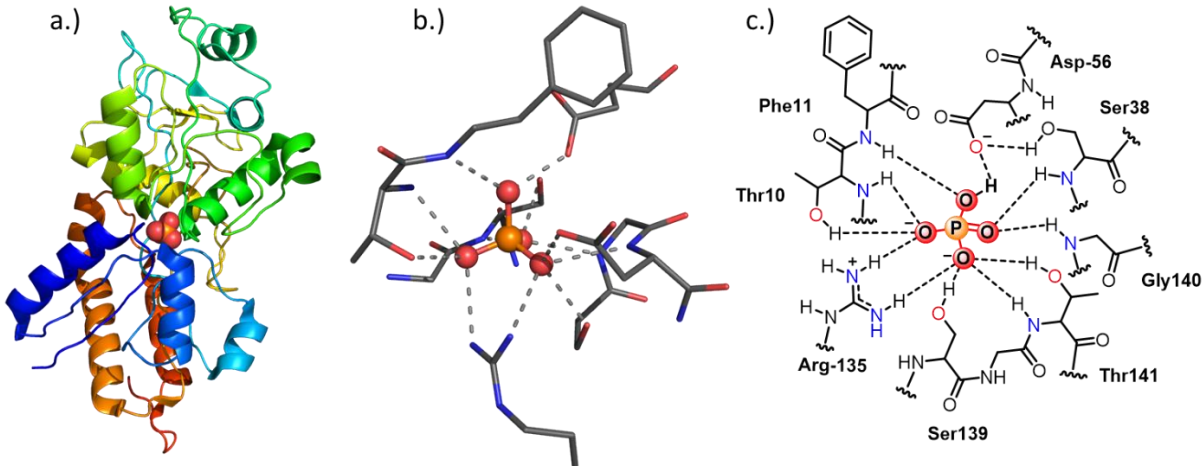



*Figure 1.13. Phosphate-binding protein (PBP), a.) X-ray crystallography structure of the protein (PDB: 1PBP)[95], b.) truncated X-ray crystal structure of binding cavity depicting H-bonding trough dashed lines, c.) two-dimensional projection of binding cavity.*

In contrast to SBP, which possesses only HB donors in the binding cavity (Figure 1.12 c), the binding site of the phosphate binding protein (PBP) possesses a carboxylate derived aspartate residue as a HB acceptor (Figure 1.13 b, c). The presence of the hydrogen bond acceptor forms a crucial part for selective $HPO_4^{2-}$ substrate recognition.[94]

### 1.3.2 Anion Receptor Design Considerations

The inherent properties of anions provide a challenge for their selective recognition.[50] The following section surveys these properties which must be taken into account in anion receptor design.

Anions are typically larger than their isoelectronic cation counterparts, lowering the relative charge density for these species (Table 1.1).[18, 96] As a result, electrostatic interactions are intrinsically attenuated relative to cations. Moreover, anions are known to adopt a wide range of geometries.[89] Selected inorganic anions displaying common simple anion geometries are

shown in Figure 1.14. The design of synthetic hosts containing complementary shaped cavities for specific geometrically complex anions is particularly challenging.[89]

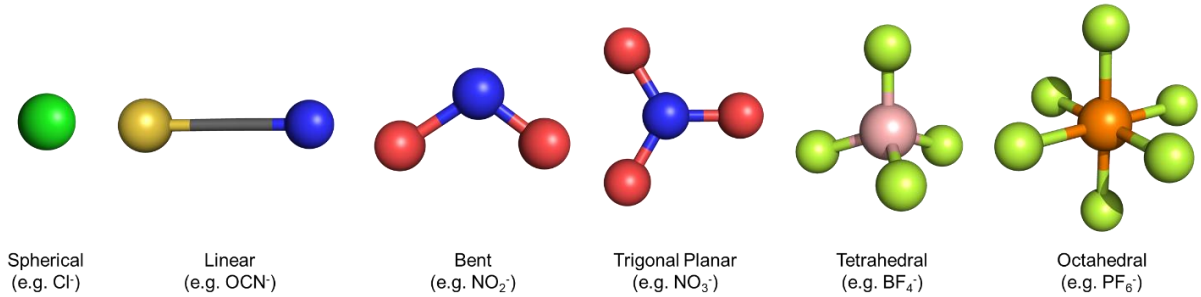



*Figure 1.14. Selected examples of common anion geometries*

For a host to recognise a target anion, the negatively charged guest must be at least partially de-solvated prior to binding, which invokes a considerable energetic penalty.[89] Indeed, an anion is typically more strongly solvated than a cation of comparable size. As shown in Table 1.1, the ionic radius of $F^-$ is comparable to $K^+$ but their free energies of hydration ($\Delta G_{hydration}$) are -465 kJ $mol^{-1}$ and -295 kJ $mol^{-1}$ respectively.[18]

*Table 1.1. Ionic radii and solvation free energies for selected anions and isoelectronic cations*

| **Anion** | **Ionic Radius (Å)** | **$\Delta G_{hydration}$ (kJ $mol^{-1}$)** | **Cation** | **Ionic Radius (Å)** | **$\Delta G_{hydration}$ (kJ $mol^{-1}$)** |
|---|---|---|---|---|---|
| $F^-$ | 1.33 | -465 | $Na^+$ | 1.02 | -365 |
| $Cl^-$ | 1.81 | -340 | $K^+$ | 1.38 | -295 |
| $Br^-$ | 1.96 | -315 | $Rb^+$ | 1.52 | - |
| $I^-$ | 2.20 | -275 | $Cs^+$ | 1.67 | -250 |

Effective ionic radii of 6-coordinate ions, values from Steed and Atwood[18], $Rb^+$ value from Shannon[96]

In aqueous media, anion solvation is reflected by the Hofmeister series which ranks anions according to their hydrophobicity and degree of hydration (Table 1.2).[18]

*Table 1.2. Hofmeister series for selected anions going from weakly hydrated (hydrophobic) to strongly hydrated (hydrophilic)*

| **Hydrophobic – Weakly Hydrated** | **Hydrophilic – Strongly hydrated** |
|---|---|
| organic anions > $ClO_4^-$ > $I^-$ > $SCN^-$ > $NO_3^-$ > $ClO_3^-$ > $Br^-$ > $Cl^-$ >> $F^-$ > $CO_3^{2-}$ > $HPO_4^{2-}$ > citrate$^{3-}$ | |

Table adapted from Steed and Atwood[18]

A further complication for anion recognition is their pH dependence. Receptors targeting anions with pH dependent speciation are required to function within a pH range in which the anion remains negatively charged.[97] This can prove a particular challenge for protonated receptors such as polyammonium systems, whose attractive electrostatic positive charge is also restricted to a specific pH window.[90] Moreover, this somewhat limits the scope of the anions that can be bound by a given receptor as strongly basic anions, such as $F^-$, cannot be used in conjunction with receptors containing acidic sites due to the anion's ability to deprotonate the host.[98]

### 1.3.3 Synthetic Anion Receptors

#### 1.3.3.1 Introduction

The chronological development of abiotic anion receptors began with Park and Simmons in 1968, reporting a positively charged protonated lipophilic cryptand-like receptor for the binding of halide anions in acidic aqueous media (Figure 1.15 a).[99] Approximately a decade later, Lehn[100] and Schmidtchen[101] built upon this work reporting positively charged, macrocyclic polyammonium and quaternary ammonium anion receptors respectively (Figure 1.15 b, c). Acknowledging the lack of directionality and selectivity of the electrostatic interactions employed by these highly charged cationic systems, a shift to lower positively charged and neutral HB donor receptor designs was subsequently made over the following decades. For

example, Fabbrizzi[102] and Sessler[103] utilised neutral urea and pyrrole N-H hydrogen bond donor acyclic and macrocyclic systems for anion binding (Figure 1.15 d, e).

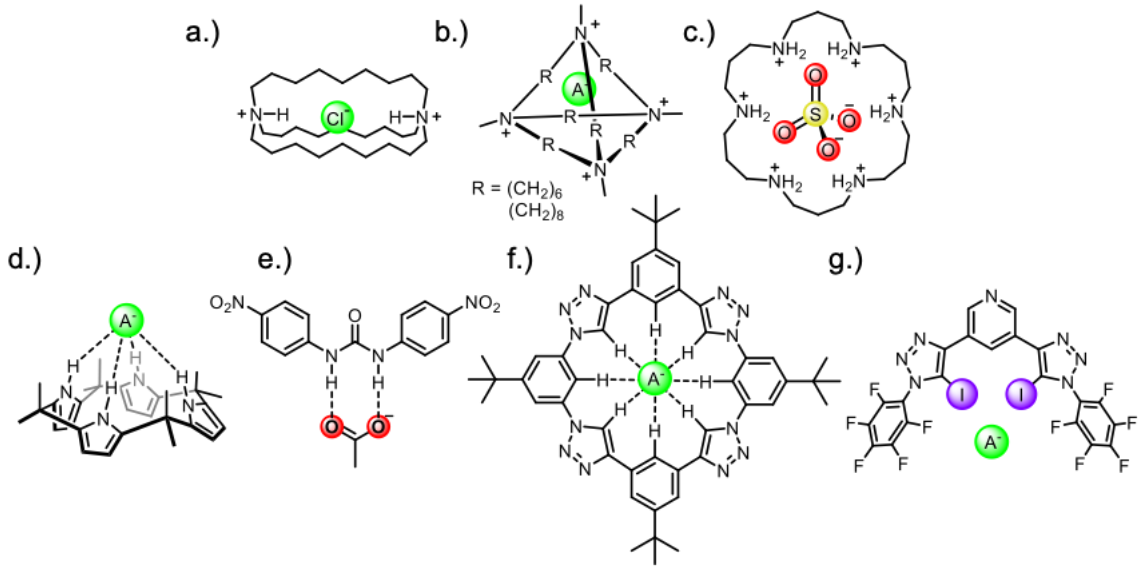



*Figure 1.15. Seminal anion receptors with a.) Simmons and Park's first reported abiotic anion receptor[99], b.) Schmidtchen's cationic ammonium cage[101], c.) Lehn's cationic sulfate receptor[100], d.) Sessler's pyrrole-based neutral receptor[103], e.) Fabbrizzi's urea-based neutral acetate receptor[102], f.) Flood's C-H based receptor[104] and g.) Beer's XB receptor[105].*

Notably, Flood further expanded the collection of neutral HB based anion receptors by incorporating multiple polarised triazole based C-H bond donor motifs into acyclic foldamer and macrocyclic structural frameworks (Figure 1.15 f).[104] The most recent advances in anion receptor design include the integration of potent σ-hole interactions, in particular XB, for the strong and selective binding of anions (Figure 1.15 g).[105]

The following sections discuss notable examples of abiotic charged anion receptors followed by neutral receptors, including those incorporating σ-hole donor motifs.

### 1.3.3.2 Positively Charged Receptors

Conceivably, the most intuitive way of developing host systems capable of anion recognition is by introducing positive charge to the receptor framework. Building on the first ammonium

based abiotic anion receptor systems of Park and Simmons (Figure 1.15 a),[99] Lehn and co-workers synthesised an ellipsoidal hexaprotonated cryptand for anion recognition in 1984.[106] While this highly charged bicyclic polyammonium system could bind a wide range of inorganic and organic polyatomic anions in aqueous media (Figure 1.16 b - e), the receptor exhibited selectivity for $N_3^-$, as well as a higher binding strength than predicted when comparing different anion hydration energies. X-ray crystal structure data confirmed that the cryptand cavity and its positioning of binding sites complemented the size and linear shape of the azide anion (Figure 1.16 e).[106]

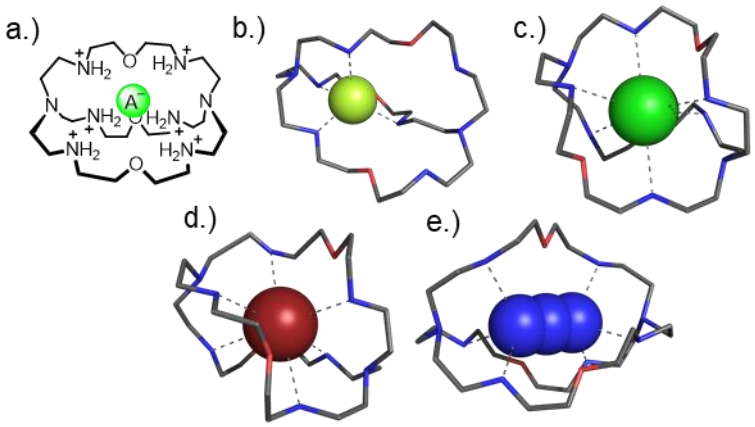



*Figure 1.16. a.) ChemDraw of Lehn's hexaprotonated cryptand and X-ray single crystal structures of cryptand binding b.) fluoride (CSD: CIDMUX), c.) chloride (CSD: CIDNAE), d.) bromide (CSD: CIDNEI) and e.) azide (CSD: CIMOR).*[106]

The spherical halides chloride and bromide displayed 6 HB N-H···anion contacts in an octahedral arrangement (Figure 1.16 c, d), similarly to $N_3^-$, while the smaller fluoride anion is bound in a tetrahedral fashion on only one side of the cryptand cavity (Figure 1.16 b).[106] This example highlights the importance of host-anion guest structural complementarity to achieve strong and selective binding.

Guanidinium, amidinium, imidazolium, triazolium, pyridinium and thiouronium have all since emerged as common cationic motifs (Figure 1.17) incorporated into a range of acyclic and

macrocyclic receptor structural frameworks for binding anions in organic as well as aqueous media *via* electrostatic and hydrogen-bonding interactions.[89]

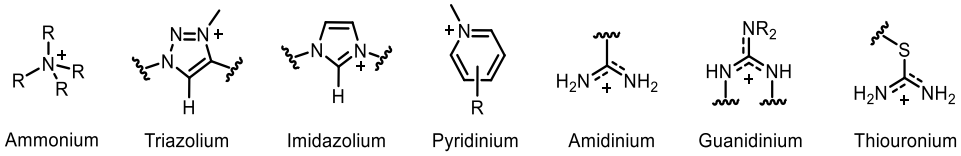



*Figure 1.17. Common motifs for charged anion receptors[89]*

Guanidinium has been shown to be a powerful cationic anion receptor motif with two protons capable of engaging in bidentate HB, as well as retaining its protonated state over a wide pH range.[107] Due to its $pK_a$ of 13.6, it is considered a virtually pH independent receptor motif.[89] It is commonly encountered in biotic systems and has inspired the design of many synthetic receptors.[108, 109] Two simple acyclic systems were reported by Hamilton[110] (Figure 1.18 a) and Göbel[111] (Figure 1.18 b) respectively, both containing two guanidinium motifs.

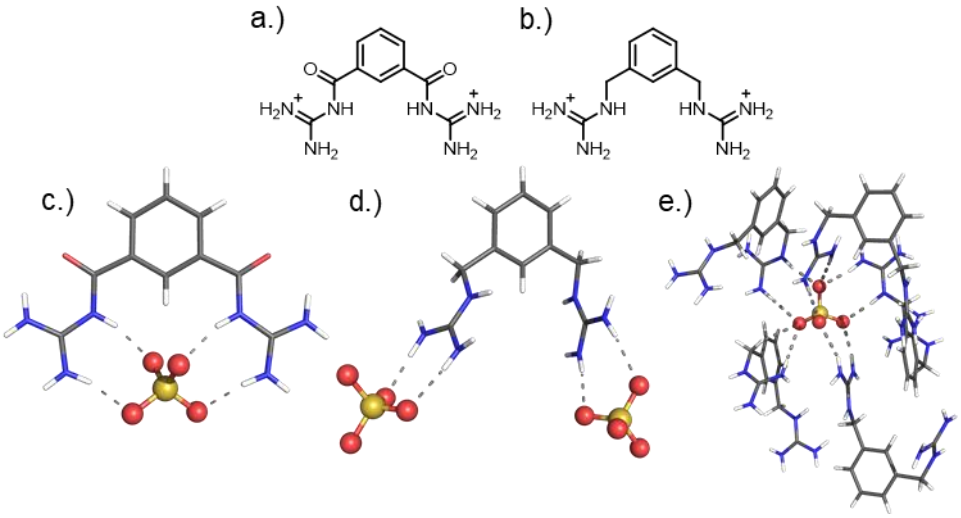



*Figure 1.18. Guanidinium-based receptors with a.) Hamilton's anion receptor[110], b.) Göber's anion receptor[111], c.) single crystal X-ray structure of a binding sulfate (CSD: QUAFVAV)[112], d.) single crystal X-ray structure of b binding sulfate (CSD: QUJQOB)[113], and e.) HB network surrounding sulfate for b (CSD: QUJQOB)[113]. HB shown as grey dashes.*

These receptors are capable of binding phosphate-based anions as well as showing promise as catalysts.[114-117] However, solid state analysis of these quite similar receptors with sulfate anions

showed a clear difference in their preorganisation.[112, 113] The receptor containing carbonyl groups can engage in intramolecular hydrogen bonding, resulting in an almost completely planar geometry of the receptor with one sulfate anion being bound within the cavity (Figure 1.18 c).[112] The receptor containing a simple alkyl linkage instead is twisted, with the guanidinium motifs being almost perpendicular to the central aromatic unit (Figure 1.18 d).[113] Here, each anion receptor motif is pointing towards a separate sulfate anion. The sulfate anions are surrounded by a HB network arising from guanidinium motifs from several different receptor units (Figure 1.18 e), which is unlike the preorganised receptor which shows clear binding in the desired binding pocket.[112, 113]

Quaternary ammonium receptors have the unique advantage that their charge is pH independent unlike other ammonium-based receptors.[89] However, they lack the ability to partake in hydrogen bonding.[89]

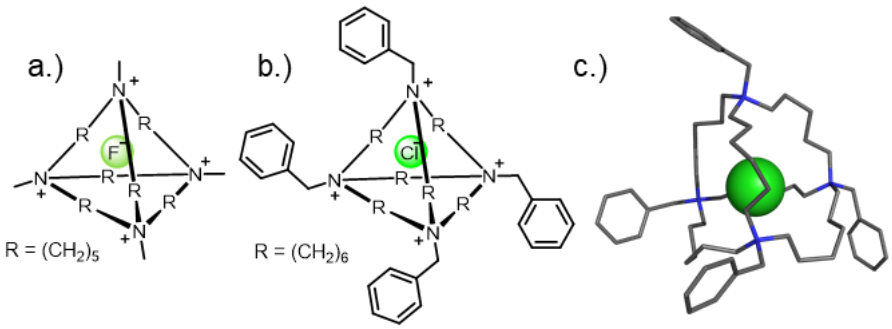



*Figure 1.19. Macrotricyclic quaternary ammonium receptors with a.) fluoride receptor[118], b.) chloride receptor[119] and d.) single crystal X-ray structure of chloride receptor (CSD: TOCXEO)[119].*

Inspired by Schmidtchen's macrotricyclic quaternary ammonium receptor (Figure 1.19 b),[101] Ichikawa and co-workers reported an analogous receptor with a shorter alkyl chain capable of selective fluoride binding within its small and preorganised binding pocket (Figure 1.18 a).[118] The X-ray single crystal structure of another analogous chloride complex further confirms the position of the halide within the cavity of the receptor (Figure 1.19 b, c).[119]

Receptors containing imidazolium or triazolium motifs also offer pH independence while being able to partake in charge assisted C-H based hydrogen bonding with anionic guest species.[120] In 2005, a calix[4]imidazolium[2]pyridine anion receptor capable of strong and selective binding of fluoride in both acetonitrile and DMSO was reported (Figure 1.20).[121] The single crystal X-data revealed a symmetrical macrocyclic host with all four imidazolium motifs engaging in the concerted binding of the $F^-$ anion through C-H HB interactions (Figure 1.20).

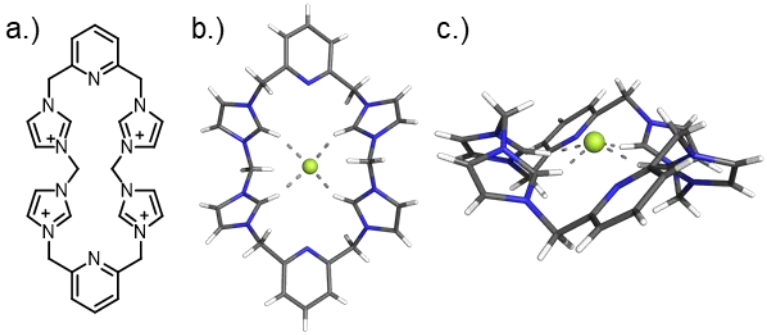



*Figure 1.20. Calix[4]imidazolium[2]pyridine anion receptor with a.) ChemDraw representation and b.) and c.) single crystal X-ray structure of chloride receptor (CSD: NAQMOI) with front side view respectively.*[121]

### 1.3.3.3 Neutral Receptors

Neutral anion receptors are often primarily designed to operate in aprotic organic solvent media.[122] They commonly function by solely employing HB-anion interactions, which are individually weaker than the attractive ion-ion Coulombic electrostatic interactions present in positively charged anion receptors.[8]

However, HB interactions are much more directional and can impart a higher degree of selectivity, especially when used in a concerted fashion as often observed in biotic systems (see section 1.3.1).[8] Furthermore neutral receptor systems do not possess counter-anions, unlike a charged receptor, where the counter-anion needs to be 'non-coordinating' to prevent strong

competition with the target anion guest species of interest.[89, 122] Some common neutral receptor motifs are shown in Figure 1.21.

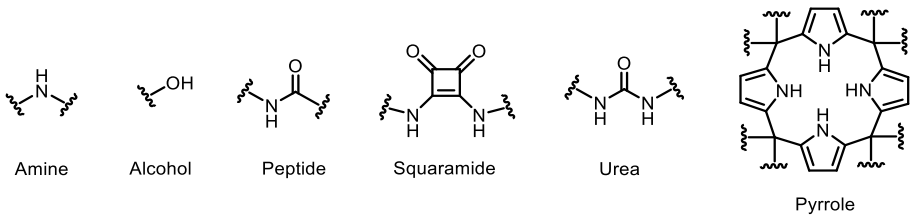



*Figure 1.21. Common motifs for neutral anion receptors[89]*

In a seminal publication in 1997, Crabtree *et al.* reported a simple, readily synthetically accessible neutral acyclic isophthalamide receptor capable of binding halides strongly in $CD_2Cl_2$ ($6.1\times10^4$ $M^{-1}$ for $Cl^-$).[123] Upon halide complexation, the molecule adopts the less favoured *syn-syn* conformation, binding the halide in a cooperative bidentate HB manner, confirmed by XRD (Figure 1.22 a, b).

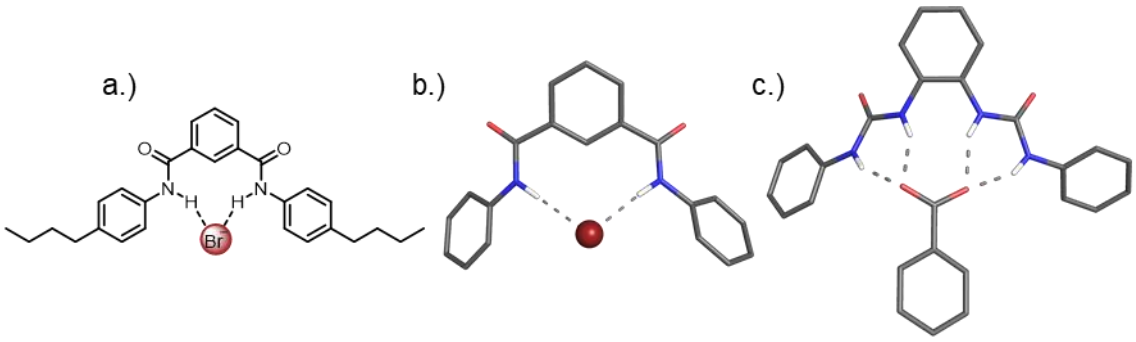



*Figure 1.22. a.) Crabtree's neutral halide receptor with receptor appended with solubilising groups, b.) single crystal X-ray structure of $Br^-$ binding receptor (CSD: RINGOK)[123] and c.) Gale's urea-based carboxylate receptor (CSD: HAWQEC)[124].*

$^1$H NMR binding studies in $CD_2Cl_2$ revealed a preference for $Cl^->Br^->I^-$ consistent with the charge densities and relative basicities of the halides. A similar bis-urea containing receptor was reported by Gale in 2005 (Figure 1.22 c).[124] The anion binding properties of the receptor were studied *via* $^1$H NMR in DMSO-$d_6$ with 0.5% $D_2O$. The receptor was shown to be selective for the carboxylate anions benzoate and acetate, with moderate binding observed for phosphate and very weak binding for sulfate as well as chloride and bromide.[124] This often observed selectivity for urea-based acyclic receptors is in accordance with the basicity of the anion guest

species.[125] However, selectivity can also be achieved through the careful positioning of multiple urea motifs in order to match the geometric requirements of a particular anionic guest.[125] Solid state analysis of a co-crystal of the receptor with benzoate (Figure 1.22 c) revealed that the carboxylate complexation occurs *via* four concerted hydrogen bonds.[124]

Sessler and co-workers have exploited macrocyclic calixpyrroles as neutral, multidentate N-H based HB donor arrays for the purposes of anion recognition.[126, 127] For example, in 2000, the anion binding abilities of a fluorinated calix[4]pyrrole was compared to its hydrogen substituted analogue (Figure 1.23 a, b).[126] Using $^{1}H$ and $^{19}F$ NMR as well as fluorescence spectroscopy, both receptors were shown to bind fluoride, chloride, and phosphate anions in acetonitrile-$d_3$ with 0.5% $D_2O$. A binding strength enhancement of up to 7-fold for phosphate was observed with the fluorinated receptor, attributed to enhanced N-H acidity. Solid state analysis of a co-crystal of the fluorinated receptor with TBAF confirmed the expected binding mode with the halide anion bound centrally in a capped geometry through four concerted hydrogen bonds (Figure 1.23 c).[126]

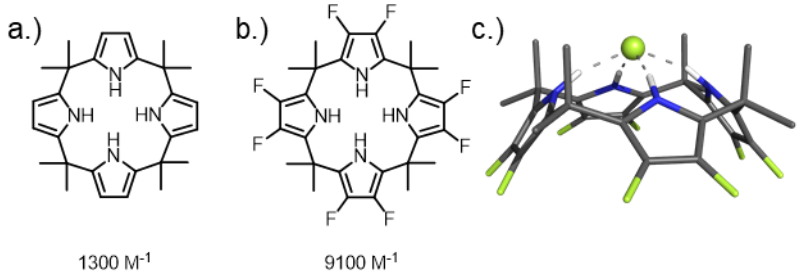
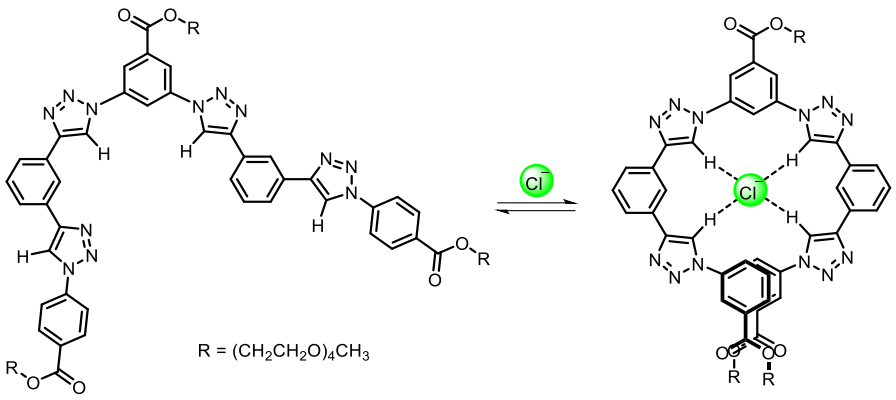



*Figure 1.23. Sessler's neutral pyrrole anion receptors with a.) non-fluorinated receptor, b.) fluorinated receptor with binding constants based on a 1:1 stoichiometric host-guest binding of $H_2PO_4^-$ in acetonitrile-$d_3$ with 0.5% v/v $D_2O$ at 295 K and c.) single-crystal X-ray structure with TBAF (CSD: VIQJAG).* [126]

Recently, Flood and others have demonstrated that preorganised arrays of unconventional C-H based HB donors can also function as potent anion recognition motifs, particularly with the 1,2,3-triazole moiety offering a highly polarised C-H bond.[120, 128, 129] In 2008, Craig reported a 1,2,3-proto-triazole based foldamer receptor, which exhibits anion-induced helical folding

(Scheme 1.3).[130] The receptor contains four polarised C-H moieties and is capable of $Cl^-$, $Br^-$ and $I^-$ binding in acetone *via* all four triazoles, as confirmed by $^1H$ NMR 2D NOESY experiments.[130]




*Scheme 1.3. Craig's proto-triazole based receptor exhibiting anion-induced folding*[130]

### 1.3.3.4 Sigma-Hole Anion Receptors

Sigma-hole interactions (see section 1.2.4) have recently been proven to be powerful additions to the arsenal of interactions exploited for anion complexation. They exhibit several desirable features such as remarkable potency and a relatively more stringent linear binding geometry for anion recognition than HB.[131-133] Another advantage of σ-hole based anion receptors is their enhanced hydrophobicity in comparison to more acidic HB donors, aiding the dehydration of anions in aqueous media.[50] Moreover, it has been observed that σ-hole interactions can impart contrasting anion selectivity trends in receptors when compared to HB receptor analogues.[134] In particular, the XB and ChB receptors reported to date commonly display preferences for halides over more basic oxoanions, whereas the selectivity of analogous HB receptors is often primarily dictated by anion basicity.[135-137]

Among the first examples of XB being exploited in solution phase anion receptor design are those reported by Taylor. His pioneering work described a series of neutral, acyclic XB

receptors, which relied upon the cooperative action of XB iodoperfluoroarene motifs (Figure 1.24).[138] The receptor's anion binding abilities were studied in solution *via* $^{19}$F NMR in acetone-$d_6$ and a clear trend could be observed for an increase in binding strength with an increase in the number of XB donors (Figure 1.24).[138] The tridentate XB receptor was identified as the most potent anion receptor, binding halides strongly with a preference for $Cl^->Br^->I^-$ consistent with their charge densities. However, p-toluenesulfonate, nitrate, and bisulfate were all bound weakly, in the range of 10 $M^{-1}$ or less.[138]

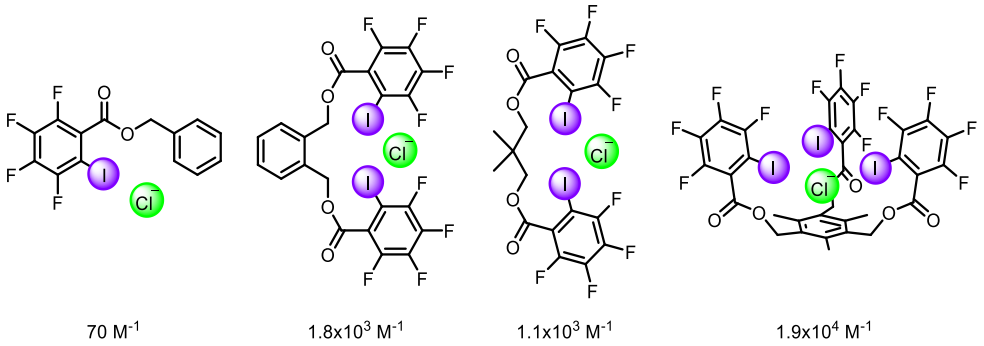



*Figure 1.24. Taylor's iodoperfluoroarene XB anion receptors. Binding constants based on a 1:1 stoichiometric host-guest binding of $Cl^-$ in acetone-$d_6$ at 295 K.*[138]

Recent years have witnessed the emergence of a number of other XB donor motifs with the most potent XB donors containing bromine and iodine attached to neutral and positively charged electron withdrawing nitrogen heterocyclic groups (Figure *1.25*).[139]

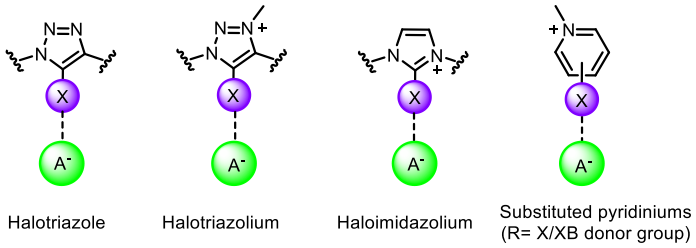



*Figure 1.25. Common XB-donor motifs, X = Br, I, $A^-$ = anion.*[60]

In particular, the 5-iodo-1,2,3-triazole motif has become a commonly used XB donor to integrate into various structural frameworks, being readily prepared *via* Cu(I)-catalysed azide-iodoalkyne cycloaddition (CuAAC) reactions.[132, 133, 137, 140, 141] Beer reported the first example of a tetradentate XB foldamer (Figure 1.26 a), which preferentially bound the heavier halides over

selected oxoanions, such as acetate and dihydrogen phosphate as determined by $^{1}$H NMR anion binding studies in $CDCl_3$.[132] Notably, the HB foldamer analogues bound all anions less strongly than the XB counterpart.[132] Single crystal XRD of the foldamer co-crystallised with NaI revealed that the iodide anion is bound through four convergent halogen bonds (Figure 1.26 b). As shown in Figure 1.26 c, the anion is situated above the plane of the phenylene backbone with the iodotriazoles being tilted out of the plane to allow for binding of the guest through linear XB.[132] The sodium counter cation is bound by the tri(ethylene glycol) chain (Figure 1.26 b, c).

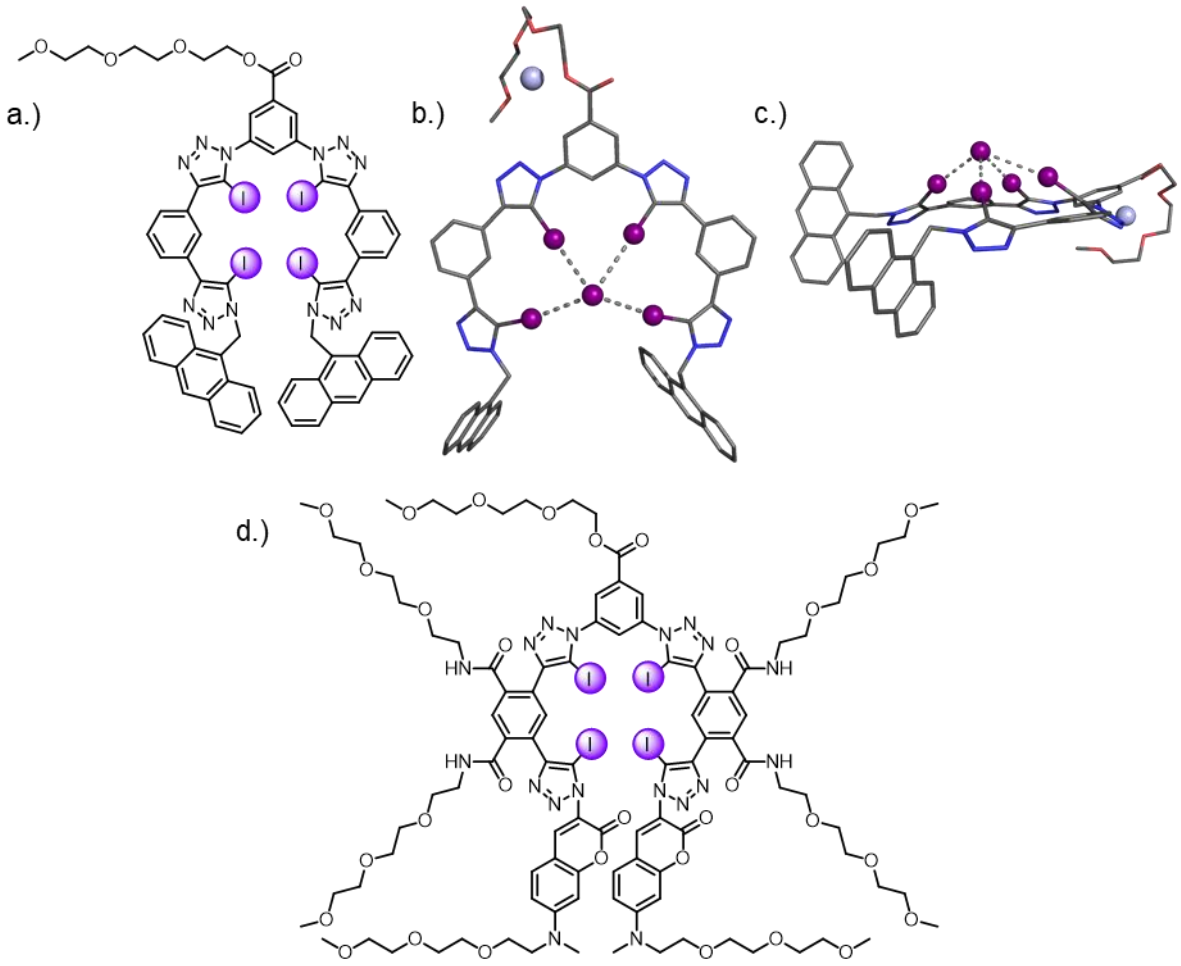



*Figure 1.26. Beer's XB foldamers with a.) selected XB foldamer for anion recognition in acetone, b.), c.) front and side view respectively of single-crystal X-ray structure of foldamer complexed with NaI (CSD: SAMXIQ), and d.) water soluble XB foldamer for selective $I^-$ recognition. Na shown in light purple complexed additionally by solvent molecule and adjacent triazole N (not pictured).*[132, 142]

A modified water soluble XB foldamer containing tri(ethylene glycol) substituents on the outer rim and a central hydrophobic XB donor cavity was reported by the same group in 2019 (Figure

1.26 d).[142] In $D_2O$, the XB foldamer binds anions in a 2:1 host to guest stoichiometry. This can be explained by the binding mode of the XB receptor and its sterically demanding iodotriazole units, which require the bound anion to be sitting slightly above the plane of the foldamer, as previously observed in the solid state (Figure 1.26 c).[132, 142] This 'capped' complexation geometry allows for a second foldamer receptor to coordinate to the anion, resulting in the extremely strong and selective binding of $I^-$, with an association constant of $1.68\times10^{11}$ $M^{-2}$ (Figure 1.26 d).[142]

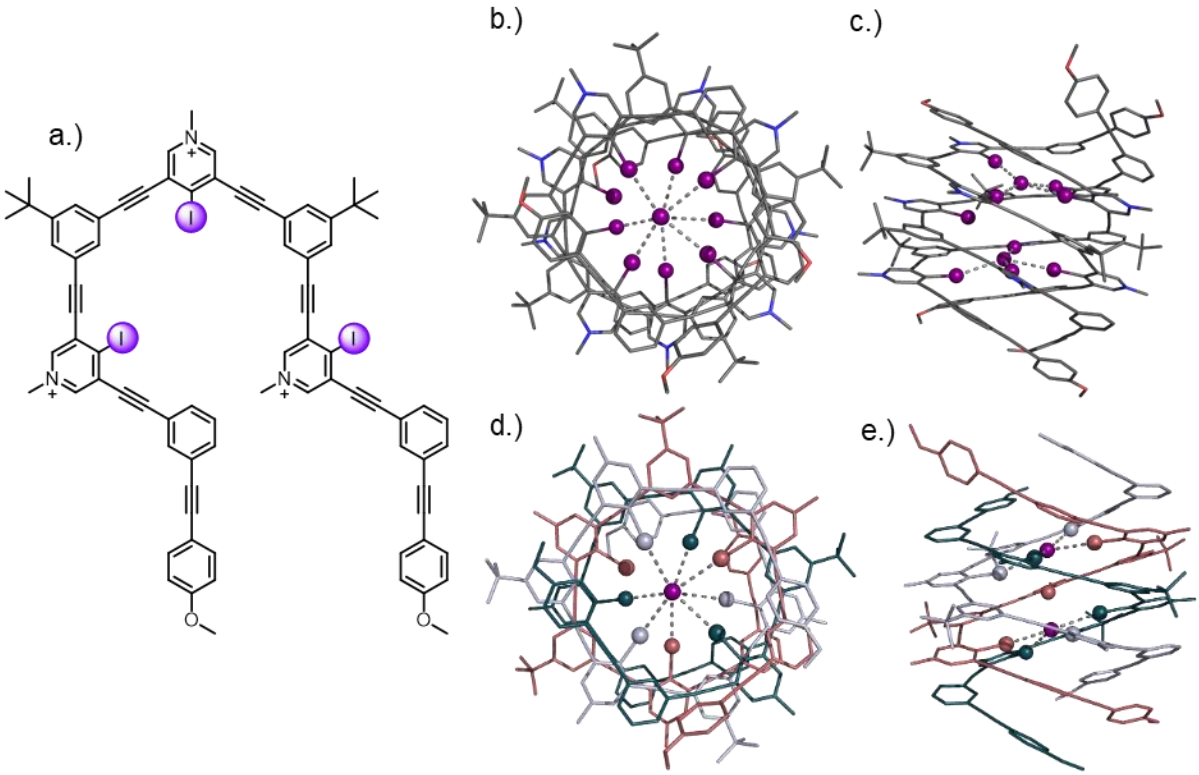



*Figure 1.27. Berryman's helical anion receptor with a.) monomer structure, b.) and c.) single crystal X-ray structure of helical assembly encapsulating two $I^-$ anions with XB bonds shown as grey dashes (CSD: ORAVIO), e.) and d.) single crystal X-structure with each monomer coloured in grey, pink, or green respectively.*[143]

Berryman used the iodopyridinium motif to construct a diethynyl benzene linked tri-cationic XB receptor which upon addition of iodide forms a triple helicate assembly (Figure 1.27 a).[143] Solid state X-ray structural analysis revealed the triple helical structure consisting of three intertwined monomers encapsulating two iodide anions in the central channel, each stabilised by four halogen bonds, with one iodopyridinium unit not contributing to the overall binding

process (Figure 1.27 b – e).[143] $^{1}$H NMR titration data provided evidence for the helix to reversibly assemble in a 1:3 DMF:acetonitrile mixture.[143]

Arguably, the most attractive feature of XB mediated anion recognition is the persistent observation of XB supramolecular host structures outperforming their HB analogues in terms of binding strength and selectivity.[144-147] This has no doubt stimulated the development of XB supramolecular chemistry in applications such as anion sensing, membrane transport as well as material design and nanotechnology.[50, 148, 149] However, the sister σ-hole interactions, ChB and PnB, have been much less explored for anion recognition purposes, especially in the solution phase.[150]

A seminal report by Gabbaï *et al.* described the synthesis and study of the first tellurium-based ChB anion receptor (Figure 1.28 a).[151]

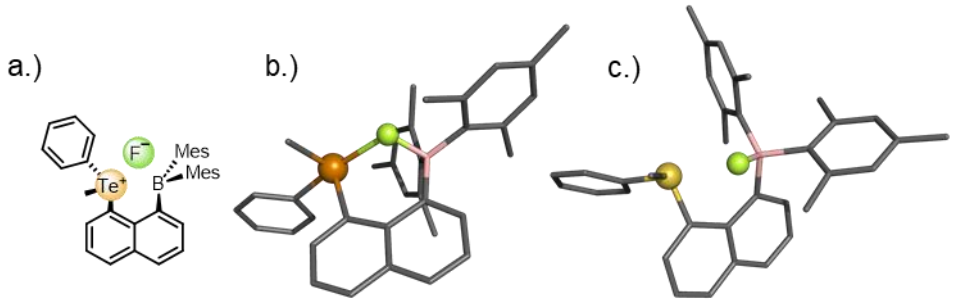



*Figure 1.28. Gabbaï's ChB anion receptor with a.) bidentate 1,8-boron-telluronium-naphthalene receptor binding fluoride, b.) X-ray single crystal structure of Te receptor (CSD: GAGYAQ) and c.) X-ray single crystal structure of S based receptor (CSD: GAGYOE)[151]*

This bidentate 1,8-boron-telluronium-naphthalene compound was capable of selective fluoride binding in methanol, with $^{19}$F and $^{125}$Te NMR titration investigations supporting solution state binding.[151] Analysis of single-crystal XRD data showed an almost linear Ph-Te-F$^{-}$ contact (174.0°), as well as a short Te-F bond distance (Figure 1.28 b), which is shorter than the S-F analogue despite the smaller size of the sulfur atom (Figure 1.28 c).[151] However, the sulfur-based

receptor showed no evidence for fluoride binding in solution, indicating that sulfur is too weak of a ChB donor to participate in solution-state anion recognition (Figure 1.28).[151]

Five years later Taylor *et al.* reported a series of neutral chalcogenadiazole and chalcogenophene receptors.[152, 153] The strongest anion receptors contained Te-based ChB donors covalently linked to electron withdrawing fluorinated aryl substituents (Figure 1.29 a - c), which results in a deeper σ-hole on the Te atom.[152, 153] In the organic media THF, all receptors showed a preference for $Cl^-$>$Br^-$, consistent with the charge densities of these halides. Interestingly, despite a higher anion basicity of some oxoanions tested, the ChB receptors showed a preference for the 'softer' halides, which is often observed for XB and regarded as characteristic of σ-hole interactions, not generally observed for HB analogues.[42]

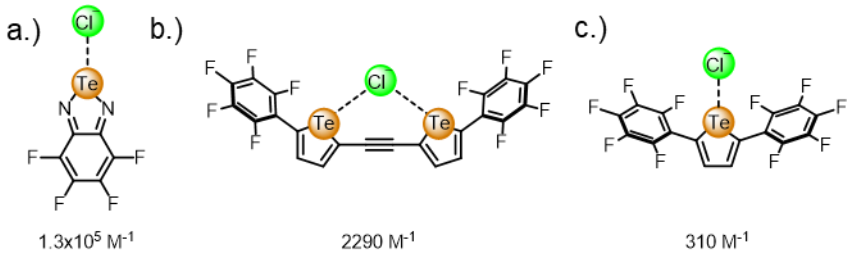



*Figure 1.29.Taylor's ChB receptors with a.) benzotelluradiazole[153], b.) bidentate tellurophene and c.) monodentate tellurophene[152]. Binding constants based on a 1:1 stoichiometric host-guest binding of $Cl^-$ in THF based on UV-vis absorbance.*

The monodentate benzotelluradiazole derivative (Figure 1.29 a) is the strongest chloride binding receptor of the series as determined by both $^1$H NMR and UV-vis titration studies performed in THF. The receptor binds bromide much more weakly, with decomposition of the receptor observed when titrated with TBA iodide.[153] UV-vis absorbance titrations in THF revealed that both the monodentate tellurophene receptor (Figure 1.29 c) as well as its bidentate analogue (Figure 1.29 b) bind chloride less strongly than the previously reported monodentate benzotelluradiazole receptor.[152, 153] However, an enhancement in chloride binding by a factor of

7 was observed when going from the monodentate tellurophene receptor to the bidentate analogue (Figure 1.29).[152]

Respective reports by Matile[154] and Huber[155] highlight the potential of utilising ChB for anion transport and organocatalysis. Matile's dithienothiophene based receptor (Figure 1.30 a), represents the first example of utilising ChB to transport chloride and nitrate anions across lipid bilayers.[154] Huber reported the first selenium chalcogen bond donor organocatalyst (Figure 1.30 b) capable of activating the solvolysis of benzhydryl bromide in wet acetonitrile.[155] The cationic receptor activates this reaction through halide abstraction *via* ChB, with HB based control compounds showing no conversion of the substrate, proving that the activation is due to the σ-hole interaction between receptor and halide.[155] These examples serve to further highlight the potential of ChB as a valuable addition to the toolbox for the design of functional supramolecular anion receptors.

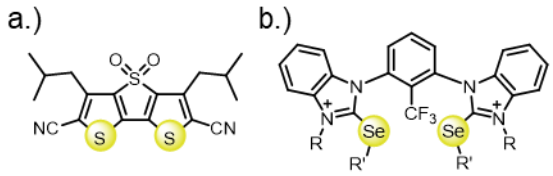



*Figure 1.30. a.) Matile's dithienothiophene based ChB anion transporter[154] and b.) Huber's Se based ChB donor capable of C-Br bond activation with bis(benzimidazolium) centre with variable R groups[155]*

While there have been computational[77, 156-158] as well as some solid state[80, 159, 160] studies on PnB anion interactions, examples of solution phase PnB receptor anion binding investigations are extremely rare.

Gabbaï *et al.* reported the synthesis of a simple antimony-indole derivative (Figure 1.31 a) capable of binding halide anions in acetonitrile, as confirmed by $^{1}$H NMR studies and optical absorbance experiments in acetonitrile.[161] Single crystal X-ray diffraction of the $Cl^-$ bound complex revealed almost linear binding along the Sb(III)-Cl bond (Figure 1.31 b). Changing the

Cl substituent to a phenyl group (Figure 1.31 c) caused the receptor to no longer bind halide anions, highlighting the importance of an electron withdrawing substituent for the deepening of the σ-holes on the Sb(III) atom.[161]

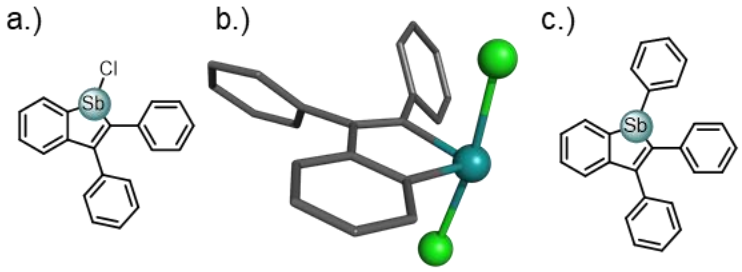



*Figure 1.31. Gabbaï's stibaindole PnB anion receptors with a.) active receptor, b.) X-ray single crystal structure of receptor binding chloride (CSD: GEHXOJ)and c.) inactive receptor with phenyl substituent.*[161]

The examples above highlight the exciting recent developments in anion receptor chemistry, in particular the potential use of σ-hole interactions for achieving the goal of strong and selective anion recognition in competitive solvent media.

## 1.4 Interlocked Structures

### 1.4.1 Introduction and Historical Context

The term 'interlocked structure' refers to a mechanically interlocked molecule (MIM), which consists of two or more molecular components connected *via* a molecular bond that cannot be separated without the cleavage of a covalent bond.[16, 162, 163]

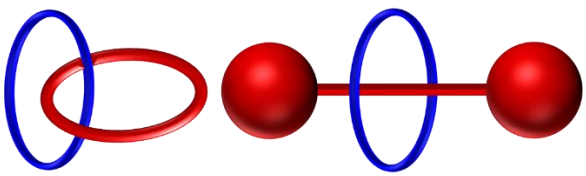


*Figure 1.32. [2]Catenane (left) and [2]rotaxane (right) as examples of MIMs*

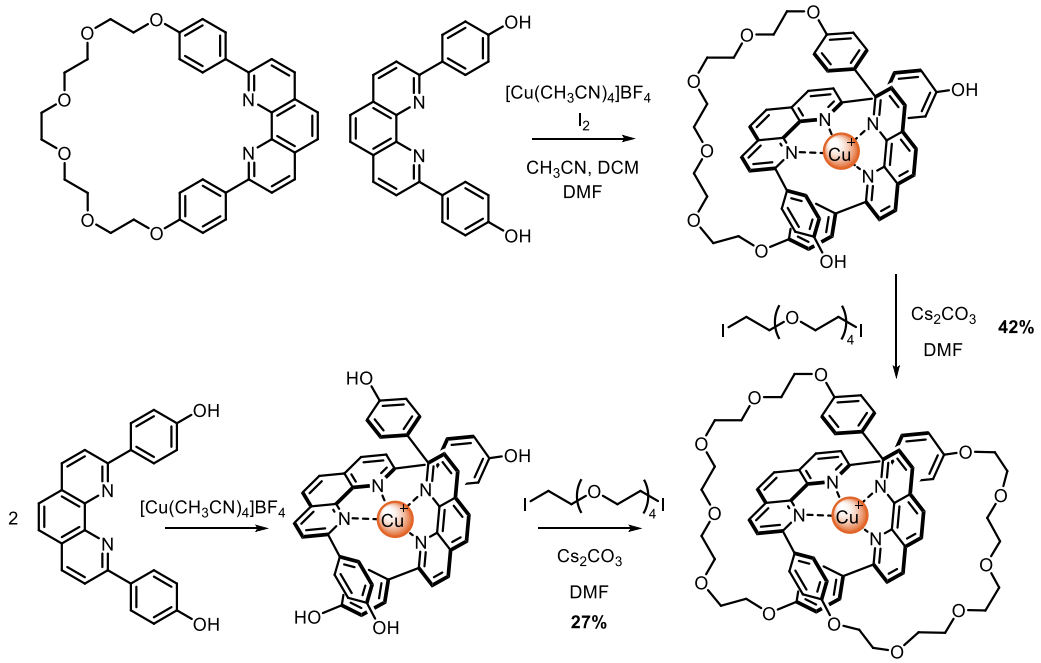
Catenanes and rotaxanes (Figure 1.32) are common examples of MIMs. The number of molecular components, which are mechanically bonded is denoted by the number in brackets before the type of MIMs (Figure 1.32).[162]

These unique molecules have been of interest to chemists since the 1960s, but their preparation was regarded as a great synthetic challenge.[163] Early attempts at forming interlocked structures were undertaken using a statistical approach,[164, 165] where the chance ring closing or stoppering reaction of a threaded macrocycle is statistically low resulting in extremely low yields.[166] Schill and Lüttringhaus were able to form a [2]catenane *via* a directed synthesis method in 1964.[167] In their multi-step approach they managed to covalently link the components for the macrocycles of a catenane together in such a way that favoured the formation of an interlocked structure. Schill's work produced a number of interlocked structures using this method and even higher order [3]catenanes were synthesised.[168, 169] However, this method required a great deal of synthetic expertise and manipulation, which still prevented MIMs from being readily synthetically available. In 1983 Sauvage first introduced the use of a metal template for the formation of interlocked structures in unprecedented high yields.[170, 171] During the ensuing years this subsequently led to various efficient templating methods being employed in MIM construction, such as aromatic donor-acceptor π-π stacking,[172, 173] anion templation,[174-178] hydrophobic effects,[179, 180] HB interactions,[181, 182] and recently radical interactions[183]. The ability to prepare these topologically unique structures in larger quantities has enabled their study in a wide variety of applications including host-guest recognition and sensing,[184-186] molecular switches[187, 188] and as molecular machines[14, 17, 189, 190]. The latter potential nanotechnological use of MIMs was notably recognised by the 2016 Chemistry Nobel Prize being awarded to Sauvage and Stoddart.[15, 16]

## 1.5 Template Synthesis of MIMs

### 1.5.1 Metal Templates

In Dietrich-Buchecker and Sauvage's seminal 1983 publication, a copper(I) metal template was exploited to construct a [2]catenane in an impressive yield.[171] Their synthetic pathway (Scheme 1.4) involved the formation of a tetrahedral copper(I) complex between 2,9-bis(4-hydroxyphenyl)-1,10-phenanthroline and a macrocycle containing a 2,9-diphenyl-1,10-phenanthroline ligand linked by a polyethylene glycol chain. A Williamson ether macrocyclisation reaction between the Cu(I) templated complex and a bis-iodine functionalised polyether under basic conditions produced the Cu(I) complexed homo[2]catenane in an overall yield of 42%.[8] A subsequent paper described a double cyclisation clipping synthetic pathway (Scheme 1.4), producing the copper(I) [2]catenane in 27% yield.[170] Demetallation of the Cu(I) template to give the metal-free catenane was achieved quantitatively on addition of tetramethylammonium cyanide.[170]




*Scheme 1.4. Formation of Sauvage's metallo-[2]catenane using a passive metal template*[170, 171]

Solid state single-crystal XRD structure determinations confirmed the catenane ligand's tetrahedral complexation of Cu(I) by the four nitrogen donor atoms of the two interlocked phenanthroline ligands (Figure 1.33 a).[191] It is noteworthy that the metal-free [2]catenane structure exhibits a dramatically altered conformation (Figure 1.33 b), showing the macrocycles have circo-rotated around each other upon demetallation.[191]

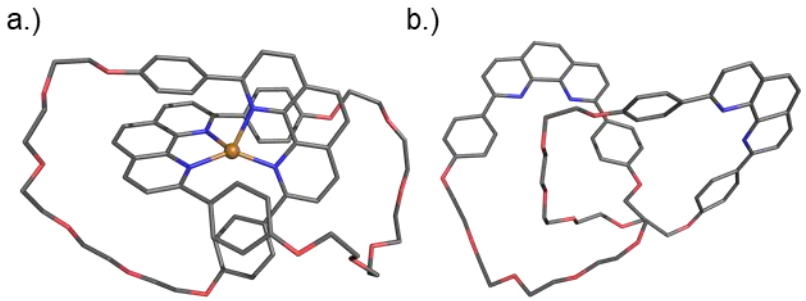



*Figure 1.33. X-ray single crystal structure of Sauvage's a.) metallo[2]catenane (CSD: CUFHEQ) and b.) demetallated homo[2]catenane (CSD: CUFHIU).*[191]

A range of transition metal templates with varying coordination geometries and chemical properties have since been employed in MIM synthesis, in particular by Leigh and co-workers (Figure 1.34).[192-195]

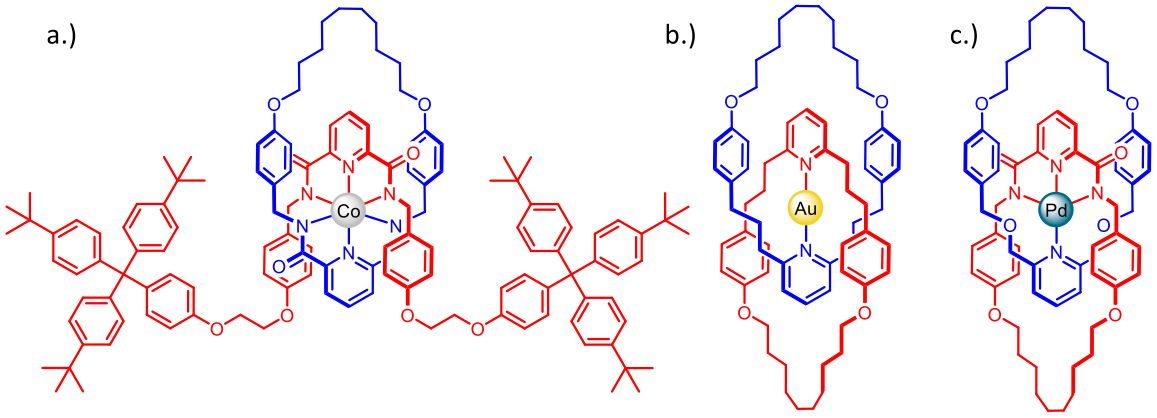


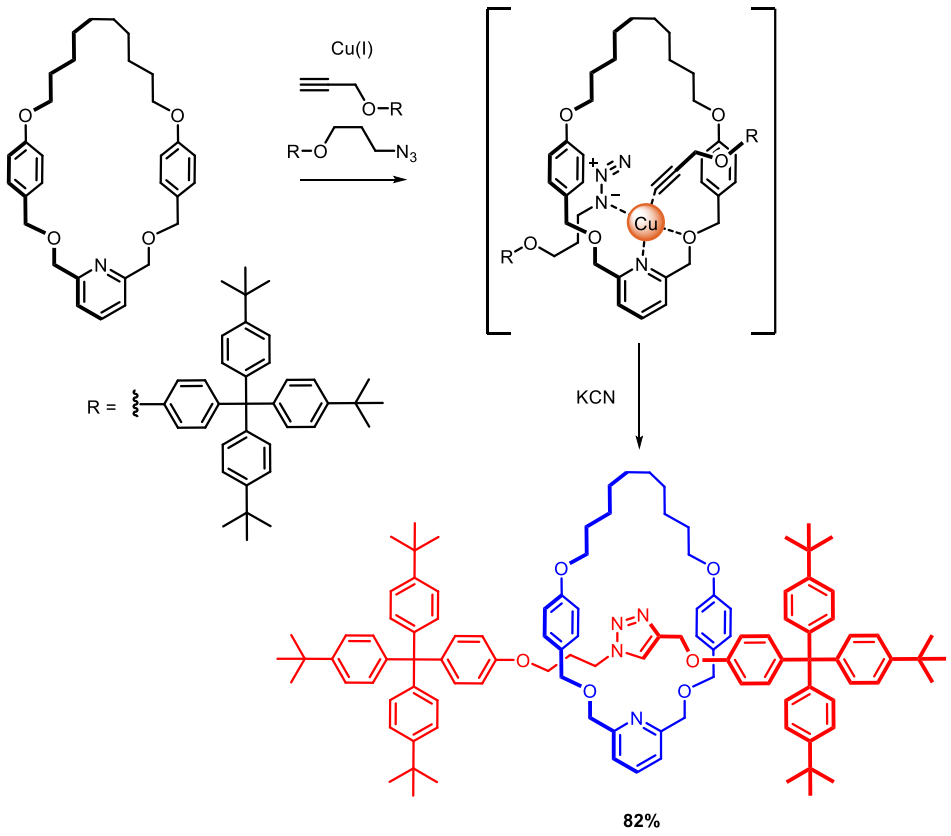

*Figure 1.34. Leigh's examples of MIMs formed via passive metal templates with a.) Co(III) rotaxane*[194]*, b.) Au(I) catenane*[196] *and c.) Pd(II) catenane*[193]

For example a [2]rotaxane was isolated in 61% yield using a Co(III) metal cation to coordinate two tridentate bis-anionic pyridine-2,6-dicarboxamido ligands in an octahedral fashion (Figure 1.34 a).[194] They were also able to exploit the linear coordination geometry of Au(I) for the

formation of a homo[2]catenane (Figure 1.34 b) in 41% yield.[196] Another notable example utilised the square planar directing Pd(II) cation template for hetero[2]catenane synthesis in 78% yield (Figure 1.3 c).[193] These examples serve to demonstrate the successful exploitation of the various stereochemical preferences of transition metals, which allow for the template synthesis of a wide range of MIMs in high yields.[196-200]

### 1.5.2 Active Metal Templates

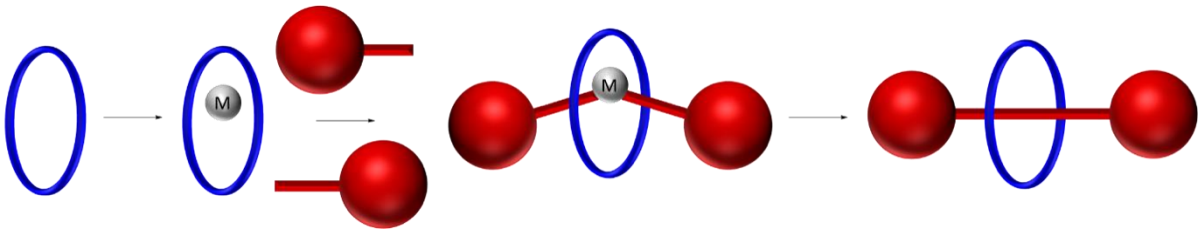
In a more recent MIM synthetic development, the metal cation has been used both as a template and a catalyst for mechanical bond formation, contrasting the 'passive' metal template approach discussed in the previous section. The use of this active metal template (AMT) method for the formation of interlocked structures was first introduced by Leigh and co-workers in 2006.[201]




*Scheme 1.5. Leigh's [2]rotaxane formed via AMT with proposed monometallic intermediate shown.*[201]

Sub-stoichiometric quantities of copper(I) were used to both template and catalyse the formation of a [2]rotaxane *via* a copper(I) catalysed click azide-alkyne cycloaddition (CuAAC) reaction (Scheme 1.5).

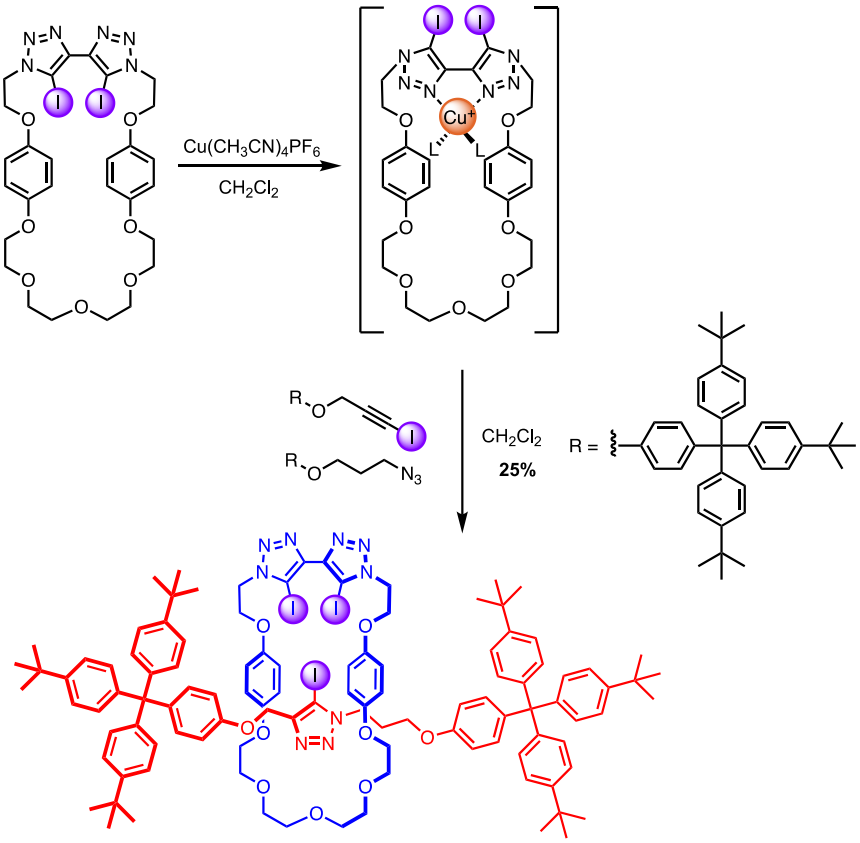
In an AMT reaction, the metal is endotopically bound in the cavity of the macrocycle, with metal-catalysed mechanical bond formation occurring within the cyclic cavity to form the axle component of the rotaxane product (Scheme 1.6).[201]




*Scheme 1.6. Schematic representation of a [2]rotaxane synthesis via AMT*

In recent years, AMT CuAAC triazole mechanical bond forming methodology in particular, has been intensely exploited in MIM synthesis due to functional group compatibility, mild reaction conditions, and accessible coupling partners. However, other metals, such as Pd,[202, 203] Zn,[204] and Ni[205-207] have also been employed in AMT synthesis using a range of organic reactions.[208] Overall, AMT allows for the reliable synthesis of many complex interlocked structures in good yield.[206, 209-213] Importantly, in contrast to passive metal templation, which relies on the formation of a thermodynamically stable complex, AMT is under kinetic control, like other catalytic processes.[208]

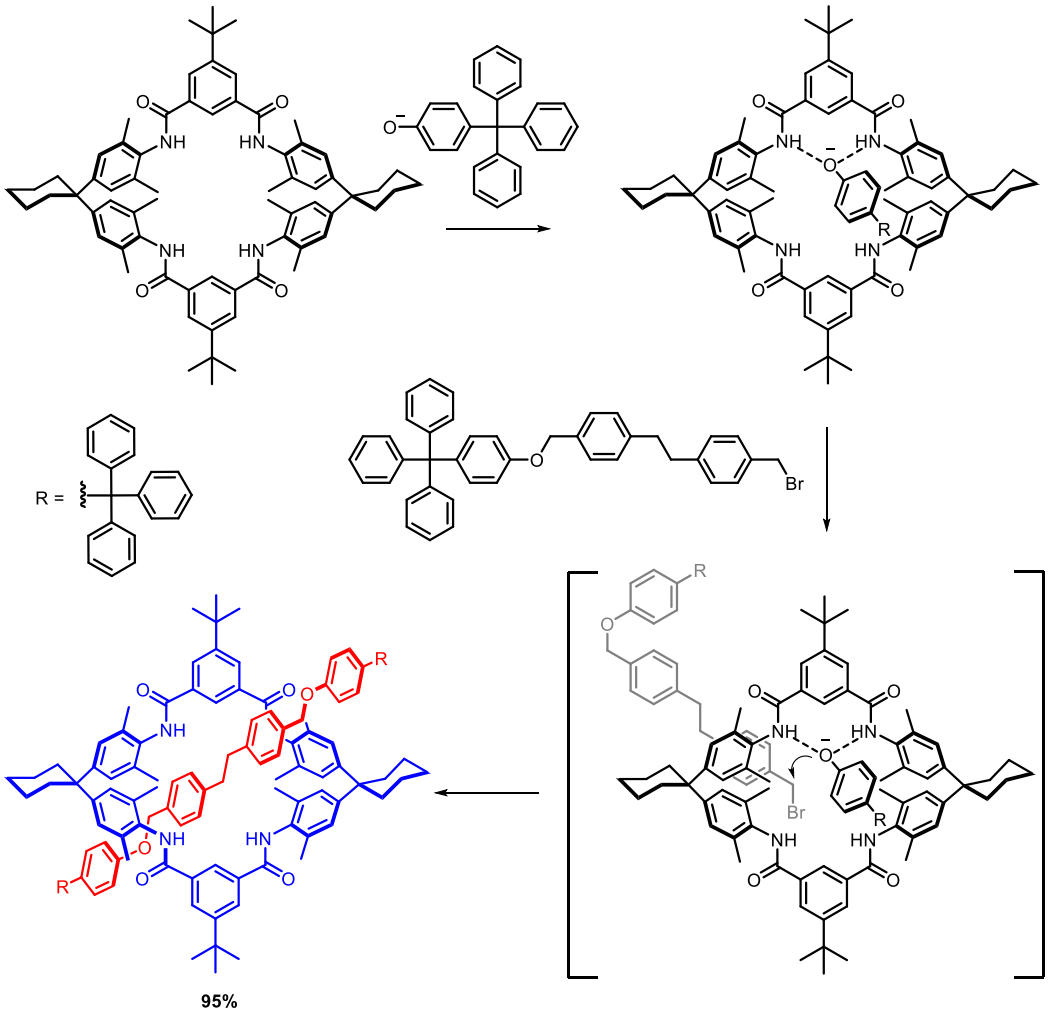
Incorporating iodotriazole units into a macrocycle allows for Cu(I) complexation *via* the Lewis basic triazole nitrogens (Scheme 1.7).[214] The iodotriazoles can then further be exploited by utilising the Lewis acidic iodo-group for XB anion recognition.[214] Several XB functionalised MIMs have been prepared *via* AMT, which exploits this ambidentate nature of the iodotriazole units.[147, 215, 216]




*Scheme 1.7. All XB [2]rotaxane made via AMT using N-triazole Cu(I) ligation*[214]

### 1.5.3 Anion Templation

In 1999, Vögtle reported the first example of an anion templated [2]rotaxane synthesis using a tetralactam based macrocycle, capable of binding an anionic phenolate stopper unit in its centre (Scheme 1.8).[217] This bound supramolecular nucleophilic anionic species can further react with a bromo-functionalised semi-axle to form the interlocked rotaxane structure in a near quantitative yield of 95% (Scheme 1.8).[217]




*Scheme 1.8. Vögtle's [2]rotaxane formed via an anionic template*[217]

An elegant example of the formation of a higher order [3]rotaxane prepared using an anion template approach comes from Flood and co-workers (Figure 1.35 b, c).[218] Their pentagonal cyanostilbene macrocycle (Figure 1.35 a) binds large anions, such as $BF_4^-$, $ClO_4^-$, $PF_6^-$ and $H_2PO_4^-$ in a stoichiometric 2:1 host:guest sandwich complex through highly polarised C-H bonds.[218] The macrocycle's strong $H_2PO_4^-$ binding affinity in particular led to a bis-alkyne functionalised phosphate ester anion template species being employed to prepare the [3]rotaxane *via* by a CuAAC stoppering reaction. The formation of the MIM was confirmed by single-crystal X-ray diffraction (Figure 1.35 b, c), as well as by $^1$H NMR and NOESY.[218]

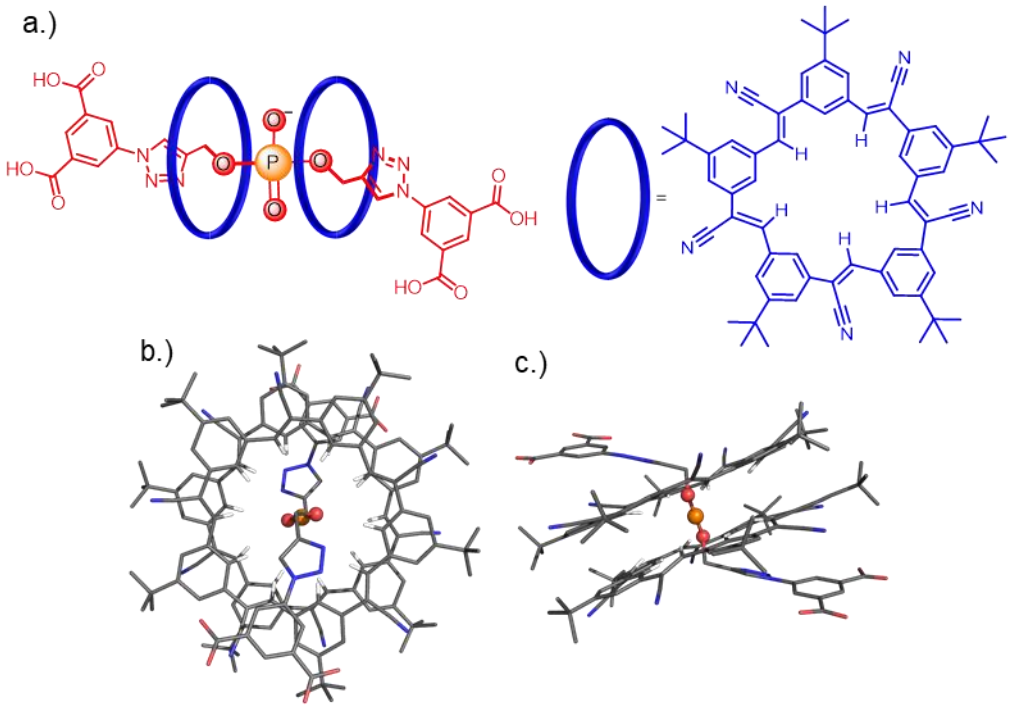



*Figure 1.35. Flood's pentagonal "cyanostar" based [3]rotaxane with a.) cartoon representation, b.) single-crystal X-ray structure front view and c.) side view of the [3]rotaxane (CSD: RIFNIF)*[218]

Following their seminal report in 2002 on the formation of a HB [2]rotaxane assembled using a discreet chloride anion template,[219] Beer and co-workers described the synthesis of the first XB [2]rotaxane *via* bromide anion templation (Figure 1.36 a).[131] The XB [2]rotaxane consists of an iodotriazolium functionalised axle, as well as a HB isophthalamide containing macrocycle (Figure 1.36 a).[131] A single-crystal X-ray structure determination further confirmed the rotaxane's concerted HB and XB binding mode of $Br^-$ (Figure 1.36 b).[131]

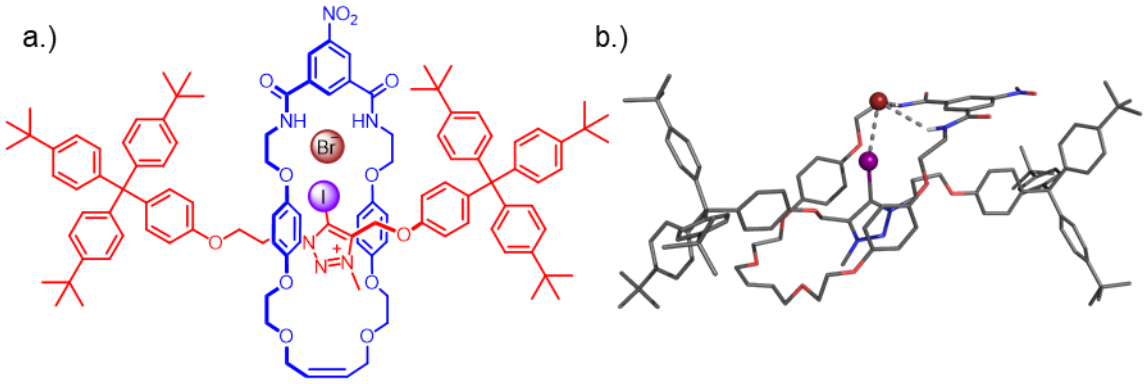



*Figure 1.36. Beer's anion templated XB MIM with a.) $Br^-$ templated [2]rotaxane and b.) single-crystal X-ray structure of Br binding [2]rotaxane (CSD: TACPUK) with XB and HB shown as grey dashes.*[131]

## 1.6 Interlocked Structures for Host-Guest Recognition

Nature's ability to utilise encapsulating three-dimensional protein-based cavities to achieve remarkable levels of selectivity, such as the sulfate and phosphate oxoanion selective proteins described in section 1.3.1,[92, 94] has influenced the employment of MIMs for host-guest recognition applications. Their cavities can be viewed as ideal three dimensional, preorganised coordination environments, which are shielded from the bulk environment.[185]

Roessler and Goldup described a series of [2]rotaxanes (Figure 1.37) synthesised *via* CuAAC AMT, with varying numbers of nitrogen-based donors present in the rotaxane cavity.[220] These tri-, tetra-, and pentadentate rotaxane-based ligands were studied as potential receptors for Co(II), Zn(II), Cu(II) and Ni(II) transition metal cations. Their investigations revealed a mechanical bond effect with the mechanical bond enhancing the binding strength of the metal-cation complexes in comparison to non-interlocked ligand controls.[220] Furthermore these rotaxane metal cation complexes exhibited unusual binding geometries, such as five-coordinate $Co^{2+}$ and $Ni^{2+}$ complexes for the pentadentate rotaxane (Figure 1.37 c) as confirmed by single-crystal XRD.[220] Electrochemical studies reveal that the stability and redox properties of the metal is altered when bound by the MIM in comparison to non-interlocked complexes. In the case of Ni(II) bound by the pentadentate rotaxane (Figure 1.37 c), electrochemical reduction to a stable Ni(I) complex was observed.[220] The pentacoordinate Co(II) rotaxane complex furthermore exhibits an unusual mixture of both high- and low spin states. Moreover, the tetradentate rotaxane (Figure 1.37 b) is an ideal ligand for the stabilisation of Cu(I) as confirmed by the high positive redox potential for the Cu(II)/Cu(I) redox couple.[220] Studies with analogous non-interlocked ligands reveal that these unique properties are only observed for the rotaxane-complexes.[220]

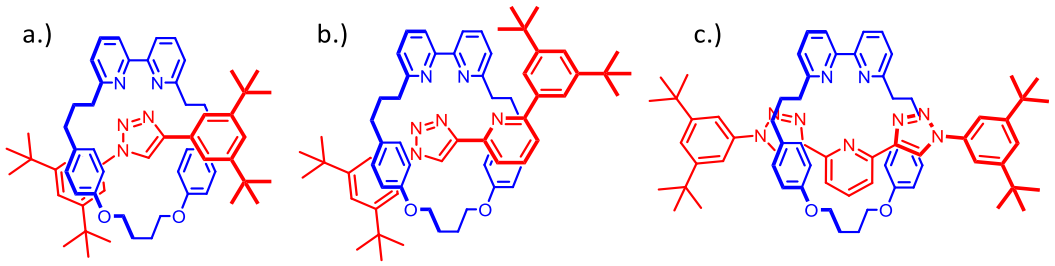



*Figure 1.37. Goldup and Roessler's [2]rotaxanes with a.) three, b.) four and c.) five nitrogen donors*

A [2]catenane (Figure 1.38) based on indolocarbazole ligands was reported by Jeong *et al.*[221] This MIM is capable of strong chloride anion recognition *via* four concerted hydrogen bonds within the central cavity of the interlocked structure.[221] $^1$H NMR as well as fluorescence anion titrations in acetone with 1% water, determined a stoichiometric 1:1 host:guest complex binding constant of 1.4 × $10^5$ $M^{-1}$ for $Cl^-$, impressively almost 20-fold greater than with the non-interlocked analogous macrocycle.[221] The catenane also bound $AcO^-$, $N_3^-$, $H_2PO_4^-$, $Br^-$ and $HSO_4^-$, anions more weakly, with no binding observed for $NO_3^-$ or $I^-$. These binding trends are in accordance with anion basicity as well as geometry.[221]

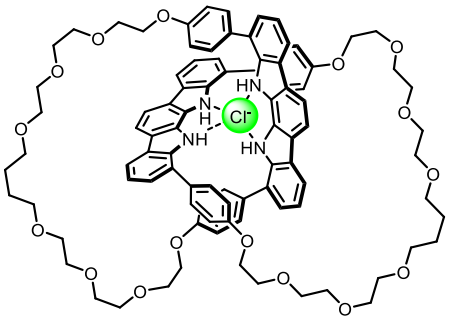



*Figure 1.38. Joeng's indolocarbazole-based [2]catenane capable of anion recognition*[221]

In more recent years, XB has been employed in the design of synthetic interlocked anion receptors to help increase the hydrophobic character of their cavities, as well as to create a more pre-organised binding site due to the σ-hole interaction's linear directionality in anion recognition.[62,222]

An all XB [2]catenane capable of selective chloride and bromide recognition and sensing was reported by Beer in 2012.[223]

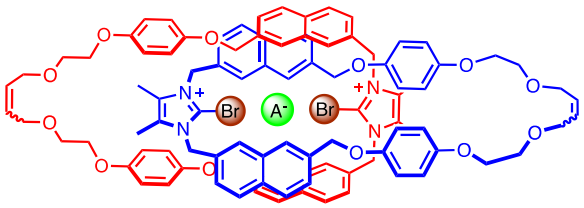



*Figure 1.39. Beer's all XB [2]catenane*[223]

The catenane, which contained two bromoimidazolium XB donor motifs, was prepared *via* bromide templation in 24% yield (Figure 1.39). Naphthalene spacer units incorporated into the MIM facilitated the determination of anion binding strength by fluorescence spectroscopy (Figure 1.39).[223] The macrocycle alone showed no significant binding for the anions tested, namely $F^-$, $Cl^-$, $Br^-$, $I^-$, $AcO^-$, $H_2PO_4^-$, $NO_3^-$ and $HCO_3^-$. However, the [2]catenane is capable of binding chloride and bromide in acetonitrile, with binding strengths of $3.71\times10^6$ $M^{-1}$ and $1.48\times10^5$ $M^{-1}$ respectively. These observations demonstrated that the mechanical bond was integral for the anion recognition and selectivity.[223]

Whereas in recent years XB receptors operating in organic media have become more common, water-soluble XB receptors remain rare.[224-226] A seminal report comparing HB and XB functionalised [2]rotaxane anion receptors in pure water was presented 2014 (Figure 1.40).[145] Water solubility was achieved by employing permethylated β-cyclodextrins as stopper units on the axle, which furthermore contained a bis-iodotriazole pyridinium XB donor motif. The XB [2]rotaxane selectively bound iodide with a binding constant of 2200 $M^{-1}$ in deuterated water solution, which is unusually high for such a low charged system in aqueous media.[145] The binding is drastically reduced for the all HB analogue, which binds even weaker than the acyclic XB axle alone. An analysis of the thermodynamic parameters reveals that the binding of iodide

by the XB functionalised rotaxane was enthalpically driven, contrasting the dominant entropic contribution observed for the all HB rotaxane.[145]

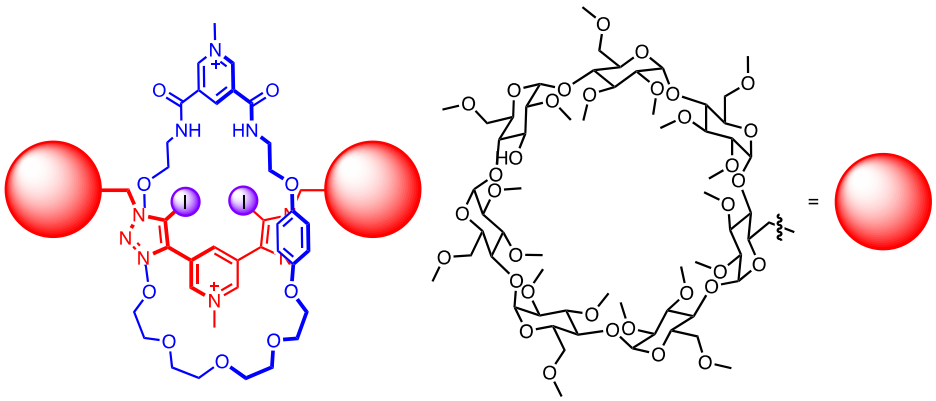


*Figure 1.40. Beer's water soluble XB [2]rotaxane capable of selective iodide recognition*[145]

The incorporation of ChB motifs into complex supramolecular structures is very rare, in part due to the weak C-Ch bond and resulting chemical instability of ChB receptors, especially those containing the heavier and more potent chalcogens, such as Te. The first report of MIMs containing ChB motifs was described in 2017 by Beer (Figure 1.10).[227] The neutral Te ChB rotaxane (Figure 1.41 a) displayed strong binding for sulfate in acetone, whereas the Se [2]rotaxane analogue showed considerably weaker ChB anion interactions in the same solvent and binding was too weak to be quantified. Methylation to form the tricationic Se [2]rotaxane (Figure 1.41 b) resulted in enhanced anion affinity compared to its neutral analogue when studied by $^{1}$H NMR in a 4:1 mixture of acetone and water.[227]

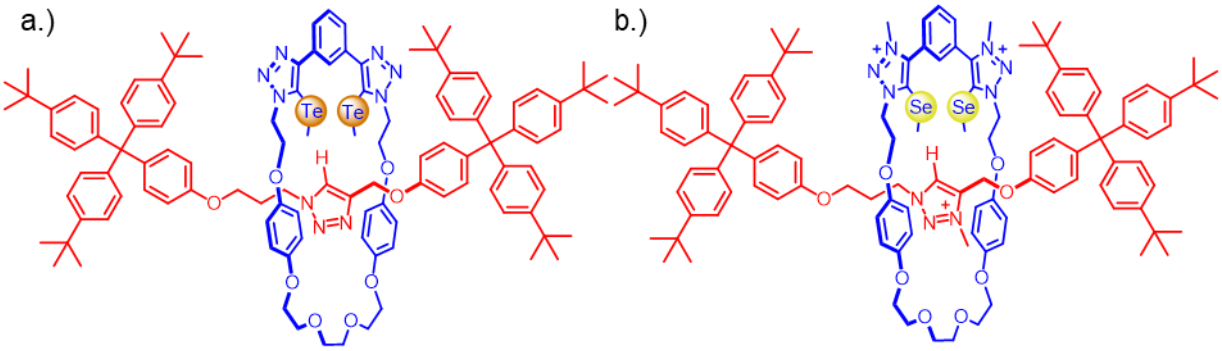
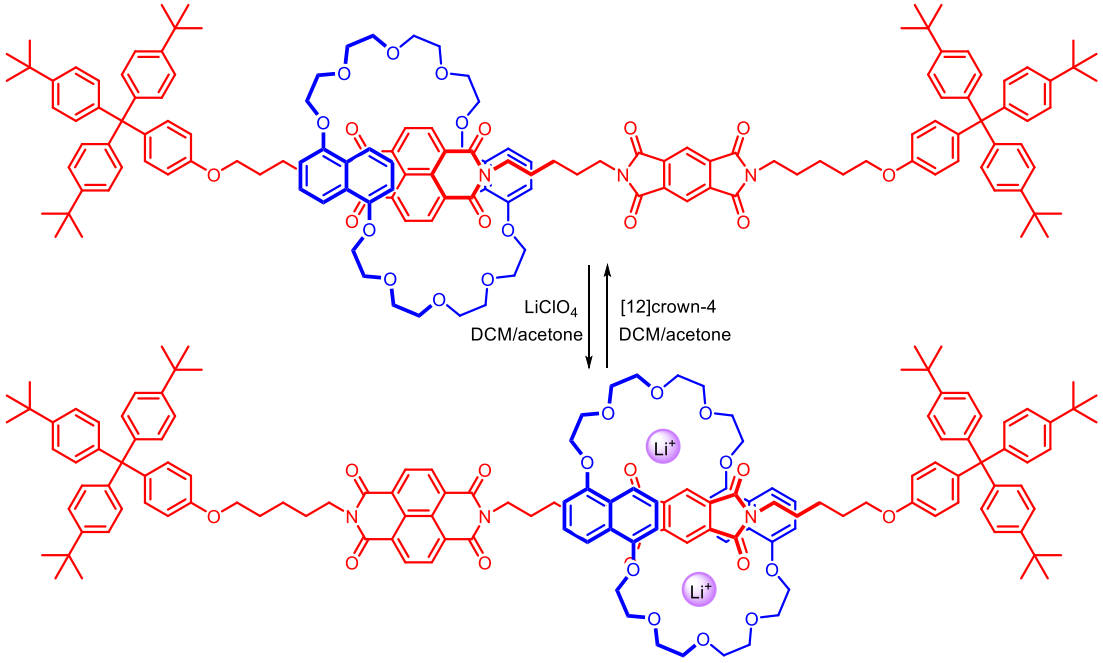



*Figure 1.41. Beer's a.) neutral Te and b.) triple cationic Se based [2]rotaxanes*[227]

Another aspect that has attracted considerable interest in interlocked systems is their inherent ability to undergo controlled molecular motion and potential to operate as synthetic molecular machines.[16, 17] Electrochemical,[228] light,[229] or chemical stimuli[230] can be used to control the position of one component with respect to another. Indeed, cation or anion recognition can also be used to induce motion within a MIM.[176, 177, 231]

Sanders and Stoddart reported a two station axle containing [2]rotaxane that upon lithium cation binding displayed switchable shuttling behaviour (Scheme 1.9).[232]

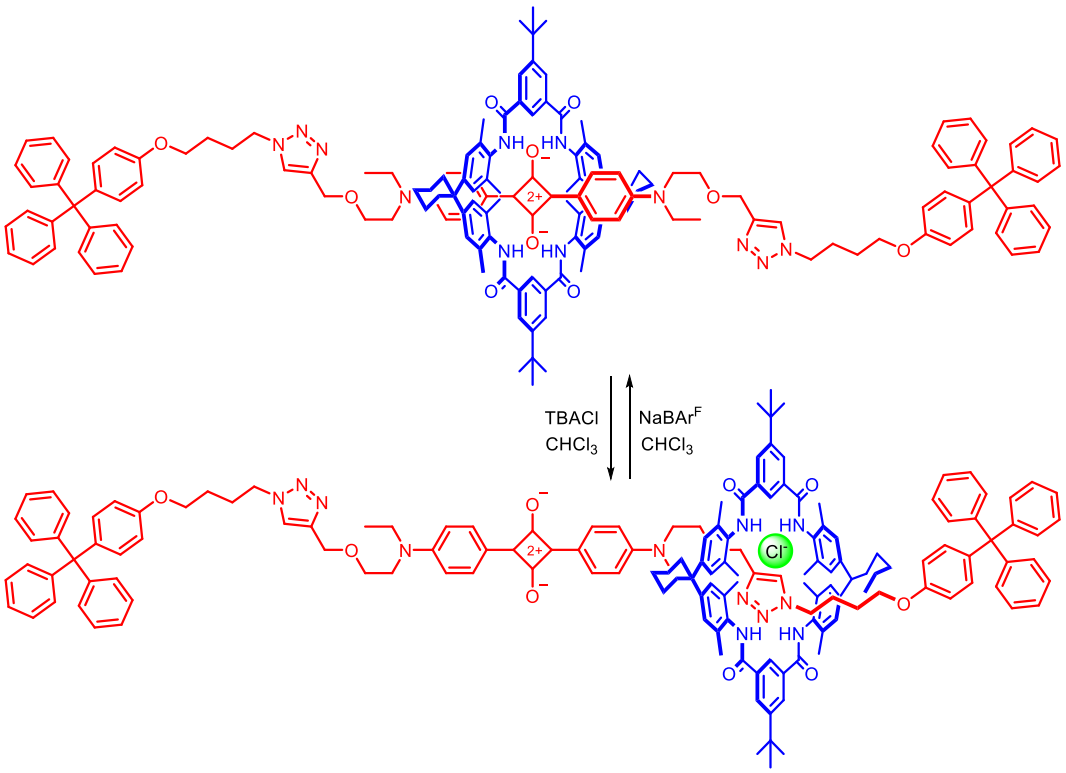



*Scheme 1.9. [2]Rotaxane based molecular switch with cation induced shuttling*[232]

The rotaxane's components consist of an axle integrated with naphthalenediimide (NDI) and pyromellitic diimide station sites and a 1,5-dinaphtho[38]crown-10 macrocycle. The macrocycle initially resides on the NDI station due to favourable aromatic π-π donor-acceptor interactions.[232] However, introduction of lithium cations caused a macrocycle translocation to the pyromellitic diimide site as confirmed by $^1$H NMR studies in a 4:1 $CD_2Cl_2$ to acetone-$d_6$ mixture.[232] The cation binding was determined to be a stoichiometric 1:2 host-guest binding, with $Li^+$ coordinating between the pyromellitic diimide site and the polyether oxygen donors of

the macrocycle as shown in Scheme 1.9.[232] The introduction of an excess of [12]crown-4 successfully removed the alkali cation from the MIM and resulted in the macrocycle translocating back to the NDI station. Furthermore, this shuttling behaviour can also be controlled *via* a one electron reduction of the NDI station, making this [2]rotaxane a dual cation- and redox-driven molecular shuttle.[232]

A functional squaraine [2]rotaxane capable of sensing chloride was reported by Smith *et al.* in 2010.[233] The tetralactam macrocycle resides on the central squaraine station (Scheme 1.10), causing the quenching of the deep-red fluorescence of the squaraine dye.




*Scheme 1.10. Smith's chloride sensing [2]rotaxane*[233]

$^1$H NMR and fluorescence titration studies revealed that introducing chloride to the MIM causes a binding event with a translocation of the macrocycle, which causes an increase in the fluorescence emission.[233] Chloride binding causes a three-fold increase in fluorescence, with acetate, dihydrogen phosphate and iodide all causing much smaller fluorescence enhancements

indicating that this is a chloride selective response. This process can be reversed by introducing $NaBAr^F$, which causes the precipitation of NaCl and the translocation of the macrocycle back to the squaraine station accompanied by a quenching of the fluorescence.[233]

## 1.7 Objectives

The overall theme of this research project is the incorporation of halogen bonding (XB) and pnictogen bonding (PnB) sigma(σ)-hole donor motifs into a variety of supramolecular host structural frameworks for investigating XB and PnB Lewis base recognition, as well as the stabilisation of reactive halonium species through macrocyclic ligands.

In **Chapter 2** the synthesis of a series of acyclic PnB tripodal Bi(III) and Sb(III) triaryl pnictogen anion receptors containing various electron withdrawing aryl substituents is described. Extensive $^1$H NMR binding investigations are undertaken to elucidate the strength and selectivity of PnB anion recognition as well as how this σ-hole interaction can be modulated. Furthermore, the chapter discusses the synthesis and study of more complex stibanotriazole-based receptors as well as a series of mixed PnB/HB donor Bi(III) and Sb(III) based tripods.

**Chapter 3** explores different synthetic routes towards the design and construction of a functional [1]rotaxane capable of anion recognition through halogen bonding. To that end, the synthesis of a series of XB functionalised lariat macrocycle precursors is described together with attempts to prepare the target [1]rotaxane interlocked structure *via* a range of anion and metal cation templating methods.

**Chapter 4** investigates halonium complexes and their stabilisation through macrocyclic bis-pyridine-based ligands. The solid-state structures of the bromonium complexes as well as their

parent Ag(I) and electronically related $d^{10}$ Au(I) complexes, determined by single-crystal X-ray diffraction, are discussed, and compared. In addition, $^{1}$H NMR data evaluating the stabilisation of the reactive bromonium species through a macrocyclic ligand is presented and serves as evidence for the presence of a macrocyclic effect for halonium guest species.

## 1.8 References


1. J.-M. Lehn, *Angewandte Chemie International Edition*, 1988, **27**, 89-112.

2. J.-M. Lehn, *Science*, 1985, **227**, 849-856.

3. J. F. Stoddart, *Annu. Rep. Prog. Chem., Sect. B: Org. Chem.*, 1988, **85**, 353-386.

4. D. J. Cram, *Angewandte Chemie International Edition*, 1986, **25**, 1039-1057.

5. K. Ariga, J. P. Hill, M. V. Lee, A. Vinu, R. Charvet and S. Acharya, *Science and Technology of Advanced Materials*, 2008, **9**, 014109.

6. J. Li, *Supramolecular chemistry of biomimetic systems*, Springer, Singapore, 2017.

7. A. Andrievsky, F. Ahuis, J. L. Sessler, F. Vögtle, D. Gudat and M. Moini, *Journal of the American Chemical Society*, 1998, **120**, 9712-9713.

8. P. D. Beer, T. A. Barendt and J. Y. C. Lim, *Supramolecular chemistry : fundamentals and applications*, Oxford University Press, Oxford, Second edn., 2022.

9. M. J. Webber and R. Langer, *Chemical Society Reviews*, 2017, **46**, 6600-6620.

10. S. Bernhard and M. W. Tibbitt, *Advanced Drug Delivery Reviews*, 2021, **171**, 240-256.

11. W. Feng, M. Jin, K. Yang, Y. Pei and Z. Pei, *Chemical Communications*, 2018, **54**, 13626-13640.

12. M. Teresa Albelda, J. C. Frías, E. García-España and H.-J. Schneider, *Chemical Society Reviews*, 2012, **41**, 3859.

13. B. O. Okesola and D. K. Smith, *Chemical Society Reviews*, 2016, **45**, 4226-4251.

14. E. R. Kay, D. A. Leigh and F. Zerbetto, *Angewandte Chemie International Edition*, 2007, **46**, 72-191.

15. J.-P. Sauvage, *Angewandte Chemie International Edition*, 2017, **56**, 11080-11093.

16. J. F. Stoddart, *Angewandte Chemie International Edition*, 2017, **56**, 11094-11125.

17. A. W. Heard and S. M. Goldup, *ACS Central Science*, 2020, **6**, 117-128.

18. J. W. Steed and J. L. Atwood, *Supramolecular chemistry*, Wiley, Chichester, UK, 2nd edn., 2009.

19. Y. Yang, W. Feng, J. Hu, S. Zou, R. Gao, K. Yamato, M. Kline, Z. Cai, Y. Gao, Y. Wang, Y. Li, Y. Yang, L. Yuan, X. C. Zeng and B. Gong, *Journal of the American Chemical Society*, 2011, **133**, 18590-18593.

20. Ł. Tabisz, Z. Rozwadowski, A. Katrusiak and B. Łęska, *Scientific Reports*, 2020, **10**.

21. E. Arunan, G. R. Desiraju, R. A. Klein, J. Sadlej, S. Scheiner, I. Alkorta, D. C. Clary, R. H. Crabtree, J. J. Dannenberg, P. Hobza, H. G. Kjaergaard, A. C. Legon, B. Mennucci and D. J. Nesbitt, *Pure and Applied Chemistry*, 2011, **83**, 1637-1641.

22. J. D. Bernal and R. H. Fowler, *The Journal of Chemical Physics*, 1933, **1**, 515-548.

23. H. R. Drew, R. M. Wing, T. Takano, C. Broka, S. Tanaka, K. Itakura and R. E. Dickerson, *Proceedings of the National Academy of Sciences*, 1981, **78**, 2179-2183.

24. B. Morosin, *Acta Crystallographica Section B Structural Crystallography and Crystal Chemistry*, 1970, **26**, 1635-1637.

25. L. J. Prins, D. N. Reinhoudt and P. Timmerman, *Angewandte Chemie International Edition*, 2001, **40**, 2382-2426.

26. P. W. Atkins and J. De Paula, *Atkins' Physical chemistry*, Oxford University Press, Oxford, Tenth edn., 2014.

27. X.-J. Wang, L.-C. Gui, Q.-L. Ni, Y.-F. Liao, X.-F. Jiang, L.-H. Tang, Z. Zhang and Q. Wu, *CrystEngComm*, 2008, **10**, 1003.

28. A. Frontera, D. Quiñonero and P. M. Deyà, *Wiley Interdisciplinary Reviews: Computational Molecular Science*, 2011, **1**, 440-459.

29. S. Grimme, *Angewandte Chemie International Edition*, 2008, **47**, 3430-3434.

30. M. O. Sinnokrot and C. D. Sherrill, *The Journal of Physical Chemistry A*, 2006, **110**, 10656-10668.

31. C. R. Martinez and B. L. Iverson, *Chemical Science*, 2012, **3**, 2191.

32. J. C. Ma and D. A. Dougherty, *Chemical Reviews*, 1997, **97**, 1303-1324.

33. S. Yamada, *Chemical Reviews*, 2018, **118**, 11353-11432.

34. A. J. Neel, M. J. Hilton, M. S. Sigman and F. D. Toste, *Nature*, 2017, **543**, 637-646.

35. P. Sarri, F. Venturi, F. Cuda and S. Roelens, *The Journal of Organic Chemistry*, 2004, **69**, 3654-3661.

36. R. E. Dawson, A. Hennig, D. P. Weimann, D. Emery, V. Ravikumar, J. Montenegro, T. Takeuchi, S. Gabutti, M. Mayor, J. Mareda, C. A. Schalley and S. Matile, *Nature Chemistry*, 2010, **2**, 533-538.

37. O. B. Berryman, A. C. Sather, B. P. Hay, J. S. Meisner and D. W. Johnson, *Journal of the American Chemical Society*, 2008, **130**, 10895-10897.

38. D. Quiñonero, C. Garau, C. Rotger, A. Frontera, P. Ballester, A. Costa and P. M. Deyà, *Angewandte Chemie International Edition*, 2002, **41**, 3389-3392.

39. L. M. Salonen, M. Ellermann and F. Diederich, *Angewandte Chemie International Edition*, 2011, **50**, 4808-4842.

40. O. B. Berryman, V. S. Bryantsev, D. P. Stay, D. W. Johnson and B. P. Hay, *Journal of the American Chemical Society*, 2007, **129**, 48-58.

41. M. Mascal, A. Armstrong and M. D. Bartberger, *Journal of the American Chemical Society*, 2002, **124**, 6274-6276.

42. S. Huber, *Halogen bonding in solution*, Wiley-VCH, Weinheim, 1st edn., 2020.

43. O. Hassel, *Science*, 1970, **170**, 497-502.

44. J. S. Murray, K. Paulsen and P. Politzer, *Proceedings of the Indian Academy of Sciences - Chemical Sciences*, 1994, **106**, 267-275.

45. T. Brinck, J. S. Murray and P. Politzer, *International Journal of Quantum Chemistry*, 1992, **44**, 57-64.

46. P. Politzer and J. S. Murray, *ChemPhysChem*, 2013, **14**, 278-294.

47. P. Politzer, P. Lane, M. C. Concha, Y. Ma and J. S. Murray, *Journal of Molecular Modeling*, 2007, **13**, 305-311.

48. E. V. Bartashevich and V. G. Tsirelson, *Russian Chemical Reviews*, 2014, **83**, 1181-1203.

49. J. S. Murray, P. Lane, T. Clark, K. E. Riley and P. Politzer, *Journal of Molecular Modeling*, 2012, **18**, 541-548.

50. J. Y. C. Lim and P. D. Beer, *Chem*, 2018, **4**, 731-783.

51. J. S. Murray, P. Lane and P. Politzer, *Journal of Molecular Modeling*, 2009, **15**, 723-729.

52. A. Bauzá and A. Frontera, *Angewandte Chemie International Edition*, 2015, **54**, 7340-7343.

53. P. Politzer and J. Murray, *Crystals*, 2017, **7**, 212.

54. A. Bauzá, T. J. Mooibroek and A. Frontera, *Angewandte Chemie International Edition*, 2013, **52**, 12317-12321.

55. M. S. Taylor, *Coordination Chemistry Reviews*, 2020, **413**, 213270.

56. A. C. Legon, *Physical Chemistry Chemical Physics*, 2017, **19**, 14884-14896.

57. M. D. Esrafili, S. Asadollahi and M. Vakili, *International Journal of Quantum Chemistry*, 2016, **116**, 1254-1260.

58. H. A. Bent, *Chemical Reviews*, 1968, **68**, 587-648.

59. N. L. Kilah, M. D. Wise and P. D. Beer, *Crystal Growth & Design*, 2011, **11**, 4565-4571.

60. P. Metrangolo and G. Resnati, *Crystal Growth & Design*, 2012, **12**, 5835-5838.

61. P. Metrangolo, H. Neukirch, T. Pilati and G. Resnati, *Accounts of Chemical Research*, 2005, **38**, 386-395.

62. T. M. Beale, M. G. Chudzinski, M. G. Sarwar and M. S. Taylor, *Chemical Society Reviews*, 2013, **42**, 1667-1680.

63. M. Erdélyi, *Chemical Society Reviews*, 2012, **41**, 3547.

64. O. Dumele, D. Wu, N. Trapp, N. Goroff and F. Diederich, *Organic Letters*, 2014, **16**, 4722-4725.

65. C. Laurence, M. Queignec-Cabanetos, T. Dziembowska, R. Queignec and B. Wojtkowiak, *Journal of the American Chemical Society*, 1981, **103**, 2567-2573.

66. M. G. Sarwar, B. Dragisic, L. J. Salsberg, C. Gouliaras and M. S. Taylor, *Journal of the American Chemical Society*, 2010, **132**, 1646-1653.

67. R. Puttreddy, J. M. Rautiainen, T. Mäkelä and K. Rissanen, *Angewandte Chemie International Edition*, 2019, **58**, 18610-18618.

68. R. Cabot and C. A. Hunter, *Chemical Communications*, 2009, 2005-2007.

69. S. H. Jungbauer, D. Bulfield, F. Kniep, C. W. Lehmann, E. Herdtweck and S. M. Huber, *Journal of the American Chemical Society*, 2014, **136**, 16740-16743.

70. R. Hein, A. Docker, J. J. Davis and P. D. Beer, *Journal of the American Chemical Society*, 2022, **144**, 8827-8836.

71. A. Docker, I. Marques, H. Kuhn, Z. Zhang, V. Felix and P. D. Beer, *Journal of the American Chemical Society*, 2022, **144**, 14778-14789.

72. M. A. A. Ibrahim and E. M. Z. Telb, *ACS Omega*, 2020, **5**, 21631-21640.

73. F. De Vleeschouwer, M. Denayer, B. Pinter, P. Geerlings and F. De Proft, *Journal of Computational Chemistry*, 2018, **39**, 557-572.

74. T. Chivers and R. S. Laitinen, *Chemical Society Reviews*, 2015, **44**, 1725-1739.

75. K. T. Mahmudov, M. N. Kopylovich, M. F. C. Guedes Da Silva and A. J. L. Pombeiro, *Dalton Transactions*, 2017, **46**, 10121-10138.

76. L. J. Riwar, N. Trapp, K. Root, R. Zenobi and F. Diederich, *Angewandte Chemie International Edition*, 2018, **57**, 17259-17264.

77. S. Scheiner, *Accounts of Chemical Research*, 2013, **46**, 280-288.

78. A. Bauzá, T. J. Mooibroek and A. Frontera, *ChemPhysChem*, 2015, **16**, 2496-2517.

79. H. J. Trubenstein, S. Moaven, M. Vega, D. K. Unruh and A. F. Cozzolino, *New Journal of Chemistry*, 2019, **43**, 14305-14312.

80. K. T. Mahmudov, A. V. Gurbanov, V. A. Aliyeva, G. Resnati and A. J. L. Pombeiro, *Coordination Chemistry Reviews*, 2020, **418**, 213381.

81. M. Yang, D. Tofan, C. H. Chen, K. M. Jack and F. P. Gabbaï, *Angewandte Chemie International Edition*, 2018, **57**, 13868-13872.

82. S. Benz, A. I. Poblador-Bahamonde, N. Low-Ders and S. Matile, *Angewandte Chemie International Edition*, 2018, **57**, 5408-5412.

83. S. Moaven, J. Yu, J. Yasin, D. K. Unruh and A. F. Cozzolino, *Inorganic Chemistry*, 2017, **56**, 8372-8380.

84. S. Moaven, M. C. Andrews, T. J. Polaske, B. M. Karl, D. K. Unruh, E. Bosch, N. P. Bowling and A. F. Cozzolino, *Inorganic Chemistry*, 2019, **58**, 16227-16235.

85. D. Tofan and F. P. Gabbaï, *Chemical Science*, 2016, **7**, 6768-6778.

86. A. Gini, M. Paraja, B. Galmés, C. Besnard, A. I. Poblador-Bahamonde, N. Sakai, A. Frontera and S. Matile, *Chemical Science*, 2020, **11**, 7086-7091.

87. M. Paraja, A. Gini, N. Sakai and S. Matile, *Chemistry – A European Journal*, 2020, **26**, 15471-15476.

88. J. Zhang, J. Wei, W.-Y. Ding, S. Li, S.-H. Xiang and B. Tan, *Journal of the American Chemical Society*, 2021, **143**, 6382-6387.

89. J. L. Sessler, P. A. Gale and W.-S. Cho, *Anion receptor chemistry*, Royal Society of Chemistry, Cambridge, 2006.

90. Philip A. Gale, Ethan N. W. Howe and X. Wu, *Chem*, 2016, **1**, 351-422.

91. L. Chen, S. N. Berry, X. Wu, E. N. W. Howe and P. A. Gale, *Chem*, 2020, **6**, 61-141.

92. J. W. Pflugrath and F. A. Quiocho, *Nature*, 1985, **314**, 257-260.

93. J. J. He and F. A. Quiocho, *Protein Science*, 1993, **2**, 1643-1647.

94. H. Luecke and F. A. Quiocho, *Nature*, 1990, **347**, 402-406.

95. Z. Wang, A. Choudhary, P. S. Ledvina and F. A. Quiocho, *Journal of Biological Chemistry*, 1994, **269**, 25091-25094.

96. R. D. Shannon, *Acta Crystallographica Section A*, 1976, **32**, 751-767.

97. M. T. Albelda, M. A. Bernardo, E. Garcia-España, M. L. Godino-Salido, S. V. Luis, M. J. Melo, F. Pina and C. Soriano, *Journal of the Chemical Society, Perkin Transactions 2*, 1999, 2545-2549.

98. C. Caltagirone, G. W. Bates, P. A. Gale and M. E. Light, *Chemical Communications*, 2008, 61-63.

99. C. H. Park and H. E. Simmons, *Journal of the American Chemical Society*, 1968, **90**, 2431-2432.

100. B. Dietrich, M. W. Hosseini, J. M. Lehn and R. B. Sessions, *Journal of the American Chemical Society*, 1981, **103**, 1282-1283.

101. F. P. Schmidtchen, *Angewandte Chemie International Edition*, 1977, **16**, 720-721.

102. M. Boiocchi, L. Del Boca, D. E. Gómez, L. Fabbrizzi, M. Licchelli and E. Monzani, *Journal of the American Chemical Society*, 2004, **126**, 16507-16514.

103. P. A. Gale, J. L. Sessler, V. Král and V. Lynch, *Journal of the American Chemical Society*, 1996, **118**, 5140-5141.

104. Y. Li and A. H. Flood, *Angewandte Chemie International Edition*, 2008, **47**, 2649-2652.

105. A. Docker, C. H. Guthrie, H. Kuhn and P. D. Beer, *Angewandte Chemie International Edition*, 2021, **60**, 21973-21978.

106. B. Dietrich, J. Guilhem, J.-M. Lehn, C. Pascard and E. Sonveaux, *Helvetica Chimica Acta*, 1984, **67**, 91-104.

107. P. Blondeau, M. Segura, R. Pérez-Fernández and J. De Mendoza, *Chemical Society Reviews*, 2007, **36**, 198-210.

108. B. Dietrich, D. L. Fyles, T. M. Fyles and J.-M. Lehn, *Helvetica Chimica Acta*, 1979, **62**, 2763-2787.

109. B. Dietrich, T. M. Fyles, J.-M. Lehn, L. G. Pease and D. L. Fyles, *Journal of the Chemical Society, Chemical Communications*, 1978, 934.

110. R. P. Dixon, S. J. Geib and A. D. Hamilton, *Journal of the American Chemical Society*, 1992, **114**, 365-366.

111. R. Gross, G. Dürner and M. W. Göbel, *Liebigs Annalen der Chemie*, 1994, **1994**, 49-58.

112. M. C. Grossel, D. A. S. Merckel and M. G. Hutchings, *CrystEngComm*, 2003, **5**, 77-81.

113. M. G. Hutchings, M. C. Grossel, D. A. S. Merckel, A. M. Chippendale, M. Kenworthy and G. McGeorge, *Crystal Growth & Design*, 2001, **1**, 339-342.

114. U. Scheffer, A. Strick, V. Ludwig, S. Peter, E. Kalden and M. W. Göbel, *Journal of the American Chemical Society*, 2005, **127**, 2211-2217.

115. H. H. Zepik and S. A. Benner, *The Journal of Organic Chemistry*, 1999, **64**, 8080-8083.

116. V. Jubian, A. Veronese, R. P. Dixon and A. D. Hamilton, *Angewandte Chemie International Edition*, 1995, **34**, 1237-1239.

117. V. Jubian, R. P. Dixon and A. D. Hamilton, *Journal of the American Chemical Society*, 1992, **114**, 1120-1121.

118. M. A. Hossain and K. Ichikawa, *Tetrahedron Letters*, 1994, **35**, 8393-8396.

119. K. Ichikawa and M. A. Hossain, *Chemical Communications*, 1996, 1721.

120. J. Cai and J. L. Sessler, *Chemical Society Reviews*, 2014, **43**, 6198-6213.

121. K. Chellappan, N. J. Singh, I.-C. Hwang, J. W. Lee and K. S. Kim, *Angewandte Chemie International Edition*, 2005, **44**, 2899-2903.

122. P. D. Beer and P. A. Gale, *Angewandte Chemie International Edition*, 2001, **40**, 486-516.

123. K. Kavallieratos, S. R. De Gala, D. J. Austin and R. H. Crabtree, *Journal of the American Chemical Society*, 1997, **119**, 2325-2326.

124. S. J. Brooks, P. A. Gale and M. E. Light, *Chemical Communications*, 2005, 4696.

125. V. Amendola, M. Boiocchi, B. Colasson and L. Fabbrizzi, *Inorganic Chemistry*, 2006, **45**, 6138-6147.

126. P. Anzenbacher, A. C. Try, H. Miyaji, K. Jursíková, V. M. Lynch, M. Marquez and J. L. Sessler, *Journal of the American Chemical Society*, 2000, **122**, 10268-10272.

127. J. L. Sessler, J. Pavel Anzenbacher, J. A. Shriver, K. Jursíková, V. M. Lynch and M. Marquez, *Journal of the American Chemical Society*, 2000, **122**, 12061-12062.

128. R. M. Meudtner and S. Hecht, *Angewandte Chemie International Edition*, 2008, **47**, 4926-4930.

129. J. Lauko, P. H. J. Kouwer and A. E. Rowan, *Journal of Heterocyclic Chemistry*, 2017, **54**, 1677-1699.

130. H. Juwarker, J. M. Lenhardt, D. M. Pham and S. L. Craig, *Angewandte Chemie International Edition*, 2008, **47**, 3740-3743.

131. N. L. Kilah, M. D. Wise, C. J. Serpell, A. L. Thompson, N. G. White, K. E. Christensen and P. D. Beer, *Journal of the American Chemical Society*, 2010, **132**, 11893-11895.

132. A. Borissov, J. Y. C. Lim, A. Brown, K. E. Christensen, A. L. Thompson, M. D. Smith and P. D. Beer, *Chemical Communications*, 2017, **53**, 2483-2486.

133. R. Tepper, B. Schulze, M. Jäger, C. Friebe, D. H. Scharf, H. Görls and U. S. Schubert, *The Journal of Organic Chemistry*, 2015, **80**, 3139-3150.

134. H. Kuhn, A. Docker and P. D. Beer, *Chemistry – A European Journal*, 2022, **28**, e202201838.

135. Y. C. Tse, A. Docker, Z. Zhang and P. D. Beer, *Chemical Communications*, 2021, **57**, 4950-4953.

136. L. E. Bickerton, A. Docker, A. J. Sterling, H. Kuhn, F. Duarte, P. D. Beer and M. J. Langton, *Chemistry – A European Journal*, 2021, **27**, 11738-11745.

137. D. Mungalpara, S. Stegmüller and S. Kubik, *Chemical Communications*, 2017, **53**, 5095-5098.

138. M. G. Sarwar, B. Dragisic, S. Sagoo and M. S. Taylor, *Angewandte Chemie International Edition*, 2010, **49**, 1674-1677.

139. A. Brown and P. D. Beer, *Chemical Communications*, 2016, **52**, 8645-8658.

140. F. Ostler, D. G. Piekarski, T. Danelzik, M. S. Taylor and O. García Mancheño, *Chemistry – A European Journal*, 2021, **27**, 2315-2320.

141. D. N. Barsoum, N. Okashah, X. Zhang and L. Zhu, *The Journal of Organic Chemistry*, 2015, **80**, 9542-9551.

142. A. Borissov, I. Marques, J. Y. C. Lim, V. Félix, M. D. Smith and P. D. Beer, *Journal of the American Chemical Society*, 2019, **141**, 4119-4129.

143. C. J. Massena, N. B. Wageling, D. A. Decato, E. Martin Rodriguez, A. M. Rose and O. B. Berryman, *Angewandte Chemie International Edition*, 2016, **55**, 12398-12402.

144. S. Chakraborty, R. Dutta and P. Ghosh, *Chemical Communications*, 2015, **51**, 14793-14796.

145. M. J. Langton, S. W. Robinson, I. Marques, V. Félix and P. D. Beer, *Nature Chemistry*, 2014, **6**, 1039-1043.

146. N. B. Wageling, G. F. Neuhaus, A. M. Rose, D. A. Decato and O. B. Berryman, *Supramolecular Chemistry*, 2016, **28**, 665-672.

147. J. Y. C. Lim, T. Bunchuay and P. D. Beer, *Chemistry - A European Journal*, 2017, **23**, 4700-4707.

148. K. Rissanen, *CrystEngComm*, 2008, **10**, 1107.

149. A. Priimagi, G. Cavallo, P. Metrangolo and G. Resnati, *Accounts of Chemical Research*, 2013, **46**, 2686-2695.

150. L. Vogel, P. Wonner and S. M. Huber, *Angewandte Chemie International Edition*, 2019, **58**, 1880-1891.

151. H. Zhao and F. P. Gabbaï, *Nature Chemistry*, 2010, **2**, 984-990.

152. G. E. Garrett, E. I. Carrera, D. S. Seferos and M. S. Taylor, *Chemical Communications*, 2016, **52**, 9881-9884.

153. G. E. Garrett, G. L. Gibson, R. N. Straus, D. S. Seferos and M. S. Taylor, *Journal of the American Chemical Society*, 2015, **137**, 4126-4133.

154. S. Benz, M. Macchione, Q. Verolet, J. Mareda, N. Sakai and S. Matile, *Journal of the American Chemical Society*, 2016, **138**, 9093-9096.

155. P. Wonner, L. Vogel, M. Düser, L. Gomes, F. Kniep, B. Mallick, D. B. Werz and S. M. Huber, *Angewandte Chemie International Edition*, 2017, **56**, 12009-12012.

156. Y. Chen, L. Yao and X. Lin, *Computational and Theoretical Chemistry*, 2014, **1036**, 44-50.

157. S. Scheiner, *Chemistry - A European Journal*, 2016, **22**, 18850-18858.

158. S. Scheiner, *Faraday Discussions*, 2017, **203**, 213-226.

159. G. Müller, J. Brand and S. E. Jetter, *Zeitschrift für Naturforschung B*, 2001, **56**, 1163-1171.

160. J. Starbuck, N. C. Norman and A. Guy Orpen, *New Journal of Chemistry*, 1999, **23**, 969-972.

161. A. M. Christianson and F. P. Gabbaï, *Organometallics*, 2017, **36**, 3013-3015.

162. D. B. Amabilino and J. F. Stoddart, *Chemical Reviews*, 1995, **95**, 2725-2828.

163. C. J. Bruns and J. F. Stoddart, *The Nature of the Mechanical Bond : From Molecules to Machines*, John Wiley & Sons, Incorporated, New York, UNITED STATES, 2016.

164. E. Wasserman, *Journal of the American Chemical Society*, 1960, **82**, 4433-4434.

165. I. T. Harrison and S. Harrison, *Journal of the American Chemical Society*, 1967, **89**, 5723-5724.

166. G. Gil-Ramírez, D. A. Leigh and A. J. Stephens, *Angewandte Chemie International Edition*, 2015, **54**, 6110-6150.

167. G. Schill and A. Lüttringhaus, *Angewandte Chemie International Edition*, 1964, **3**, 546-547.

168. G. Schill and C. Zürcher, *Angewandte Chemie International Edition*, 1969, **8**, 988-988.

169. G. Schill, *Catenanes, rotaxanes, and knots*, Academic Press, New York, 1971.

170. C. O. Dietrich-Buchecker, J. P. Sauvage and J. M. Kern, *Journal of the American Chemical Society*, 1984, **106**, 3043-3045.

171. C. O. Dietrich-Buchecker, J. P. Sauvage and J. P. Kintzinger, *Tetrahedron Letters*, 1983, **24**, 5095-5098.

172. P. R. Ashton, T. T. Goodnow, A. E. Kaifer, M. V. Reddington, A. M. Z. Slawin, N. Spencer, J. F. Stoddart, C. Vicent and D. J. Williams, *Angewandte Chemie International Edition*, 1989, **28**, 1396-1399.

173. D. G. Hamilton, J. K. M. Sanders, J. E. Davies, W. Clegg and S. J. Teat, *Chemical Communications*, 1997, 897-898.

174. M. R. Sambrook, P. D. Beer, J. A. Wisner, R. L. Paul and A. R. Cowley, *Journal of the American Chemical Society*, 2004, **126**, 15364-15365.

175. M. S. Vickers and P. D. Beer, *Chemical Society Reviews*, 2007, **36**, 211-225.

176. T. A. Barendt, L. Ferreira, I. Marques, V. Félix and P. D. Beer, *Journal of the American Chemical Society*, 2017, **139**, 9026-9037.

177. T. A. Barendt, A. Docker, I. Marques, V. Félix and P. D. Beer, *Angewandte Chemie International Edition*, 2016, **55**, 11069-11076.

178. G. T. Spence and P. D. Beer, *Accounts of Chemical Research*, 2013, **46**, 571-586.

179. H. Ogino, *Journal of the American Chemical Society*, 1981, **103**, 1303-1304.

180. D. Armspach, P. R. Ashton, R. Ballardini, V. Balzani, A. Godi, C. P. Moore, L. Prodi, N. Spencer, J. F. Stoddart, M. S. Tolley, T. J. Wear, D. J. Williams and J. F. Stoddart, *Chemistry - A European Journal*, 1995, **1**, 33-55.

181. C. A. Hunter, *Journal of the American Chemical Society*, 1992, **114**, 5303-5311.

182. M. S. Deleuze, D. A. Leigh and F. Zerbetto, *Journal of the American Chemical Society*, 1999, **121**, 2364-2379.

183. C. Barnes Jonathan, C. Fahrenbach Albert, D. Cao, M. Dyar Scott, M. Frasconi, A. Giesener Marc, D. Benítez, E. Tkatchouk, O. Chernyashevskyy, H. Shin Weon, H. Li, S. Sampath, L. Stern Charlotte, A. Sarjeant Amy, J. Hartlieb Karel, Z. Liu, R. Carmieli, Y. Botros Youssry, W. Choi Jang, M. Z. Slawin Alexandra, B. Ketterson John, R. Wasielewski Michael, A. Goddard William and J. F. Stoddart, *Science*, 2013, **339**, 429-433.

184. A. Brown, K. M. Mennie, O. Mason, N. G. White and P. D. Beer, *Dalton Transactions*, 2017, **46**, 13376-13385.

185. A. Caballero, F. Zapata and P. D. Beer, *Coordination Chemistry Reviews*, 2013, **257**, 2434-2455.

186. M. J. Langton and P. D. Beer, *Accounts of Chemical Research*, 2014, **47**, 1935-1949.

187. A. R. Pease, J. O. Jeppesen, J. F. Stoddart, Y. Luo, C. P. Collier and J. R. Heath, *Accounts of Chemical Research*, 2001, **34**, 433-444.

188. Y.-L. Huang, W.-C. Hung, C.-C. Lai, Y.-H. Liu, S.-M. Peng and S.-H. Chiu, *Angewandte Chemie*, 2007, **119**, 6749-6753.

189. B. Champin, P. Mobian and J.-P. Sauvage, *Chemical Society Reviews*, 2007, **36**, 358-366.

190. V. Balzani, A. Credi, S. Silvi and M. Venturi, *Chemical Society Reviews*, 2006, **35**, 1135.

191. M. Cesario, C. O. Dietrich-Buchecker, J. Guilhem, C. Pascard and J. P. Sauvage, *Journal of the Chemical Society, Chemical Communications*, 1985, 244-247.

192. J. E. Beves, B. A. Blight, C. J. Campbell, D. A. Leigh and R. T. McBurney, *Angewandte Chemie International Edition*, 2011, **50**, 9260-9327.

193. A.-M. L. Fuller, D. A. Leigh, P. J. Lusby, A. M. Z. Slawin and D. B. Walker, *Journal of the American Chemical Society*, 2005, **127**, 12612-12619.

194. D. A. Leigh, P. J. Lusby, R. T. McBurney, A. Morelli, A. M. Z. Slawin, A. R. Thomson and D. B. Walker, *Journal of the American Chemical Society*, 2009, **131**, 3762-3771.

195. D. A. Leigh, P. J. Lusby, S. J. Teat, A. J. Wilson and J. K. Y. Wong, *Angewandte Chemie International Edition*, 2001, **40**, 1538-1543.

196. S. M. Goldup, D. A. Leigh, P. J. Lusby, R. T. McBurney and A. M. Z. Slawin, *Angewandte Chemie International Edition*, 2008, **47**, 6999-7003.

197. A.-M. Fuller, D. A. Leigh, P. J. Lusby, I. D. H. Oswald, S. Parsons and D. B. Walker, *Angewandte Chemie International Edition*, 2004, **43**, 3914-3918.

198. L. Hogg, D. A. Leigh, P. J. Lusby, A. Morelli, S. Parsons and J. K. Y. Wong, *Angewandte Chemie International Edition*, 2004, **43**, 1218-1221.

199. J. C. Chambron, V. Heitz and J. P. Sauvage, *Journal of the American Chemical Society*, 1993, **115**, 12378-12384.

200. P. Mobian, J.-M. Kern and J.-P. Sauvage, *Journal of the American Chemical Society*, 2003, **125**, 2016-2017.

201. V. Aucagne, K. D. Hänni, D. A. Leigh, P. J. Lusby and D. B. Walker, *Journal of the American Chemical Society*, 2006, **128**, 2186-2187.

202. J. D. Crowley, K. D. Hänni, A.-L. Lee and D. A. Leigh, *Journal of the American Chemical Society*, 2007, **129**, 12092-12093.

203. J. Berná, J. D. Crowley, S. M. Goldup, K. D. Hänni, A.-L. Lee and D. A. Leigh, *Angewandte Chemie International Edition*, 2007, **46**, 5709-5713.

204. J. D. Crowley, K. D. Hänni, D. A. Leigh and A. M. Z. Slawin, *Journal of the American Chemical Society*, 2010, **132**, 5309-5314.

205. J. D. Crowley, S. M. Goldup, N. D. Gowans, D. A. Leigh, V. E. Ronaldson and A. M. Z. Slawin, *Journal of the American Chemical Society*, 2010, **132**, 6243-6248.

206. J. J. Danon, D. A. Leigh, P. R. McGonigal, J. W. Ward and J. Wu, *Journal of the American Chemical Society*, 2016, **138**, 12643-12647.

207. S. M. Goldup, D. A. Leigh, R. T. McBurney, P. R. McGonigal and A. Plant, *Chemical Science*, 2010, **1**, 383.

208. M. Denis and S. M. Goldup, *Nature Reviews Chemistry*, 2017, **1**, 0061.

209. R. Barat, T. Legigan, I. Tranoy-Opalinski, B. Renoux, E. Péraudeau, J. Clarhaut, P. Poinot, A. E. Fernandes, V. Aucagne, D. A. Leigh and S. Papot, *Chemical Science*, 2015, **6**, 2608-2613.

210. P. E. Barran, H. L. Cole, S. M. Goldup, D. A. Leigh, P. R. McGonigal, M. D. Symes, J. Wu and M. Zengerle, *Angewandte Chemie International Edition*, 2011, **50**, 12280-12284.

211. H. M. Cheng, D. A. Leigh, F. Maffei, P. R. McGonigal, A. M. Z. Slawin and J. Wu, *Journal of the American Chemical Society*, 2011, **133**, 12298-12303.

212. S. M. Goldup, D. A. Leigh, P. R. McGonigal, V. E. Ronaldson and A. M. Z. Slawin, *Journal of the American Chemical Society*, 2010, **132**, 315-320.

213. R. J. Bordoli and S. M. Goldup, *Journal of the American Chemical Society*, 2014, **136**, 4817-4820.

214. M. J. Langton, Y. Xiong and P. D. Beer, *Chemistry - A European Journal*, 2015, **21**, 18910-18914.

215. X. Li, J. Y. C. Lim and P. D. Beer, *Chemistry - A European Journal*, 2018, **24**, 17788-17795.

216. J. Y. C. Lim, I. Marques, V. Félix and P. D. Beer, *Journal of the American Chemical Society*, 2017, **139**, 12228-12239.

217. G. M. Hübner, J. Gläser, C. Seel and F. Vögtle, *Angewandte Chemie International Edition*, 1999, **38**, 383-386.

218. S. Lee, C.-H. Chen and A. H. Flood, *Nature Chemistry*, 2013, **5**, 704-710.

219. J. A. Wisner, P. D. Beer, M. G. B. Drew and M. R. Sambrook, *Journal of the American Chemical Society*, 2002, **124**, 12469-12476.

220. M. Cirulli, A. Kaur, J. E. M. Lewis, Z. Zhang, J. A. Kitchen, S. M. Goldup and M. M. Roessler, *Journal of the American Chemical Society*, 2019, **141**, 879-889.

221. M. K. Chae, J.-m. Suk and K.-S. Jeong, *Tetrahedron Letters*, 2010, **51**, 4240-4242.

222. S. W. Robinson, C. L. Mustoe, N. G. White, A. Brown, A. L. Thompson, P. Kennepohl and P. D. Beer, *Journal of the American Chemical Society*, 2015, **137**, 499-507.

223. A. Caballero, F. Zapata, N. G. White, P. J. Costa, V. Félix and P. D. Beer, *Angewandte Chemie International Edition*, 2012, **51**, 1876-1880.

224. R. Tepper and U. S. Schubert, *Angewandte Chemie International Edition*, 2018, **57**, 6004-6016.

225. M. J. Langton, C. J. Serpell and P. D. Beer, *Angewandte Chemie International Edition*, 2016, **55**, 1974-1987.

226. E. J. Mitchell, A. J. Beecroft, J. Martin, S. Thompson, I. Marques, V. Félix and P. D. Beer, *Angewandte Chemie International Edition*, 2021, **60**, 24048-24053.

227. J. Y. C. Lim, I. Marques, A. L. Thompson, K. E. Christensen, V. Félix and P. D. Beer, *Journal of the American Chemical Society*, 2017, **139**, 3122-3133.

228. C. Cheng, P. R. McGonigal, S. T. Schneebeli, H. Li, N. A. Vermeulen, C. Ke and J. F. Stoddart, *Nature Nanotechnology*, 2015, **10**, 547-553.

229. A. M. Brouwer, C. Frochot, F. G. Gatti, D. A. Leigh, L. Mottier, F. Paolucci, S. Roffia and G. W. Wurpel, *Science*, 2001, **291**, 2124-2128.

230. M. Asakawa, P. R. Ashton, V. Balzani, A. Credi, C. Hamers, G. Mattersteig, M. Montalti, A. N. Shipway, N. Spencer, J. F. Stoddart, M. S. Tolley, M. Venturi, A. J. P. White and D. J. Williams, *Angewandte Chemie International Edition*, 1998, **37**, 333-337.

231. T. A. Barendt, I. Rašović, M. A. Lebedeva, G. A. Farrow, A. Auty, D. Chekulaev, I. V. Sazanovich, J. A. Weinstein, K. Porfyrakis and P. D. Beer, *Journal of the American Chemical Society*, 2018, **140**, 1924-1936.

232. S. A. Vignon, T. Jarrosson, T. Iijima, H.-R. Tseng, J. K. M. Sanders and J. F. Stoddart, *Journal of the American Chemical Society*, 2004, **126**, 9884-9885.

233. J. J. Gassensmith, S. Matthys, J.-J. Lee, A. Wojcik, P. V. Kamat and B. D. Smith, *Chemistry - A European Journal*, 2010, **16**, 2916-2921.

# 2 Anion Recognition with Sb(III) and Bi(III)-Based Pnictogen Bonding Receptors

## 2.1 Introduction

Pnictogen bonding (PnB), the attractive non-covalent interaction between an electrophilic region, or sigma (σ)-hole, of a group 15 element and a nucleophilic Lewis base, shares many characteristics of other σ-hole interactions.[1] Whilst widely acknowledged for many decades as a pervasive structural characteristic in solid-state inorganic chemistry,[2-5] the application of pnictogen centred Lewis acidity has only recently been realised in the solution phase, primarily for the application of catalysis[6-9]. However, in the context of anion recognition, the strategy of employing PnB in receptor host design is rare.

Pioneering examples by Matile and co-workers, have demonstrated impressive applications of PnB driven anion recognition for the purposes of halide abstraction catalysis and transmembrane anion transport.[7-10]

Their seminal 2018 report highlights the synthesis of a series of neutral PnB receptors appended with electron withdrawing perfluorophenyl substituents.[6] Quantitative $^{1}$H NMR halide anion titration analysis in THF-$d_8$ revealed that the PnB based receptor outperformed its ChB and XB analogues significantly.[6] As can be seen in Figure 2.1, the chloride binding potency of the Sb(III) receptors is greatly reduced when switching to the lighter PnB As, ChB Se and XB Br donors. However, the PnB>ChB>XB general trend of receptor potency is still being observed.[6] Furthermore, halide binding strength is shown to be greatly affected by the nature of the aryl substituent with the PnB donor potency being reduced greatly when the Sb(III) centre contains fewer electron withdrawing substituents (Figure 2.1).[6]

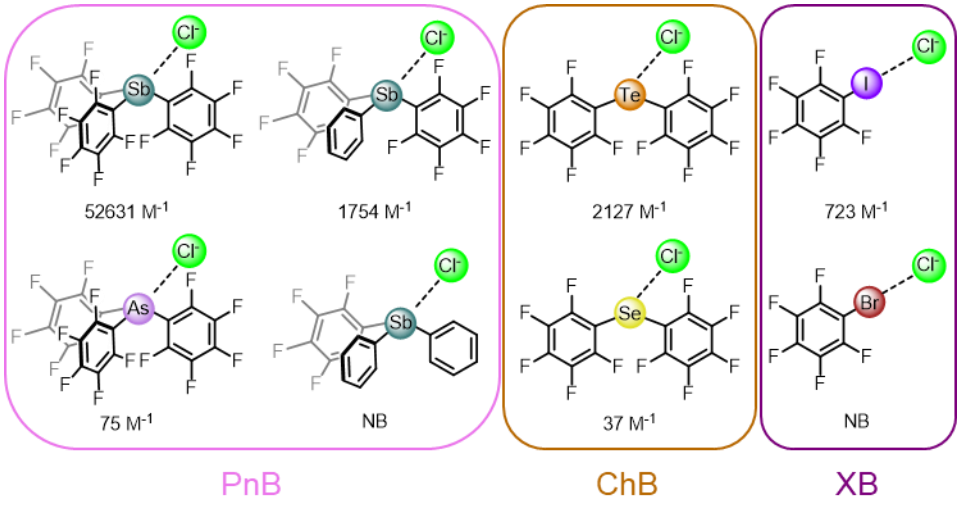



*Figure 2.1. Matile's σ-hole anion receptors. Chloride anion binding constants in THF-$d_8$ at 298 K as determined by $^{19}$F-NMR.[6]*

In a later report, the σ-hole receptors (Figure 2.1) were furthermore used as functional transmembrane chloride anion transporters.[10] When comparing the different σ-hole interactions, ChB based receptor bis(perfluorophenyl)tellane was shown to be the most active carrier, outperforming the chloride transport activity of the XB based carrier by three orders of magnitude.[10] The PnB based receptor tris(perfluorophenyl)stibine, which formed the strongest chloride anion complex as described above, unfortunately caused leakage during the experiment precluding an exact measurement of transport activity.[10]

Notwithstanding the promising examples presented above, surprisingly to date there have been no reports of systematic investigations to elucidate the electronic and structural factors which underpin anion recognition by PnB-based receptors.

In the context of ChB and XB mediated anion recognition, Beer and co-workers have recently undertaken such an investigation on a series of structurally homologous telluromethyl-, and iodo- functionalised 3,5-bis-triazole pyridine based receptors appended with either perfluorophenyl or phenyl substituents (Figure 2.2).[11] Extensive $^{1}$H NMR anion titration

experiments in acetone-$d_6$ solution, or acetone-$d_6$-$D_2O$ mixtures revealed that the ChB and XB receptors containing the highly electron withdrawing perfluorophenyl moieties exhibited remarkable enhancements in their halide binding potency with increased chloride binding potencies of over 30-fold and 8-fold respectively.[11] In stark contrast, the anion binding ability of the HB receptor, which consistently exhibited the weakest halide affinity relative to ChB and XB analogues, appeared unaffected with respect to perfluorophenyl incorporation.

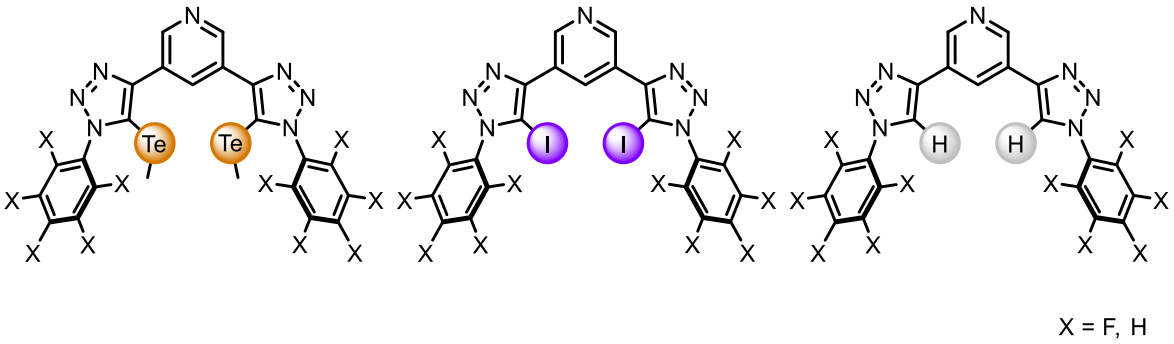



*Figure 2.2. ChB, XB and HB phenyl- and perfluorophenyl appended anion receptors*

## 2.2 Project Aims

The aim of this project is to investigate the electronic and structural factors which govern PnB mediated anion recognition. To achieve this, the first section of the chapter reports the synthesis of a library of triaryl Sb(III) and Bi(III) acyclic receptors, wherein systematic variation of appended electron withdrawing aryl substituents on anion binding strength and selectivity behaviour is investigated through quantitative $^1$H NMR titration studies. The second section describes the synthesis and characterisation of four novel tripodal Sb(III) and Bi(III) receptors containing a central PnB donor atom together with electron-deficient proto-triazole HB donors. The capabilities of these mixed PnB-HB receptors as chloride receptors are investigated and compared through $^1$H NMR anion titration studies. Finally, the third section details the synthesis of a range of receptors containing stibanotriazole units. Their characterisation is described together with preliminary $^1$H NMR chloride titration studies.

## 2.3 Triaryl Antimony(III) and Bismuth(III) Receptors

### 2.3.1 Synthesis

A series of antimony(III) and bismuth(III) triaryl compounds were synthesised with varying electron withdrawing substituents (Figure 2.3).

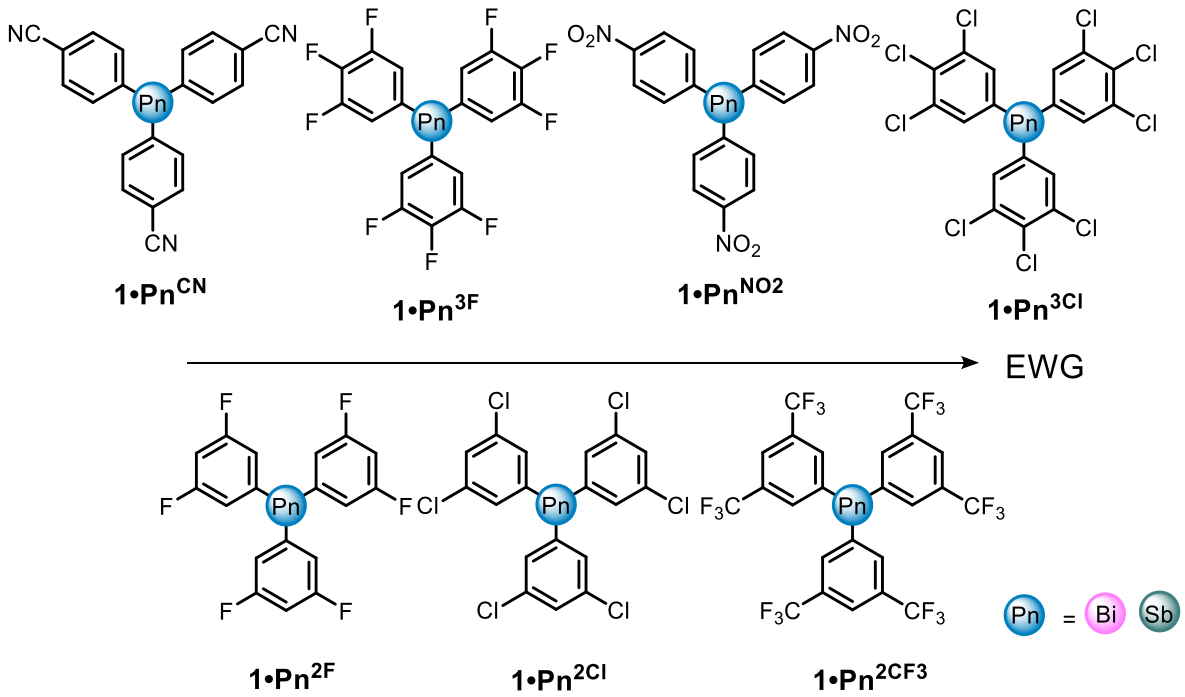
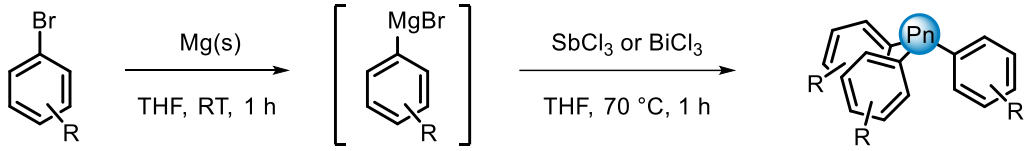



*Figure 2.3. Series of PnB Receptors with various electron withdrawing groups (EWG)*

The synthesis of the target Sb(III) and Bi(III) triaryl receptors containing electron-withdrawing chlorine- or fluorine-based substituents was achieved by the addition of the respective pnictogen trichloride to the appropriate aryl magnesium bromide Grignard reagent, formed *in situ* from the commercially available aryl bromide and freshly activated magnesium turnings in anhydrous THF. Purification by silica gel flash column chromatography afforded the target triaryl pnictogen receptors in variable yields (Scheme 2.1).

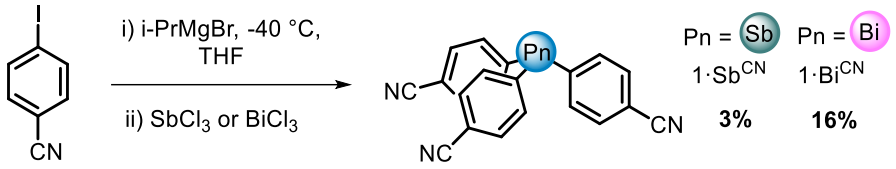



| | | Pn = Sb | | Pn = Bi | |
|---|---|---|---|---|---|
| R = | m-2F | 1·Sb$^{2F}$ | 59% | 1·Bi$^{2F}$ | 48% |
| | m-2Cl | 1·Sb$^{2Cl}$ | 17% | 1·Bi$^{2Cl}$ | 32% |
| | 3,4,5-trifluoro | 1·Sb$^{3F}$ | 19% | 1·Bi$^{3F}$ | 41% |
| | 3,4,5-trichloro | 1·Sb$^{3Cl}$ | 49% | 1·Bi$^{3Cl}$ | 32% |
| | m-2CF$_3$ | 1·Sb$^{2CF3}$ | 24% | 1·Bi$^{2CF3}$ | 35% |

*Scheme 2.1. Synthesis of PnB receptors via Grignard formation*

For the cyano- and nitro-aryl appended receptors, which are incompatible with the Grignard conditions described above, metal-halogen exchange reactions between the appropriately functionalised aryl iodide and phenyllithium or isopropylmagnesium bromide were used following literature procedures.[12, 13]

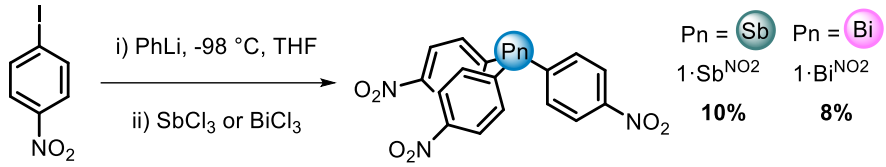
To prepare the cyano aryl appended receptors **1·Sb$^{CN}$** and **1·Bi$^{CN}$**, 4-iodobenzonitrile was treated with a 0.75 M isopropylmagnesium bromide THF solution at -40 °C before addition of the pnictogen trichloride salt to form the desired products (Scheme 2.2). TLC analysis and silica gel flash column chromatography revealed a very complex reaction profile; however, the desired products were successfully isolated albeit in low yields.




*Scheme 2.2. Synthesis of Receptors **1·Bi$^{CN}$** and **1·Sb$^{CN}$***

The corresponding nitro-aryl appended tripodal **1·Sb$^{NO2}$** and **1·Bi$^{NO2}$** receptors were formed from commercially available 4-iodonitrobenzene to which a 1.9 M phenyllithium solution in

THF was added dropwise over half an hour at -98 °C. The respective pnictogen trichloride salt was then added to the cooled mixture to form the final product, which was isolated in modest yields after column chromatographic purification (Scheme 2.3).




*Scheme 2.3. Synthesis of Receptors* ***1·Bi$^{NO2}$*** *and* ***1·Sb$^{NO2}$***

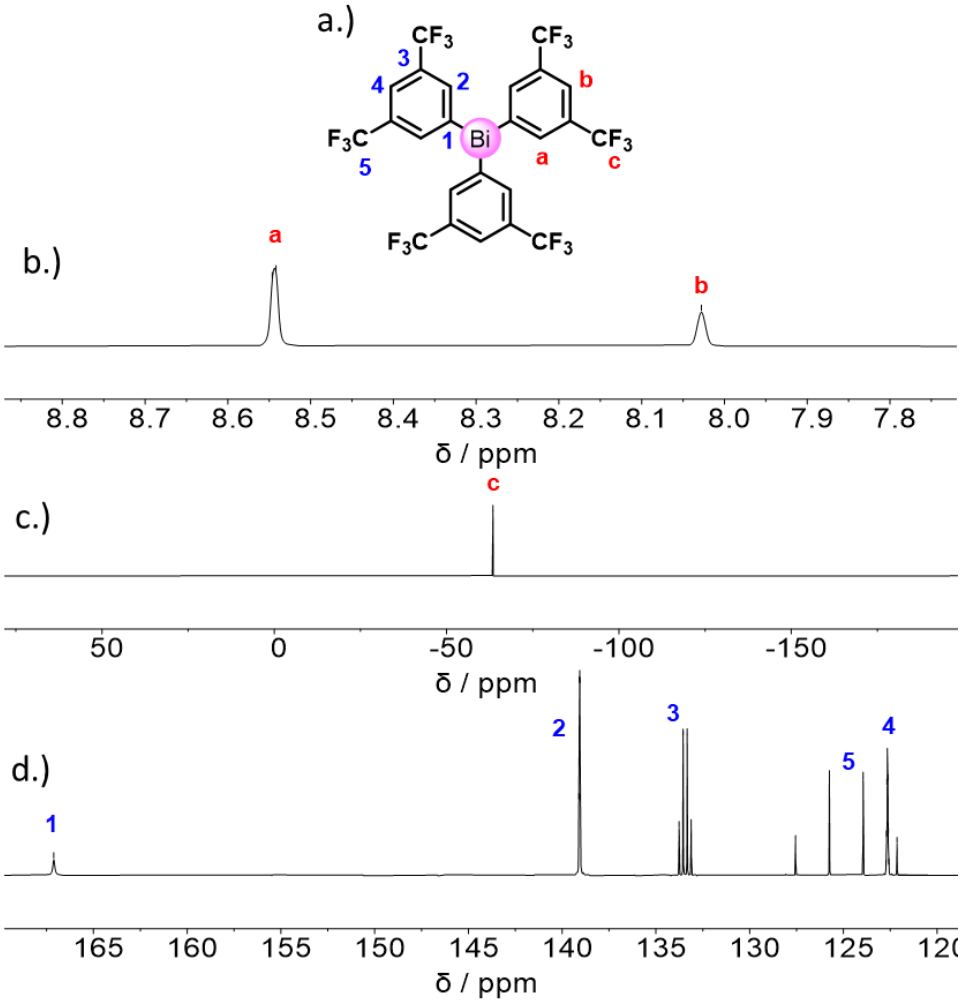



*Figure 2.4. a.) Chemical structure of* ***1·Bi$^{2CF3}$*** *b.) Truncated $^{1}$H NMR spectrum of* ***1·Bi$^{2CF3}$*** *(acetone-$d_6$, 600 mHz, 298K), c.) Truncated $^{19}$F NMR spectrum of* ***1·Bi$^{2CF3}$*** *(acetone-$d_6$, 377 mHz, 298K), d.) Truncated $^{13}$C NMR spectrum of* ***1·Bi$^{2CF3}$*** *(acetone-$d_6$, 151 mHz, 298K).*

All receptors were characterised by $^{1}H$ and $^{13}C$ NMR as well as $^{19}F$ NMR where appropriate. Representative NMR spectroscopic data for **1·Bi$^{2CF3}$** is shown in Figure 2.4.

### 2.3.2 Single-Crystal XRD Characterisation

Receptors **1·Sb$^{2Cl}$** and **1·Bi$^{2Cl}$** (Figure 2.5 a, d), **1·Sb$^{3Cl}$** and **1·Bi$^{3Cl}$** (Figure 2.5 b, e) and **1·Sb$^{2CF3}$** and **1·Bi$^{2CF3}$** (Figure 2.5 c, f) were also characterised by single crystal XRD. Crystals suitable for XRD structural analysis were grown from ethyl acetate and hexane mixtures. All single-crystal XRD data presented here was collected and refined by the author of this thesis.

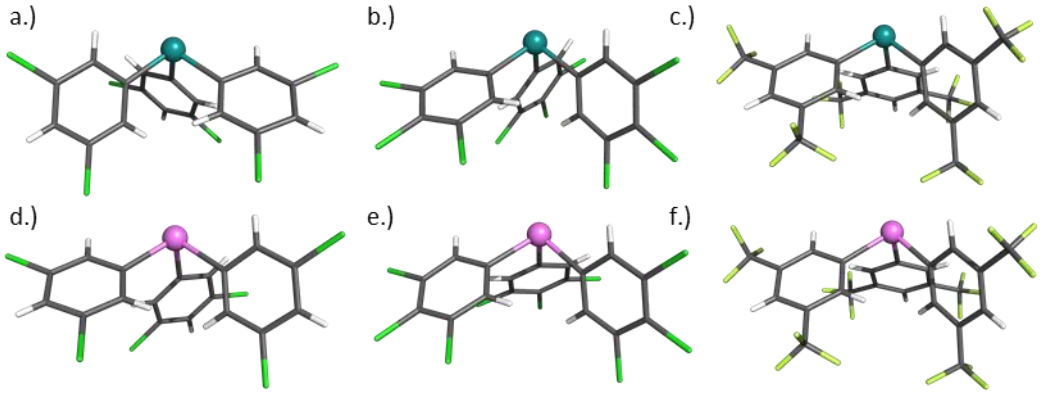



*Figure 2.5.Solid state structures of a.) **1·Sb$^{2Cl}$**, b.) **1·Sb$^{3Cl}$**, c.) **1·Sb$^{2F3I}$**, d.) **1·Bi$^{2Cl}$**, e.) **1·Bi$^{3Cl}$** and f.) **1·Bi$^{2CF3}$** with Grey = carbon, white = hydrogen, green = fluorine, dark green = chlorine, teal = antimony, pink = bismuth.*

The distances and angles around the Pn atom centres were calculated from the solid-state structures using PLATON and are summarised in Table 2.1. Sb-C bond distances within the Sb(III) receptors are on average 2.156 Å with average angles of 95.47°. The Bi-C bond distances are approximately 0.1 to 0.2 Å longer than their Sb analogues with an average Bi-C distance of 2.256 Å and a slightly smaller average bond angle of 94.12°. Importantly, the solid-state structures indicate structural homogeneity of the series with the various substituted aryl appendages not resulting in significant bond length or angle distortion. Hence this solid-state

observation ensures that the comparative anion binding properties of the tripodal PnB receptors reflects PnB donor potency.

*Table 2.1.Distances and angles around the Pn centre measured from the single-crystal XRD structures of* ***1·Sb$^{2Cl}$, 1·Sb$^{3Cl}$, 1·Sb$^{2F3I}$, 1·Bi$^{2Cl}$, 1·Bi$^{3Cl}$*** *and* ***1·Bi$^{2CF3}$***

| **R =** | **2Cl** | | **3Cl** | | **2CF$_3$** | |
|---|---|---|---|---|---|---|
| | **Distance (Å) Pn-C** | **Angle (°) C-Pn-C** | **Distance (Å) Pn-C** | **Angle (°) C-Pn-C** | **Distance (Å) Pn-C** | **Angle (°) C-Pn-C** |
| **Sb** | 2.152(2) | 92.46(8) | 2.150(2) | 93.54(8) | 2.1505(18) | 94.79(8) |
| | 2.153(2) | 95.80(9) | 2.158(2) | 94.42(8) | 2.157(2) | 96.02(7) |
| | 2.159(2) | 99.08(7) | 2.161(2) | 96.27(9) | 2.166(2) | 96.88(7) |
| **Bi** | 2.249(3) | 90.57(9) | 2.251(4) | 91.56(14) | 2.239(4) | 92.87(19) |
| | 2.255(3) | 93.97(9) | 2.264(4) | 93.99(14) | 2.250(6) | 94.97(17) |
| | 2.263(3) | 97.55(9) | 2.277(4) | 96.25(15) | 2.259(5) | 95.31(18) |

### 2.3.3 Anion Binding Studies of **1·Pn$^R$** Receptors

The anion recognition properties of the variously substituted triaryl PnB receptors were initially investigated by $^1$H-NMR titrations with TBACl in THF-$d_8$. In general, the addition of chloride induced significant aryl proton chemical shift perturbations of the respective receptor, typically with the largest changes observed in the protons *ortho* to the Pn centre (Figure 2.6 a). This observation is consistent with chloride anion recognition through PnB and possible aryl C-H HB at the Bi(III) and Sb(III) centres.

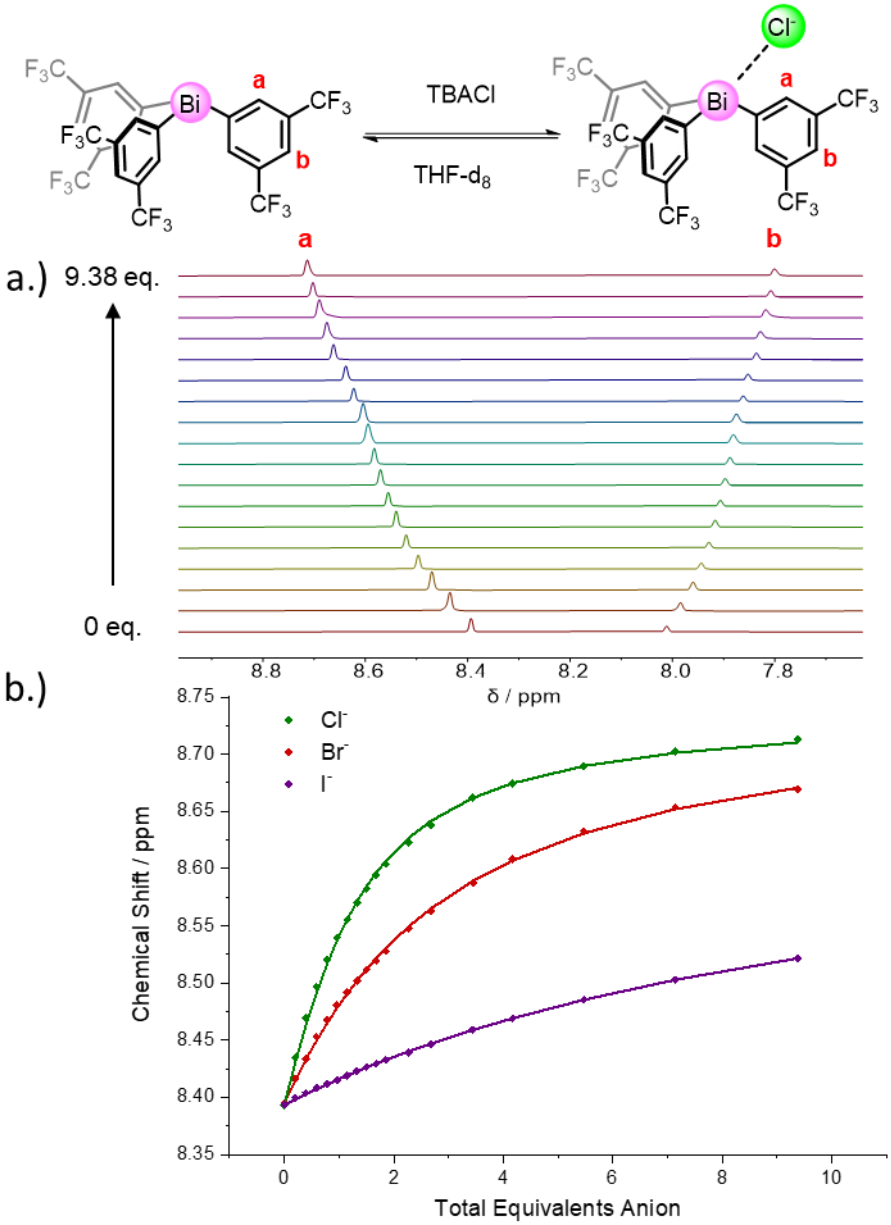



*Figure 2.6 a.) Stacked $^{1}$H-NMR TBACl titration and b.) binding isotherm for halide anions with dots representing experimental data and solid lines representing the fitted binding isotherm for* ***1·Bi$^{2CF3}$****. Solvent = THF-$d_8$. T = 298 K.*

For the determination of quantitative binding data, the chemical shift of the *ortho* aryl protons was monitored as a function of chloride anion concentration (Figure 2.6 b). BindFit analysis of the titration isotherms determined the 1:1 stoichiometric host-guest chloride association constants for the halide-receptor complexes, which are summarised in Table 2.2.[14-16]

*Table 2.2. Chloride anion association constants for Pn-receptors. $K_a(M^{-1})$ values calculated using BindFit software using a 1:1 stoichiometric host-guest binding model. Errors (±) are in parentheses. Solvent = THF-$d_8$. T = 298 K.*

| | **Chloride association constants for the PnB receptor series ($K_a$ / $M^{-1}$)** | | **Binding enhancement factor** | **Summed Hammett constant** |
|---|---|---|---|---|
| **R** | **1·Sb$^R$** | **1·Bi$^R$** | **$\alpha = (K_a^{Bi} / K_a^{Sb})$** | **Σσ** |
| **CN** | 36(2) | 76(1) | 2.1 ± 0.12 | 0.66 |
| **2F** | 61(2) | 152(2) | 2.5 ± 0.09 | 0.674 |
| **2Cl** | 52(1) | 213(1) | 4.0 ± 0.08 | 0.746 |
| **$NO_2$** | 94(2) | 227(3) | 2.4 ± 0.06 | 0.778 |
| **3F** | 253(3) | 580(7) | 2.3 ± 0.04 | 0.736 |
| **3Cl** | 341(6) | 716(8) | 2.1 ± 0.04 | 0.973 |
| **2$CF_3$** | 702(16) | 1300(43) | 1.8 ± 0.12 | 0.86 |

Several general trends can be observed for the binding constants determined (Table 2.2). Firstly, the bismuth receptors universally exhibit larger anion association constant ($K_a$) values than their antimony analogues, as anticipated based on the decreased electronegativity of bismuth relative to antimony and arguments originating from σ-hole polarisation being more pronounced in heavier elements. To provide a quantitative measure of this enhancement, a binding enhancement factor, $\alpha = (K_a^{Bi} / K_a^{Sb})$, was calculated.

Interestingly, inspection of the determined α values indicated a relatively constant α value of 2 (Table 2.2), the exception being the dichloro-substituted derivative. Whilst it is not immediately

clear as to the origin of this, tentatively it may arise from solution phase conformational changes, or potential C-H contributions to the overall anion binding process.

Furthermore, a clear influence of the nature of the substituent on the strength of anion binding can be observed, namely that an increasing value of the summed Hammett constants ($\Sigma\sigma$) for each aryl group, (*i.e.*, the larger $\Sigma\sigma$ value indicates the more electron-withdrawing aryl substituent) is generally accompanied by an increasing chloride $K_a$ value. This is rationalised by the electronic inductive activation of the pnictogen centre by the electron withdrawing functional groups. Whilst a linear correlation between the receptor's summed Hammett substituent constants ($\Sigma\sigma$) and log($K_a$) could not be established for either Sb or Bi, it is clear that electron withdrawing potency and chloride $K_a$ values are positively correlated. The strongest receptors for Sb and Bi respectively were those appended with two *meta*-trifluoromethyl aryl groups, namely **1·Sb$^{2CF3}$**, **1·Bi$^{2CF3}$**.

Choosing to further investigate the anion selectivity studies of these most potent triaryls **1·Sb$^{2CF3}$** and **1·Bi$^{2CF3}$** receptor systems, analogous $^1$H-NMR titrations in THF-$d_8$ were undertaken with the remaining halides and a range of oxoanions. Downfield perturbations in the shifts corresponding to the *ortho* protons accompanied by upfield shifts of the *para* protons were again observed (Figure 2.7 a). The isotherm binding titration data was analysed using BindFit (Figure 2.7 b) and the 1:1 stoichiometric host-guest anion association constants determined are summarised in Table 2.3.[14-16]

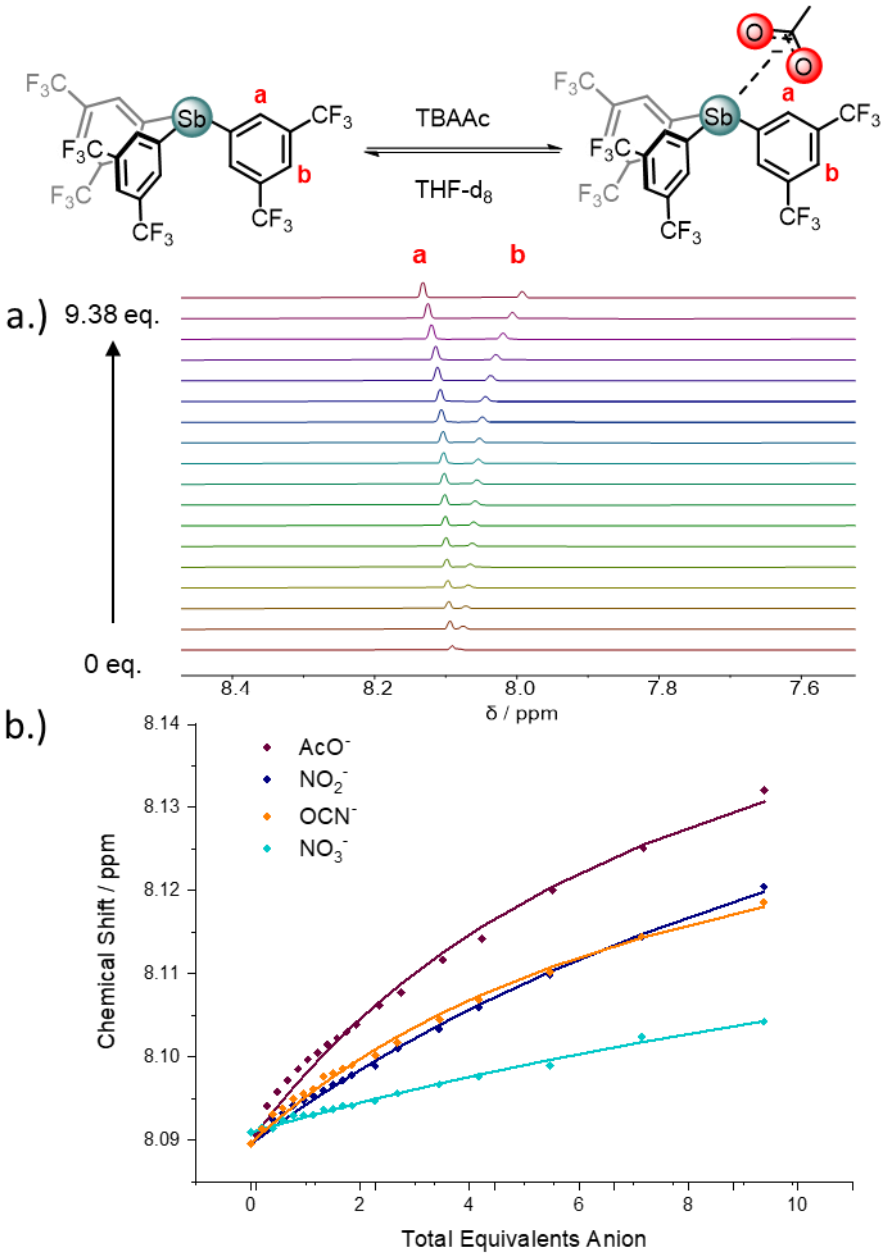



*Figure 2.7. a.) Stacked $^{1}$H-NMR TBA acetate titration and b.) binding isotherm for oxo-anions with dots representing experimental data and solid lines representing the fitted binding isotherm for* ***1·Sb$^{2CF3}$****. Solvent = THF-$d_8$. T = 298K.*

As was the case for chloride binding, the Bi-based anion receptor **1·Bi$^{2CF3}$** consistently displays stronger anion binding affinities than the Sb analogue **1·Sb$^{2CF3}$** for all anions investigated. Both **1·Sb$^{2CF3}$** and **1·Bi$^{2CF3}$** demonstrated a halide binding trend of $Cl^- > Br^- > I^-$ in accordance with halide charge densities and anion basicity (Table 2.3). The oxoanions studied showed a preference of $OCN^- > NO_2^- > NO_3^-$ for both **1·Sb$^{2CF3}$** and **1·Bi$^{2CF3}$**. However, comparisons of

acetate selectivity were compromised by the decomposition of **1·Bi$^{2CF3}$** upon the addition of TBAOAc, presumably reflective of the weaker Bi-C bond.

Interestingly, the selectivity behaviour of both **1·Sb$^{2CF3}$** and **1·Bi$^{2CF3}$** receptors does not follow anion basicity, with the binding of chloride remaining the strongest by far despite the lower basicity of the halide compared to the oxoanions investigated. This selectivity behaviour is in accordance with selectivity trends elucidated for some XB and ChB receptor systems but is not observed for traditional HB receptors.[11, 17, 18]

*Table 2.3. Anion association constants for Pn-receptors. $K_a(M^{-1})$ values calculated using BindFit software using a 1:1 stoichiometric host-guest binding model. All using TBA salts. Errors (±) are in parentheses. Solvent = THF-$d_8$. T = 298 K*

| | **Association constants for the PnB receptor series ($K_a$ / $M^{-1}$)** | | **p$K_a$** |
|---|---|---|---|
| **Anion** | **1·Sb$^{2CF3}$** | **1·Bi$^{2CF3}$** | |
| **Cl$^-$** | 702(16) | 1300(43) | -8.0 |
| **Br$^-$** | 207(3) | 432(8) | -9.0 |
| **I$^-$** | 147(4) | 192(2) | -10.0 |
| **AcO$^-$** | 268(15) | - | 4.8 |
| **OCN$^-$** | 263(11) | 344(12) | 3.9 |
| **NO$_2^-$** | 125(4) | 332(6) | 3.3 |
| **NO$_3^-$** | 79(3) | 124(4) | -1.3 |

### 2.3.4 Conclusions

The anion recognition studies of a series of acyclic triaryl Sb(III) and Bi(III) receptors has demonstrated that the anion binding potency of PnB receptors is dictated by the respective polarisabilty of the PnB donor with Bi consistently outperforming its Sb analogues. Moreover, anion binding strength is highly sensitive to the nature of the aryl substituents, with the electrophilicity of the PnB donor being notably increased through electron-withdrawing substituents. Furthermore, the PnB receptors have been shown to be chloride selective over more basic oxoanions. This selectivity profile is often seen in both ChB and XB σ-hole receptor systems but is in stark contrast to the selectivity trend commonly observed for HB based receptor systems, which follows anion basicity.

## 2.4 PnB-HB Tripodal Receptors

### 2.4.1 Synthesis of mixed PnB-HB Tripodal based Receptors

Having proven the ability to modulate the σ-hole PnB Lewis acidity of the Pn(III) centre electronically through inductive electron withdrawing aryl substituents, a novel receptor design was envisioned in which the incorporation of additional HB donors into the tripodal pnictogen atom scaffold would allow for the cooperative binding of anions through concerted HB and PnB interactions (Figure 2.8).

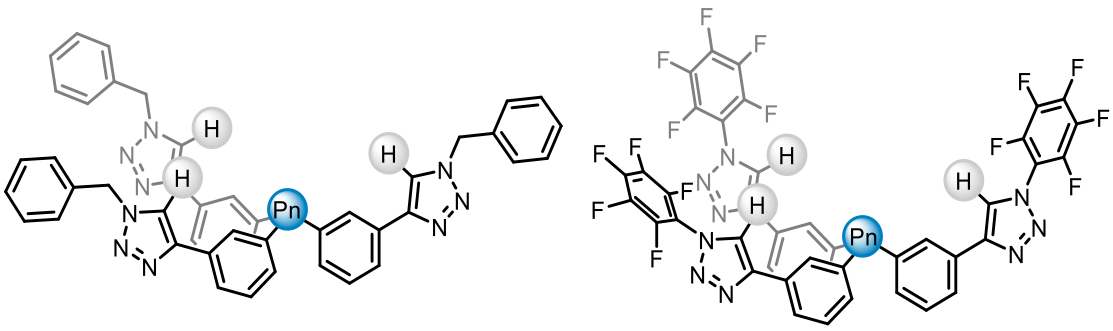
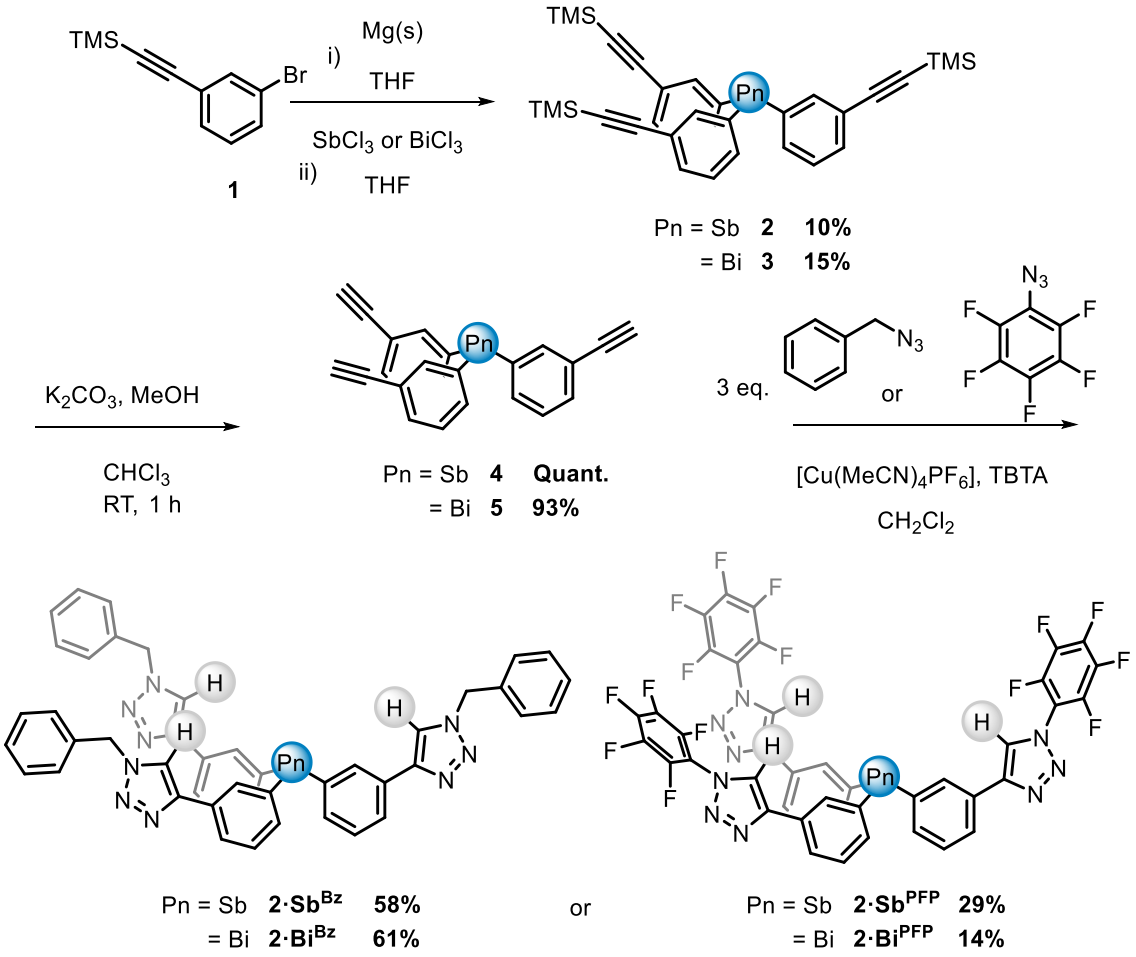



*Figure 2.8. Mixed HB and PnB receptor design*

To this end, the integration of proto-triazole groups into the receptor design surrounding the Lewis acidic pnictogen centre could be facilitated *via* a CuAAC click reaction using a tris-alkyne functionalised triaryl pnictogen scaffold.

The synthetic route undertaken for the formation of the target mixed PnB-HB receptors is shown in Scheme 2.4.




*Scheme 2.4.Formation of mixed HB-PnB tripodal anion receptors*

2-(3-Bromophenyl)ethynyltrimethylsilane **1** was prepared using a chemoselective Sonogashira reaction between commercially available 1-bromo-3-iodobenzene and TMS acetylene.[19] The Grignard reagent was then prepared *in situ* by the dropwise addition of the TMS protected alkyne **1** to a suspension of Mg turnings in either dry diethyl ether or dry THF. Once activated, a solution of either antimony(III)- or bismuth(III) trichloride was added to the Grignard

reagent. The corresponding TMS protected triaryl pnictogen alkynes **2** and **3** were then purified using silica gel flash column chromatography and characterised by $^{1}H$ and $^{13}C$ NMR before being subjected to TMS deprotection using mildly basic hydrolysis in the presence of $K_2CO_3$ to form **4** and **5** in excellent yields. The triaryl pnictogen alkynes **4** and **5** were then subjected to CuAAC click conditions using precomplexed $[Cu(MeCN)_4]PF_6$ and TBTA as the catalyst and 3.3 equivalents of either perfluorophenyl azide or benzyl azide. All products were purified using silica gel flash column chromatography.

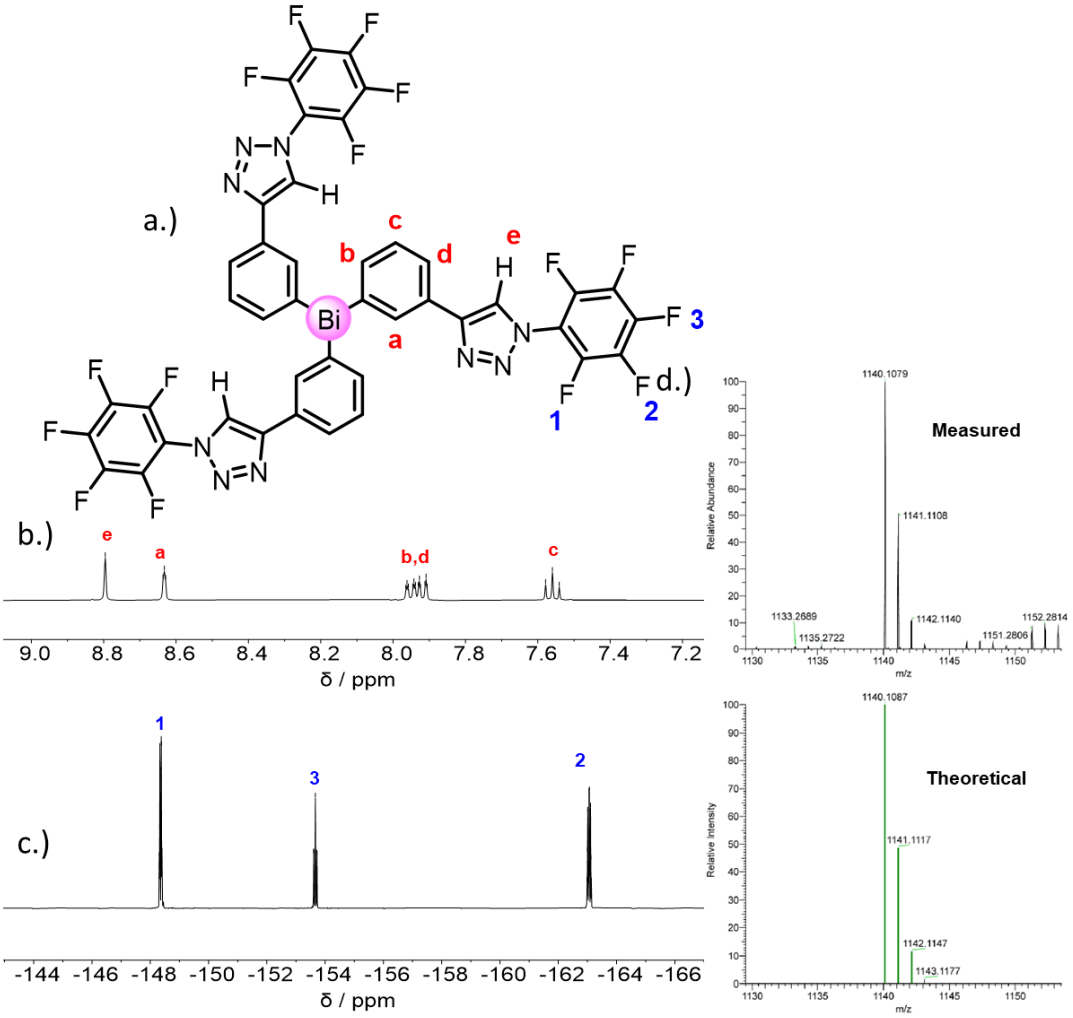



*Figure 2.9. a.) Chemical structure of* ***2·Bi$^{PFP}$*** *b.) Truncated $^{1}H$ NMR spectrum of* ***2·Bi$^{PFP}$*** *(acetone-$d_6$, 400 mHz, 298K), c.) Truncated $^{19}F$ NMR spectrum of* ***2·Bi$^{PFP}$*** *(acetone-$d_6$, 377 mHz, 298K), d.) theoretical (bottom) and measured (top) high resolution ESI spectra.*

The four novel tripodal receptors were fully characterised by $^{1}H$, $^{13}C$ NMR and $^{19}F$ NMR where appropriate, as well as high-resolution ESI-MS. Representative spectroscopic data is shown in Figure 2.9.

Furthermore, single crystals were obtained for both **2·Sb$^{PFP}$** and **2·Bi$^{PFP}$** receptors by slow evaporation from $CDCl_3$ and their solid-state structures elucidated using XRD (Figure 2.10). The distances and angles around the respective Pn centres determined from the solid-state structures are summarised in Table 2.4. The Sb-C bond distances within the Sb(III) receptor are on average 2.147 Å with an average angle of 96.90°. The Bi-C bond distances are once again longer than their Sb analogues by approximately 0.1 Å, with an average Bi-C distance of 2.263 Å and a comparative average bond angle of 96.47°.

*Table 2.4. Distances and angles around the Pn centre measured from the single-crystal XRD structures of **2·Sb$^{PFP}$** and **2·Bi$^{PFP}$***

| **R =** | **PFP** | |
|---|---|---|
| | **Distance (Å)**<br>**Pn-C** | **Angle (°)**<br>**C-Pn-C** |
| **Sb** | 2.139(6) | 96.5(2) |
| | 2.143(6) | 96.8(2) |
| | 2.159(7) | 97.4(2) |
| **Bi** | 2.251(4) | 94.42(15) |
| | 2.268(4) | 96.11(14) |
| | 2.269(4) | 98.89(14) |

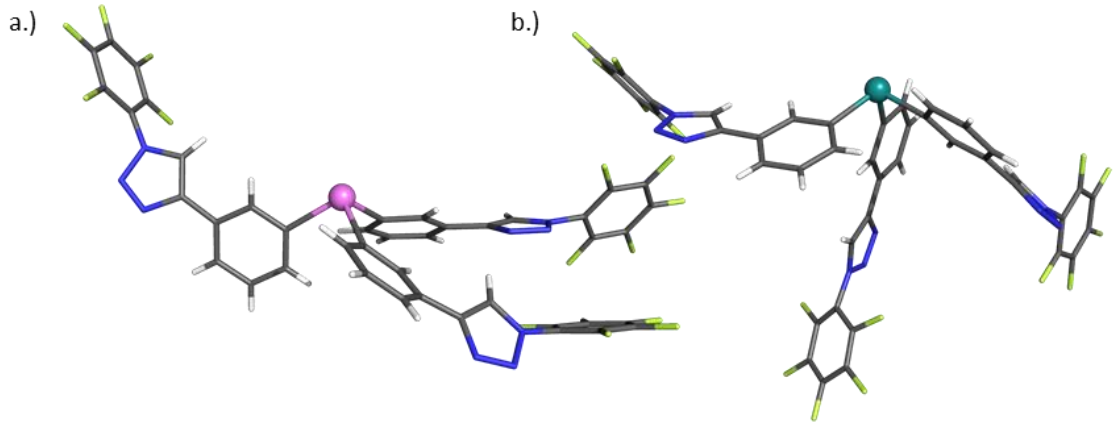



*Figure 2.10. Solid state structures of a.) bismuth(III) and b.) antimony(III) mixed HB-PnB tripods with Grey = carbon, white = hydrogen, green = fluorine, dark green = chlorine, teal = antimony, pink = bismuth*

### 2.4.2 Anion Binding Studies of **2·Pn$^R$** Receptors

The anion binding abilities of all four tripodal receptors were studied using $^1$H-NMR titrations with TBACl in THF-$d_8$. Upon addition of the TBACl salt, significant respective receptor chemical shift perturbations of both the triaryl framework and the triazole protons were observed, indicating that the halide binding mode included both HB and PnB interactions (Figure 2.11).

For all four receptors the triazole protons notably moved downfield and their chemical shifts were monitored as a function of halide anion concentration. BindFit analysis of the titration isotherms (Figure 2.11) determined the 1:1 stoichiometric host-guest chloride association constant values which are summarised in Table 2.5.[14-16]

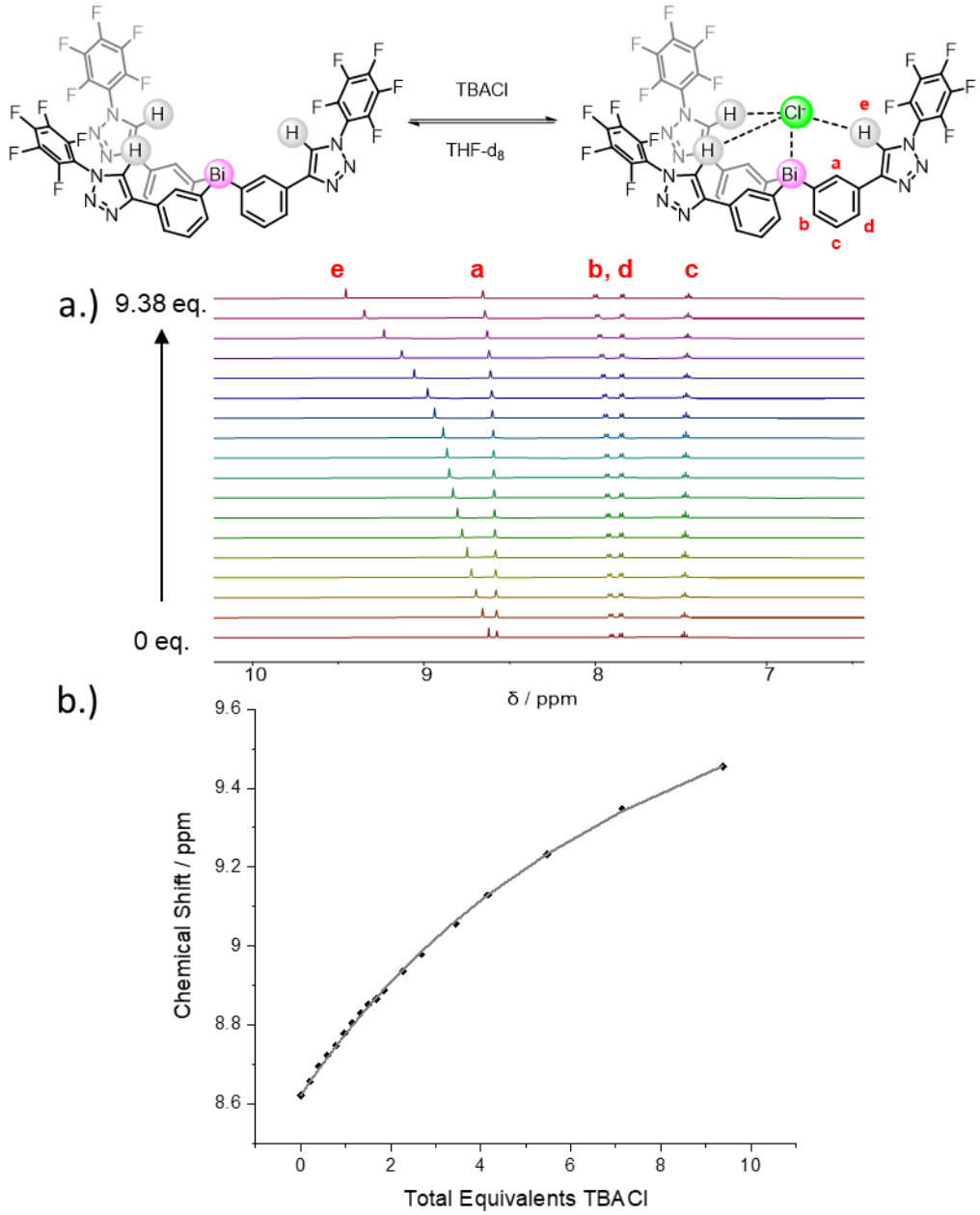



*Figure 2.11. a.) a.) Stacked $^{1}$H-NMR TBACl titration and b.) binding isotherm for chloride with dots representing experimental data and solid lines representing the fitted binding isotherm for* ***2·Bi$^{PFP}$****. Solvent = THF-$d_8$. T = 298 K.*

In a similar manner to the triaryl receptors, the more electrophilic Bi(III) receptors exhibited an approximate 2-fold increase in binding strength in comparison to the analogous Sb(III) receptors, with $\alpha \approx 2$ (Table 2.5). Furthermore, switching from the benzyl substituent to the much more electron withdrawing perfluorophenyl causes an approximate two-fold increase in chloride binding strength due to the enhanced C-H acidity of the HB donor motif. Overall,

**2·Bi$^{PFP}$** is the most potent chloride receptor, with a binding strength approximately four times greater than the weakest receptor, **2·Sb$^{Bz}$** (Table 2.5). It should be noted that the parent triphenylbismuth and triphenylantimony compounds do not exhibit any chloride affinity under these THF-$d_8$ solvent conditions, providing strong evidence that concerted HB and PnB anion interactions are responsible for anion recognition.

*Table 2.5 Chloride anion association constants for tripodal Pn-receptors. $K_a(M^{-1})$ values calculated using BindFit software using a 1:1 stoichiometric host-guest binding model. All using TBA salts. Errors (±) are in parentheses. Solvent = THF-$d_8$. T = 298 K*

| | **Chloride association constants for the PnB receptor series ($K_a$ / $M^{-1}$)** | | **Binding enhancement factor $\alpha = (K_a^{Bi} / K_a^{Sb})$** |
|---|---|---|---|
| **R** | **2·Sb$^R$** | **2·Bi$^R$** | |
| **PFP** | 58(1) | 115(1) | **2.0** |
| **Benz** | 25(1) | 63(1) | **2.5** |
| **Binding enhancement factor $\beta = (K_a^{5F} / K_a^{Benz})$** | **1.8** | **2.3** | |

## 2.4.3 Conclusions

The successful synthesis and characterisation of the first examples of mixed HB and PnB anion receptors was achieved. Preliminary $^1$H NMR titration chloride binding studies determined that concerted PnB and triazole HB donor interactions were responsible for halide recognition. In addition, it was demonstrated that chloride anion binding strength can be modulated through

changing the Pn centre for the more polarisable Bi and employing electron-withdrawing substituents to inductively enhance the PnB donor atom electrophilicity.

### 2.4.4 PnB-XB Tripodal Receptors

Following the successful synthesis of the series of mixed PnB-HB receptors, attempts were made to synthesise the first PnB-XB Sb(III) receptors (Figure 2.12). The aim was to further enhance halide binding affinities *via* the integration of three powerful iodotriazole XB donor motifs into the tripodal aryl Sb(III) receptor scaffold.

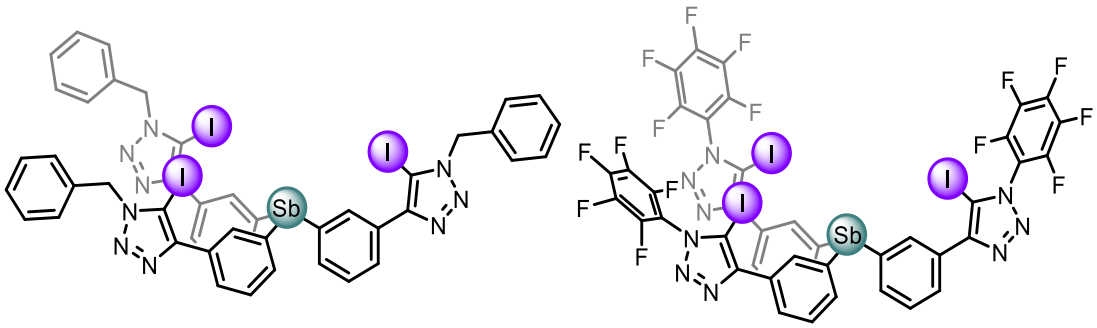



*Figure 2.12. Proposed design of tripodal mixed XB-PnB receptors*

#### 2.4.4.1 Attempted Synthesis of Mixed XB-PnB Tripods

The preparation of 5-iodo-1,2,3-triazole XB donors can be achieved under CuAAC click reaction conditions *via* iodoalkyne and organo-azide reactants.[20] This 'two-pot' method requires the initial synthesis and isolation of the iodoalkyne.[20-22]

The formation of iodoalkynes from trimethylsilyl acetylenes can be achieved in one step through treatment of the trimethylsilyl acetylene with *N*-iodosuccinimide and catalytic amounts of silver nitrate.[21] Iodination of the TMS protected alkyne **2** was therefore initially attempted *via in situ* deprotection using *N*-iodosuccinimide and silver nitrate in DMF. Whilst TLC analysis

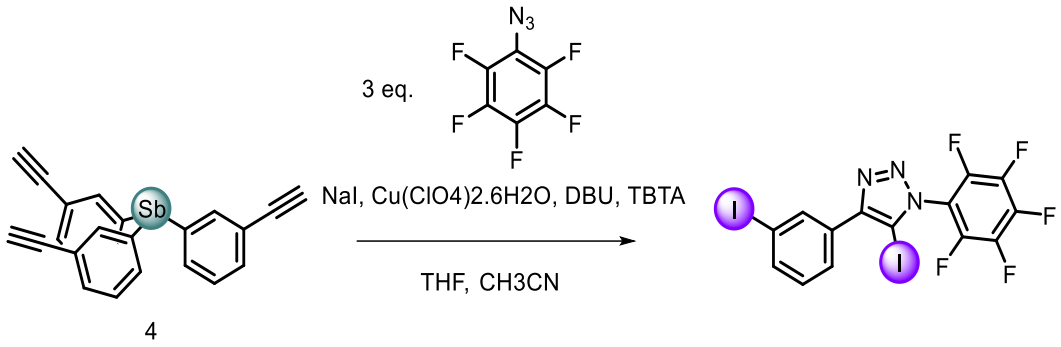
confirmed consumption of the alkyne starting material, it also revealed a complex and intractable mixture of species.

Iodoalkynes can also be prepared from the respective proto-alkynes.[20] Therefore, an alternative synthetic strategy was attempted, wherein the deprotected alkyne **4** was treated with *N*-iodomophiline·HI in the presence of CuI in dry THF.[20] Similarly, the crude $^{1}$H NMR and TLC of the iodination reaction mixture did not show any product formation despite consumption of starting material.

Another alternative synthetic route involves the treatment of proto-alkynes with *n*-BuLi for the *in situ* formation of the lithiated alkyne, which can be treated with elemental iodine to afford the respective iodoalkyne.[22] A further attempt at synthesising the iodoalkyne was therefore made following this established iodination method *via* lithiation of the proto-alkyne **4** and treatment with iodine. Unfortunately, however, no formation of the desired tris-iodoalkyne product was observed by TLC analysis of the reaction mixture.

The inability to successfully prepare the desired tris-iodo-alkyne led to employing a 'one-pot' methodology for the *in situ* formation of 5-iodo-1,2,3-triazoles from the corresponding proto-alkyne and organo-azide, first reported by Zhu in 2012.[23] For this methodology a Cu(II) source is mixed together with NaI in the presence of base causing the *in situ* formation of Cu(I) and triiodide, which facilitate the CuAAc reaction resulting in the formation of the desired iodotriazole.[23] Here, three equivalents of the respective perfluorophenyl azide or benzyl azide were initially dissolved in a mixture of 1:1 THF and acetonitrile, followed by the addition of NaI, copper(II) perchlorate hexahydrate, TBTA and DBU (Scheme 2.5). The subsequent addition of one equivalent of the tris-alkyne Sb(III) **9** and stirring of the reaction overnight, resulted in a complex reaction mixture profile as observed by TLC.

For the 'one pot' CuAAC reaction with perfluorophenylazide, attempts to isolate the major products *via* column chromatography resulted in the isolation of a perfluorophenyl functionalised iodotriazole decomposition product shown in Scheme 2.5 as identified by $^{1}H$, $^{13}C$ NMR and HRESI-MS, with no evidence for the synthesis of the desired XB-PnB receptor. Similarly, the corresponding functionalised benzyl iodotriazole decomposition product was isolated from the reaction using benzyl azide, characterised by $^{1}H$ and $^{13}C$ NMR.




*Scheme 2.5.Formation of decomposition product when reacting compound **4** with perfluorophenylazide under 'one-pot' CuAAC click conditions*

## 2.5 Stibanotriazole Receptors

As discussed in a recent paper by Beer and co-workers,[11] covalently linking electron withdrawing substituents to a tellurium triazole ChB σ-hole donor strongly affects anion receptor potency *via* through bond electronic inductive activation of the σ-hole. Motivated by this and the ability to modulate the anion binding potency of organoantimony and organobismuth triaryl PnB donors *via* the introduction of inductively activating electron-withdrawing aryl substituent groups, another avenue was sought in which the Sb(III) PnB donor atom is directly covalently linked to the 1,2,3-triazole motif as shown in Figure 2.13

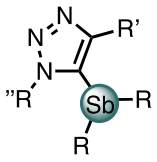



*Figure 2.13. General structure of the 5-stibano-1H-1,2,3-triazole motif*

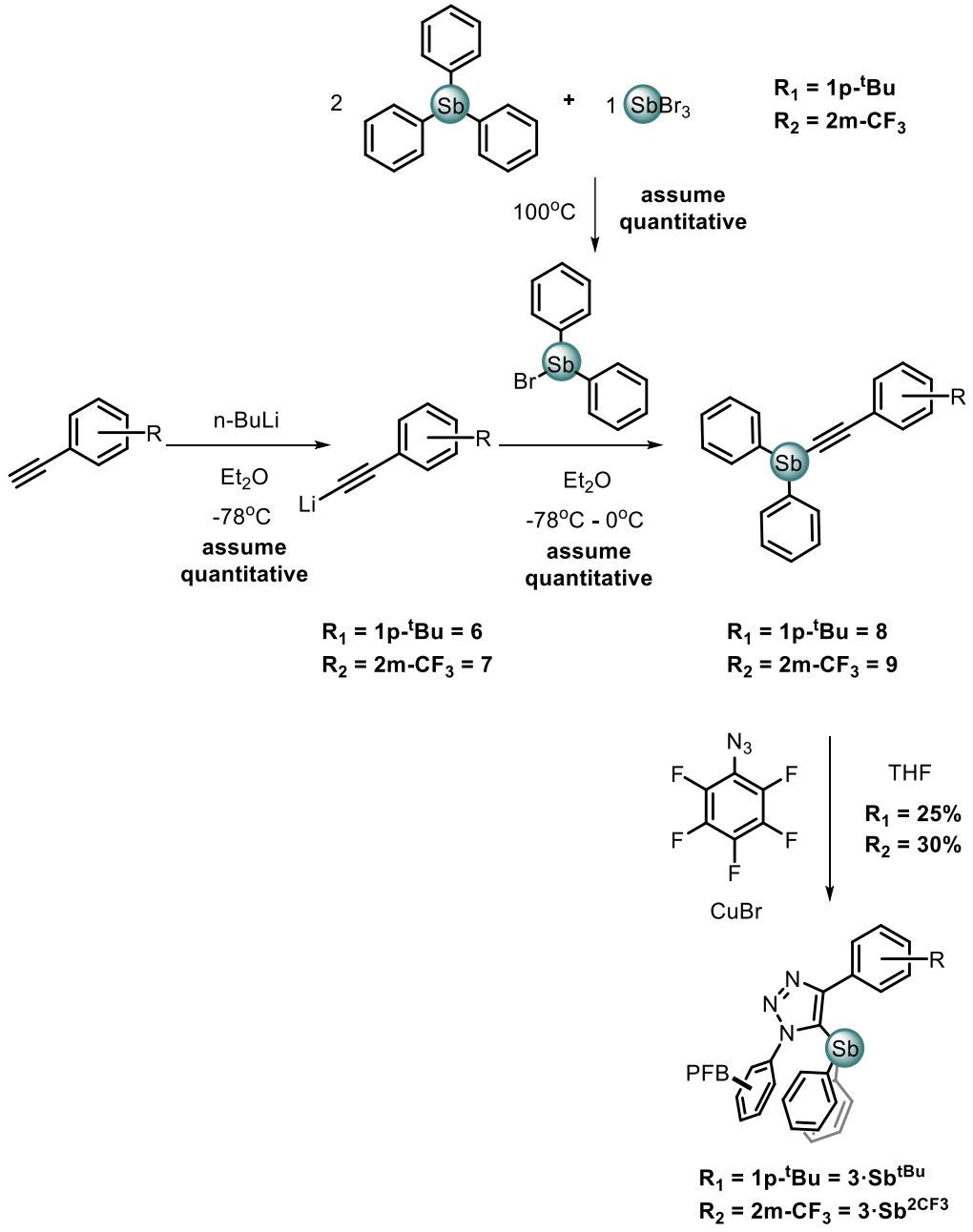
### 2.5.1 Synthesis of 5-Stibano-1H-1,2,3-Triazole Receptors

The recently reported synthesis of trisubstituted 5-stibano-1H-1,2,3-triazoles by Yasuike *et al.* served as the basis for the synthetic procedures undertaken initially to prepare monodentate Sb(III)-functionalised triazole targets (Scheme 2.6).[24-26] These previous reports demonstrated that stibanotriazoles can be accessed in a similar fashion to iodotriazole derivatives through a Cu(I) mediated azide alkyne cycloaddition (CuAAC) between an appropriately functionalised antimony-alkyne and an azide.[24-26]

To this end, the corresponding diphenyl appended antimony alkynes **8** and **9** were prepared by the methodology described in Scheme 2.6.

Two equivalents of triphenylantimony(III) and one equivalent of antimony(III) bromide were mixed and heated to 100 °C under an inert nitrogen atmosphere to facilitate a redistribution reaction for the formation of diphenylantimony(III) bromide. Commercially available 4-*tert*-butylphenylacetylene and 3,5-bis(trifluoromethyl)phenylacetylene were treated with *n*-BuLi in dry, degassed diethyl ether to form the lithiated salts **6** and **7** *in situ*. The previously formed diphenylantimony(III) bromide was then added as a suspension in dry diethyl ether to form the respective diphenylantimony functionalised alkynes **8** and **9**. The alkynes were subjected to an aqueous workup but no further purification was performed due to their presumed instability on silica.

The crude **8** and **9** synthons were immediately reacted with one equivalent of pentafluorophenyl azide under CuAAC conditions with CuBr as the catalyst to afford the respective mono-stibanotriazole receptors **3·Sb$^{tBu}$** and **3·Sb$^{2CF3}$**, which were isolated in yields of 25% and 30% respectively after silica gel flash column chromatographic purification.




*Scheme 2.6. Successful synthesis of mono-stibanotriazole receptors **3·Sb$^{tBu}$** and **3·Sb$^{2CF3}$***

The two mono-triazole receptors **3·Sb$^{tBu}$** and **3·Sb$^{2CF3}$** were fully characterised by $^{1}$H NMR, $^{13}$C NMR, $^{19}$F NMR and HRESI. Representative spectroscopic data for **3·Sb$^{2CF3}$** are shown in Figure 2.14.

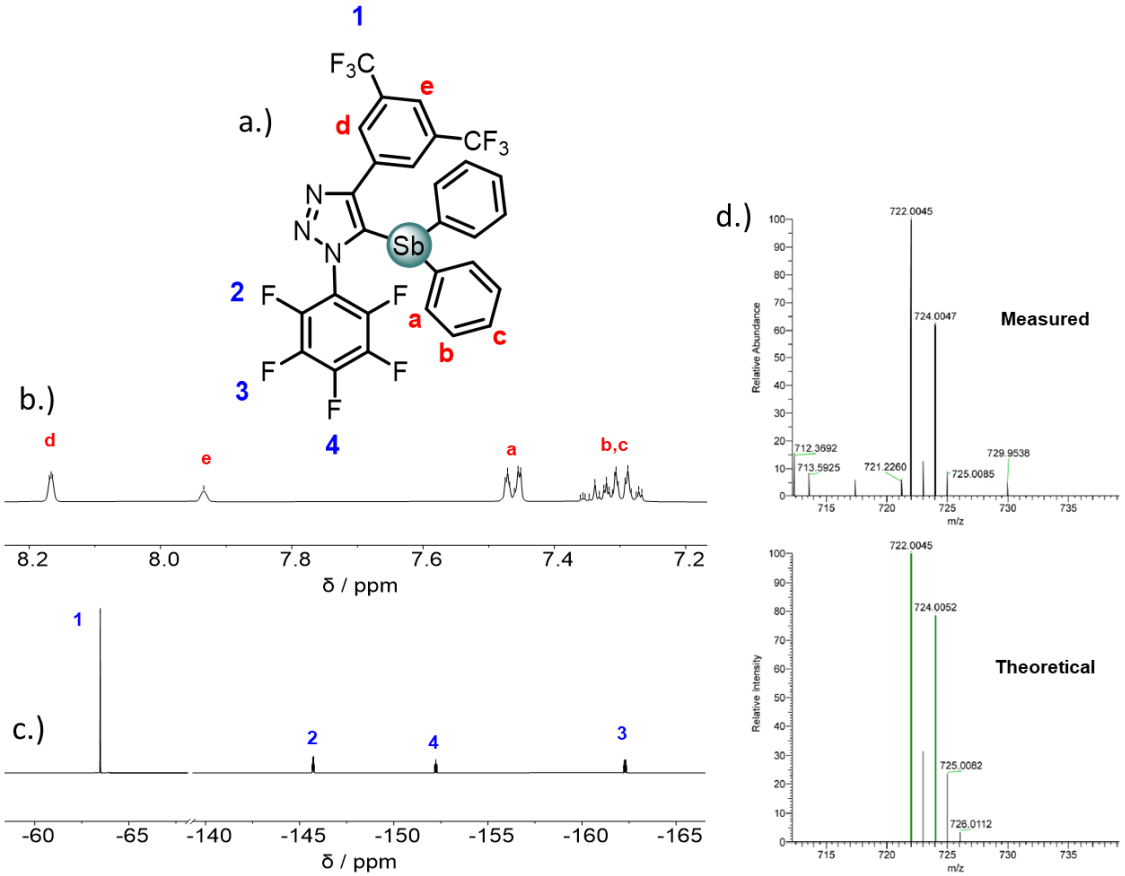
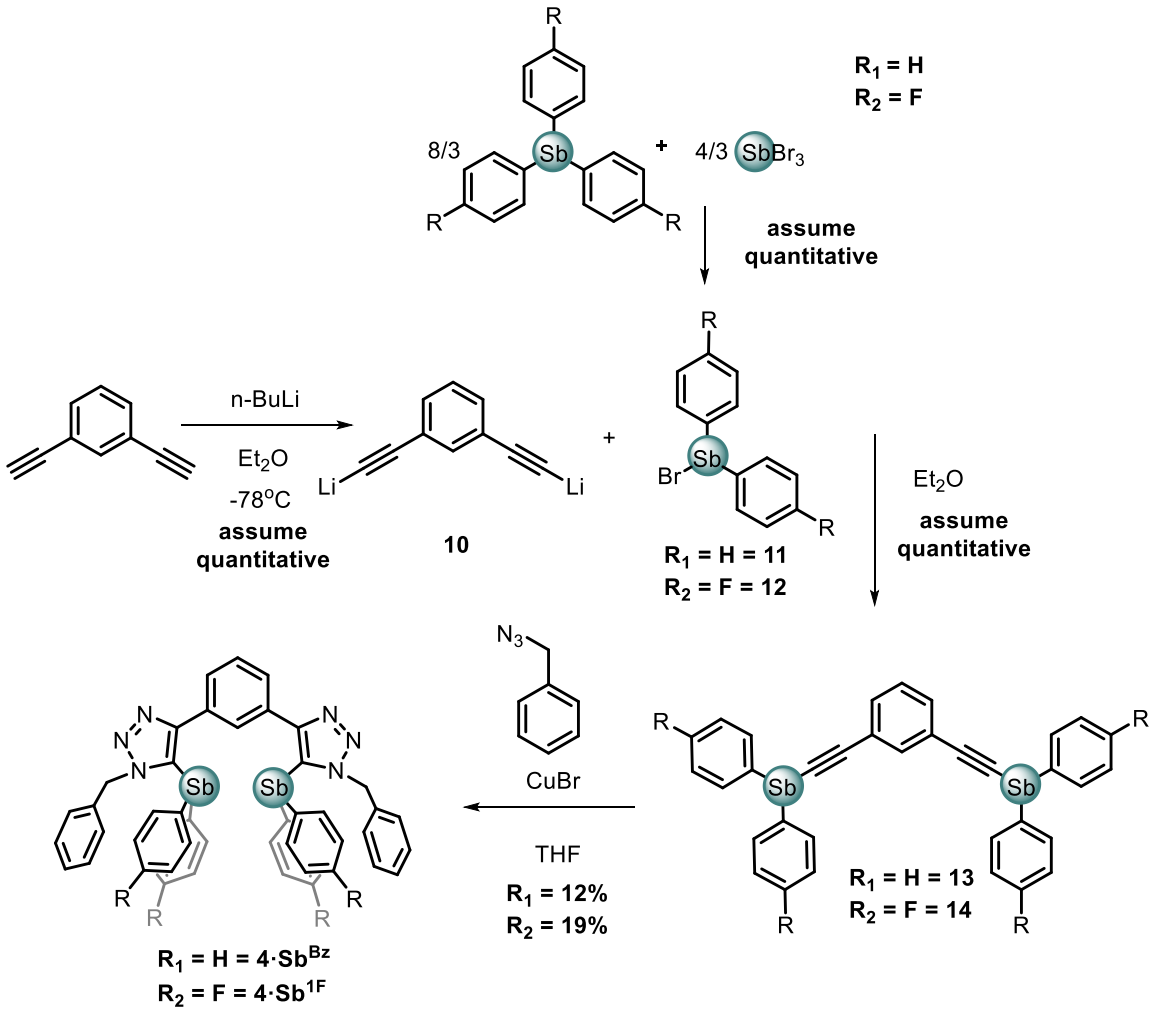



*Figure 2.14. a.) Chemical structure of* ***3·Sb$^{2CF3}$*** *b.) Truncated $^{1}$H NMR spectrum of* ***3·Sb$^{2CF3}$*** *(acetone-$d_6$, 400 mHz, 298K), c.) Truncated $^{19}$F NMR spectrum of* ***3·Sb$^{2CF3}$*** *(acetone-$d_6$, 377 mHz, 298K), d.) theoretical (bottom) and measured (top) high resolution ESI spectra*

An analogous synthetic protocol was undertaken to prepare novel bidentate stibanotriazole receptor systems (Scheme 2.7).

1,3-Diethynylbenzene was subjected to a lithiation reaction to form **10** *in situ*, which was allowed to react immediately with four equivalents of the respective freshly generated redistribution product **11** and **12**, prepared from either triphenylantimony or tri-p-fluorophenylstibine and antimony tribromide, to afford the corresponding diphenylantimony functionalised bis-alkynes **13** and **14**. After aqueous workup, the alkynes were immediately reacted with benzyl azide under CuAAC conditions to afford the respective bis-stibanotriazole receptors **4·Sb$^{Bz}$** and **4·Sb$^{1F}$** in moderate yields. Purification was again performed using silica gel flash-column chromatography.




*Scheme 2.7. Synthetic route for the formation of bis-stibanotriazole products* ***4·Sb$^{Bz}$*** *and* ***4·Sb$^{1F}$***

While the redistribution reaction readily proceeded for triphenylstibine and tri-*p*-fluorophenylstibine, attempts to repeat the reaction with more fluorinated triarylstibines were unsuccessful. The relatively weak Sb-C bond also proved to be a limitation for the target receptor design as product decomposition was frequently observed upon aqueous work-up or purification by silica gel flash column chromatography. This was especially the case when attempts were made to synthesise a modified receptor containing a central pyridine unit, as well as attempts to perform the CuAAC with more electron withdrawing pentafluorophenyl azide instead of benzyl azide. Commonly $^{1}$H NMR observed side products contained proto-triazole units with mixed proto- and stibanotriazole receptors. Indeed, Yasuike has previously reported

that proto-triazole decomposition by-products are formed from stibanotriazole instability, highlighting the weak Sb-C bond is prone to further reaction.[25]

However, the two successfully synthesised bis-stibanotriazole receptors **4·Sb$^{Bz}$** and **4·Sb$^{1F}$** could be fully characterised by $^{1}$H NMR, $^{13}$C NMR, HRESI as well as $^{19}$F NMR for **4·Sb$^{1F}$**. Representative spectroscopic data for **4·Sb$^{1F}$** is shown in Figure 2.15. To the best of our knowledge these are the first examples of molecules containing more than one stibanotriazole unit.

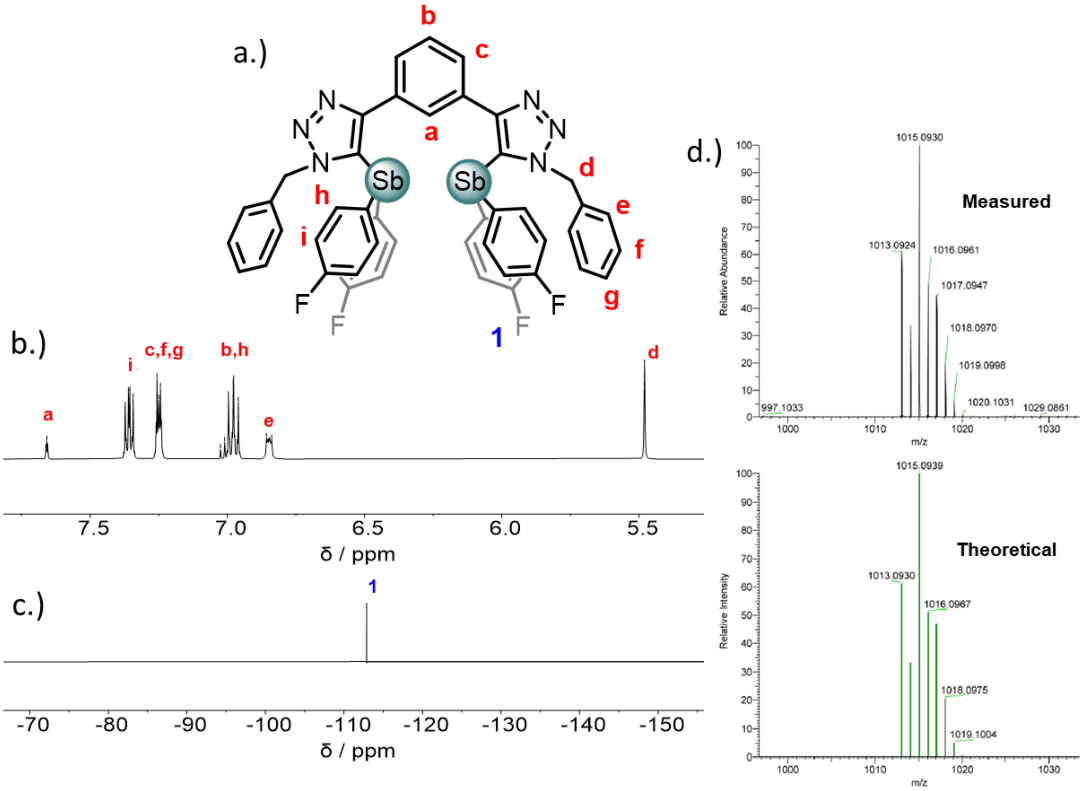



*Figure 2.15. a.) Chemical structure of **4·Sb$^{1F}$** b.) Truncated $^{1}$H NMR spectrum of **4·Sb$^{1F}$** (acetone-$d_6$, 400 mHz, 298K), c.) Truncated $^{19}$F NMR spectrum of **4·Sb$^{1F}$** (acetone-$d_6$, 377 mHz, 298K), d.) theoretical (bottom) and measured (top) high resolution ESI spectra.*

### 2.5.2 Anion Binding Studies of Stibanotriazole Receptors

The chloride binding abilities of the all four stibanotriazole receptors **3·Sb$^{tBu}$**, 3·**Sb$^{2CF3}$**, **4·Sb$^{Bz}$** and **4·Sb$^{1F}$** were studied *via* $^{1}$H-NMR titration experiments with TBACl in THF-$d_8$ (Figure 2.16 - Figure 2.19).

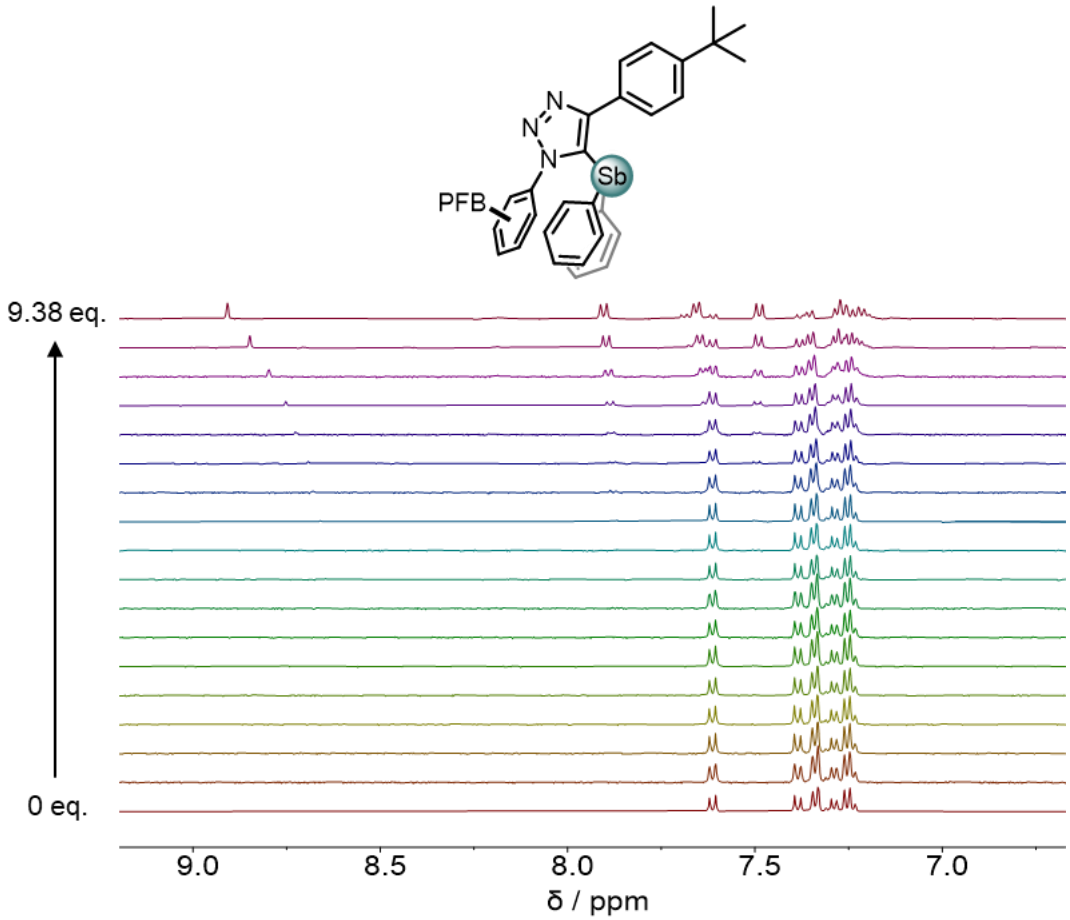



*Figure 2.16. $^{1}$H-NMR spectra of mono-stibanotriazole receptor **3·Sb$^{tBu}$** upon incremental addition of 9.38 equivalents of TBACl (bottom to top). Solvent = THF-$d_8$. T = 298 K.*

The **3·Sb$^{tBu}$** receptor exhibited no significant proton perturbations indicative of halide binding and partial decomposition to the proto-triazole derivative occurred at higher TBACl concentrations, as evidenced by the appearance of a new triazole proton peak at approximately 8.7 ppm (Figure 2.16).

Unfortunately, the more electron deficient **3·Sb$^{2CF3}$** receptor readily decomposed to the proto-triazole analogue as evidenced with the appearance of a new triazole proton peak upon addition of as little as 0.2 equivalents of TBACl (Figure 2.17). Due to the halide anion induced decomposition of both receptors, no reliable quantitative binding data could be determined from the $^{1}$H NMR titration experiments.

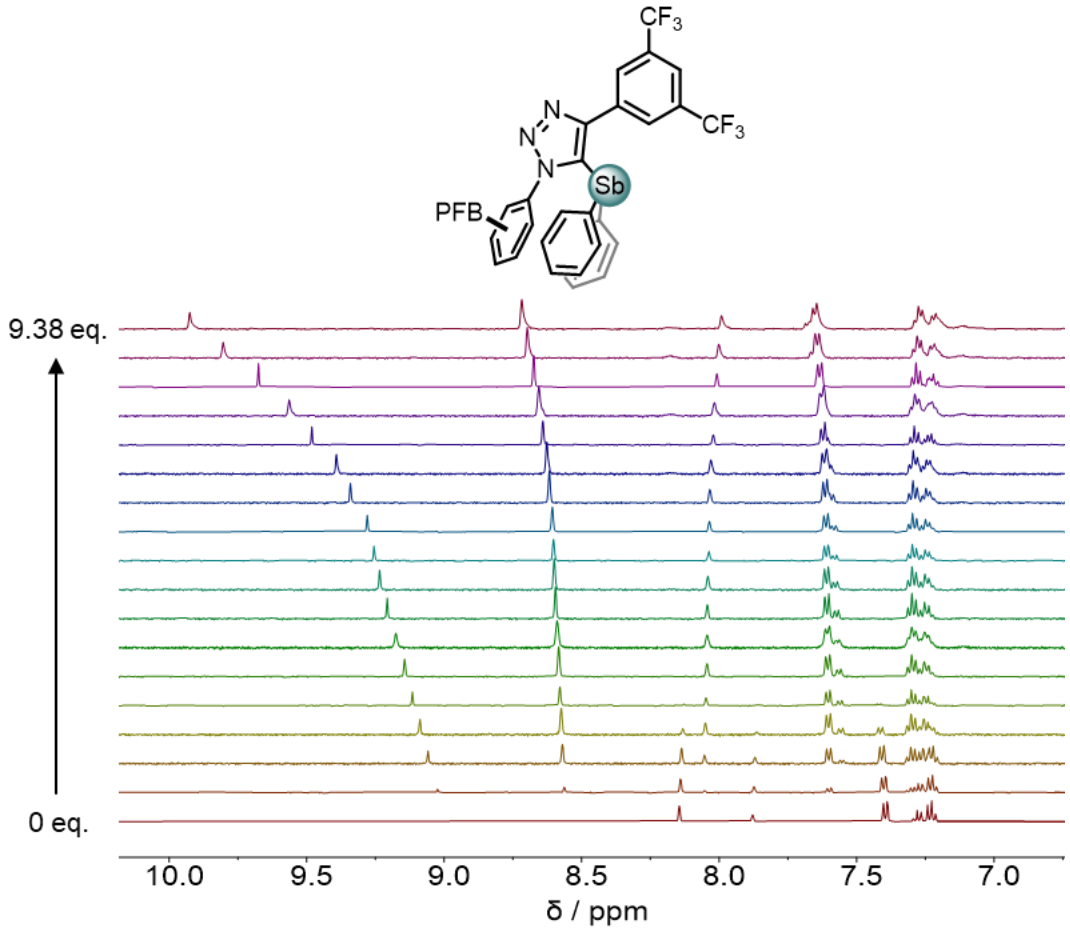



*Figure 2.17. $^{1}$H-NMR spectra of mono-stibanotriazole receptor **3·Sb$^{2CF3}$** upon incremental addition of 9.38 equivalents of TBACl (bottom to top). Solvent = THF-$d_8$. T = 298 K.*

Although the bis-stibanotriazole based-receptor, **4·Sb$^{Bz}$** receptor remained stable and showed no evidence of decomposition throughout the $^{1}$H NMR TBACl titration investigation, no significant receptor proton shifts were observed, indicative of no PnB binding of the chloride anion (Figure 2.18).

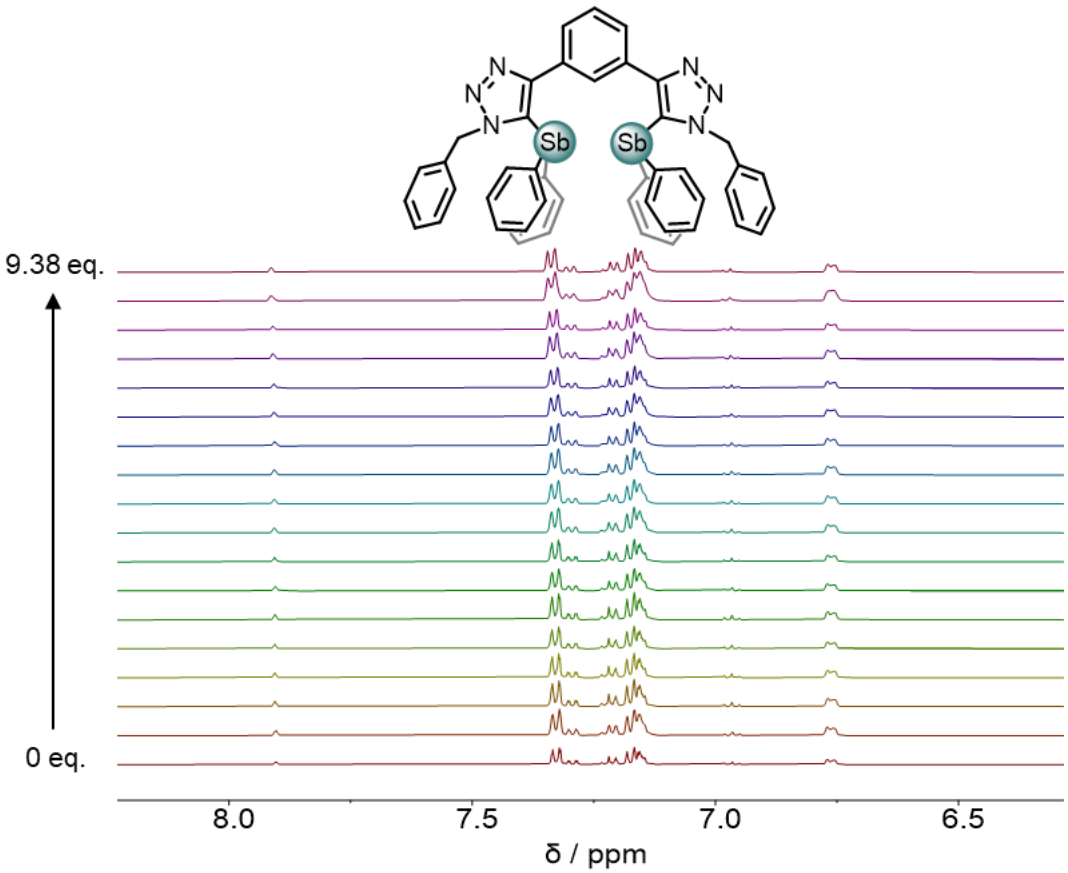



*Figure 2.18. $^{1}$H-NMR spectra of receptor **4·Sb$^{Bz}$** upon incremental addition of 9.38 equivalents of TBACl (bottom to top). Solvent = THF-$d_8$. T = 298 K.*

Pleasingly, the *para*-fluoro analogue **4·Sb$^{1F}$** did display receptor proton perturbations in the $^{1}$H NMR spectra indicative of chloride binding, however, partial decomposition to the proto-triazole was observed at higher TBACl concentrations (Figure 2.19). The decomposition of the receptor once again precluded a reliable quantitative analysis of the anion binding event.

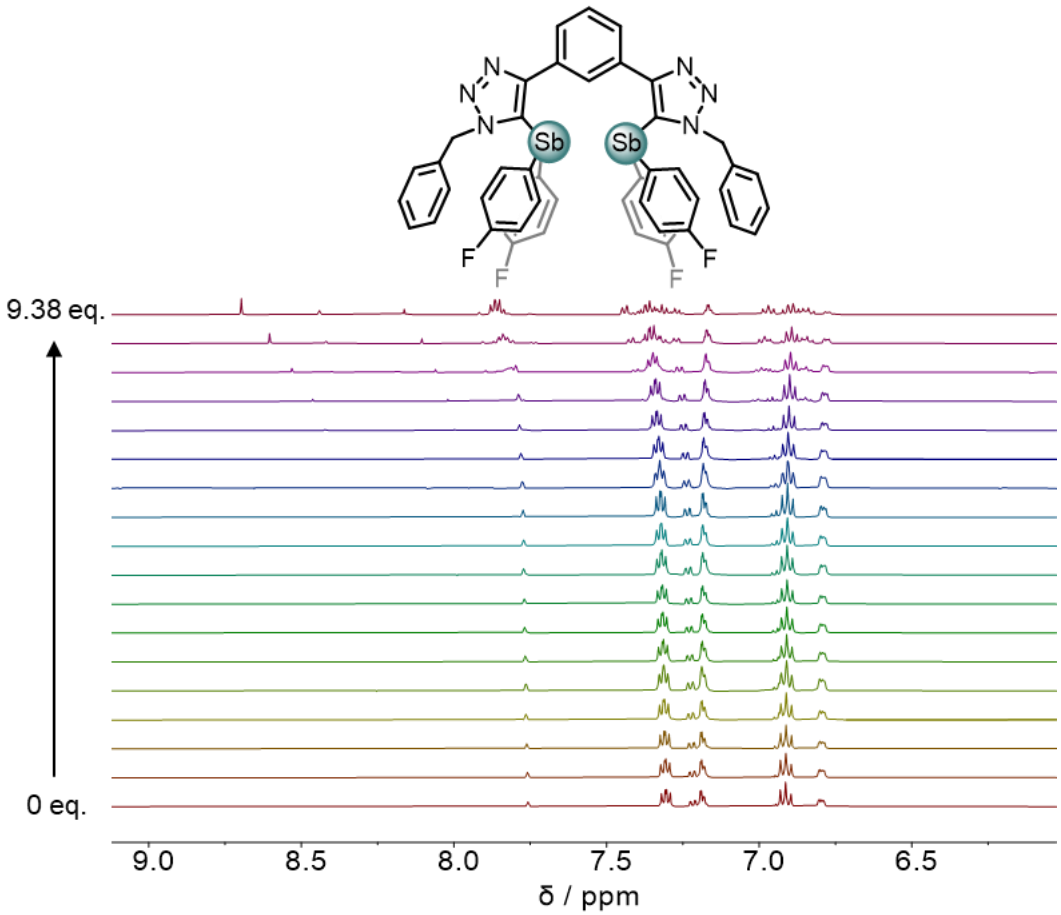



*Figure 2.19. $^{1}$H-NMR spectra of receptor **4·Sb$^{1F}$** upon incremental addition of 9.38 equivalents of TBACl (bottom to top). Solvent = THF-$d_8$. T = 298.*

## 2.5.3 Conclusions

The successful synthesis and characterisation of four novel stibanotriazole based PnB receptors was achieved, with receptors **4·Sb$^{Bz}$** and **4·Sb$^{1F}$** constituting the first examples of the successful incorporation of two stibanotriazole units into a potential acyclic anion receptor structural framework.

Preliminary $^{1}$H NMR anion titration studies with TBACl and receptor **4·Sb$^{1F}$** revealed receptor proton perturbations in the $^{1}$H NMR spectra, which are indicative of chloride binding. However, the lability of the Sb-C bond precluded quantitative analysis of receptors **4·Sb$^{1F}$** as well as **3·Sb$^{2CF3}$** and **3·Sb$^{tBu}$**, with observed halide anion induced decomposition of the receptor

framework to the corresponding proto-triazole as indicated by the appearance of a diagnostic proto-triazole peak in the $^{1}$H NMR spectra.

This study has demonstrated that functional PnB receptor design necessitates the incorporation of electron withdrawing substituents for receptor potency, whilst maintaining host stability that considers the inherently weak Pn-C bond. This remains a significant synthetic challenge to overcome.

## 2.6 Conclusions and Further Outlook

This chapter presented the study of three different groups of PnB based anion receptors. Firstly, the systematic investigation of acyclic triaryl based Bi(III) and Sb(III) receptors appended with various electron withdrawing aryl substituents was reported. $^{1}$H NMR anion titration experiments revealed that receptor potency is directly influenced by the electronic nature of the substituents, as well as the nature of the PnB donor, with the heavier Bi containing hosts outperforming the analogous Sb receptors. Furthermore, in line with other σ-hole receptors and in contrast to classic acyclic HB receptor systems, the PnB receptors displayed notable chloride selectivity over more basic oxoanions.

Secondly, the synthesis of four novel mixed PnB-HB tripodal host systems has shown that Pn atoms can be successfully incorporated into multidentate receptor scaffolds. As observed with the triaryl based Bi(III) and Sb(III) receptors, $^{1}$H NMR anion titration investigations demonstrated the Bi receptors outperformed their Sb analogues, as well as receptor potency increasing upon incorporation of electron withdrawing substituents.

Thirdly, the incorporation of Sb(III) into more advanced receptor designs was undertaken with the successful synthesis and characterisation of the first bis-stibanotriazole to date. However, in this host system the inherently weak Pn-C bond necessitates finding a compromise between electronic substituent polarisation and anion stability in future PnB receptor design.

Overall, this study provides important insights into the properties of the underexplored PnB interaction and can serve as a foundation for the considered development of more potent and selective Pn-based anion receptors.

Future work could include the incorporation of Pn(III) centres into cage-like scaffolds (Figure 2.20), which could provide more well defined and preorganised anion binding environments. As mentioned above, the challenge for the design of powerful PnB anion receptors remains the balance between a stable receptor and a sufficiently polarised C-Pn bond to facilitate strong σ-hole anion interactions.

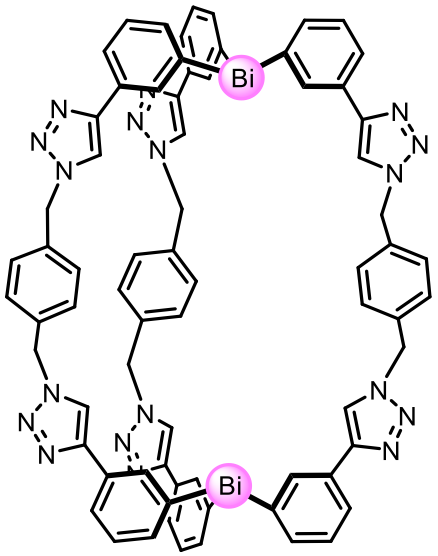



*Figure 2.20. Example of a Bi(III) cage design*

While the study presented here sought to employ Pn(III) derivatives as the main PnB donor, conceivably the potency of PnB interactions can be increased by accessing higher oxidation

states of the pnictogen centre. Indeed, Gabbaï and co-workers have demonstrated this by preparing Sb(V) systems, displaying enhanced Lewis acidity when compared to analogous Sb(III) receptors (see section 1.2.4.3).[27] A systematic study could therefore enable the determination of the electronic and structural factors which govern Pn(V) mediated anion recognition to further aid PnB based receptor design diversification.

## 2.7 References


1. S. Scheiner, *Accounts of Chemical Research*, 2013, **46**, 280-288.

2. J. Ramler, K. Hofmann and C. Lichtenberg, *Inorganic Chemistry*, 2020, **59**, 3367-3376.

3. R. Kannan, S. Kumar, A. P. Andrews, E. D. Jemmis and A. Venugopal, *Inorganic Chemistry*, 2017, **56**, 9391-9395.

4. J. Ramler and C. Lichtenberg, *Chemistry – A European Journal*, 2020, **26**, 10250-10258.

5. S. S. Chitnis, A. P. M. Robertson, N. Burford, B. O. Patrick, R. McDonald and M. J. Ferguson, *Chemical Science*, 2015, **6**, 6545-6555.

6. S. Benz, A. I. Poblador-Bahamonde, N. Low-Ders and S. Matile, *Angewandte Chemie International Edition*, 2018, **57**, 5408-5412.

7. A. Gini, M. Paraja, B. Galmés, C. Besnard, A. I. Poblador-Bahamonde, N. Sakai, A. Frontera and S. Matile, *Chemical Science*, 2020, **11**, 7086-7091.

8. M. Paraja, A. Gini, N. Sakai and S. Matile, *Chemistry – A European Journal*, 2020, **26**, 15471-15476.

9. H. V. Humeniuk, A. Gini, X. Hao, F. Coelho, N. Sakai and S. Matile, *JACS Au*, 2021, **1**, 1588-1593.

10. L. M. Lee, M. Tsemperouli, A. I. Poblador-Bahamonde, S. Benz, N. Sakai, K. Sugihara and S. Matile, *Journal of the American Chemical Society*, 2019, **141**, 810-814.

11. A. Docker, C. H. Guthrie, H. Kuhn and P. D. Beer, *Angewandte Chemie International Edition*, 2021, **60**, 21973-21978.

12. T. Murafuji, K. Nishio, M. Nagasue, A. Tanabe, M. Aono and Y. Sugihara, *Synthesis*, 2000, **2000**, 1208-1210.

13. A. F. M. M. Rahman, T. Murafuji, M. Ishibashi, Y. Miyoshi and Y. Sugihara, *Journal of Organometallic Chemistry*, 2005, **690**, 4280-4284.

14. D. Brynn Hibbert and P. Thordarson, *Chemical Communications*, 2016, **52**, 12792-12805.

15. P. Thordarson, *Chemical Society Reviews*, 2011, **40**, 1305-1323.

16. BindFit v0.5 | Supramolecular, http://app.supramolecular.org/bindfit/).

17. L. E. Bickerton, A. Docker, A. J. Sterling, H. Kuhn, F. Duarte, P. D. Beer and M. J. Langton, *Chemistry – A European Journal*, 2021, **27**, 11738-11745.

18. Y. C. Tse, A. Docker, Z. Zhang and P. D. Beer, *Chemical Communications*, 2021, **57**, 4950-4953.

19. J. C. Burnett, C. Lim, B. D. Peyser, L. P. Samankumara, M. Kovaliov, R. Colombo, S. L. Bulfer, M. G. Laporte, A. R. Hermone, C. F. McGrath, M. R. Arkin, R. Gussio, D. M. Huryn and P. Wipf, *Organic & Biomolecular Chemistry*, 2017, **15**, 4096-4114.

20. J. E. Hein, J. C. Tripp, L. B. Krasnova, K. B. Sharpless and V. V. Fokin, *Angewandte Chemie International Edition*, 2009, **48**, 8018-8021.

21. T. Nishikawa, S. Shibuya, S. Hosokawa and M. Isobe, *Synlett*, 1994, 485-486.

22. A. Docker, X. Shang, D. Yuan, H. Kuhn, Z. Zhang, J. J. Davis, P. D. Beer and M. J. Langton, *Angewandte Chemie International Edition*, 2021, **60**, 19442-19450.

23. W. S. Brotherton, R. J. Clark and L. Zhu, *The Journal of Organic Chemistry*, 2012, **77**, 6443-6455.

24. S. Yasuike, K. Nakata, W. Qin, M. Matsumura, N. Kakusawa and J. Kurita, *Journal of Organometallic Chemistry*, 2015, **788**, 9-16.

25. M. Yamada, M. Matsumura, Y. Uchida, M. Kawahata, Y. Murata, N. Kakusawa, K. Yamaguchi and S. Yasuike, *Beilstein Journal of Organic Chemistry*, 2016, **12**, 1309-1313.

26. M. Yamada, M. Matsumura, M. Kawahata, Y. Murata, N. Kakusawa, K. Yamaguchi and S. Yasuike, *Journal of Organometallic Chemistry*, 2017, **834**, 83-87.

27. M. Yang, D. Tofan, C. H. Chen, K. M. Jack and F. P. Gabbaï, *Angewandte Chemie International Edition*, 2018, **57**, 13868-13872.

# 3 Towards a Functional [1]Rotaxane

## 3.1 Introduction

[1]Rotaxanes constitute a unique class of mechanically interlocked molecules (MIMs), in which, similar to their [2]rotaxane counterparts, they possess an axle component which penetrates the aperture of a macrocyclic unit that cannot become de-threaded due to a bulky terminus.[1] However, they are distinct in the fact that all these units are covalently linked together (Figure 3.1).[2]

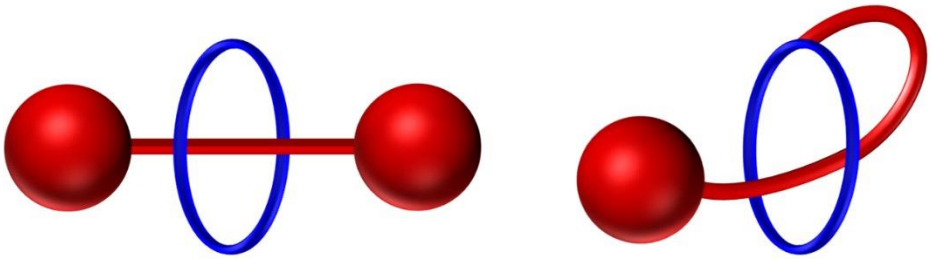


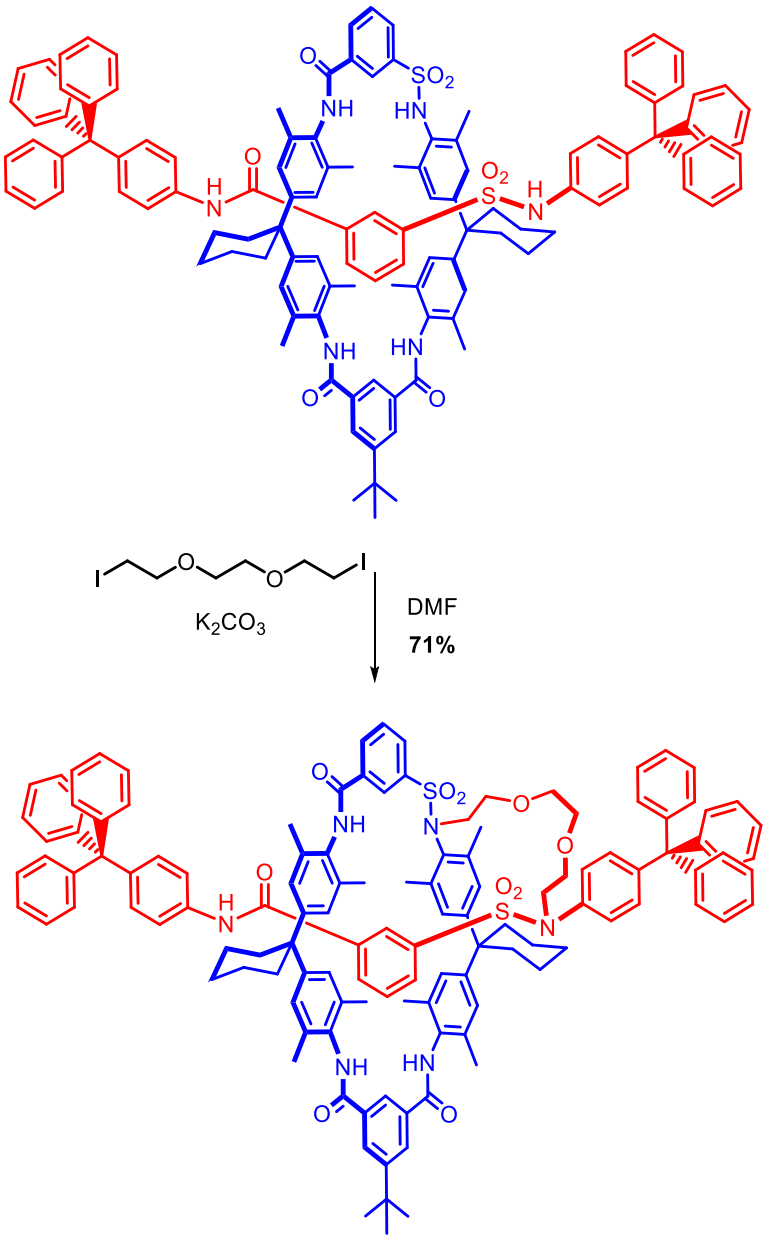
*Figure 3.1. Schematic representation of a [2]rotaxane (left) and [1]rotaxane (right)*

Despite being relatively rare in the field of MIMs, this form of topology can be found in the natural world and is prevalent throughout the bacterial domain.[3] Termed lasso peptides, these mechanically interlocked biomacromolecules exhibit a diverse array of biological functions, some of which are thought to be solely due to their interpenetrated nature.[3, 4]

The [1]rotaxane topology has stimulated considerable interest as a particular synthetic challenge to access and several methodologies have been used to achieve this type of mechanical bond formation.[5]

Some of the earliest examples were constructed by post-functionalisation of [2]rotaxanes.[6-8] An example by Vögtle in 1996 involved the synthesis of a [2]rotaxane, which itself was assembled

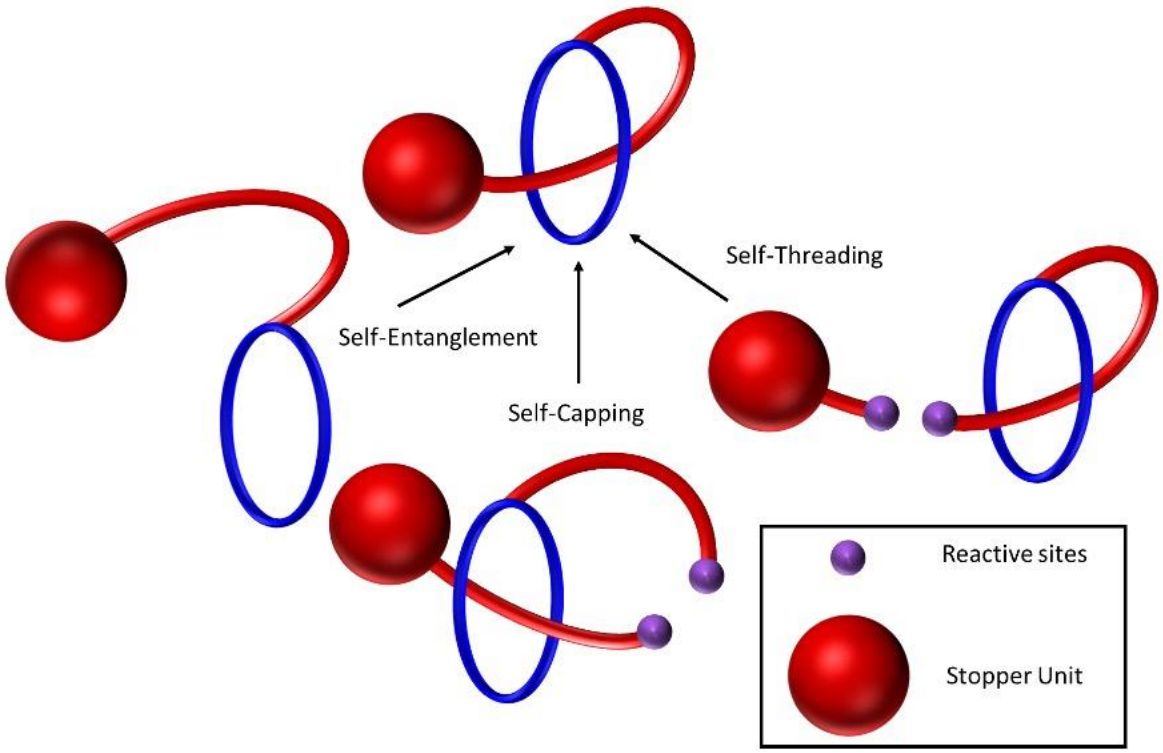
through a hydrogen bonding templated methodology.[6] The sulfonamide groups on both the axle and macrocycle components were reacted with a bis-iodo functionalised ether alkylating agent, such that the two components became covalently linked to give the [1]rotaxane in an impressive 71% yield (Scheme 3.1).[6]




*Scheme 3.1. Vögtle's [1]rotaxane synthesis*[6]

However, the synthetic utility of this strategy is somewhat limited by the precursor being a MIM. In more recent years, mechanical bond forming synthetic approaches have emerged for

[1]rotaxane formation. The most common include self-threading[9, 10], self-capping[11] and self-entanglement[12-14] (Scheme 3.2).

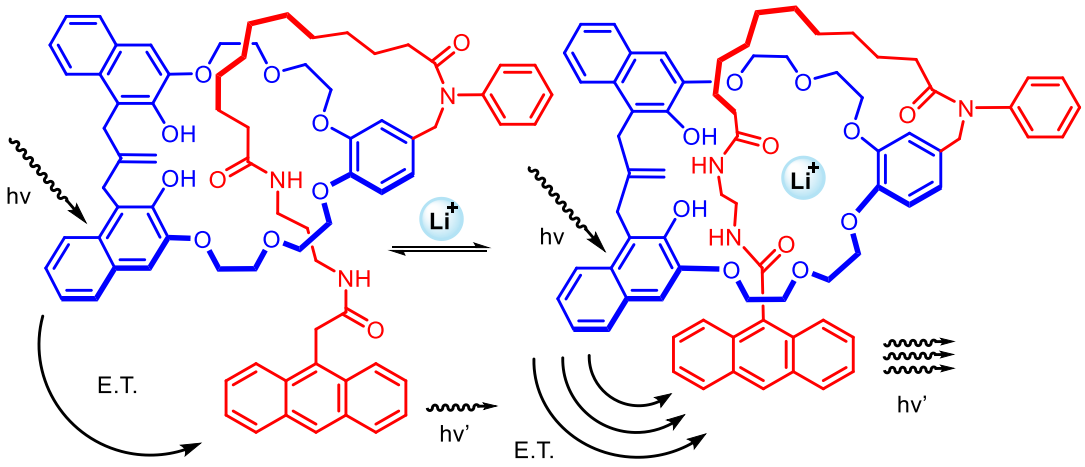



*Scheme 3.2. Schematic representation of [1]rotaxane formation through self-entanglement, self-capping and self-threading*

The templating strategy employed to achieve the interpenetrated assembly of the reactants arises from either an inherent interaction between the two components, such as π-π stacking[15] or electrostatics,[11, 16] or alternatively the addition of a discrete template, typically a metal cation,[14] to preorganise the components into the desired arrangement.

In 2004, Hiratani prepared a functional [1]rotaxane system capable of lithium cation sensing *via* a covalent bond formation mechanism involving an intramolecular bridge, which is broken *via* aminolysis to form the MIM and non-interlocked isomer by-products, which are separated using preparative gel permeation chromatography.[1] In this seminal report, the authors detailed that the crown-ether like macrocycle component, in concert with Lewis basic amide oxygens integrated in the axle, are capable of lithium cation complexation (Scheme 3.3). Crucially, $Li^+$

cation binding induced a conformational change, which increased the proximity of the macrocycle-bound naphthol group and the anthracene terminated axle (Scheme 3.3).[1] Consequently, the improved efficiency of energy transfer between the excited state of the naphthol and anthracene unit, presumably through a Förster resonance energy transfer (FRET) mechanism, dramatically improved the anthracene based fluorescence.[1] The [1]rotaxane thereby functions as a fluorescent sensor for lithium. Importantly, it was shown that the non-interlocked analogue exhibited no such fluorescent response upon lithium addition.[1]

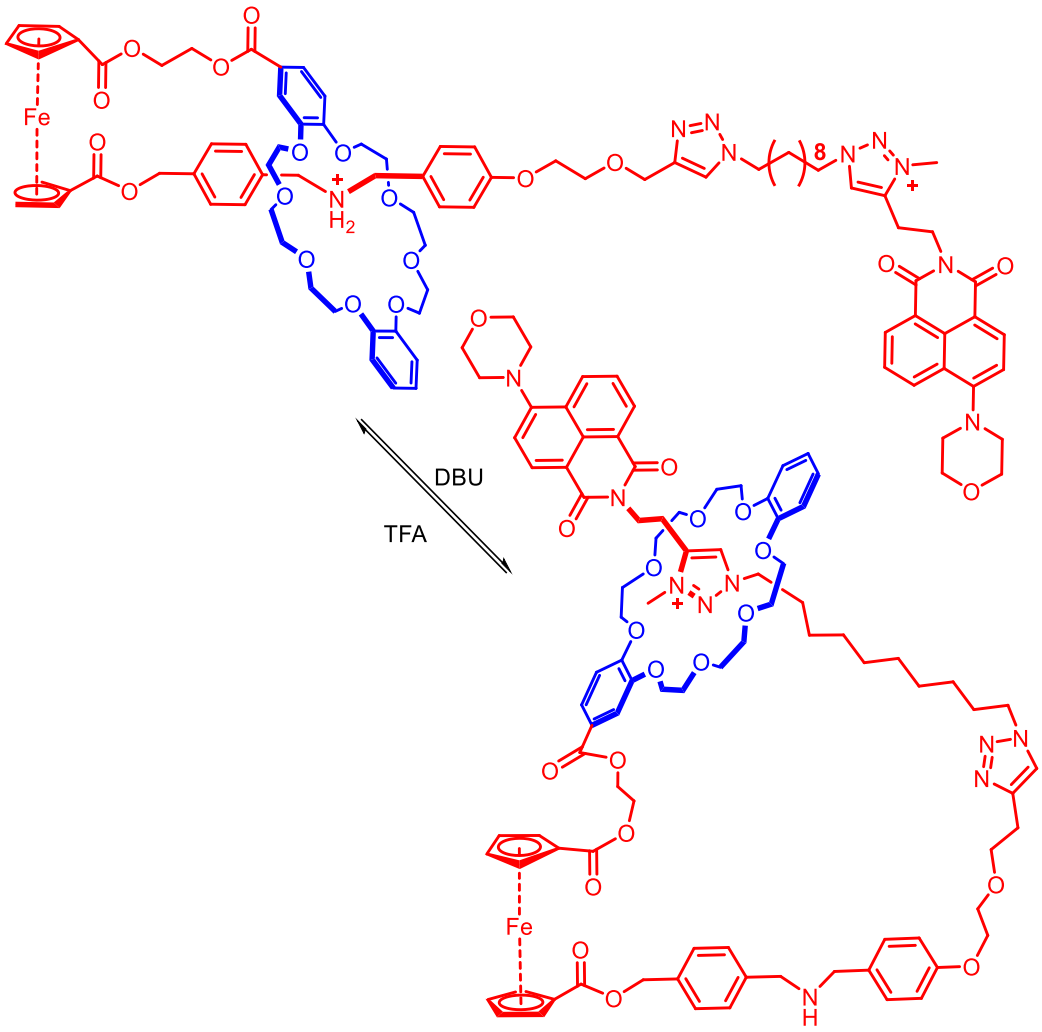



*Scheme 3.3. Lithium binding of Hiratani's functional [1]rotaxane[1]*

A subsequent example by Qu from 2013 reported the synthesis of a [1]rotaxane *via* self-templation of a pseudo[1]rotaxane through HB and electrostatic interactions followed by a CuAAC stoppering reaction for the formation of the MIM.[16] The unique dynamism of this [1]rotaxane was exploited by utilising a pH-based stimulus to initiate a controlled conformation change.[16]

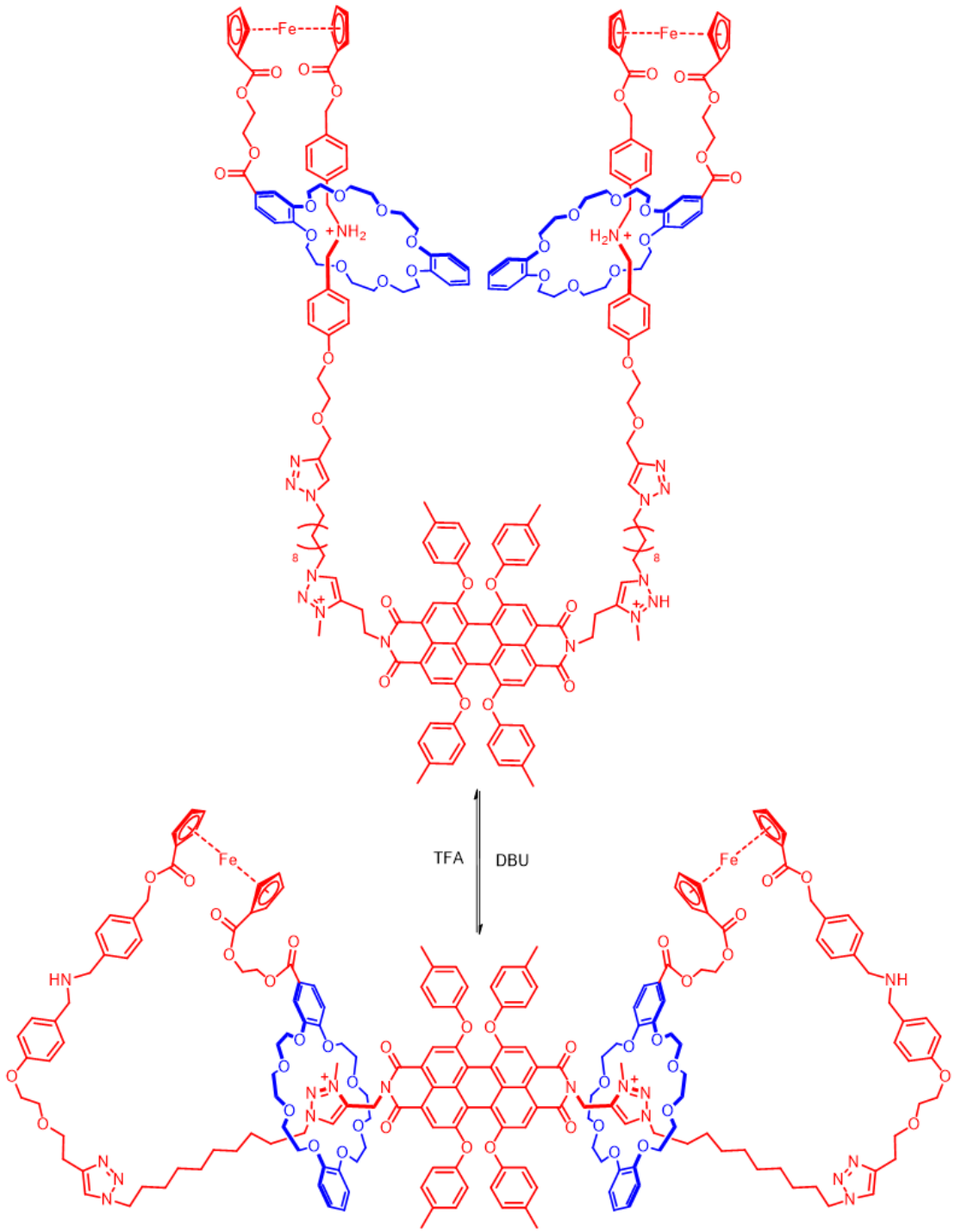
A bifunctional ferrocene motif was used as a molecular hinge or pivot wherein the relatively free mutual rotation of the cyclopentadienyl rings facilitated the ability of the dibenzo-24-crown-8 macrocycle to translocate along the axle length of the [1]rotaxane structure (Scheme 3.4).[16] Despite the steric ability to move freely, the presence of a secondary ammonium group

in the axle component strongly favoured the crown ether macrocycle to reside over this station through ammonium-ether hydrogen bonding interactions. However, upon the addition of the strong base 1,8-diazabicyclo[5.4.0]undec-7-ene (DBU), ammonium deprotonation causes the dibenzo-24-crown-8 macrocycle to shuttle to the cationic triazolium station axle site resulting in quenching of fluorescence of the 4-morpholin-naphthalimide stopper unit (Scheme 3.4). [16] The motion can be reversed through the introduction of trifluoroacetic acid (TFA).[16]




*Scheme 3.4. Acid induced switching of a bistable [1]rotaxane[16]*

Another functional [1]rotaxane was reported by Qu in 2014, which contained a central perylene bisimide core with two bis-stable [1]rotaxane arms, whose motion could furthermore be controlled using acid and base stimuli (Scheme 3.5).[10]




*Scheme 3.5. Acid-base switchable bis-branched [1]rotaxane*[10]

The MIM was once again formed *via* the self-threading of the macrocycle through ammonium-ether hydrogen bonding interactions followed by a stoppering CuAAC click reaction with the functionalised central core (Scheme 3.5). The dynamic shuttling behaviour of each crown ether macrocycle from the ammonium to triazolium stations was once again demonstrated to be

under reversible acid-base control and moreover affected the aggregation and thereby fluorescence of the central perylene bisimide core.[10]

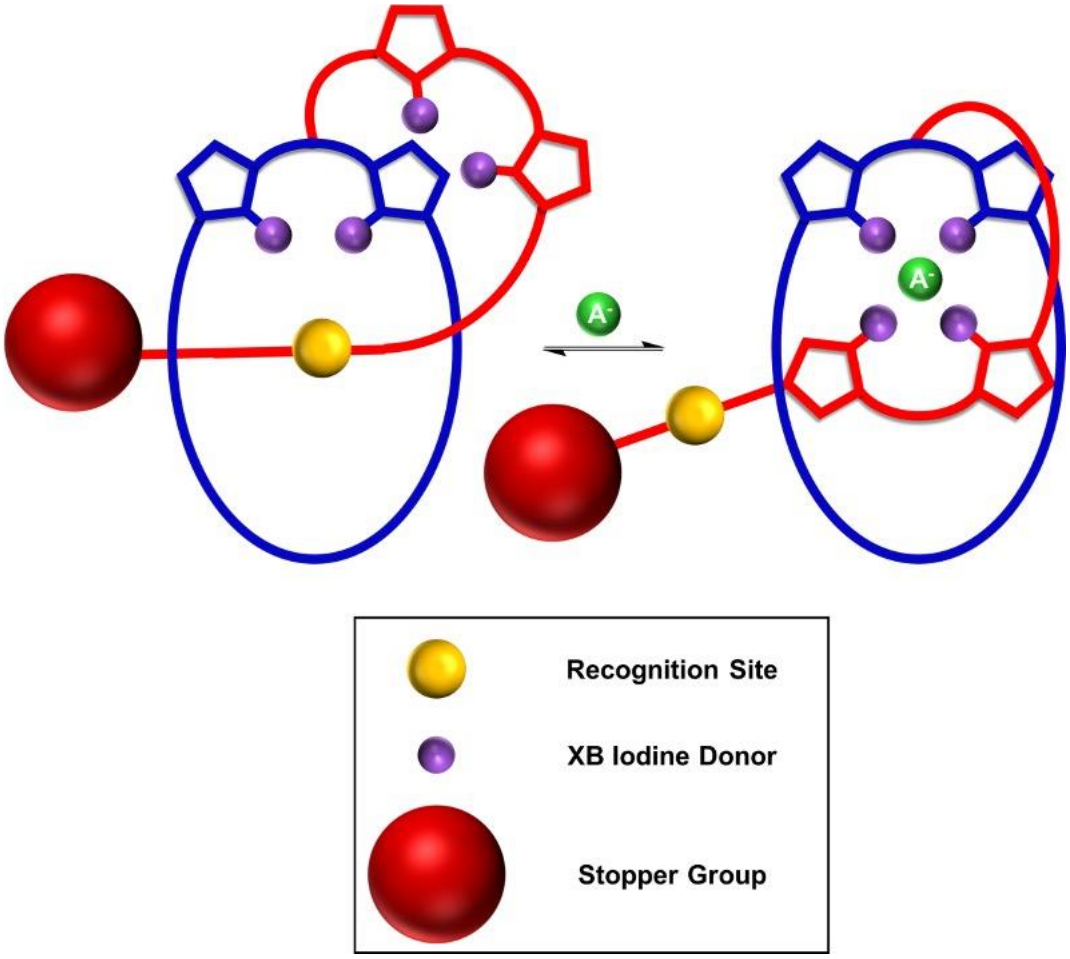
Examples of redox[17] and thermal energy[18] induced stimuli dynamic [1]rotaxanes have also been reported. However, to date the number of [1]rotaxanes reported in the literature remains limited, especially compared to the burgeoning examples of [2]rotaxanes.[17] Surprisingly, employing [1]rotaxane topology for host-guest recognition applications has not been investigated to any great extent and rarely has it been used to control motion in these systems.[1] This is presumably due to overcoming the synthetic challenge for constructing such functional [1]rotaxanes.

## 3.2 Project Aims

The aim of this project was to construct a XB [1]rotaxane for anion recognition applications. Specifically, a novel lasso-type XB [1]rotaxane was targeted that could exhibit dynamic shuttling behaviour upon anion recognition (Scheme 3.6).

As shown in Scheme 3.6, the lasso type XB [1]rotaxane was envisioned to contain a recognition site (shown as a yellow sphere), which would interact favourably with the macrocycle in the absence of a coordinating anion. This could, for example, be an electron deficient naphthalene diimide (NDI) motif, which would favourably interact with electron rich aromatic units incorporated into the macrocycle.[19] The MIM was furthermore envisioned to contain iodotriazole XB donor motifs on both the axle and macrocycle, here with the iodines depicted as purple spheres (Scheme 3.6). Upon the introduction of a coordinating anion, the macrocycle would translocate along the axle to cooperatively bind the anion *via* all four XB iodotriazole

units (Scheme 3.6). This controlled dynamic motion process would be reversible through the removal of the coordinating anion.



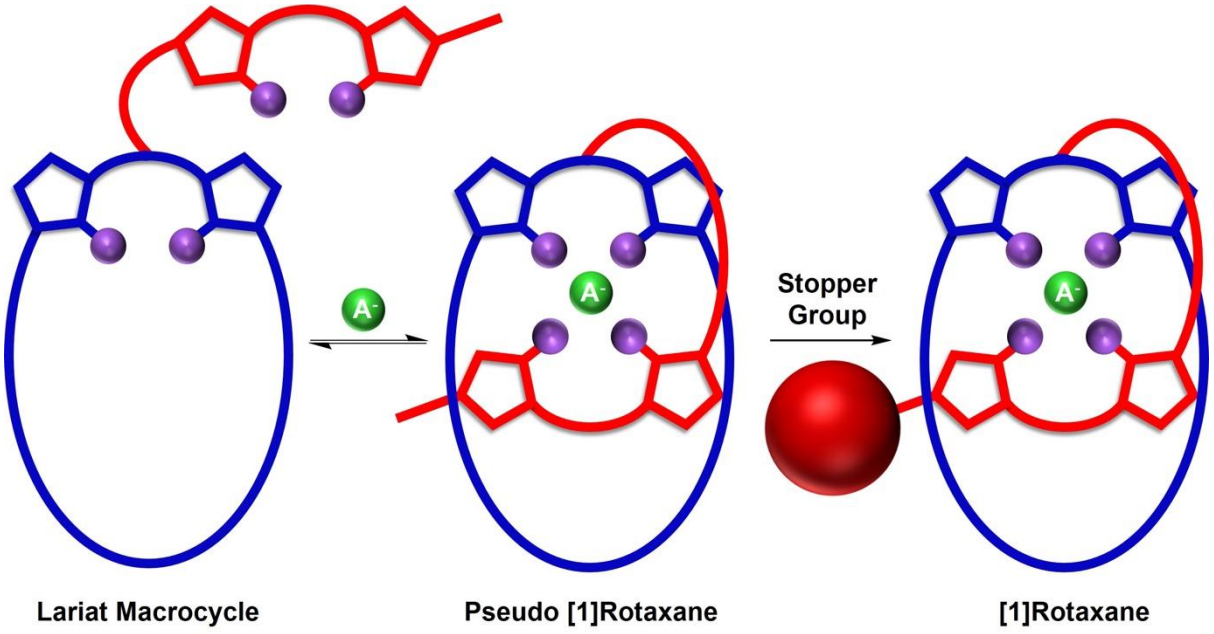

*Scheme 3.6. Schematic representation of target two-station lasso XB [1]rotaxane*

Initial investigations therefore focused on attempts to establish a viable synthetic route towards a [1]rotaxane topology employing either anion, cation, or active metal template methodologies.

## 3.3 Iodotriazole-Lariat Macrocycle for Pseudo [1]Rotaxane Investigation

A macrocycle which has been functionalised with an arm appenditure can be described as a lariat macrocycle (Scheme 3.7). As such, through the integration of appropriate recognition sites in the macrocycle and lariat arm components, a lariat macrocycle can be designed to undergo self-threading upon anion or cation templation and thereby serve as a potential precursor for

(pseudo) [1]rotaxane assembly (Scheme 3.7). Following the self-threading, a stoppering reaction can be performed resulting in the formation of a [1]rotaxane (Scheme 3.7).




*Scheme 3.7. Schematic representation of a lariat macrocycle forming a pseudo [1]rotaxane upon anion recognition followed by a stoppering reaction for the formation of a [1]rotaxane. With purple spheres representing XB donor motifs.*

The incorporation of ambidentate iodotriazole motifs into the macrocycle and lariat axle units allows for the recognition of both anions and cations *via* the heterocycle's Lewis acidic XB donor iodine atoms and Lewis basic nitrogen triazole donors respectively. Therefore, cooperative binding of either an anion or cation template coordinating species through both the macrocycle and axle triazole motifs could potentially be used for self-threading pseudo[1]rotaxane formation (Scheme 3.7).

### 3.3.1 Pseudo [1]Rotaxane Design Strategy

The initial design for the formation of a pseudo [1]rotaxane was based on a previously reported XB [2]rotaxane, which exploits the ambidentate nature of a secondary amine bis-iodotriazole motif incorporated into the macrocycle and axle components (Figure 3.2).[20] The neutral

rotaxane was shown to bind zinc (II) metal cations in an orthogonal pseudo six-coordinate octahedral meridian (mer) isomer fashion *via* the tridentate Lewis basic triazole nitrogen- and secondary amine nitrogen donors of the macrocycle and axle (Figure 3.2).[20] Conversely the dicationic protonated rotaxane strongly bound chloride through concerted XB and charge assisted HB interactions (Figure 3.2).[20]

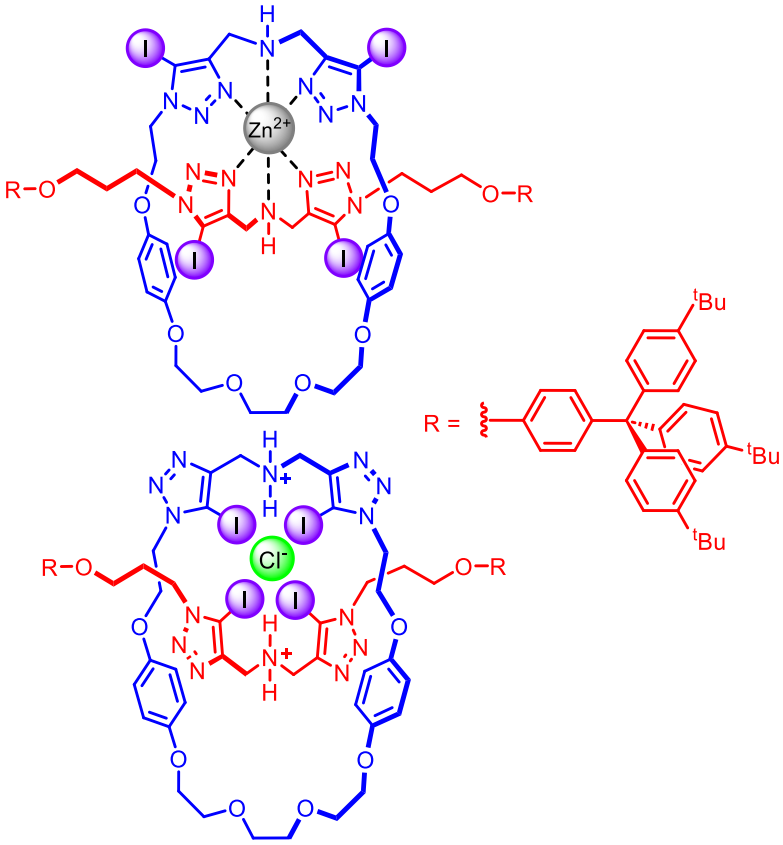



*Figure 3.2. [2]Rotaxane capable of cation and anion binding*

It was therefore envisioned that appending an appropriate bis-iodotriazole functionalised lariat arm on to the secondary amine functional group of the bis-iodotriazole containing macrocycle component would facilitate cation template, or upon protonation, anion template pseudo [1]rotaxane assembly threading through the macrocycle cavity.

Two lariat macrocycle molecules were targeted initially that contained a lariat arm linked *via* 'long' and 'short' methylene groups depicted in Figure 3.3. The long-armed lariat macrocycle

**LM-2** was predicted to be capable of pseudo [1]rotaxane formation *via* anion or metal cation templation whereas this would not be possible using short lariat macrocycle **LM-1**, which would serve as a control.

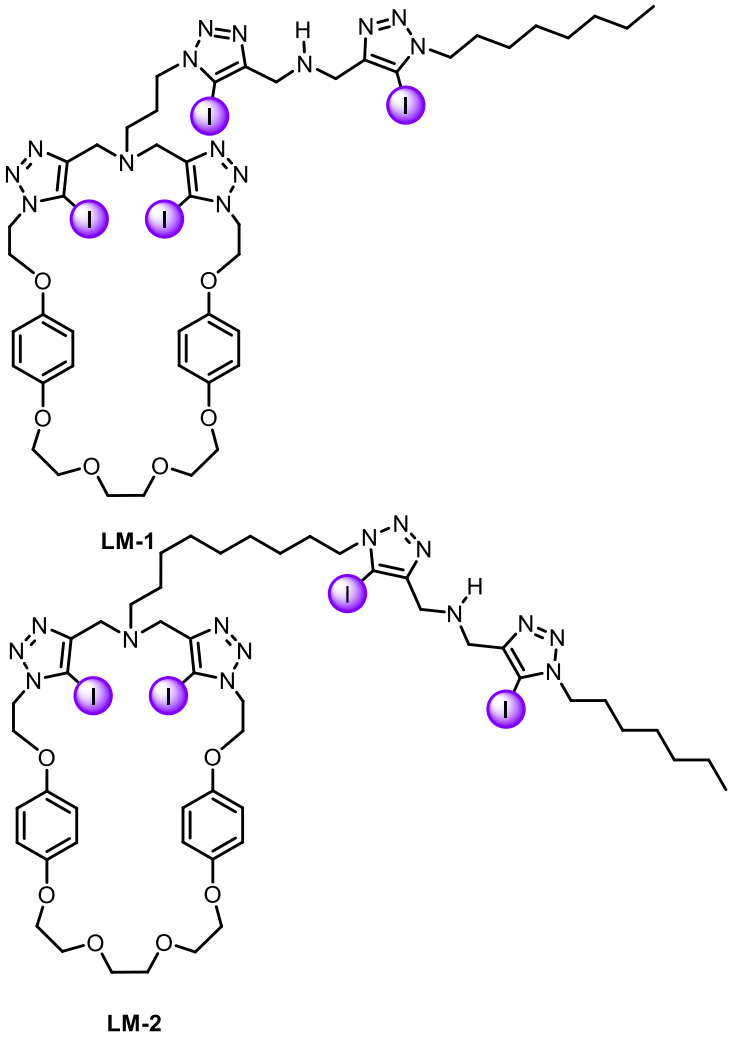
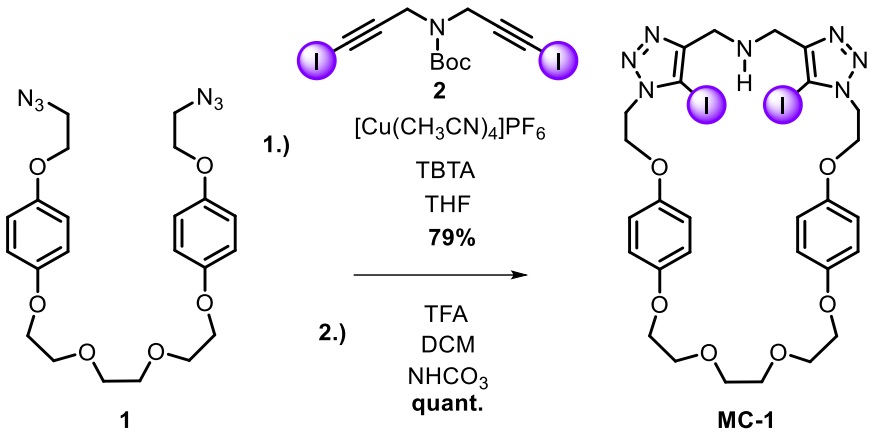



*Figure 3.3. Target lariat macrocycles with either short (top) or long (bottom) lariat arm*

### 3.3.2 Synthesis of Lariat Macrocycles

Macrocycle **MC-1** was synthesised according to a previously reported CuAAC mediated macrocyclization reaction.[20] *N*-Boc-protected bis-iodoalkyne **2** was reacted with equimolar amounts of the bis-azide **1** under high-dilution conditions in the presence of $Cu(MeCN)_4PF_6$ and the Cu(I) stabilising ligand TBTA to give the *N*-Boc protected macrocycle *via* CuAAC reaction in 79% yield after chromatographic purification. Subsequent *N*-Boc deprotection using

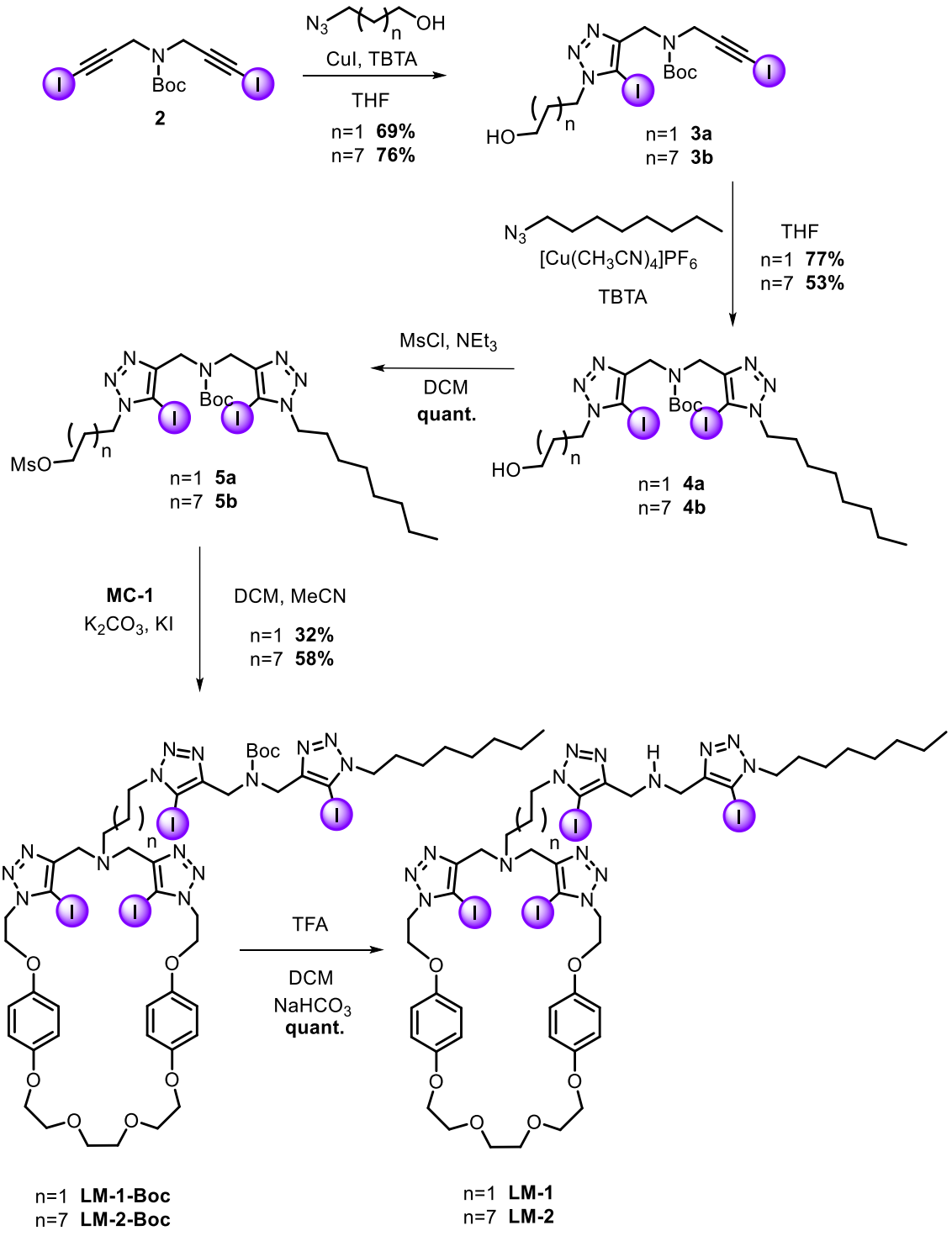
trifluoroacetic acid (TFA) gave quantitative conversion to **MC-1** following neutralisation by washing with an aqueous solution of sodium hydrogencarbonate (Scheme 3.8).




*Scheme 3.8. Macrocycle **MC-1** synthesis*

The synthesis of the requisite mesylate functionalised lariat arms was achieved according to Scheme 3.9.

Five equivalents of *N*-Boc-protected bis-iodoalkyne **2** were reacted with one equivalent of 3-azido-propan-1-ol and 9-azido-1-nonanol respectively to afford iodotriazole iodo-alkynes **3a** in 69% and **3b** in 76% yields after silica gel column chromatography. Compounds **3a** and **3b** were again subjected to CuAAC conditions with octyl-azide to give products **4a** in 77% and **4b** in 53% yield after chromatographic purification. The terminal alcohols were subsequently converted to the corresponding mesylates **5a** and **5b**.




*Scheme 3.9. Lariat macrocycle **LM-1** and **LM-2** synthesis*

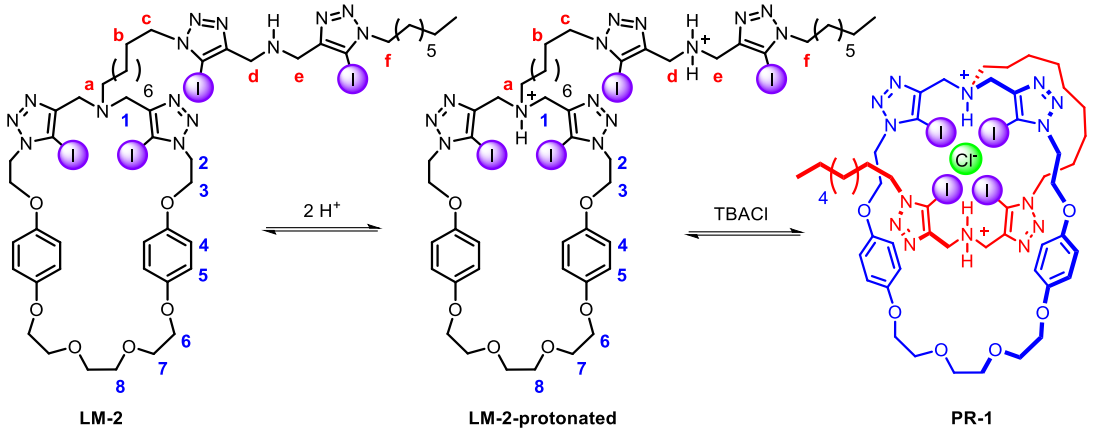
The lariat arms were attached to the central Lewis basic amine of the macrocycle *via* treatment of **MC-1** with the mesylated components **5a** and **5b** in mixtures of $CH_2Cl_2$ and acetonitrile in the presence of $K_2CO_3$. The reaction mixtures were heated at 70°C for two days and the

resulting *N*-Boc protected lariat macrocycles were purified by silica gel column chromatography to afford the lariat macrocycles **LM-1-Boc** and **LM-2-Boc** in 17% and 58% respective yield. Deprotection of the *N*-Boc group using trifluoroacetic acid afforded the target lariat macrocycle **LM-2** in 98% yield after neutralising the molecule using sodium hydrogen carbonate. For **LM-1** further purification by preparative TLC was required following deprotection to afford the target molecule in 65% yield. Both lariat macrocycles were fully characterised by $^{1}$H and $^{13}$C-NMR and high-resolution ESI mass spectrometry.

## 3.4 $^{1}$H-NMR Pseudo [1]Rotaxane Assembly Investigation *via* Anion Templation

With the target lariat macrocycles in hand attention turned to investigating whether pseudo [1]rotaxane interpenetrated assembly would occur *via* an anion template protocol involving initial protonation and subsequent introduction of a chloride anion template (Scheme 3.10). A preliminary $^{1}$H-NMR study was therefore performed in acetone-$d_6$ (Figure 3.4).

Both the secondary and tertiary amine motifs of **LM-2** were protonated using two equivalents of tetrafluoroboric acid ($HBF_4$) diethyl ether complex and the $^{1}$H-NMR spectrum of the doubly protonated species recorded (Figure 3.4). Downfield shifts were observed for the macrocycle methylene protons **1** and methylene protons **d** and **e** of the lariat arm, which also broadened substantially, consistent with protonation of both amine sites.




*Scheme 3.10. Proposed formation of pseudo [1]rotaxane **PR-1** via chloride templation*

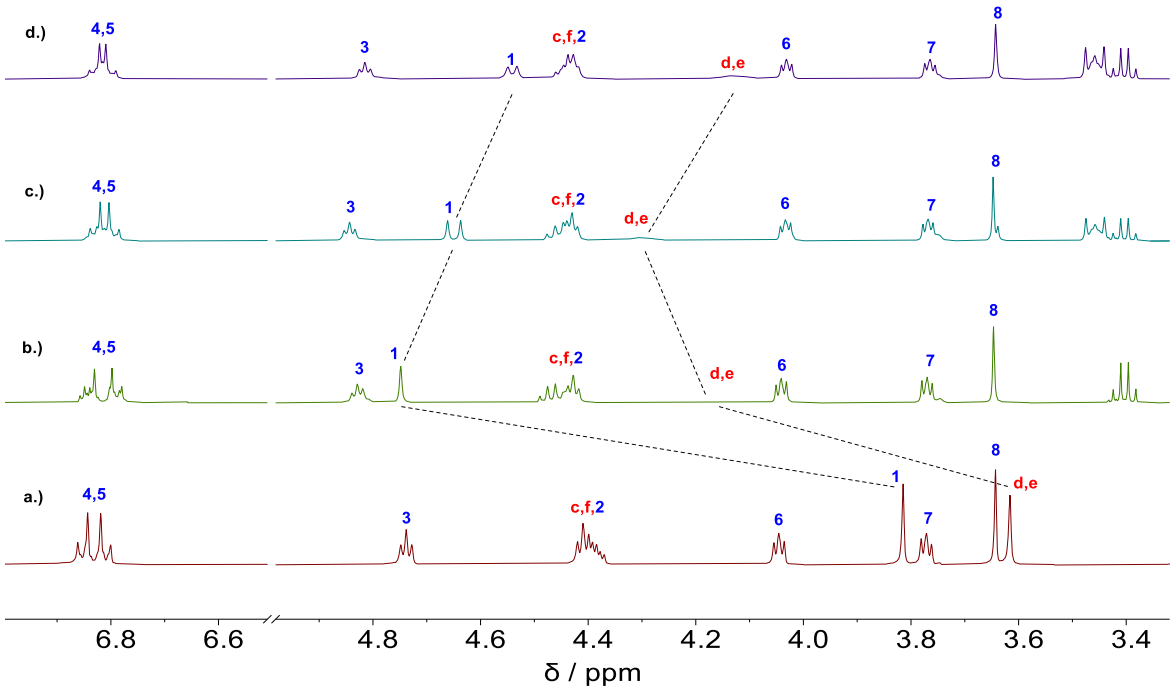



*Figure 3.4. Partial $^{1}$H-NMR spectra of a.) neutral and b.) doubly protonated **LM-2** and upon a further addition of c.) 0.5 and d.) 1.0 equivalents of TBACl (acetone-$d_6$, 298K, 500MHz)*

Upon addition of 0.5 equivalents of tetrabutylammonium chloride (TBACl) to the doubly protonated **LM-2**, several dramatic perturbations in chemical shift environments were observed. Namely, peak **1** shifted upfield and split into a doublet and the broad peak corresponding to protons **d** and **e** experienced a small shift downfield. A further 0.5 equivalents of TBACl were added, which caused further upfield shifting of signal **1** culminating in a total

0.2 ppm perturbation. Lariat arm methylene signal **d** and **e** remained broad and shifted upfield by 0.18 ppm. The splitting of peak **1** may be explained by the different chemical environments of the $CH_2$ protons, with one pointing towards the lariat arm and the other one pointing away (Figure 3.6). The splitting of signal **1** is also indicative of a rigidification of the structure upon halide binding. Furthermore, the shifts of methylene protons **d** and **e** are presumed to be due to significant conformational changes upon anion coordination which is consistent with cooperative XB-mediated recognition of the chloride template guest species.

A 2D-$^1$H-$^1$H ROESY NMR spectrum (Figure 3.5) was undertaken in an effort to elucidate the topology of the chloride complexed species.

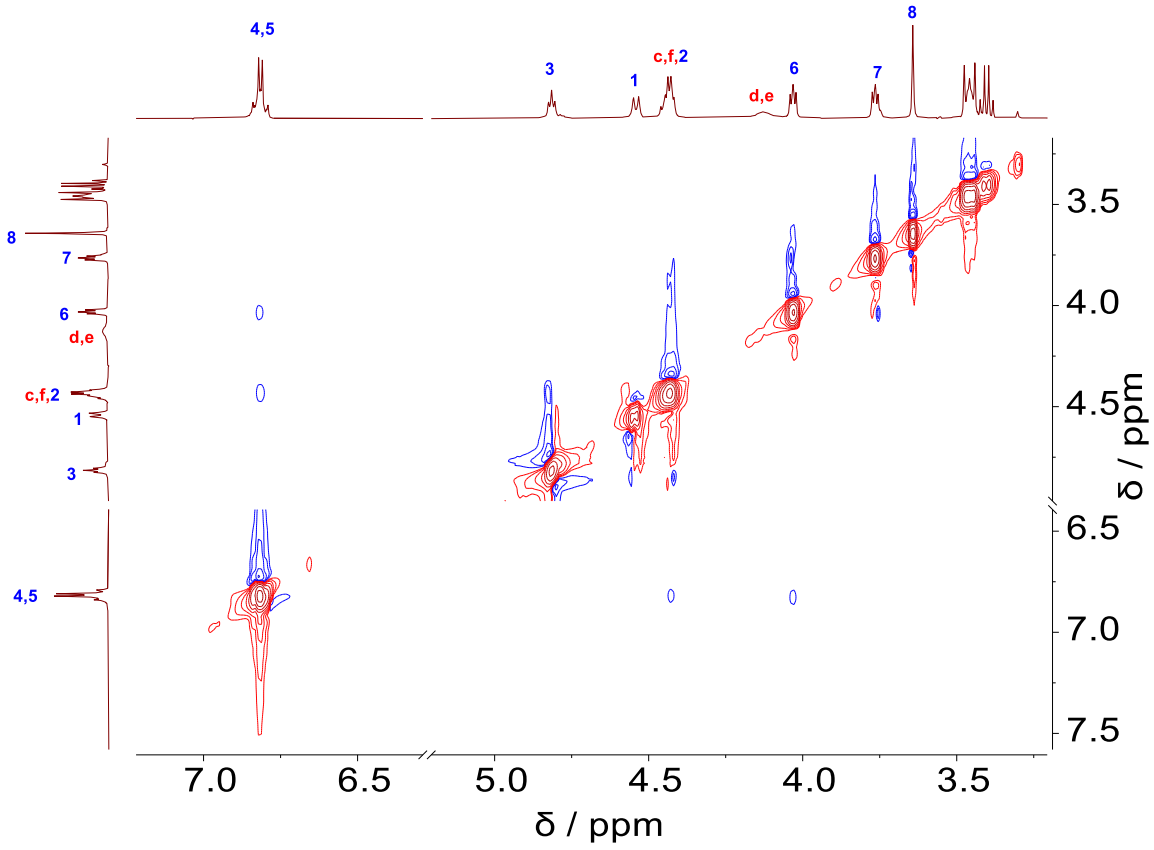



*Figure 3.5. 2D-$^1$H-$^1$H ROESY NMR spectrum of doubly protonated LM-2 with 1 eq. TBACl (acetone-$d_6$, 298K, 500MHz)*

Interestingly, no clear cross-peaks were observed between signals corresponding to the macrocycle or lariat arm suggesting that chloride binding may be occurring in an exotopic coordination mode as depicted in Figure 3.6.

Attempts to perform a control $^{1}$H NMR study with **LM-1**, which would be incapable of threading due to the short lariat arm, were unfortunately precluded by poor solubility of the smaller lariat macrocycle in acetone-$d_6$. $^{1}$H NMR studies in other solvents were not attempted as a change in solvent would preclude direct comparison to the previously performed **LM-2** study.

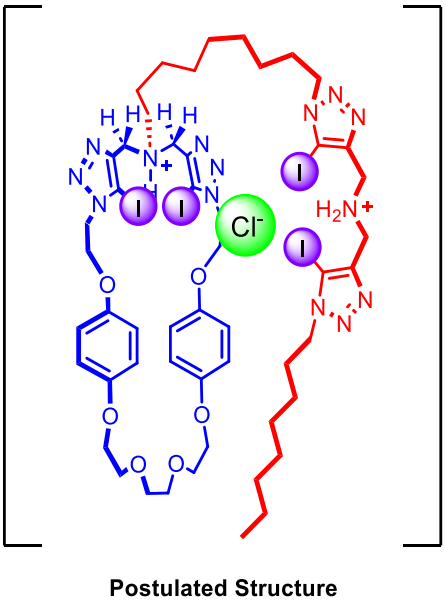
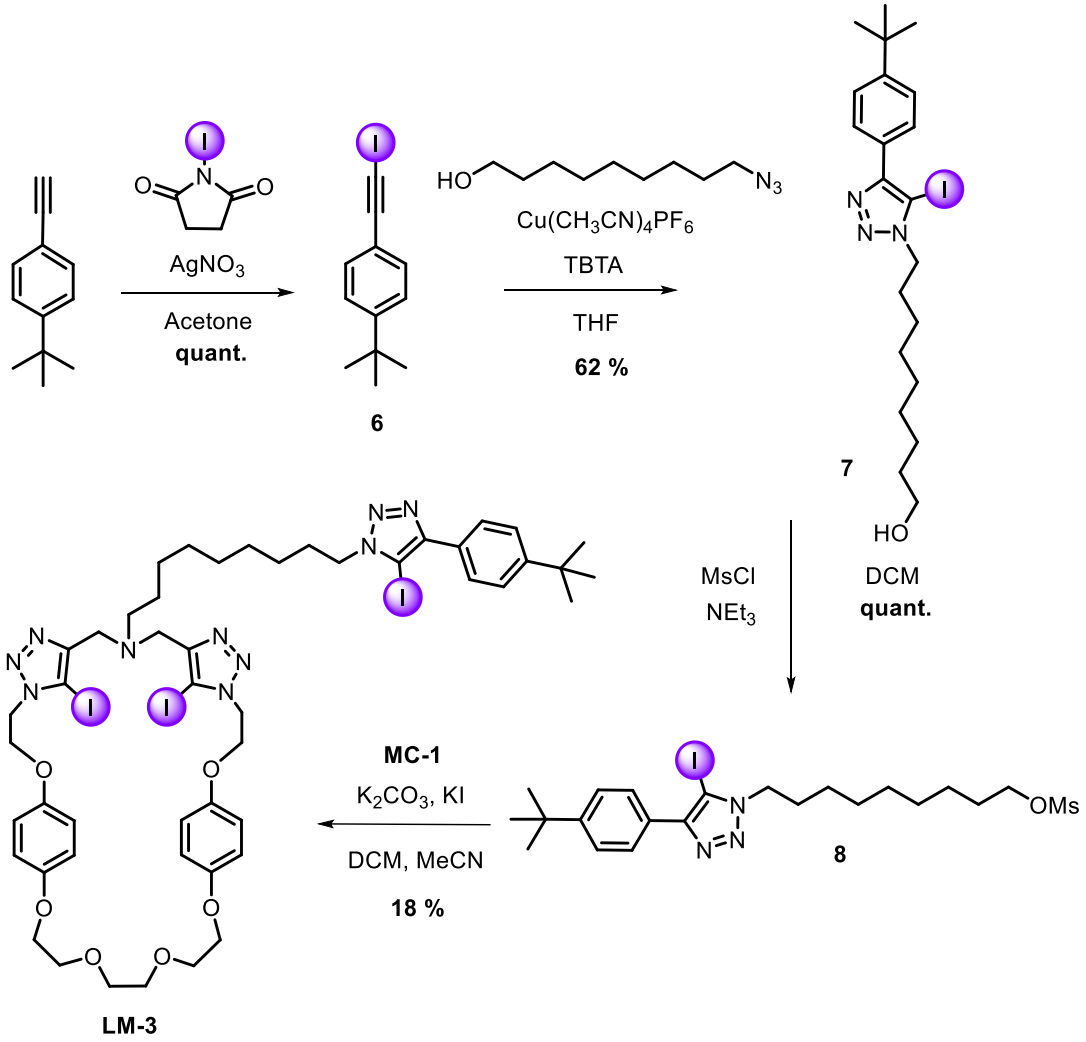



*Figure 3.6. Postulated chloride binding mode by doubly protonated **LM-2***

### 3.4.1 Modified Iodotriazole-Lariat Macrocycle

A new synthetic target **LM-3** containing the same macrocycle but only one iodotriazole motif on the lariat arm was synthesised to reduce the potential steric demand of intramolecular self-threading of multiple XB donor groups (Scheme 3.11). In addition, the terminal *tert*-butyl-phenyl motif on the arm would enable diagnostic chemical shift perturbations associated with pseudo [1]rotaxane formation to be identified using $^{1}$H-NMR.

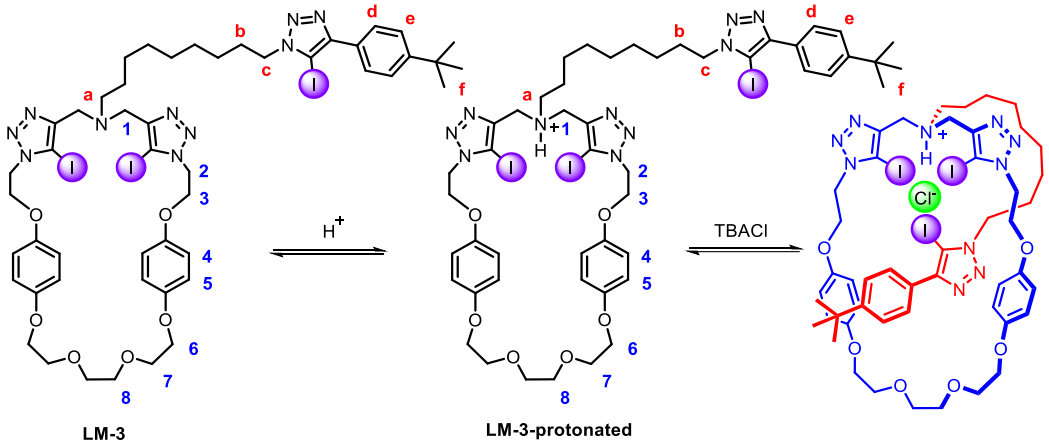
To this end, commercially available 4-*tert*-butylphenylacetylene was iodinated using N-iodosuccinimide. Product **6** was subjected to a CuAAC click reaction with 9-azido-1-nonanol to give iodotriazole **7** in 62% yield following chromatographic purification. The terminal alcohol was converted to the corresponding mesylate **8**. **LM-3** was obtained through the alkylation reaction of **MC-1** with mesylate **8** in a modest yield of 18% after silica gel flash column chromatography (Scheme 3.11). The lariat macrocycle was fully characterised by $^{1}H$ and $^{13}C$-NMR and high-resolution ESI mass spectrometry.




*Scheme 3.11. Synthesis of lariat macrocycle* ***LM-3***

### 1.1.1.1 $^{1}$H-NMR Pseudo [1]Rotaxane Assembly Investigation *via* Anion Templation

An analogous $^{1}$H NMR anion template pseudo [1]rotaxane assembly investigation was undertaken with lariat macrocycle **LM-3** (Scheme 3.12).




*Scheme 3.12. Proposed formation of pseudo [1]rotaxane **PR-3** via chloride templation*

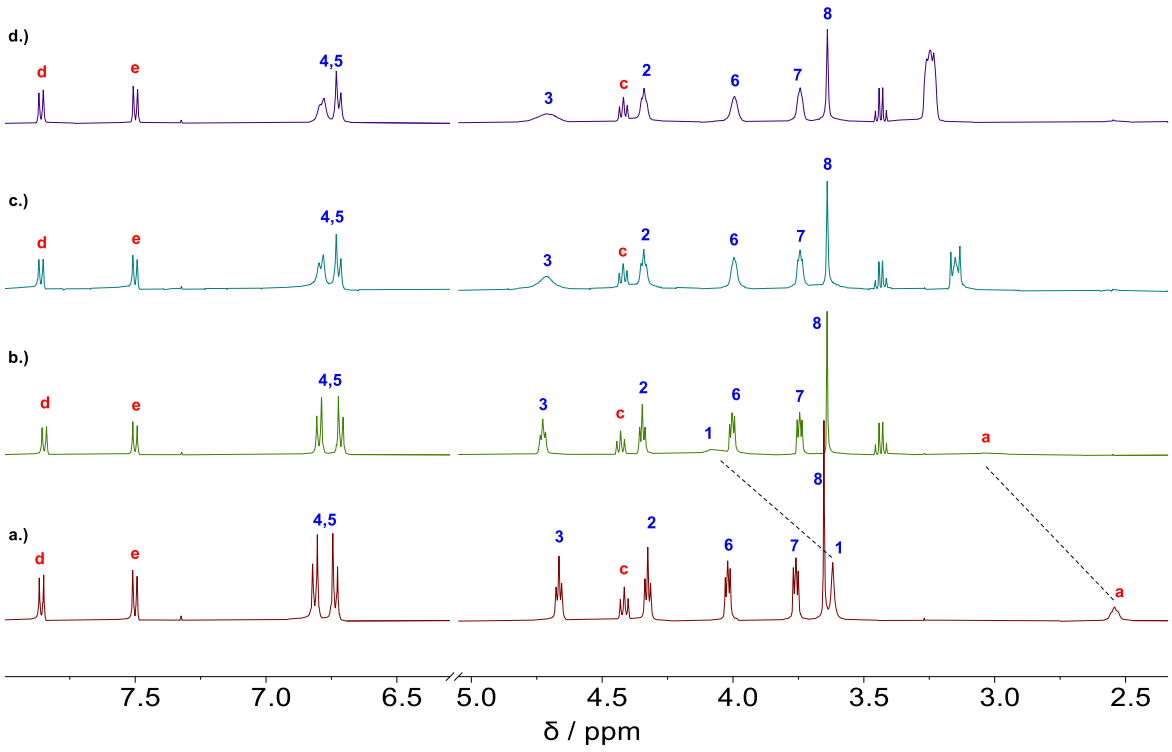



*Figure 3.7. Partial $^{1}$H-NMR spectra of a.) neutral and b.) protonated **LM-3**, and upon a further addition of c.) 0.5 and d.) 1.0 equivalents of TBACl ($CD_2Cl_2$, 298K, 500MHz)*

Upon protonation of **LM-3** with one equivalent of $HBF_4$ (Figure 3.7), a significant downfield shift and broadening of the methylene protons **1** and **a** adjacent to the site of protonation was observed consistent with the formation of the cationic species. Following the addition of 0.5 and 1 equivalents of TBACl chloride, both peaks **1** and **a** broadened to the point where they could no longer be observed clearly in the spectra. Notably, all proton peaks belonging to the macrocycle also broadened whereas the proton signals of the lariat arm remained sharp and unperturbed (Figure 3.7). As can be seen in Figure 3.7, phenyl protons d and e as well as methylene protons c do not experience any change in shift or shape indicating that they are not involved in the halide binding process. Methylene protons b overlap with the water peak and cannot be clearly identified in the spectrum.

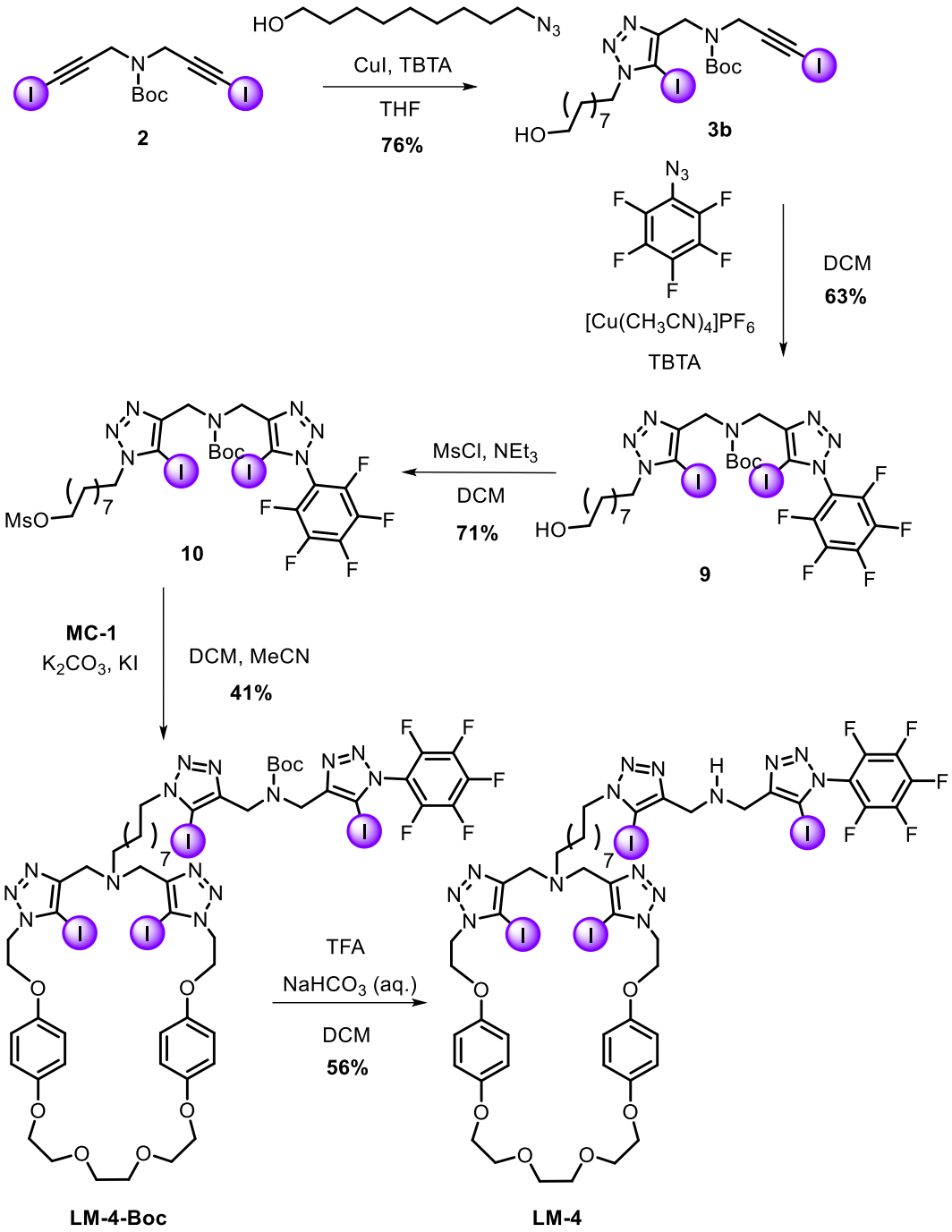
Hence, as expected, no evidence for the formation of a pseudo [1]rotaxane assembly could be found in the corresponding $^{1}H$-$^{1}H$ ROESY NMR spectrum. This suggested a stronger XB donor anion-binding motif would be needed on the lariat arm to facilitate the formation of a pseudo [1]rotaxane through anion templation.

### 3.4.2 Pentafluorophenyl-Lariat Macrocycle

Recently it has been demonstrated that appending strongly electron withdrawing aryl groups to the iodotriazole motif dramatically improves its XB donor potency.[21] Taking this into account a pentafluorophenyl group was incorporated into the lariat arm design (Scheme 3.13).

The synthesis for the pentafluorophenyl containing lariat arm is summarised in Scheme 3.13. Iodo-alkyne **3b** was reacted with pentafluorophenyl azide under CuAAC click conditions to form **9** in 62% yield following silica gel flash column chromatography. The primary alcohol was subsequently converted into the corresponding mesylate **10** in 72% yield. **LM-4-Boc** was

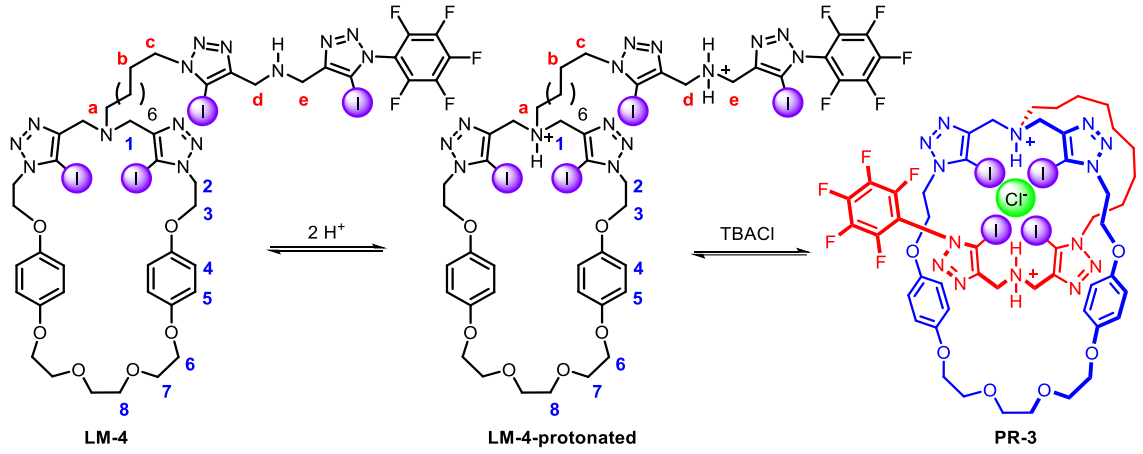
obtained through alkylation of **MC-1** with mesylate **10** in 41% yield after silica gel flash column chromatography. Deprotection of **LM-4-Boc** using TFA afforded **LM-4** in 56% yield after neutralisation using sodium hydrogencarbonate and purification by preparative TLC. The lariat macrocycle was fully characterised by $^{1}H$ and $^{13}C$-NMR and high-resolution ESI mass spectrometry.




*Scheme 3.13. Synthesis of pentafluorophenyl lariat macrocycle **LM-4***

### 3.4.2.1 $^{1}$H-NMR Pseudo [1]Rotaxane Assembly Investigation *via* Anion Templation

A preliminary $^{1}$H-NMR study was performed to investigate whether **LM-4** would form pseudo [1]rotaxane **PR-3** upon protonation and subsequent introduction of a chloride anion template (Scheme 3.14).




*Scheme 3.14. Proposed formation of pseudo [1]rotaxane **PR-3** via chloride anion templation*

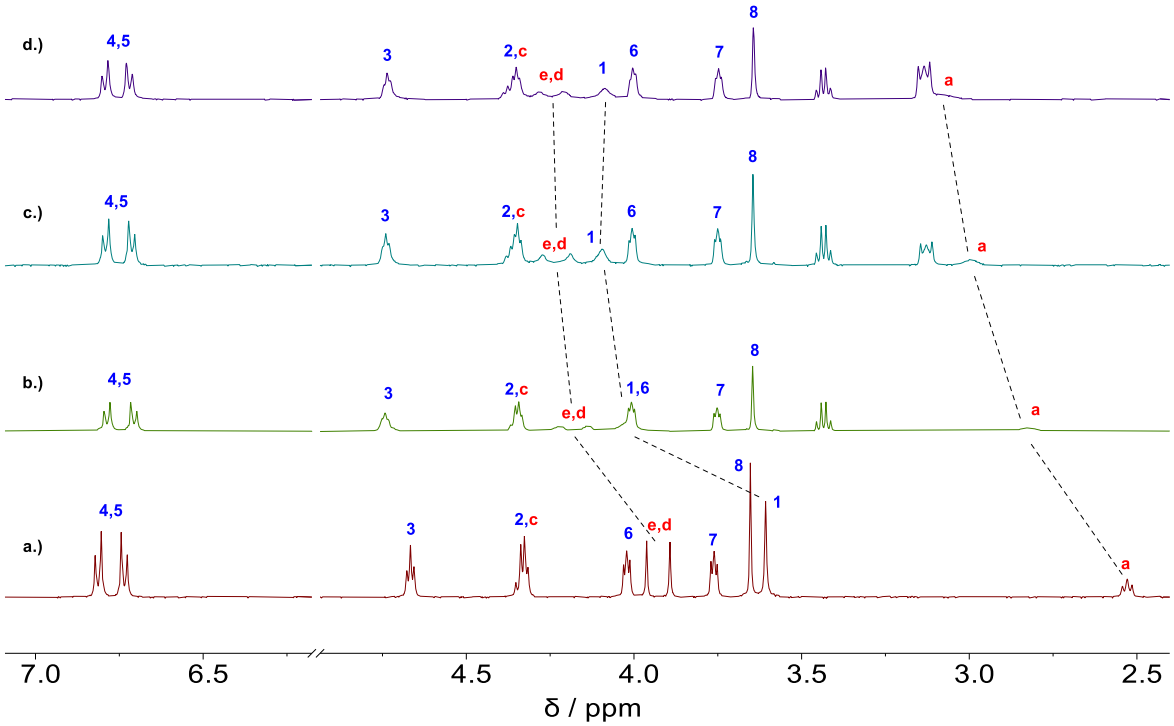



*Figure 3.8. Partial $^{1}$H-NMR spectra of a.) neutral and b.) doubly protonated **LM-4**, and upon a further addition of c.) 0.5 and d.) 1.0 equivalents of TBACl ($CD_2Cl_2$, 298K, 500MHz)*

These studies were performed in dichloromethane-$d_2$ due to the non-competitive nature of the solvent and enhanced solubility of the receptor in this solvent over acetone-$d_6$.[22] Both the secondary and tertiary amine motifs of **LM-4** were protonated using two equivalents of $HBF_4$ acid diethyl ether complex (Figure 3.8). As observed with **LM-2**, downfield shifts in the $^1$H-NMR spectrum were observed for the methylene protons **1** adjacent to the tertiary amine on the macrocycle and the methylene protons **d** and **e** adjacent to the secondary amine on the lariat arm. The peaks for protons **d**, **e** and **1** also broadened substantially. This provides strong evidence that both amines had been protonated.

Upon addition of 0.5 equivalents of tetrabutylammonium chloride (TBACl), peak **1** shifted downfield while remaining broad (Figure 3.8). The broad peaks corresponding to protons **d** and **e** also experienced a slight downfield shift. A further 0.5 equivalents of TBACl were added. Peak **1** shifted slightly upfield. Peak **d** and **e** remained very broad and shifted further downfield. Unlike for **LM-2** (Figure 3.4), the peak for protons **1** did not split and remained broad. The shifts of the methylene protons **d** and **e** are presumed to be due to conformational changes upon halide anion coordination. Overall, the chemical shift perturbations of proton signal peaks **1**, **d** and **e** indicate macrocycle-lariat arm cooperative binding of $Cl^-$ in the vicinity of the XB donor groups (Figure 3.9).

As observed for previous $^1$H-NMR pseudo [1]rotaxane assembly investigations *via* anion templation, a 2D-$^1$H-$^1$H ROESY NMR spectrum was recorded to elucidate the topology of the chloride complexed species. However, no clear cross-peaks were observed between signals corresponding to the macrocycle or lariat arm once again suggesting that chloride binding may be occurring in an exotopic coordination mode as shown in Figure 3.9.

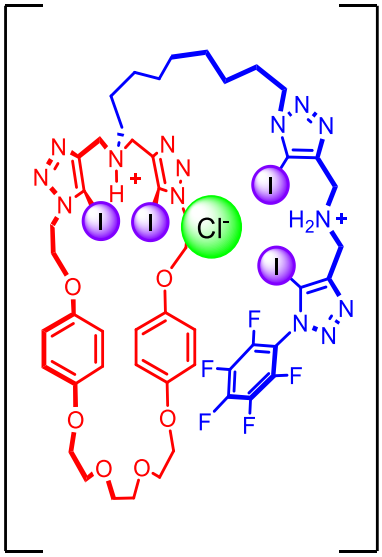
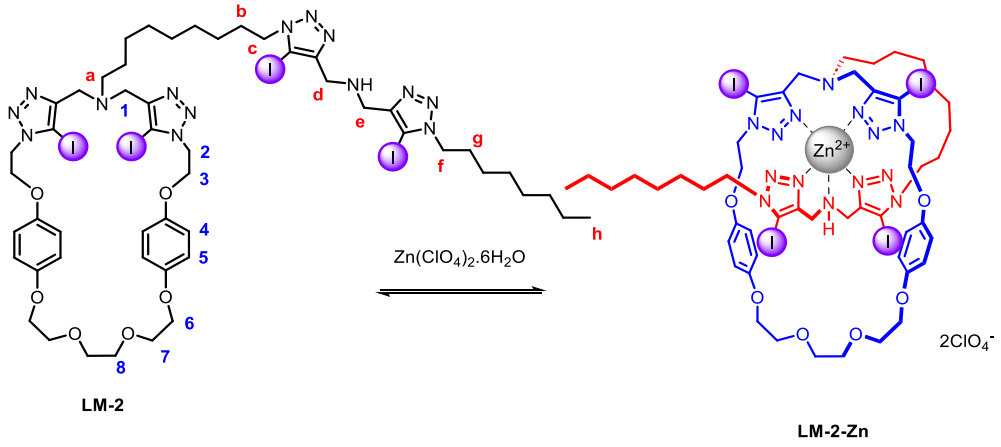


*Figure 3.9. Postulated chloride binding mode by doubly protonated **LM-4***

## 3.5 Metal Cation Template Pseudo[1]Rotaxane Assembly Investigation

### 3.5.1 $^{1}$H-NMR Study of Zinc(II) Complexation

The previously reported [2]rotaxane (Figure 3.2) was demonstrated to complex a zinc(II) cation through the nitrogen donor atoms of the bis-iodotriazole secondary amine units on both the axle and macrocycle.[20] It was therefore envisioned that a pseudo[1]rotaxane assembly may form through zinc(II) cation templation (Scheme 3.15).




*Scheme 3.15. Proposed zinc complexation of **LM-2***

Hence, an equimolar mixture of $Zn(ClO_4)_2 \cdot 6H_2O$ in methanol and **LM-2** in $CH_2Cl_2$ was stirred for one hour at room temperature. After the removal of the solvent mixture, the off-white solid residue was re-dissolved in a 1:1 mixture of $CDCl_3$ and acetonitrile-$d_3$.

A comparison of the $^1$H-NMR spectra revealed the proton peaks for the zinc(II)-complex to be broad compared to **LM-2** (Figure 3.10). In addition, the methylene protons next to the two central amines on both the arm and macrocycle have shifted. Peak **1**, which corresponds to the methylene protons on the macrocycle showed the greatest change in the spectra with a downfield shift of 1.56 ppm (Figure 3.10).

The lariat methylene protons **d** and **e** have shifted significantly upfield by 0.29 ppm. The hydroquinone proton signals have also shifted slightly upfield. Notably, the perturbation of macrocycle methylene protons **1** is similar to the shifts observed for the zinc(II)-complexed [2]rotaxane.[20]

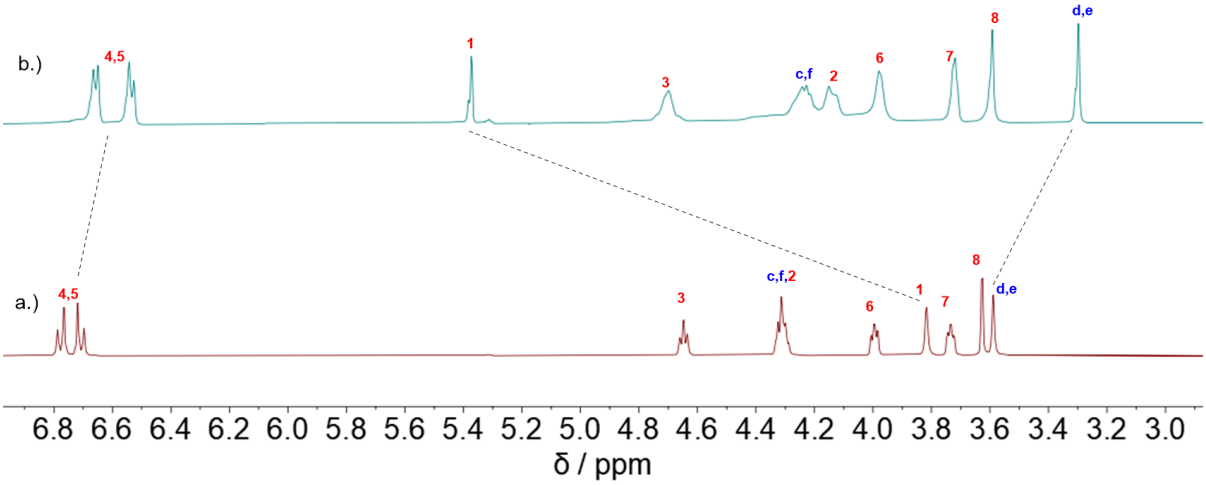
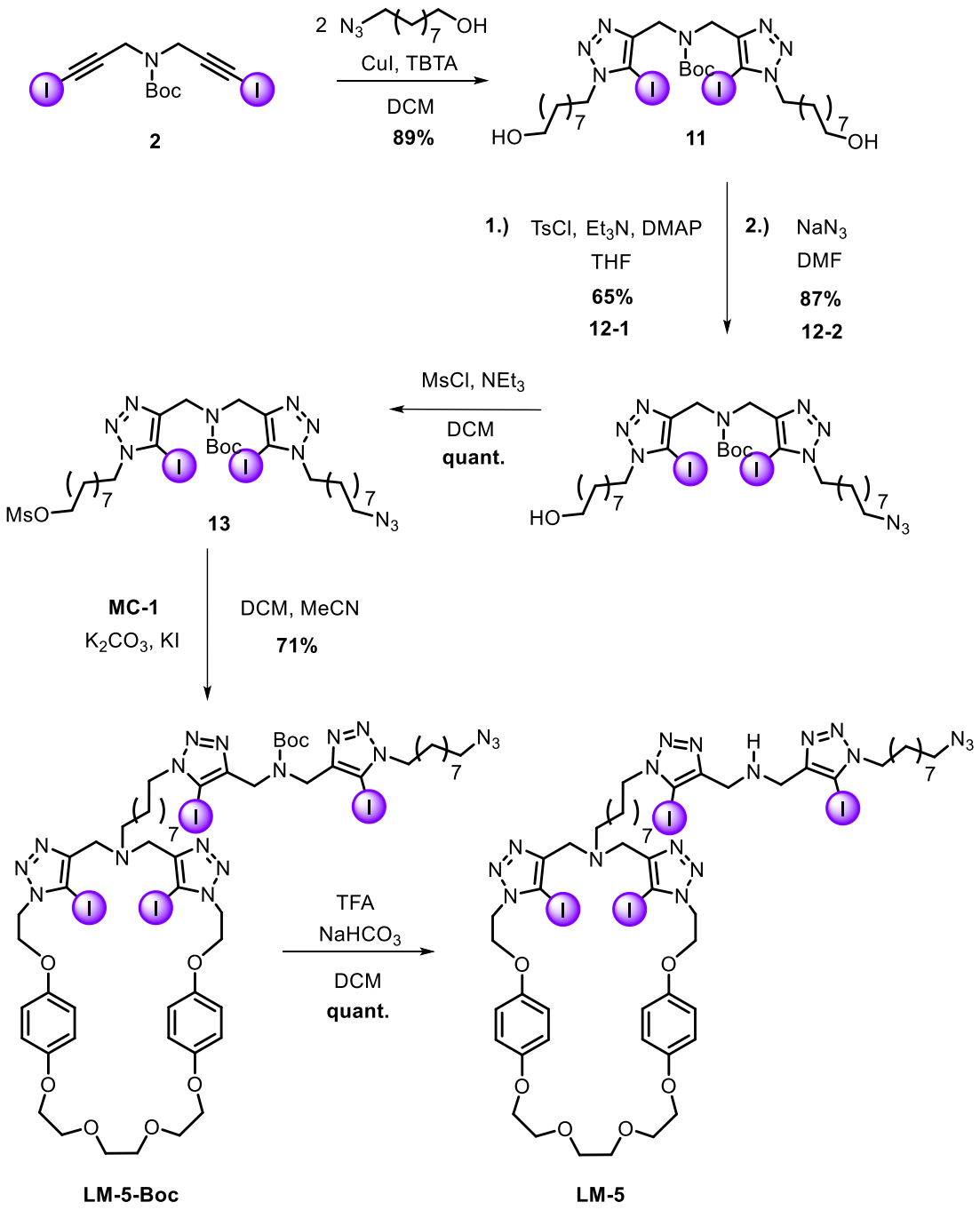



*Figure 3.10. Zinc(II) complexation of **LM-2** in 1:1 $CDCl_3$:acetonitrile-$d_3$, 298K, 500MHz with a.) **LM-2** b.) **LM-2** with 1 equivalent of $Zn(ClO_4)_2.6H_2O$*

Despite $^1$H-NMR providing evidence of successful complexation, the 2D $^1$H-$^1$H ROESY NMR spectrum of the zinc (II)-LM-2 complex displayed no crosspeaks between the arm and macrocycle indicative of pseudo [1]rotaxane formation.

### 3.5.2 Attempts to prepare a [1]Rotaxane *via* Zinc(II) Templation

Undeterred by the inconclusive $^1$H NMR observations above, attempts were made to prepare a [1]rotaxane *via* a zinc(II) template stoppering reaction. This required the initial synthesis of a new azide appended lariat macrocycle (Scheme 3.16).

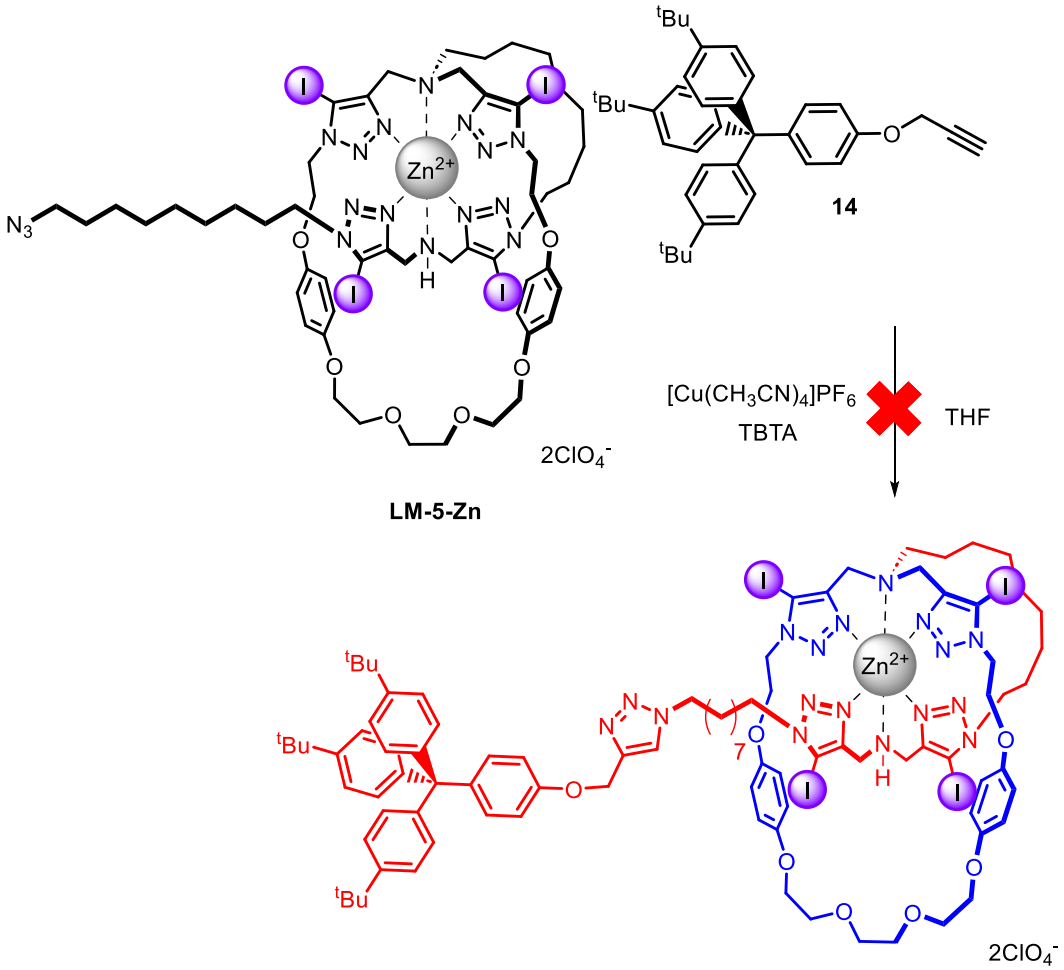



*Scheme 3.16. Synthesis of azide appended lariat macrocycle* ***LM-5***

A CuAAC click reaction between one equivalent of the *N*-Boc-protected bis-iodoalkyne **2** and 2.4 equivalents of 9-azido-1-nonanol gave the bis-iodotriazole product **11** in 86% yield after chromatographic purification. One and a half equivalents of **11** were dissolved in dry, degassed THF together with 1.5 equivalents of triethylamine and a catalytic amount of DMAP. A solution of 1 equivalent of *p*-toluenesulfonyl chloride in dry, degassed THF was added dropwise and the resulting mixture stirred for 2 days to afford the mono-tosylated product **12.1** in 65% yield, which could be isolated from the bis-tosylated side product using silica gel flash column chromatography. For the conversion of the tosyl group into the corresponding azide, **12.1** was dissolved in a small amount of DMF and stirred together with sodium azide. The monofunctionalised azide compound **12-2** was isolated in 87% yield following an aqueous workup. With the monofunctionalised azide in hand, the terminal alcohol of **12-2** was converted to the corresponding mesylate **13** through dropwise addition of a methanesulfonyl chloride solution in dry, degassed $CH_2Cl_2$ to a $CH_2Cl_2$ mixture of the precursor **12-2** and triethylamine. Mesylate product **13** was isolated in 49% yield following chromatographic purification. Alkylation of **MC-1** with the mesylated compound **13** proceeded in a mixture of acetonitrile and $CH_2Cl_2$ with $K_2CO_3$ as a mild base to afford **LM-5-Boc** in 71% following purification by silica gel flash column chromatography. The lariat arm of **LM-5-Boc** was *N*-Boc-deprotected using TFA and neutralised by washing with an aqueous solution of sodium hydrogen carbonate to give **LM-5**, which was fully characterised using $^{1}H$ and $^{13}C$-NMR spectroscopy and high-resolution ESI mass spectrometry.

The potential terphenyl stopper-alkyne motif **14** (Scheme 3.17) was prepared according to a literature procedure through the functionalisation of 4-[tris-(4-*tert*-butyl-phenyl)-methyl]-phenol with propargyl bromide.[23]

For the attempted zinc(II) template stoppering reaction to produce the target [1]rotaxane, **LM-5** was initially complexed with zinc(II) *via* the addition of an equimolar amount of $Zn(ClO_4)_2{\cdot}6H_2O$ in methanol to **LM-5** in $CH_2Cl_2$. The mixture was stirred for one hour to ensure complexation followed by the removal of the solvent.

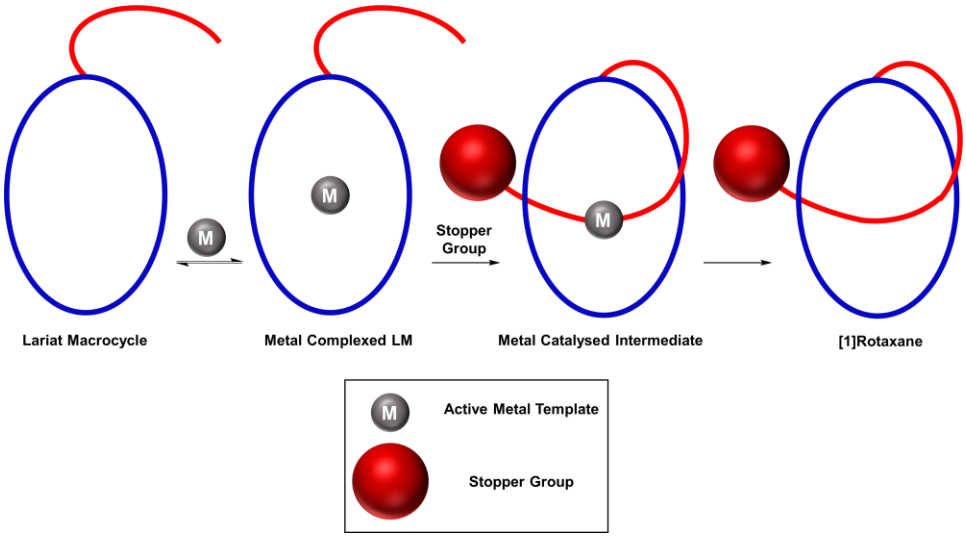



*Scheme 3.17. Attempted formation of [1]rotaxane using zinc complexation*

The **LM-5-Zn** complex was then dissolved in dry THF and added to a mixture of $[Cu(CH_3CN)_4]PF_6$ and TBTA, as well as the stopper alkyne **14** (Scheme 3.17). The resulting reaction mixture was stirred under a nitrogen atmosphere and monitored by TLC and low-resolution mass spectrometry. Unfortunately, even after allowing the mixture to stir for 7 days, neither TLC nor MS detected any evidence for [1]rotaxane product formation. Unfortunately, limited supplies of **LM-5** curtailed attempts at repeating the MIM reaction under various CuAAC 'click' conditions using different sources of copper(I).

## 3.6 Attempted [1]Rotaxane Formation *via* Active Metal Template Methodology

As previously described in section 1.5.2 of the introduction, the active metal template (AMT) approach for MIM formation was first introduced by Leigh and co-workers in 2006 for the successful synthesis of [2]rotaxanes.[23] In this methodology, the transition metal ion serves as both a preorganising template and a catalyst for mechanical bond formation. Adapting AMT for [1]rotaxane construction has not been exploited to any great extent.[24]




*Scheme 3.18. Schematic representation of a [1]rotaxane synthesis via AMT*

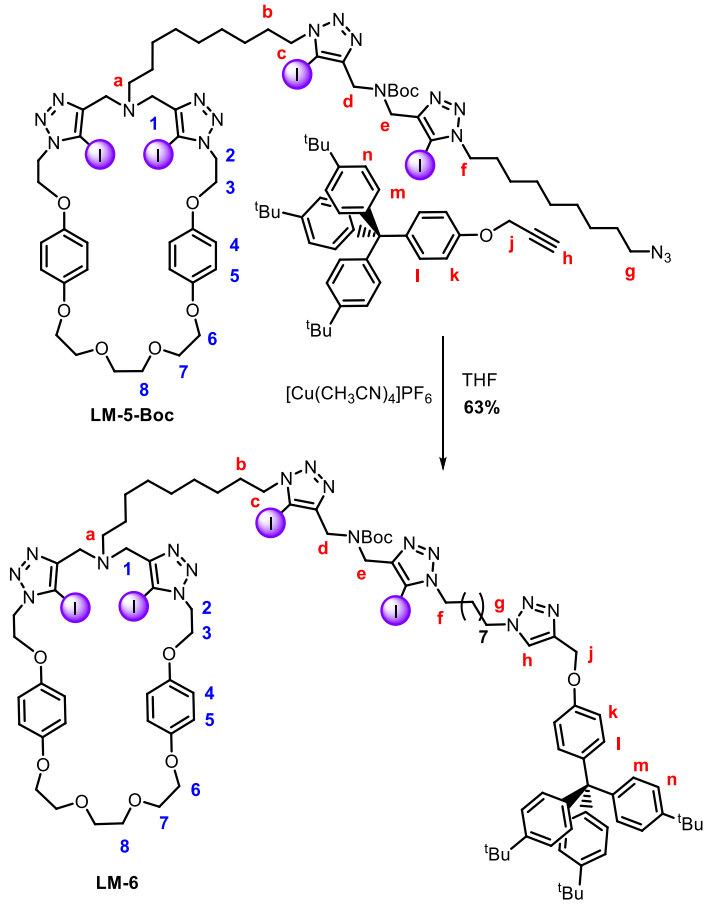
As shown in Scheme 3.18, this would entail the active metal being endotopically bound in the cavity of the lariat macrocycle to facilitate subsequent catalytic metal-mediated mechanical bond formation between the lariat arm and stopper precursor functional groups through the macrocyclic cavity. While a variety of organic reactions using different transition metals have been employed for AMT, [25-30] CuAAC triazole AMT MIM formation is the most common due to functional group compatibility, mild reaction conditions, and accessible coupling partners.[20, 31, 32]

Considering macrocycle **MC-1** has previously been shown to undergo CuAAC-AMT [2]rotaxane formation,[20] it was envisioned that Cu(I) could be endotopically bound by the azide functionalised lariat macrocycle **LM-5-Boc** for [1]rotaxane synthetic investigation.

### 3.6.1 AMT Reaction [1]Rotaxane Synthesis Attempts using a Lariat Macrocycle

The *N*-Boc-protected lariat macrocycle **LM-5-Boc** was combined with 0.95 equivalents of $[Cu(CH_3CN)_4]PF_6$ in dry $CH_2Cl_2$. After stirring for 30 minutes under an inert nitrogen atmosphere to ensure complexation of the Cu(I) metal by the macrocycle, a $CH_2Cl_2$ solution of the stopper alkyne **14** was added and the resulting mixture left to stir overnight (Scheme 3.19). Pleasingly, TLC and MS analysis of the reaction mixture confirmed the presence of a stoppered product species which was isolated in 42% yield after preparative thin layer chromatography (Scheme 3.19).

Disappointingly, the $^1$H-NMR spectrum (Figure 3.11) confirmed the product as being the non-interlocked stoppered lariat macrocycle **LM-6**, as there were no signs of interpenetration when comparing the spectra of the product and precursor. The only significant shifts were observed for the methylene protons **g** on the arm adjacent to the newly formed triazole group covalently linked to the terphenyl stopper (Figure 3.11). Furthermore, there were no clear crosspeaks in the 2D $^1$H-$^1$H ROESY NMR spectrum between signals corresponding to the macrocycle or lariat arm. Unfortunately, this all indicated that the lariat arm was stoppered without being threaded through the macrocycle first and lariat macrocycle **LM-6** was formed instead of the target [1]rotaxane. **LM-6** was fully characterised by $^1$H and $^{13}$C-NMR and high-resolution ESI mass spectrometry.




*Scheme 3.19. Attempted [1]rotaxane stoppering reaction under AMT conditions*

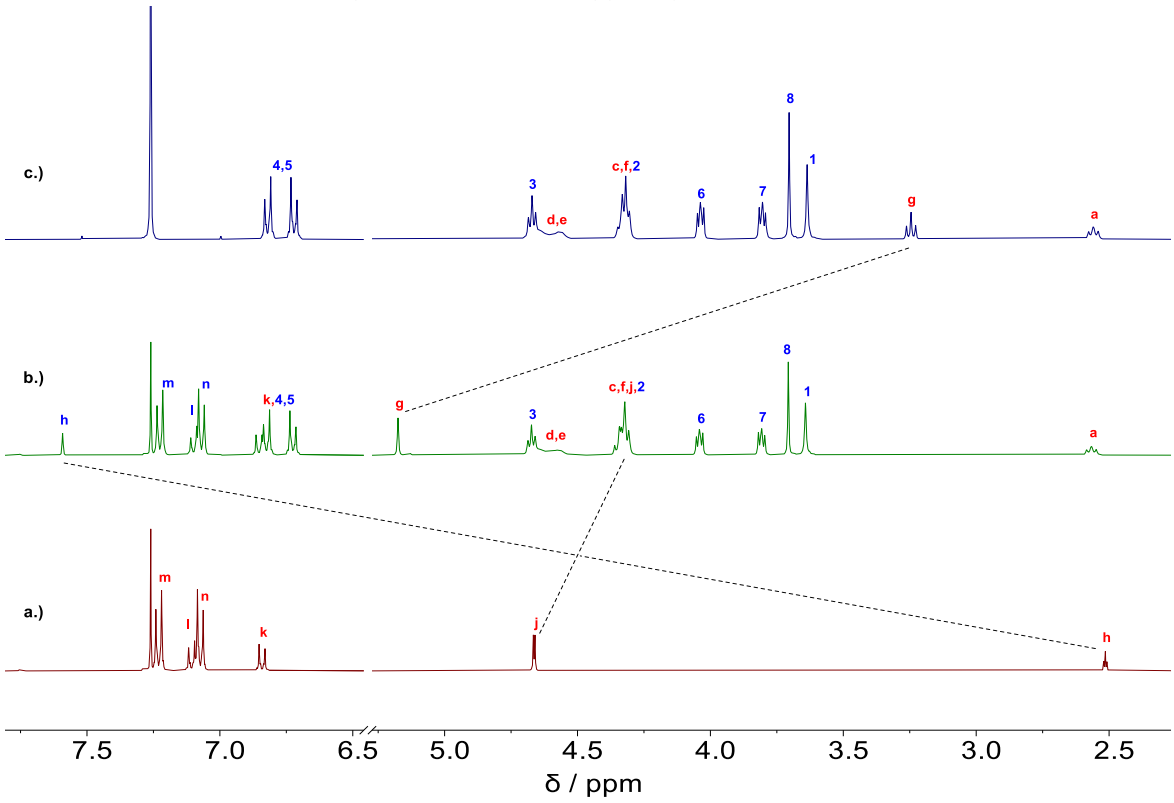
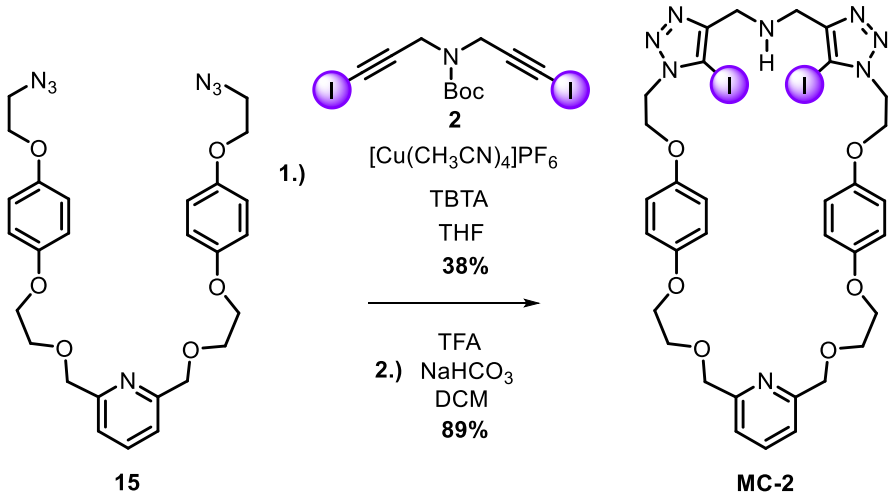



*Figure 3.11. Stacked $^{1}$H-NMR for a.) stopper, b.) **LM-6** and c.) **LM-5-Boc** in $CDCl_3$, 298K, 500MHz*

### 3.6.2 Synthesis of Pyridyl Modified Lariat Macrocycles for AMT [1]Rotaxane Investigation

In their initial 2006 report, Leigh and co-workers employed a pyridine containing macrocycle (see introduction, section 1.5.2) for the efficient high yielding formation of a [2]rotaxane *via* Cu(I) AMT.[23] The 2,6-bis-methoxy pyridyl group has since been proven to be an effective copper(I) coordinating motif to incorporate in macrocycle design for the formation of a range of interlocked structures *via* AMT.[23, 33-35] Pyridyl-based macrocycle **MC-2** (Scheme 3.20), incorporating an XB bis-iodotriazole motif, was therefore chosen as the new macrocycle precursor to prepare for azide functionalised alkyl chain lariat macrocycle design and subsequent synthesis (Scheme 3.21).

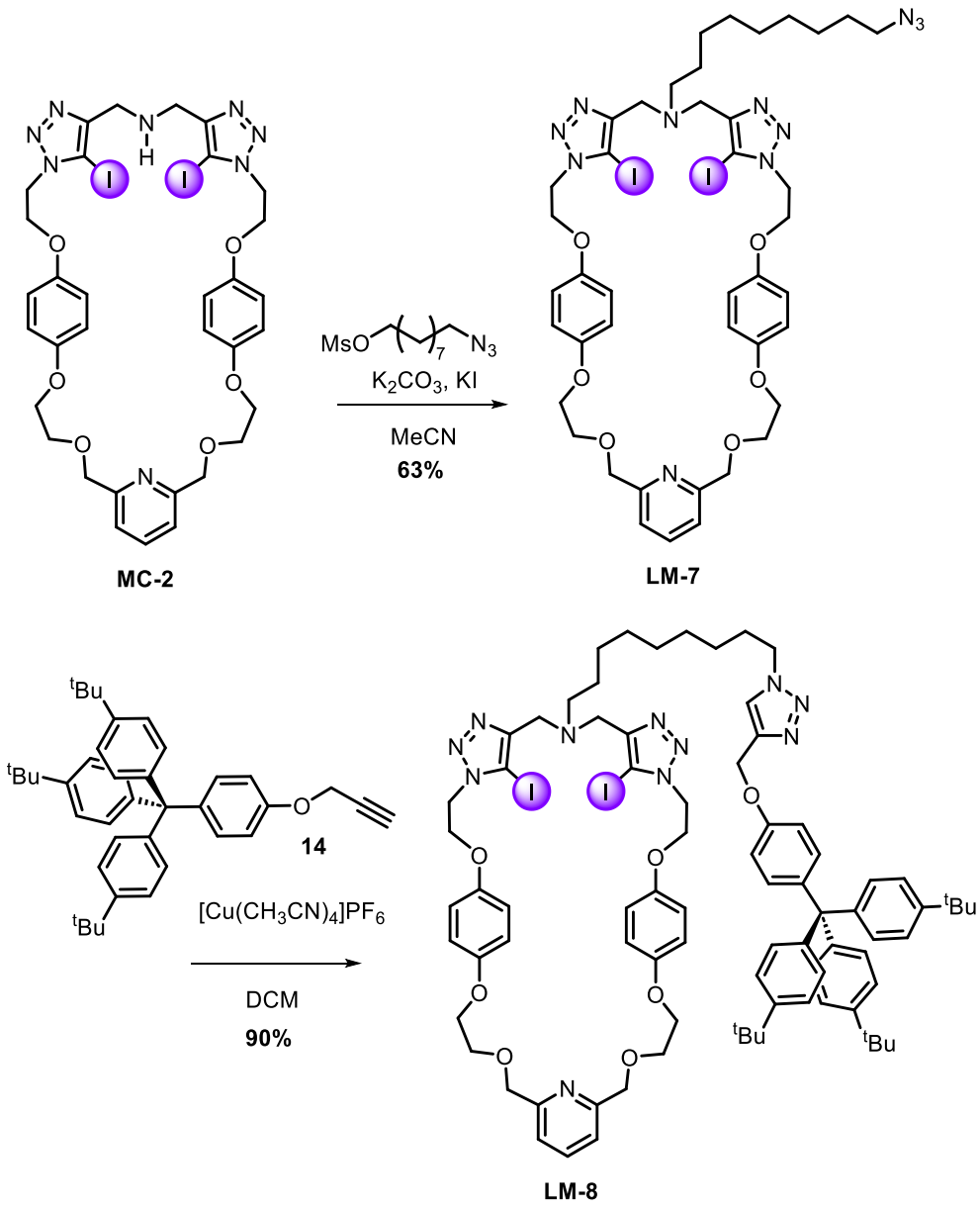
Macrocycle **MC-2** was synthesised using analogous conditions to **MC-1**, employing the same bis-iodoalkyne motif **2** together with the pyridyl-based bis-azide **15**, which was prepared according to a literature procedure.[36]




*Scheme 3.20. Formation of* ***MC-2***

The *N*-Boc-protected bis-iodoalkyne **2** was reacted with equimolar amounts of the pyridyl-based bis-azide **15** at a concentration of 3.35 mM to give the *N*-Boc protected macrocycle *via*

CuAAC click reaction in 38% yield after chromatographic purification. Subsequent *N*-Boc deprotection using trifluoroacetic acid (TFA) gave **MC-2** in 89% yield following neutralisation with sodium hydrogencarbonate (Scheme 3.20).



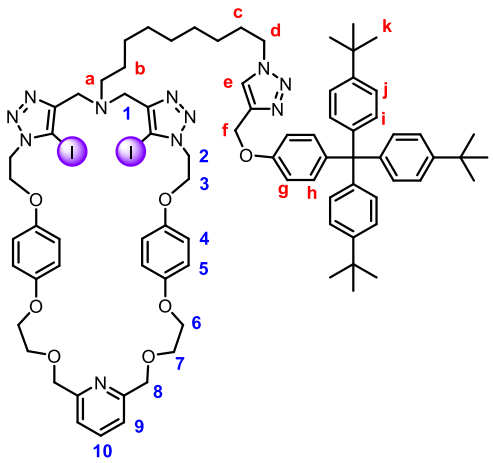

*Scheme 3.21. Stoppering reaction of **LM-7** under CuAAC-AMT conditions*

9-Azidononyl methanesulfonate was prepared according to literature procedure, starting from commercially available 9-bromo-1-nonanol in 2 steps.[37, 38] Alkylation of **MC-2** in acetonitrile with $K_2CO_3$ resulted in the formation of **LM-7** in 63% yield after purification by preparative

TLC (Scheme 3.21). The novel lariat macrocycle **LM-7** was fully characterised by $^{1}H$ and $^{13}C$-NMR and high-resolution ESI mass spectrometry.

With the target lariat macrocycle in hand, **LM-7** and the stopper alkyne **14** were subjected to CuAAC-AMT conditions. One equivalent of **LM-7** in $CH_2Cl_2$ was stirred together with 0.95 equivalents of the Cu(I) source $[Cu(CH_3CN)_4]PF_6$ for 30 minutes for copper (I) macrocycle complexation. After the introduction of 1.1 equivalents of stopper alkyne **14** in $CH_2Cl_2$, the mixture was stirred overnight at room temperature, after which a new species was identified by TLC and low-resolution MS showed a peak corresponding to the m/z of the [1]rotaxane. The product was isolated by silica gel flash column chromatography in 89% yield (Scheme 3.21).

Despite the promising preliminary MS results, $^{1}H$ NMR analysis once again only showed significant shifts in the proton environments either directly adjacent to or part of the stoppering triazole forming reaction site with no indication of threading (Figure 3.12). It has therefore been concluded that the stoppered lariat macrocycle **LM-8** was formed instead of the interlocked topological isomer (Figure 3.12).



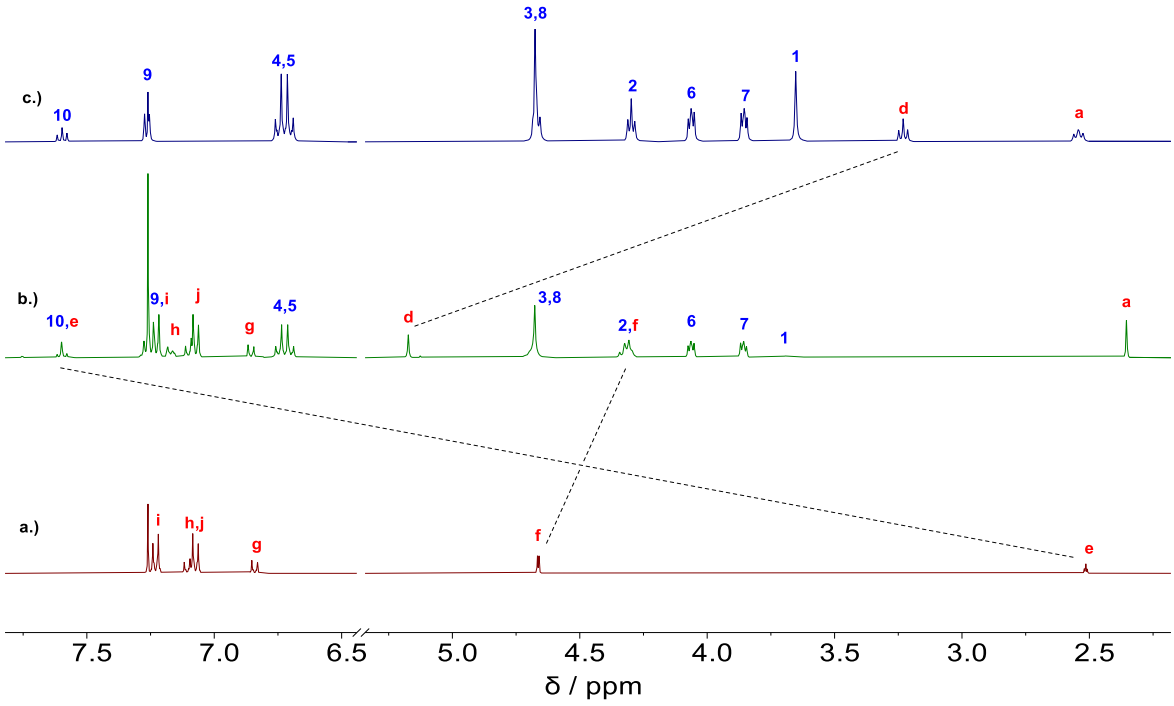
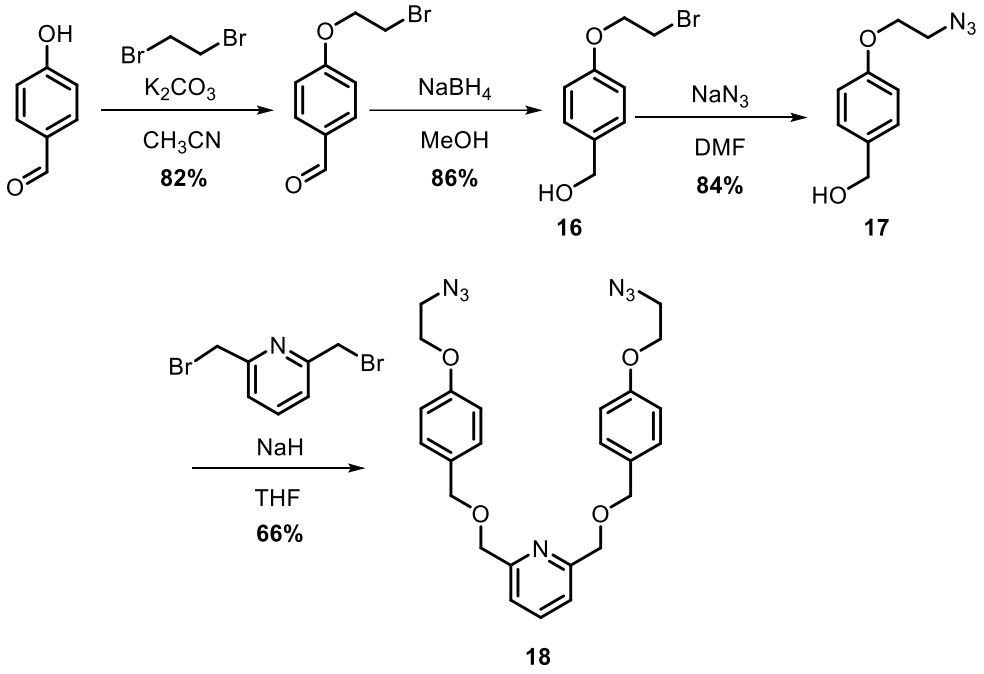



*Figure 3.12. Stacked $^{1}$H-NMR for a.) stopper, b.) **LM-8** and c.) **LM-7** in $CDCl_3$, 298K, 400MHz*

A further final attempt was made at revising the lariat macrocycle design for the formation of a [1]rotaxane *via* CuAAC-AMT. All previous attempts at forming a XB [1]rotaxane presented in this work so far have used a bis-iodotriazole-secondary amine functional motif.[20] However, a different bis-iodotriazole motif had been reported recently, which would also allow for post-modification of the macrocycle with a lariat arm once incorporated, as well as having been shown to be a powerful neutral XB donor.[39] The macrocycle **MC-3** precursor itself would once again contain a pyridine motif to allow for effective Cu(I) complexation during the AMT methodology. The macrocycle would also be slightly smaller than the previous macrocycles to ensure no de-threading would be possible if a MIM was formed. Previous reports have shown that [1]rotaxane formation can be achieved *via* CuAAC-click with a pyridine functionalised macrocycle and alkyne functionalised appended lariat arm.[24]

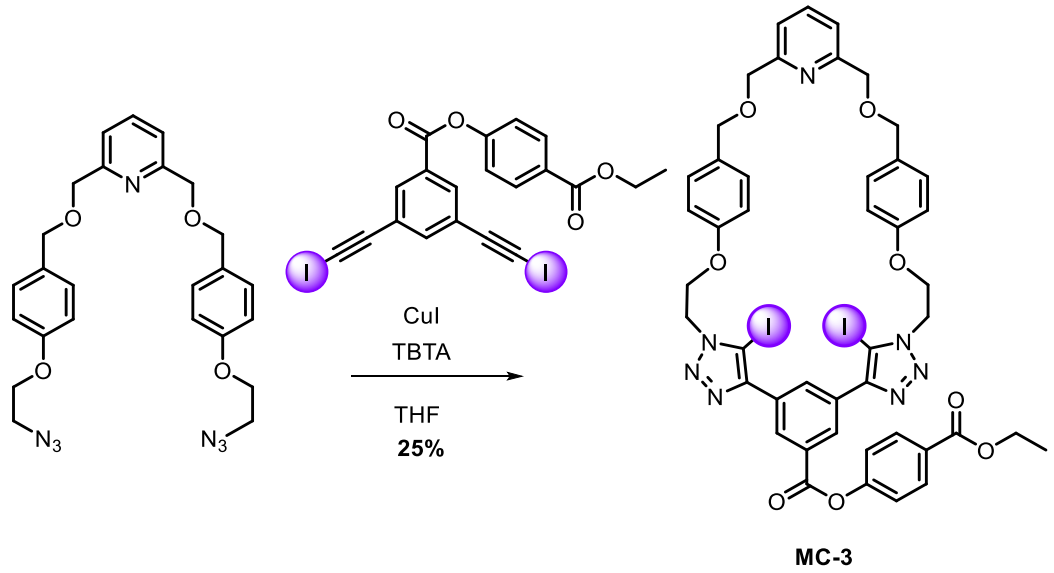
The novel macrocycle, **MC-3**, was therefore synthesised using another pyridyl-based bis-azide motif **18** (Scheme 3.22), which is similar to the motif used for the formation of **MC-2** but contains one less methylene oxygen linker for the formation of a slightly smaller macrocycle.




*Scheme 3.22. Formation of pyridine bis-azide macrocycle precursor **18***

The pyridyl-based bis-azide **18** was prepared from [4-(2-azidoethoxy)phenyl]methanol **17**, which was prepared according to a literature procedure (Scheme 3.22).[40] Commercially available 4-hydroxybenzaldehyde was alkylated with 1,2-dibromoethane in acetonitrile with $K_2CO_3$ to form 4-(2-bromoethyloxy)benzaldehyde in 82% yield before being reduced to the primary alcohol **16** by sodium borohydride in methanol. Subjecting product **16** to sodium azide in DMF afforded [4-(2-azidoethoxy)phenyl]methanol **17** in 84% yield. Just over two equivalents of **17** were then reacted with 2,6-bis(bromomethyl)pyridine in THF in the presence of 3 equivalents of sodium hydride for the formation of the desired bis-azide **18** in 66% yield following chromatographic purification (Scheme 3.22).

The macrocycle was furthermore formed with an active ester-appended bis-iodo-alkyne **19**, which had recently been reported by the Beer Group (Scheme 3.23).[39] Equimolar amounts of both precursors **18** and **19** were subjected to CuAAC-click conditions and the cyclic product was observed by TLC after 3 days of stirring at room temperature. After silica gel flash column chromatography purification, **MC-3** was isolated in 25% yield (Scheme 3.23). The novel macrocycle was fully characterised by $^{1}$H and $^{13}$C-NMR spectroscopy as well as high-resolution ESI mass spectrometry.

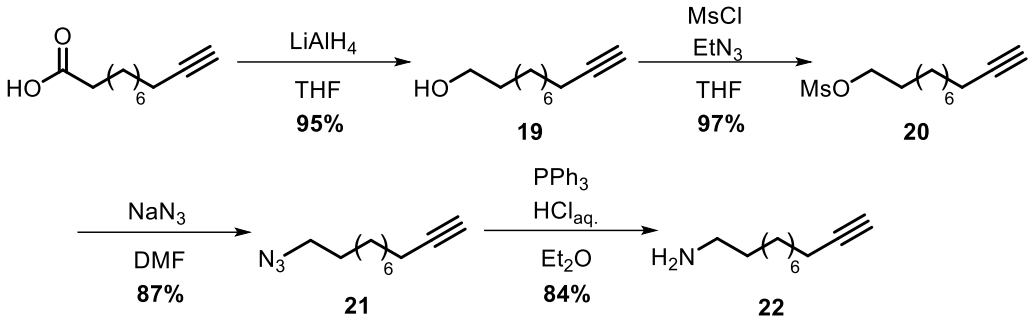



*Scheme 3.23.Formation of **MC-3***

The active ester motif of **MC-3** allows for the formation of a lariat macrocycle *via* a condensation reaction with an amine-functionalised arm rather than an alkylation using a mesylated species. It was envisioned that an alkyne appended alkyl chain would form the lariat arm of target **LM-9**.

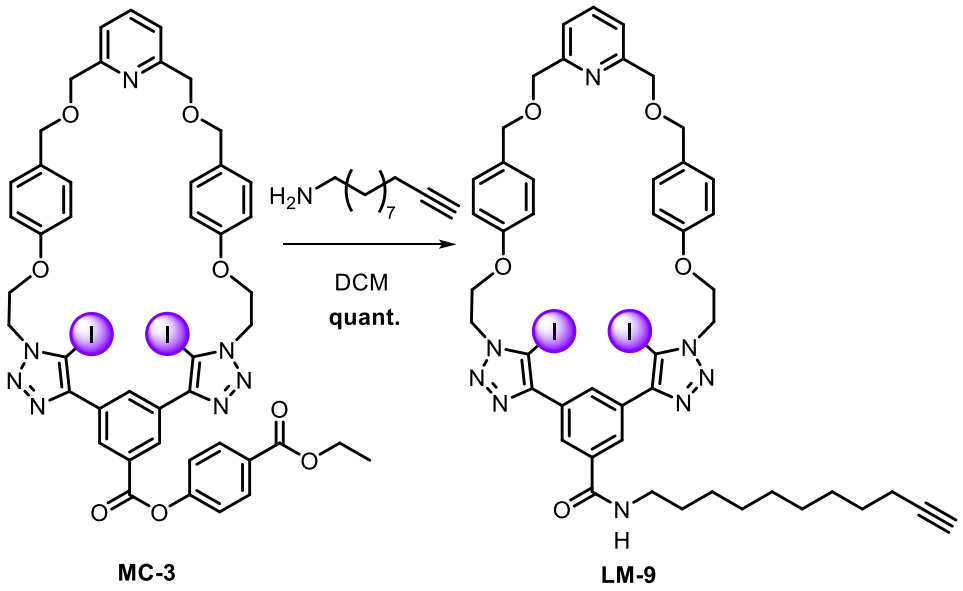
In order to form the alkyne functionalised arm precursor undec-10-ynyl-1-amine **22** (Scheme 3.24), commercially available 10-undecynoic acid underwent reduction to form undec-10-ynyl-1-ol **19** using LiAlH in 95% yield,[41] followed by the mesylation of the alcohol to form undec-10-ynyl methanesulfonate **20**.[42] The mesylate functionalised compound **20** was then converted

into the corresponding azide **21** using $NaN_3$.[43] The azide was then finally converted into the amine functionalised arm precursor **22** under Staudinger reaction conditions using a modified literature procedure in 84% yield (Scheme 3.24).[44]




*Scheme 3.24. Formation of undec-10-ynyl-1-amine*

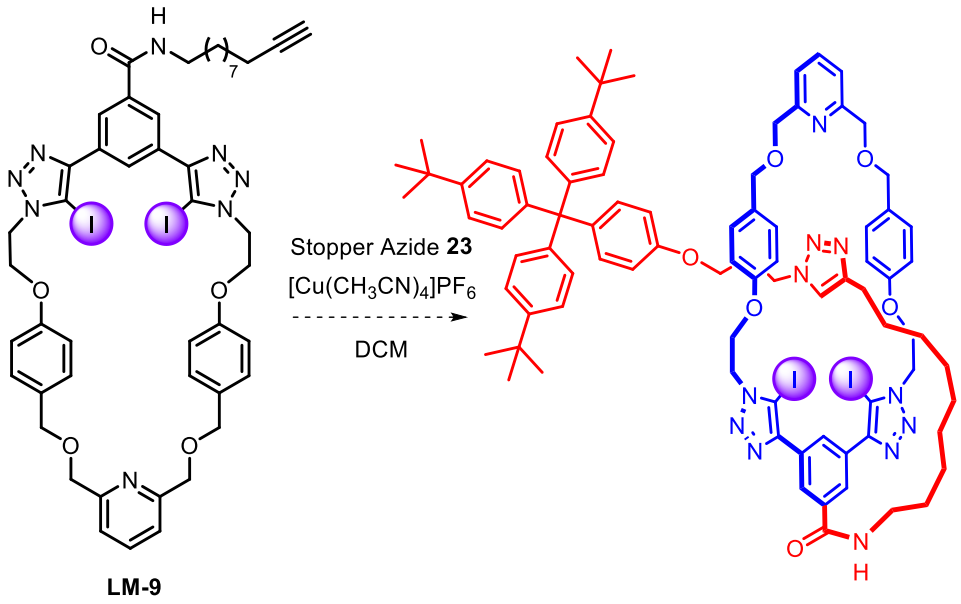
Condensation of undec-10-ynyl-1-amine **22** with **MC-3** gave **LM-9** in a quantitative yield (Scheme 3.25), characterised by $^{1}H$ and $^{13}C$-NMR spectroscopy and high-resolution ESI mass spectrometry.




*Scheme 3.25. Synthesis of **LM-9***

**LM-9** was then subjected to CuAAC-AMT conditions in an effort to synthesise the interlocked [1]rotaxane (Scheme 3.26). **LM-9** was stirred with 0.95 equivalents of $[Cu(CH_3CN)_4]PF_6$ in dry, degassed $CH_2Cl_2$ before addition of a solution of 1.1 equivalents of terphenyl stopper azide **23**,

which was prepared according to a literature procedure,[23] with an overall concentration of 10 mM with respect to **LM-5**. A new species with the correct m/z value of 1648.5885 for the desired [1]rotaxane was detected by ESI-MS and isolated in 43% yield following chromatographic purification.




*Scheme 3.26. Proposed synthesis of novel [1]rotaxane via AMT*

However, once again, the $^{1}$H-NMR spectrum of the purified product provided no evidence for the MIM structure, indicating the non-interlocked stoppered lariat macrocycle species **LM-10** had been produced (Figure 3.13).

Considering the AMT reaction is sensitive with respect to concentration of reactants,[45] a second attempt at [1]rotaxane formation *via* CuAAC-AMT was undertaken using a reduced concentration of reactants of 5 mM. Once again, disappointingly no interlocked product could be isolated.

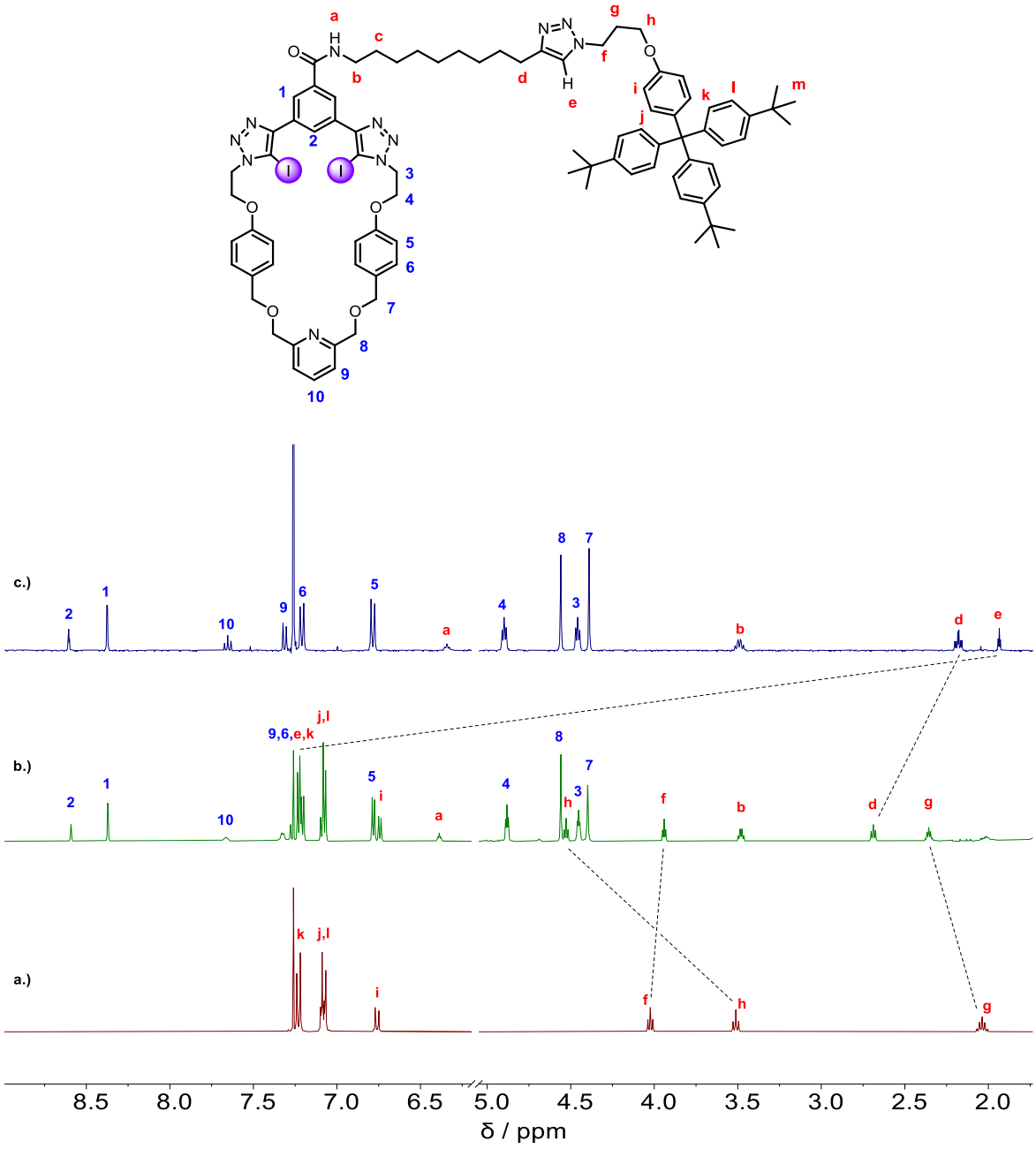



*Figure 3.13. Stacked $^{1}$H-NMR for a.) stopper, b.)* ***LM-10*** *and c.)* ***LM-9*** *in $CDCl_3$, 298K, 400MHz*

## 3.7 Conclusion and Future Work

This chapter has presented and discussed synthetic attempts to construct a XB [1]rotaxane using various anion and metal cation templating methods. The general synthetic approach was to synthesise an appropriately functionalised XB lariat macrocycle, which was envisioned to be capable of the charged guest template directed binding assembly of a pseudo [1]rotaxane *via* an

intramolecular self-threading event, which could potentially be stoppered for the formation of an XB functionalised [1]rotaxane.

Influenced by a previously reported protonated XB [2]rotaxane capable of chloride anion recognition *via* four iodotriazole motifs as well secondary ammonium-based charge assisted HB interactions,[20] the first part of this chapter focused on using various XB lariat macrocycles **LM-2**, **LM-3**, and **LM-4** to prepare a [1]rotaxane *via* chloride anion templation. Although $^{1}$H NMR titration studies suggested chloride binding by each receptor system, this was not occurring in the desired endotopic pseudo [1]rotaxane coordination mode of threading of the respective XB lariat arm through the macrocycle cavity.

Exploiting the ambidentate nature of the iodotriazole motif which can bind metal cations *via* the Lewis basic triazole nitrogen donors, attention turned to the potential formation of a (pseudo) [1]rotaxane using a zinc(II) metal cation template. The $^{1}$H NMR spectrum of the isolated zinc(II) complexes of the lariat macrocycle **LM-2** indicated successful metal coordination *via* the tridentate Lewis basic triazole nitrogen donors of the macrocycle and axle. However, it remained inconclusive whether any self-threading had occurred. An azide functionalised lariat macrocycle **LM-5** was then synthesised and the subsequent zinc(II) template [1]rotaxane stoppering reaction unfortunately gave no evidence of the desired interlocked product.

Attempts to prepare a [1]rotaxane *via* an active metal template (AMT) methodology were then made. **LM-5-Boc** was subjected to CuAAC-AMT conditions, which resulted in the formation of a non-interlocked stoppered lariat macrocycle **LM-6**. A modified lariat macrocycle design **LM-7** was then introduced which contained an integrated pyridyl motif in an effort to favour endotopic coordination of the copper(I) AMT. The pyridyl macrocycle **MC-2** was appended

with an alkyl azide functionalised lariat arm which upon CuAAC-AMT MIM stoppering conditions gave only the non-interlocked stoppered lariat macrocycle product **LM-8**.

The final attempt involved the synthesis of a smaller macrocycle containing an active ester-appended bis-iodotriazole motif, as well as a pyridine unit for Cu(I) binding. The active ester could be functionalised *via* a condensation reaction with undec-10-ynyl-1-amine for the formation of novel lariat macrocycle **LM-9**. Another attempt at [1]rotaxane formation using a CuAAC-AMT methodology was made, however, it once again resulted in the formation of the non-interlocked stopper species **LM-10** rather than the [1]rotaxane topological isomer.

In summary, a range of multidentate XB iodotriazole based lariat macrocycles were successfully synthesised and pseudo- and [1]rotaxane assembly investigated by anion, cation, and active metal template methodologies. Unfortunately, no conclusive evidence of pseudo- or [1]rotaxane formation was found, indicating further tuning of electronic and steric properties of the lariat-based macrocyclic system is required.

Future work will include new design ideas to move towards a molecular lasso-type XB [1]rotaxane capable of anion binding with multiple binding sites for dynamic molecular motion. A recent report has demonstrated the successful use of a functionalised pillar[5]arene lariat macrocycle for the formation of a [1]rotaxane capable of zinc(II) cation sensing.[46] This could for example serve as inspiration for the use of post-functionalised pillar[5]arenes for the construction of an XB [1]rotaxane capable of anion sensing.

## 3.8 References

1. K. Hiratani, M. Kaneyama, Y. Nagawa, E. Koyama and M. Kanesato, *Journal of the American Chemical Society*, 2004, **126**, 13568-13569.

2. O. Š. Miljanić, W. R. Dichtel, I. Aprahamian, R. D. Rohde, H. D. Agnew, J. R. Heath and J. Fraser Stoddart, *QSAR & Combinatorial Science*, 2007, **26**, 1165-1174.

3. J. D. Hegemann, M. Zimmermann, X. Xie and M. A. Marahiel, *Accounts of Chemical Research*, 2015, **48**, 1909-1919.

4. H. Martin-Gómez and J. Tulla-Puche, *Organic & Biomolecular Chemistry*, 2018, **16**, 5065-5080.

5. P. Waelès, C. Clavel, K. Fournel-Marotte and F. Coutrot, *Chemical Science*, 2015, **6**, 4828-4836.

6. R. Jäger, M. Händel, J. Harren, F. Vögtle and K. Rissanen, *Liebigs Annalen*, 1996, **1996**, 1201-1207.

7. C. Reuter, C. Seel, M. Nieger and F. Vögtle, *Helvetica Chimica Acta*, 2000, **83**, 630-640.

8. C. Reuter, A. Mohry, A. Sobanski and F. Vögtle, *Chemistry – A European Journal*, 2000, **6**, 1674-1682.

9. X. Ma, Q. Wang and H. Tian, *Tetrahedron Letters*, 2007, **48**, 7112-7116.

10. H. Li, X. Li, Z.-Q. Cao, D.-H. Qu, H. Ågren and H. Tian, *ACS Applied Materials & Interfaces*, 2014, **6**, 18921-18929.

11. Q. Zhou, P. Wei, Y. Zhang, Y. Yu and X. Yan, *Organic Letters*, 2013, **15**, 5350-5353.

12. C. Clavel, C. Romuald, E. Brabet and F. Coutrot, *Chemistry - A European Journal*, 2013, **19**, 2982-2989.

13. C. Clavel, K. Fournel-Marotte and F. Coutrot, *Molecules*, 2013, **18**, 11553-11575.

14. Z. Xue and M. F. Mayer, *Journal of the American Chemical Society*, 2010, **132**, 3274-3276.

15. A. B. Braunschweig, W. R. Dichtel, O. Š. Miljanić, M. A. Olson, J. M. Spruell, S. I. Khan, J. R. Heath and J. F. Stoddart, *Chemistry – An Asian Journal*, 2007, **2**, 634-647.

16. H. Li, J.-N. Zhang, W. Zhou, H. Zhang, Q. Zhang, D.-H. Qu and H. Tian, *Organic Letters*, 2013, **15**, 3070-3073.

17. H. V. Schröder, J. M. Wollschläger and C. A. Schalley, *Chemical Communications*, 2017, **53**, 9218-9221.

18. C. Zong, M. J. Wu, J. Z. Qin and A. J. Link, *Journal of the American Chemical Society*, 2017, **139**, 10403-10409.

19. T. A. Barendt, A. Docker, I. Marques, V. Félix and P. D. Beer, *Angewandte Chemie International Edition*, 2016, **55**, 11069-11076.

20. X. Li, J. Y. C. Lim and P. D. Beer, *Chemistry - A European Journal*, 2018, **24**, 17788-17795.

21. T. Bunchuay, A. Docker, A. J. Martinez-Martinez and P. D. Beer, *Angewandte Chemie International Edition*, 2019, **58**, 13823-13827.

22. M. Mohsen-Nia, H. Amiri and B. Jazi, *Journal of Solution Chemistry*, 2010, **39**, 701-708.

23. V. Aucagne, K. D. Hänni, D. A. Leigh, P. J. Lusby and D. B. Walker, *Journal of the American Chemical Society*, 2006, **128**, 2186-2187.

24. N. Pairault, A. Bessaguet, R. Barat, L. Frédéric, G. Pieters, J. Crassous, I. Opalinski and S. Papot, *Chemical Science*, 2021, **12**, 2521-2526.

25. J. D. Crowley, K. D. Hänni, A.-L. Lee and D. A. Leigh, *Journal of the American Chemical Society*, 2007, **129**, 12092-12093.

26. J. Berná, J. D. Crowley, S. M. Goldup, K. D. Hänni, A.-L. Lee and D. A. Leigh, *Angewandte Chemie International Edition*, 2007, **46**, 5709-5713.

27. J. D. Crowley, K. D. Hänni, D. A. Leigh and A. M. Z. Slawin, *Journal of the American Chemical Society*, 2010, **132**, 5309-5314.

28. J. D. Crowley, S. M. Goldup, N. D. Gowans, D. A. Leigh, V. E. Ronaldson and A. M. Z. Slawin, *Journal of the American Chemical Society*, 2010, **132**, 6243-6248.

29. J. J. Danon, D. A. Leigh, P. R. McGonigal, J. W. Ward and J. Wu, *Journal of the American Chemical Society*, 2016, **138**, 12643-12647.

30. S. M. Goldup, D. A. Leigh, R. T. McBurney, P. R. McGonigal and A. Plant, *Chemical Science*, 2010, **1**, 383.

31. J. Y. C. Lim, T. Bunchuay and P. D. Beer, *Chemistry - A European Journal*, 2017, **23**, 4700-4707.

32. J. Y. C. Lim, I. Marques, V. Félix and P. D. Beer, *Journal of the American Chemical Society*, 2017, **139**, 12228-12239.

33. V. Aucagne, J. Berná, J. D. Crowley, S. M. Goldup, K. D. Hänni, D. A. Leigh, P. J. Lusby, V. E. Ronaldson, A. M. Z. Slawin, A. Viterisi and D. B. Walker, *Journal of the American Chemical Society*, 2007, **129**, 11950-11963.

34. M. Denis and S. M. Goldup, *Nature Reviews Chemistry*, 2017, **1**, 0061.

35. J. D. Crowley, S. M. Goldup, A.-L. Lee, D. A. Leigh and R. T. McBurney, *Chemical Society Reviews*, 2009, **38**, 1530.

36. A. Brown, T. Lang, K. M. Mullen and P. D. Beer, *Organic & Biomolecular Chemistry*, 2017, **15**, 4587-4594.

37. F. F. Hilário, R. C. De Paula, M. L. T. Silveira, G. H. R. Viana, R. B. Alves, J. R. C. S. Pereira, L. M. Silva, R. P. De Freitas and F. De Pilla Varotti, *Chemical Biology & Drug Design*, 2011, **78**, 477-482.

38. N. Wolf, L. Kersting, C. Herok, C. Mihm and J. Seibel, *The Journal of Organic Chemistry*, 2020, **85**, 9751-9760.

39. A. Docker, J. G. Stevens and P. D. Beer, *Chemistry – A European Journal*, 2021, **27**, 14600-14604.

40. Y. Tian, J. Jin, C. Wang, W. Lv, X. Li, X. Che, Y. Gong, Y. Li, Q. Li, J. Hou, P. G. Wang and J. Shen, *Bioorganic & Medicinal Chemistry Letters*, 2016, **26**, 2434-2437.

41. A.-C. Bédard and S. K. Collins, *Journal of the American Chemical Society*, 2011, **133**, 19976-19981.

42. S. Butini, M. Brindisi, S. Gemma, P. Minetti, W. Cabri, G. Gallo, S. Vincenti, E. Talamonti, F. Borsini, A. Caprioli, M. A. Stasi, S. Di Serio, S. Ros, G. Borrelli, S. Maramai, F. Fezza, G. Campiani and M. Maccarrone, *Journal of Medicinal Chemistry*, 2012, **55**, 6898-6915.

43. A.-C. Bédard and S. K. Collins, *Organic Letters*, 2014, **16**, 5286-5289.

44. N. Kojima, Y. Suga, T. Matsumoto, T. Tanaka, A. Akatsuka, T. Yamori, S. Dan, H. Iwasaki and M. Yamashita, *Bioorganic & Medicinal Chemistry*, 2015, **23**, 1276-1283.

45. S. M. Goldup, D. A. Leigh, T. Long, P. R. McGonigal, M. D. Symes and J. Wu, *Journal of the American Chemical Society*, 2009, **131**, 15924-15929.

46. Y. Yao, L. Ma, R. Tang, Y. Zhou, J. Bei, T. Chen, C. Ou, Y. Wang, Y. Han and C. Yan, *Chemical Communications*, 2022, **58**, 8978-8981.

# 4 Exploiting the Macrocyclic Effect for the Stabilisation of Halonium Cations

## 4.1 Introduction

Halonium ions ($X^+$), or positively charged halogen species were first postulated in 1937 as reactive intermediates to rationalise the stereospecificity of halogen addition across alkenes.[1] Subsequent solution and solid phase spectroscopic, as well as single crystal X-ray diffraction (XRD) data have served to extensively characterise these species. Indeed, recent years have seen enormous improvements in our understanding of their structure and bonding characteristics.[2]

Perhaps unsurprisingly, the ability of the typically electronegative group 17 elements to form formally positive species is best documented with the heavier elements of the group *i.e.*, iodine and bromine.[3] This is reflected in the enhanced stability of diaryliodonium $[Ar\cdots I\cdots Ar]^+$ species having pervasive use in organic synthesis.[4, 5] In general, carbon-bonded halonium species form bent geometries with symmetrical bonds to the carbons.[3] Although rare, $[C\cdots Cl\cdots C]^+$ type complexes have been structurally characterised[6] with recent publications also revealing evidence for the existence of symmetrical $[C\cdots F\cdots C]^+$ complexes in solution[3, 7, 8], as well as the solid state[9].

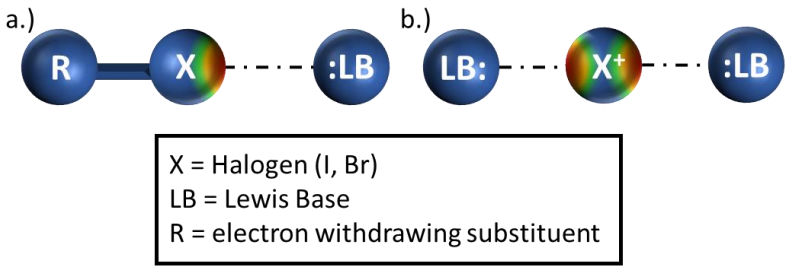



*Figure 4.1.Representation of a.) A traditional XB with red region indicating the electropositive σ-hole and b.) Halonium interaction with red regions indicating the two electropositive regions coined p-holes*

Conceivably, halogen atoms bearing a formal positive charge are potential potent halogen bond donors. From an orbital perspective, a $X^+$ species possesses a vacant p-orbital capable of interaction with a Lewis base which parallels an organic halogen bond donor (Figure 4.1).[10]

While their high oxidising power and reactivity frequently results in the chemical transformation of a Lewis base, one successful strategy in the stabilisation of haloniums has been the formation of complexes with neutral, typically nitrogenous bases such as pyridine (Py) in the form $[(Py)_2X]^+$.[11] Other reports of stabilisation by a diverse range of heteroatoms are known,[12-16] however, nitrogenous electron donors remain the most common.[17]

$[Py\cdots X\cdots Py]^+$ complexes invariably form linear geometries and in the instance where the nitrogen donors are identical the complexes typically exhibit two equivalent N···X (X= Br, I) bonds as determined by extensive solution phase and solid-state characterisation (Figure 4.2).[18, 19]

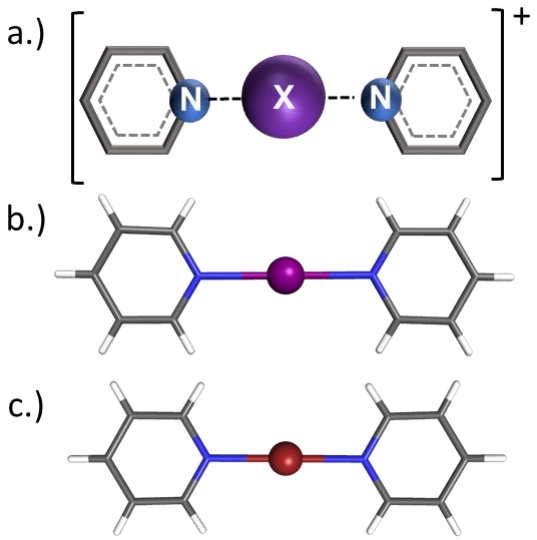



*Figure 4.2. a.) Schematic representation of a linear $[(Py)_2X]^+$ complex with X=I, Br, b.) single-crystal XRD of $[(Py)_2I]^+$(CSD: CICQIQ)[20] and c.) single-crystal XRD of $[(Py)_2Br]^+$(CSD:DOWBAU)[21]*

The bonding situation of these halonium complexes is well described by a 3-centre-4-electron model.[22] While the relative electrostatic and charge transfer contributions of these bonds are

the subject of ongoing discussion,[2, 23] several general trends have been established dependant on the exact nature of the system.

The nature of the N···$X^+$···N bonds going down the group is shaped by an increase in strong electrostatic contributions (Figure 4.3).[2, 18] These electrostatic forces are a key determinant of the strength of the XB interaction with the heavier and less electronegative halogens exhibiting the strongest interactions with XB bond strengths of up to 180 kJ $mol^{-1}$ (Figure 4.3).[10, 17, 24] An increasing covalent character dominated by charge transfer contributions can be observed for weaker halonium bonds involving the lighter and more electronegative halogens (Figure 4.3).[10]

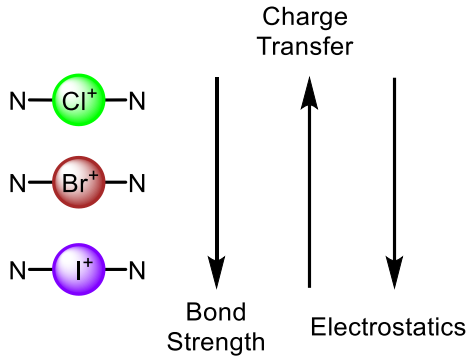



*Figure 4.3. Comparison of characteristics and nature of N···X⁺···N bonds for the different halogens*[10]

Halonium complex distances strongly depend on both the nature of the ligand and halonium cation but computational studies have determined N–X bond lengths to be 2.303 Å for iodonium, 2.140 Å for bromonium and 2.025 Å for chloronium in symmetrical bis-pyridine complexes with a $CH_2Cl_2$ solvent model.[2] The aromatic nature of the pyridine based ligands allows for a delocalisation of the positive charge on the halonium, which in turn shortens and strengthens the halonium to nitrogen bond.[17]

As a consequence of the increasing halonium stability down Group 17 and the utility of the pyridine ligands in halonium stabilisation, bis-pyridine iodonium complexes are the most commonly encountered and characterised members of the halogen(I) cations, with a

considerable source of structural and spectroscopic characterisation of these complexes (Figure 4.2).[10] They are also well known reagents for halogen transfer reactions,[25] as well as being able to function as oxidising agents,[26, 27] and catalysts[28].

Recent years have witnessed iodonium cations being incorporated into larger supramolecular structures.[29-33] Here, haloniums can serve as structurally directing motifs in solid state crystal engineering applications. With their high fidelity to form linear coordination complexes, iodonium cations in particular can act as closed shell $d^{10}$ transition metal cation analogues for Ag(I) and Au(I) or Hg(II), which also form symmetric, linear three-centre complexes with pyridyl based ligands.[34]

After reporting the first examples of symmetric, dimeric capsules in which the pyridyl-based monomers are connected *via* iodonium linker units in 2016,[29] Rissanen described the formation of dimeric and tetrameric cages using tripodal *N*-donor ligands in 2017 (Figure 4.4).[30] Two units of neutral tris(imidazole-1-ylmethyl)-2,4,6-trimethylbenzene were used as a ligand system for the formation of the dimeric capsule (Figure 4.4 a). Each ligand system contains three imidazole motifs, which can act as Lewis bases for the stabilisation of both Ag(I) and I(I) (Figure 4.4 a). The tetrameric capsule contains three cationic tris(1-methyl-1-azonia-4-azabicyclo[2.2.2]octane)-mesitylene ligands, where the substituted diazabicyclo[2.2.2]octane units serve as the nitrogenous Lewis bases for the halonium complexation (Figure 4.4 b). The halonium cages were prepared *via* the initial formation of the analogous $Ag^+$ based cages to which elemental iodine was introduced, resulting in a cation exchange reaction within the cages and the precipitation of AgI. The cages were characterised both in solution and in the solid state by $^1$H NMR and single-crystal XRD respectively (Figure 4.4).[30]

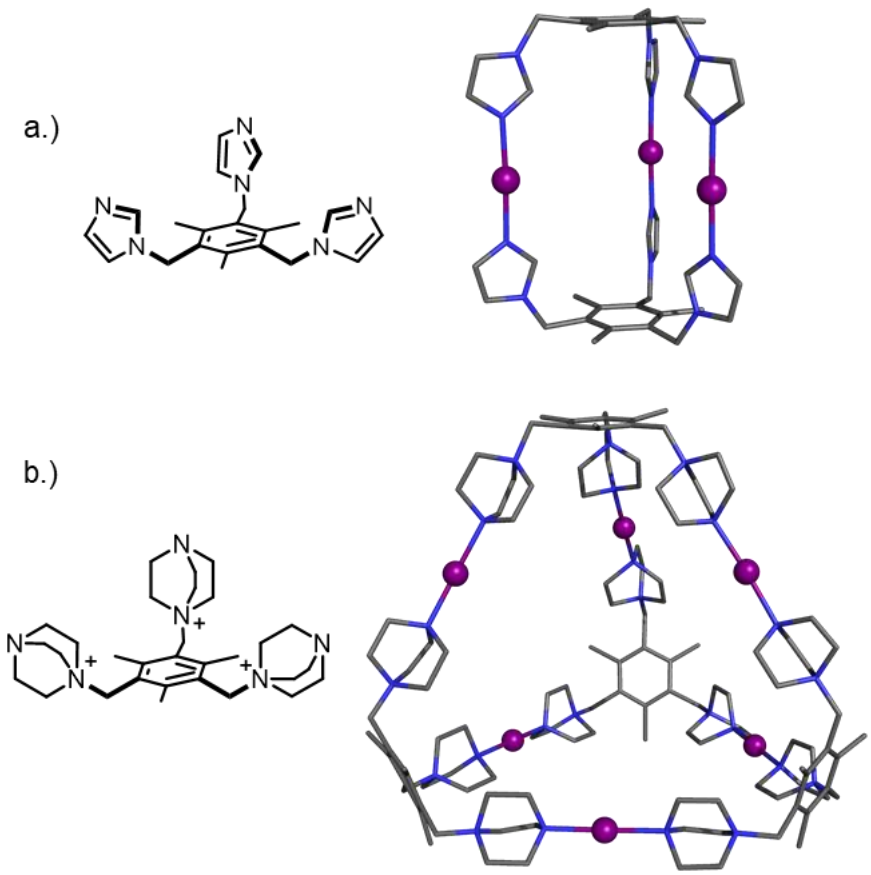



*Figure 4.4. Halonium cages from tripodal N-donor ligands with a.) tris(imidazole-1-ylmethyl)-2,4,6-trimethylbenzene ligand and dimeric cage (CSD: WEHTEL) and b.) tris(1-methyl-1-azonia-4-azabicyclo[2.2.2]octane)-mesitylene ligand and tetrameric halonium cage (CSD: WEHSUA).*[30]

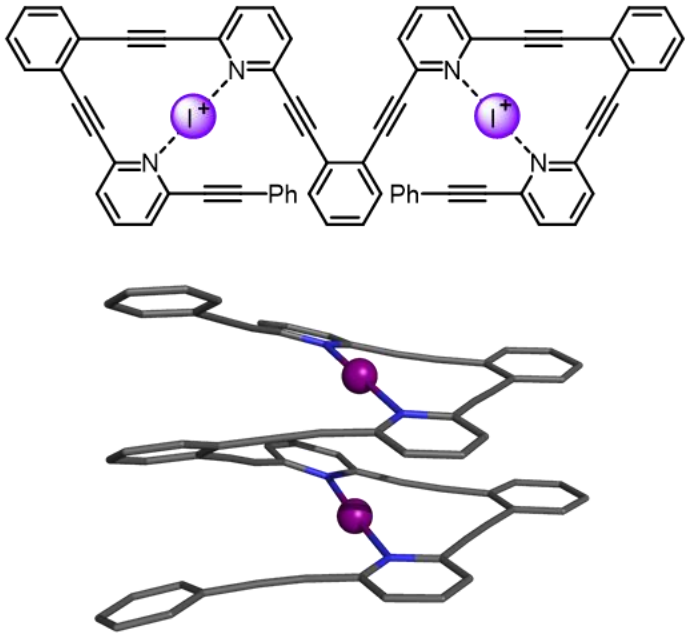
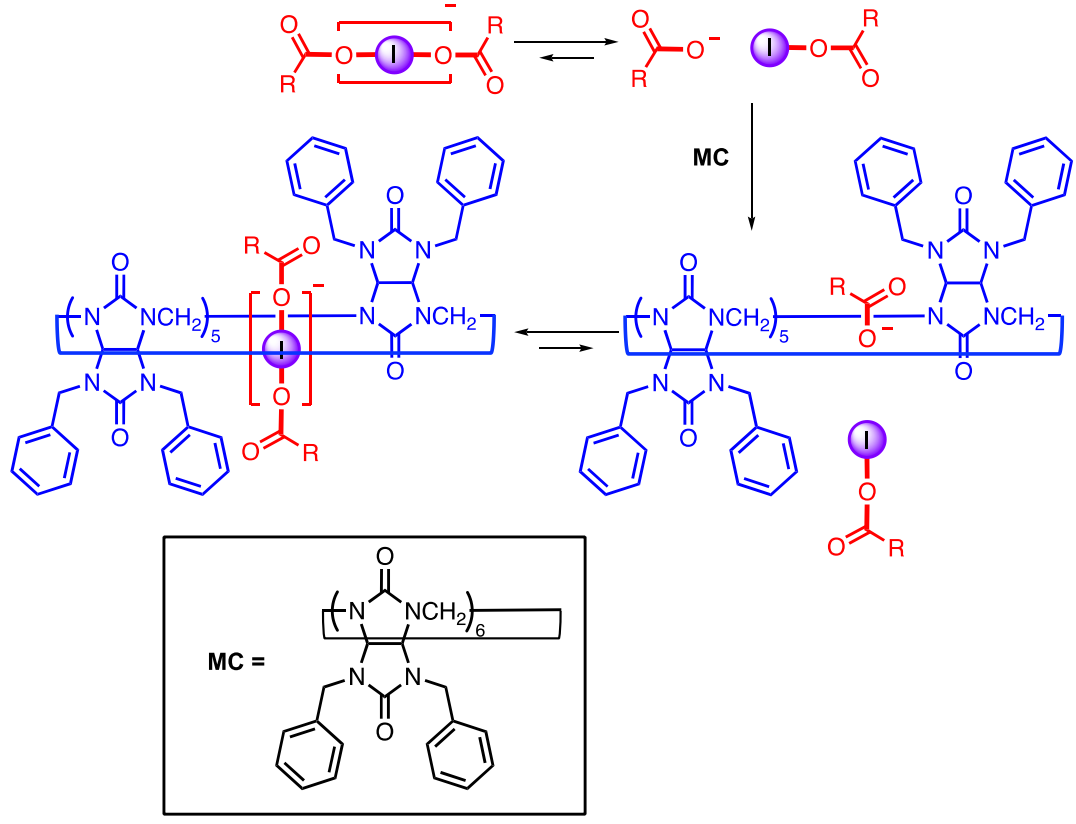



*Figure 4.5. Erdélyi's halonium helix (CSD: NOMBOJ)*[33]

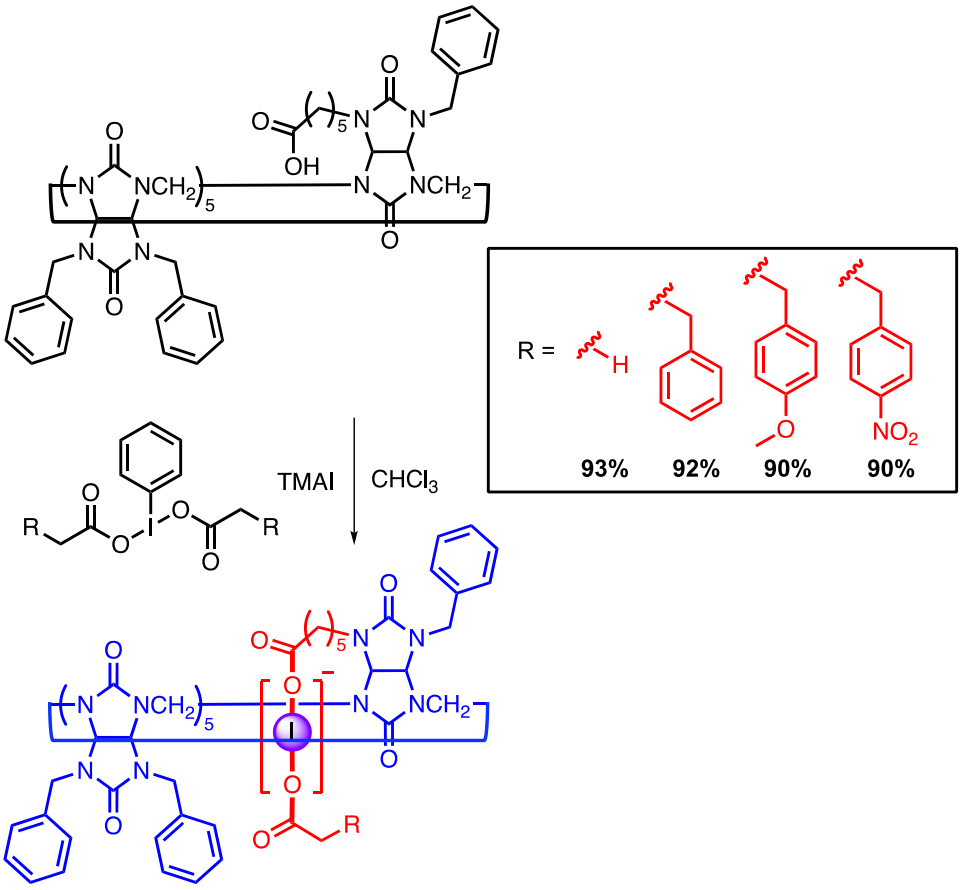
Erdélyi reported the first halonium based helicate structures in 2019.[33] The structure contains pyridine motifs as XB acceptors linked by diethynyl benzene units (Figure 4.5). The helical arrangement was predicted to be the most stable form by DFT calculations. As well as solid state characterisation, solution phase evidence included $^{1}H$, $^{13}C$ as well as $^{15}N$ NMR.[33]

Exploiting the dynamic exchange properties of bis(acyloxy)iodate complexes, Šindelář and co-workers recently reported examples of MIMs constructed through an anion recognition strategy.[35, 36] The [2]rotaxane design incorporated an anionic bis(acyloxy)iodate(I) motif into the axle with a bambus[6]uril-based macrocycle (Scheme 4.1).[35] Impressively, by exploiting the known lability of the halonium species, almost quantitative [2]rotaxane formation was achieved by mixing equimolar amounts of the dodecabenzylbambus[6]uril macrocycle and TBA salt of the bis(acyloxy)iodate(I) axle, as confirmed by $^{1}H$ NMR as well as single crystal XRD, wherein it was shown that the I(I) resides in the centre of the macrocycle (Scheme 4.1).[35]




*Scheme 4.1. Formation of [2]rotaxane via dynamic covalent bond formation*[35]

Building upon this work, the same authors demonstrated the method was also applicable in the construction of [1]rotaxanes.[36] Here a benzyl decorated bambus[6]uril scaffold was appended with a carboxylate arm, which when reacted with (diacetoxyiodo)benzene and tetramethyl iodide (TMAI) produced the bis(acyloxy)iodate(I) anionic moiety *in situ* as the precursor axle, which threaded through the macrocycle cavity to form the desired [1]rotaxane in high yields (Scheme 4.2).[36] The proposed mechanism of [1]rotaxane formation similarly relies upon the labile nature of the iodate(I) I–O bonds facilitating interpenetration, which is thermodynamically favoured by endodentate C-H interactions between the macrocycle interior and anionic axle component.[36] The interlocked nature of the structure was confirmed by $^{1}$H NMR analysis, including $^{1}$H-$^{1}$H ROESY NMR, which showed through space coupling between a selected number of axle and macrocycle protons.[36]




*Scheme 4.2. One-pot formation of a series of [1]rotaxanes*[36]

In general, the field of halonium supramolecular chemistry remains in its infancy, and the relatively few examples reported to date have focused on iodonium, as a consequence of the relative enhanced stability of the heavier halonium species.[10]

Bromonium stabilised complexes are rare, with structural characterisation often being limited to more simple acyclic complexes (Figure 4.6).[37-43] Despite some solution phase NMR spectroscopic evidence, the corresponding chloronium halonium stabilised by neutral Lewis bases remain elusive and are yet to be structurally characterised.[2] Furthermore, the existence of a symmetrical $[N\cdots F\cdots N]^+$ type complex is still subject to debate and further study.[17]

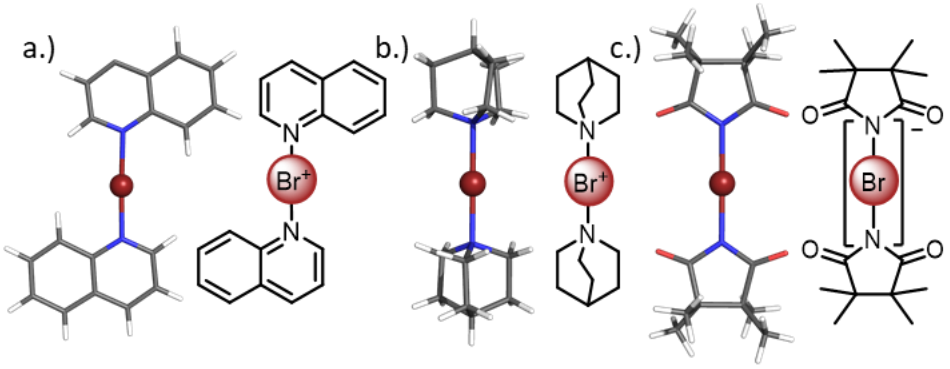



*Figure 4.6. Selected N···Br⁺···N single crystal XRD structures each with their associate ChemDraw representations with a.) quinoline ligands (CSD: QUBRPC),[37] b.) quinuclidine ligands (CSD: BUWMOV),[38]and c.) tetramethylsuccinimide ligands (CSD: JEJZED)[44]*

Overall, the instability of halonium compounds limits the scope of their applications. Indeed, if the lighter haloniums are to find supramolecular chemistry applications, for example in self-assembly, then structural characterisation and a deeper understanding of their fundamental nature is a prerequisite.

## 4.2 Project Aims

While the macrocyclic effect is a well-established concept in supramolecular chemistry,[45] its application for the stabilisation of halonium ions is unprecedented. The aim of this collaborative

project with Dr Andrew Docker, was to investigate the potential ability of a set of bis-pyridine containing macrocycles to stabilise halonium cations and to determine whether the traditionally defined kinetic and thermodynamic factors that contribute to the macrocycle effect translate to the coordination chemistry of halonium, in particular the bromonium cation. Dr Docker performed the synthetic work presented in this chapter, such as synthesising the macrocyclic bis-pyridine ligands as well as the macrocyclic Ag(I), Au(I) and Br(I) complexes, with all crystallographic work done by the author of this thesis.

## 4.3 Target Macrocycle Designs

The series of bis-pyridine containing macrocycles designed to investigate the 'halonium macrocyclic effect' included both symmetric and asymmetric ligand systems with two different ring linker sizes as well as variation in the Lewis basicity of the pyridine ligands through the incorporation of oxygen atoms into the linker alkyl chain (Figure 4.7).

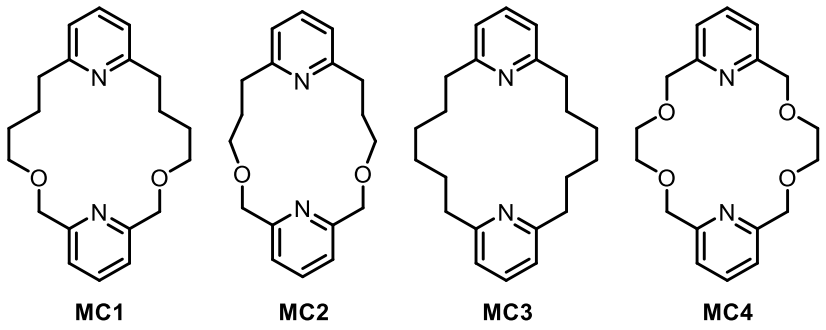



*Figure 4.7. Target bis-pyridine containing macrocycles*

All macrocycles contain pyridine motifs, which were chosen based on their proven ability to stabilise haloniums in addition to their synthetic availability. As mentioned previously, their aromatic nature allows for a delocalisation of the charge on the halonium cation leading to enhanced stability of the complex.[17] The macrocycle size needs to be sufficiently large to accommodate for the N···$X^+$···N bond lengths of approximately 4.6 Å for iodonium and 4.3

Å for bromonium. A more flexible linker system was chosen to allow for the accommodation of these halonium species with rigid macrocyclic systems with small cavities having previously failed to give strong experimental evidence for halonium complexation.[17, 46] Furthermore, the macrocycle designs were carefully chosen to allow for an investigation into the effect of the pyridine-pyridine ligand separation through different methylene and ether spacer lengths has on the type of halonium that can be stabilised (Figure 4.7). Methylene-oxygens were also incorporated into the macrocycle spacer units to investigate how the presence of other potential donor atoms affect halonium complex formation and stability.

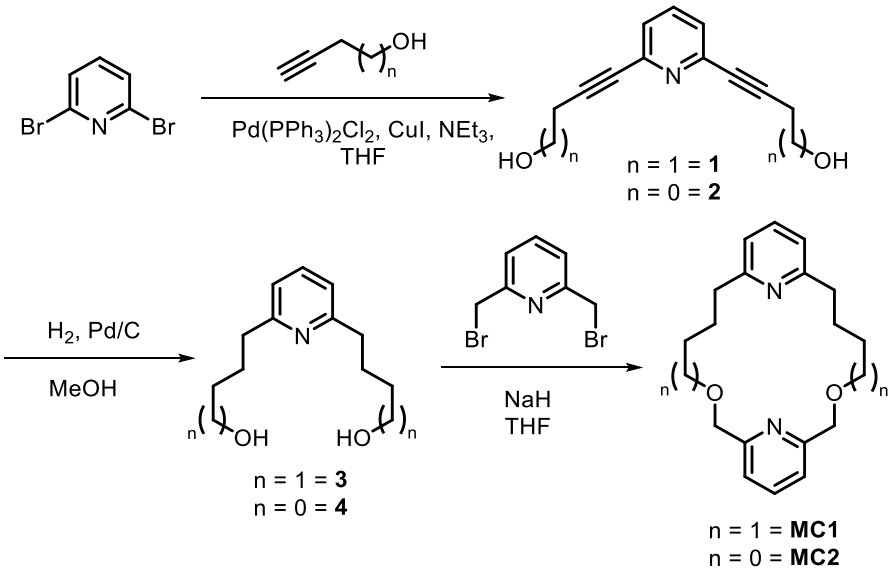
The first section of this chapter contains synthetic details for the preparation of four bis-pyridine containing macrocycles (Figure 4.7). The second section details the formation of Ag(I) and Au(I) metal $d^{10}$ complexes, the former as reagents for subsequent halonium cation complexation, which includes analysis of their solid-sate structures. The subsequent sections investigate macrocycle halonium complex formation, focusing on bromonium complexation of **MC1** and discussion of solid-state structures of the complexes. Solution phase $^{1}$H NMR exchange experiments were undertaken to provide evidence of a macrocyclic effect for halonium cation stabilisation.

## 4.4 Synthesis of Macrocyclic Bis-Pyridine Ligands for Halonium Stabilisation

### 4.4.1 Synthesis of Macrocyclic Ligands **MC1** and **MC2**

The novel macrocycles **MC1** and **MC2** were prepared in three steps under analogous conditions (Scheme 4.3). Firstly, commercially available 2,6-dibromopyridine was subjected to Sonogashira coupling reaction conditions with 3-butyn-1-ol and propargyl alcohol respectively. The resulting 4,4'-(2,6-pyridinediyl)bis[3-butyn-1-ol] **1** was isolated in 59% yield after chromatographic purification. 3,3'-(2,6-Pyridinediyl)bis[2-propyn-1-ol] **2** was purified by silica gel flash column

chromatography with the resulting purity being approximately 90% as determined by $^{1}$H NMR. The alcohol functionalised pyridine motif **2** was then subjected to further reaction without repeated purification. Both alkyne-diols were subjected to hydrogenation using 10% Pd on carbon under an atmosphere of hydrogen to afford **3** in 46% yield as well as **4** in 50% yield over two steps. Macrocyclisation was achieved through dropwise addition of the appropriate diol **3** or **4** and 2,6-bis(bromomethyl)pyridine to a refluxing suspension of NaH in THF. Following silica gel flash column chromatography in a 3:2:0.3 mixture of $CH_2Cl_2$, ethyl acetate and methanol (v/v) the macrocycles were isolated in 42% yield for **MC1** and 63% yield for **MC2**.




*Scheme 4.3. Synthesis of macrocycle **MC1** and **MC2***

Both macrocycles were fully characterised by $^{1}$H NMR, $^{13}$C NMR and high-resolution ESI mass spectrometry. Representative spectroscopic data for **MC1** is shown in Figure 4.8.

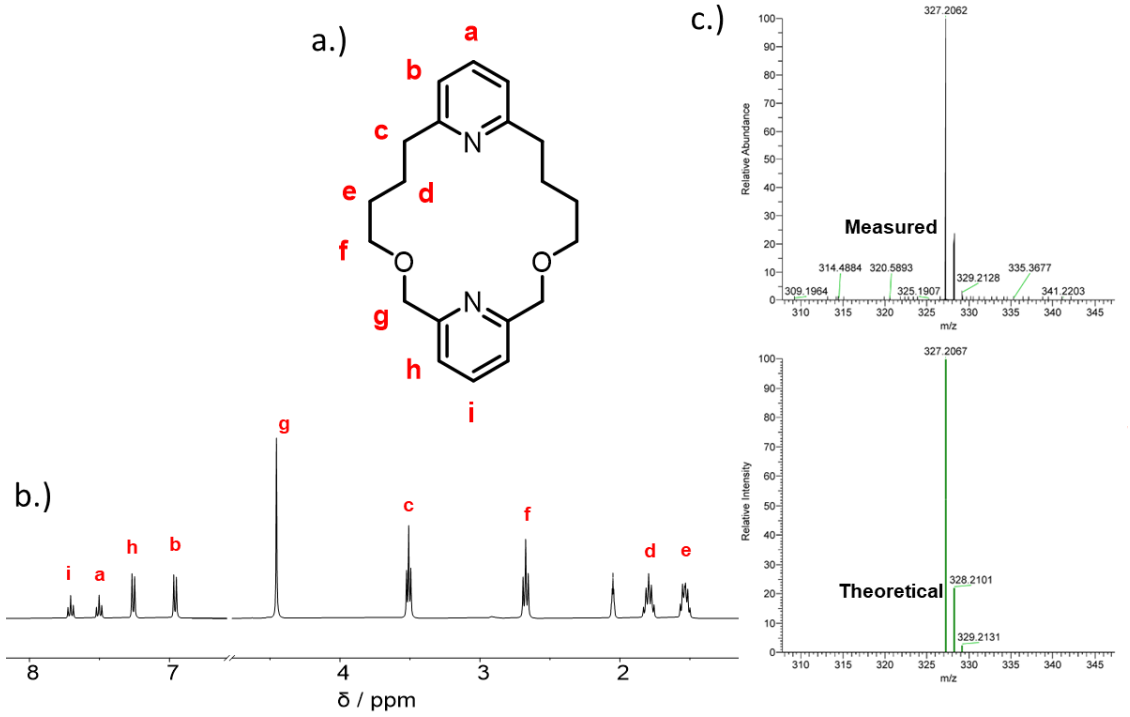
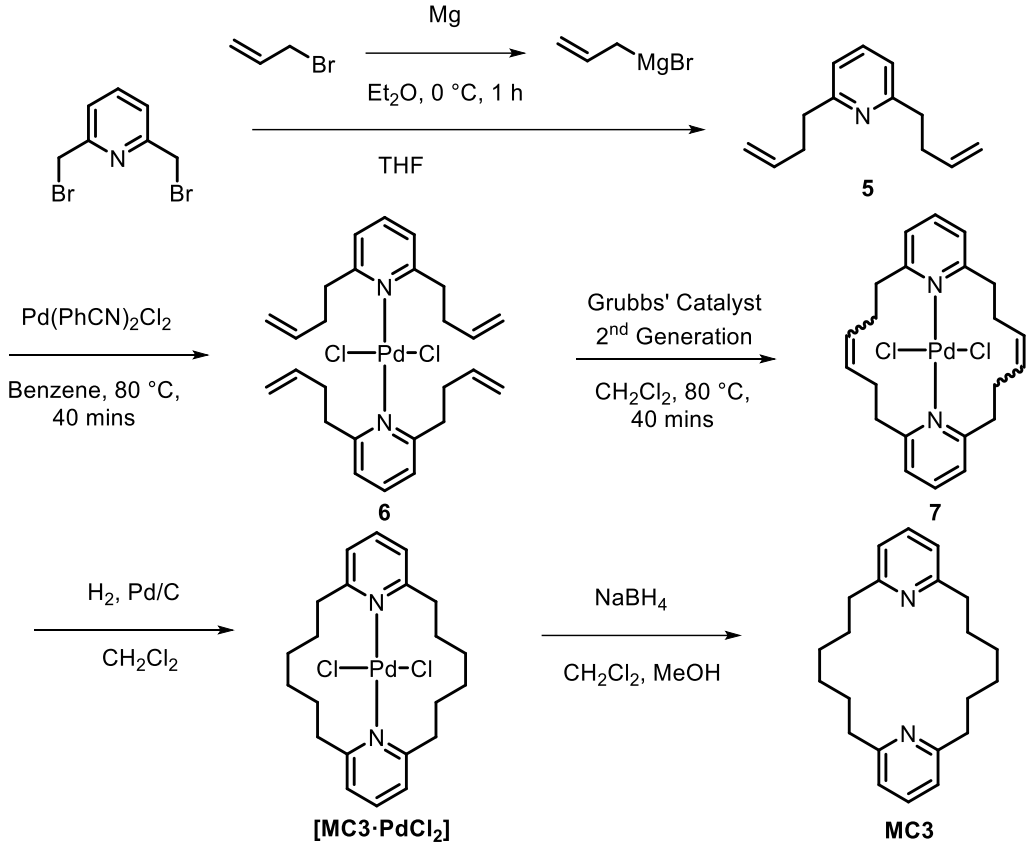



*Figure 4.8. a.) Chemical structure of **MC1** b.) Truncated $^{1}$H NMR spectrum of **MC1** (acetone-$d_6$, 400 mHz, 298K) and c.) theoretical (bottom) and measured (top) high resolution ESI spectra*

### 4.4.2 Synthesis of Macrocyclic Ligand **MC3**

The symmetric [6.6](2,6)pyridinophane macrocycle complexed with $PdCl_2$, **[MC3·PdCl$_2$]**, was prepared according to a literature procedure (Scheme 4.5).[47] Commercially available 2,6-bis(bromomethyl)pyridine was combined with *in situ* generated allylmagnesium bromide in THF. Chromatographic purification gave the doubly alkylated pyridine **5** as a yellow oil in 43% yield. The formation of the dichloropalladium bis(pyridine) complex **6** in 31% yield was achieved through combining 2.3 equivalents of **5** with 1 equivalent of bis(benzonitrile)palladium(II) chloride followed by purification using silica gel flash column chromatography. A solution of **6** was treated with Grubbs' 2$^{nd}$ generation catalyst in anhydrous $CH_2Cl_2$ to form **7** *via* a double ring-closing metathesis. The mixture was subsequently filtered and subjected to hydrogenation conditions using 10% palladium on carbon under an atmosphere of hydrogen to form **[MC3·PdCl$_2$]**. Decomplexation of palladium to form the free

macrocycle **MC3** was achieved by treatment of **[MC3·PdCl$_2$]** with $NaBH_4$. **MC3** was isolated in a 13% yield over 4 steps, following chromatographic purification and fully characterised by $^1$H NMR, $^{13}$C NMR and high-resolution ESI mass spectrometry.

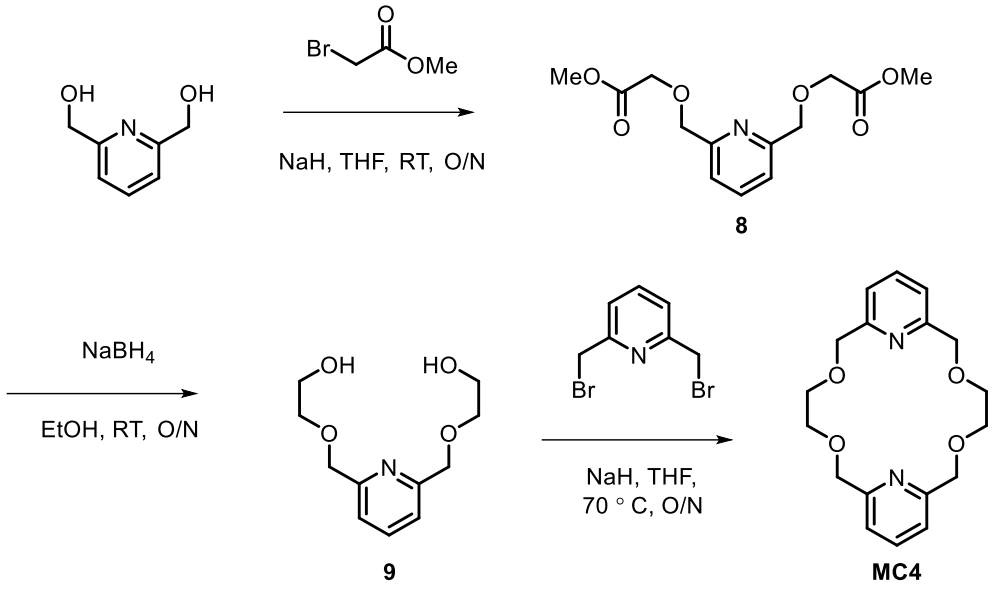



*Scheme 4.4. Synthesis of macrocycle **MC3***

### 4.4.3 Synthesis of Macrocyclic Ligand **MC4**

Bis-pyridino-18-crown-6 **MC4** is known in the literature[48] but has been prepared according to a modified procedure. Therefore, for the formation of the symmetric **MC4** (Scheme 4.5) commercially available methyl bromoacetate and 2,6-bis(hydroxymethyl)pyridine were combined with NaH in THF to form diester **8** in 13% yield after silica gel flash column chromatography. Diol **9** was formed *via* reduction of **8** using sodium borohydride in 80% yield before being added dropwise to a solution of 2,6-bis(bromomethyl)pyridine and NaH in THF

to form **MC4** in 11% yield following chromatographic purification. **MC4** was fully characterised by $^{1}$H NMR, $^{13}$C NMR and high-resolution ESI mass spectrometry.




*Scheme 4.5. Synthesis of macrocycle **MC4***

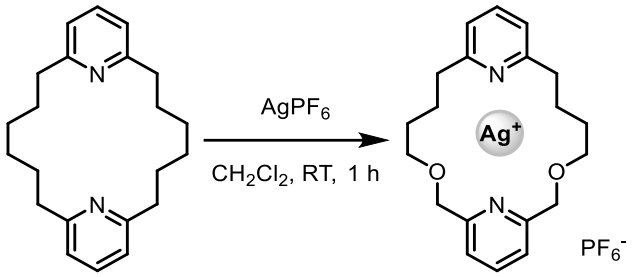
## 4.5 Formation of Ag(I) and Au(I) d$^{10}$ Metal Complexes

Both Ag(I) and Au(I) transition metal cations can be regarded as analogues of halonium cations due to their electronic nature and ability to form 2-coordinate linear complexes.[34] Furthermore, Ag(I) complexes are commonly used precursor complexes employed for the subsequent preparation of halonium complexed species *via* their reaction with elemental halogens.[30, 49] The Ag(I) and Au(I) cation binding properties of the previously prepared macrocycles were therefore firstly investigated.

### 4.5.1 Ag(I) Complex Formation

In a general procedure, each macrocycle was dissolved in anhydrous $CH_2Cl_2$ together with $AgPF_6$ and the mixture left to stir for 1 hour (Scheme 4.6). The resulting **[MC1·AgPF$_6$]**,

**[MC2·AgPF$_6$]**, **[MC3·AgPF$_6$]** and **[MC4·AgPF$_6$]** complexes were isolated by filtering the solution and solvent evaporation.




*Scheme 4.6. Formation of **[MC1·AgPF$_6$]***

### 4.5.2 Ag(I) Complex Solid-State Characterisation

Crystals suitable for X-ray diffraction analysis of the **[MC1·AgPF$_6$]**, **[MC2·AgPF$_6$]**, and **[MC3·AgPF$_6$]** complexes were obtained by slow evaporation of the $CD_2Cl_2$ solutions. The solid-state structures revealed that the Ag(I) is bound by all macrocycles endotopically, forming two N···Ag coordinate bonds (Figure 4.9).

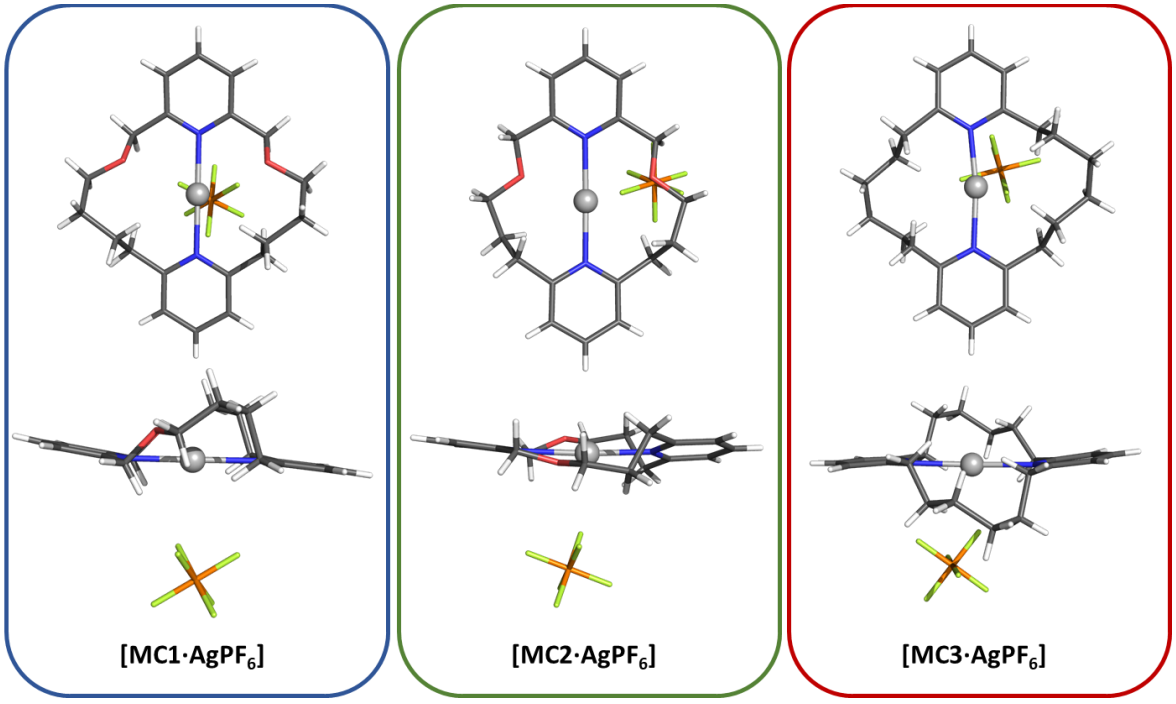



*Figure 4.9. X-ray single crystal structure of **[MC1·AgPF$_6$]**, **[MC2·AgPF$_6$]** and **[MC3·AgPF$_6$]**. Each showing one complex from two different angles.*

**[MC2·AgPF$_6$]** crystallised in the triclinic space group P –1 and **[MC3·AgPF$_6$]** in the monoclinic space group P 21/c. **[MC1·AgPF$_6$]**, which crystallised in the higher symmetry orthorhombic space group P n m a, has an asymmetric unit that only contains 'half' of the macrocycle and counter anion (Figure 4.10), with the two halves being related through a mirror plane.

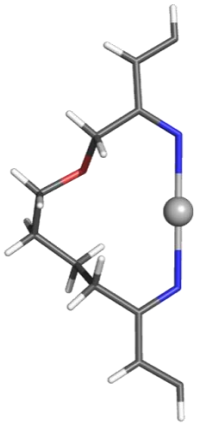


*Figure 4.10. Asymmetric unit of **[MC1·AgPF$_6$]***

Notably **[MC3·AgPF$_6$]** co-crystallised with a $CH_2Cl_2$ solvent molecule in the asymmetric unit, unlike the other two complexes, which only contain the complex and counter anion. Rapid solvent loss accompanied by crystal degradation could be observed when handling crystals of the **[MC3·AgPF$_6$]** complex outside of their mother liquor. The solid-state structure itself shows disorder in one of the alkyl chains of the macrocycle, as well as both pyridine motifs, which has been modelled as shown in Figure 4.11.

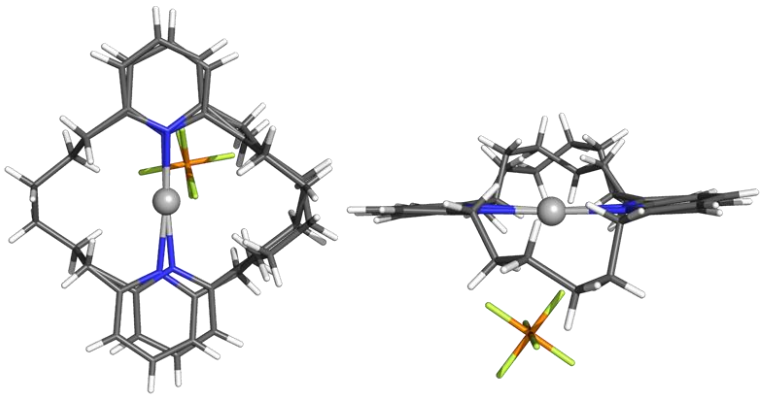


*Figure 4.11. Modelled disorder for **[MC3·AgPF$_6$]***

For the determination of distances and angles, the nitrogen atoms with the highest occupancy level were chosen, which are also the ones shown in Figure 4.9. Due to the degree of disorder in the macrocycle pyridine ligand motifs, these values are less reliable when compared to a non-disordered complex, such as **[MC1·AgPF$_6$]**. The solid-state structure, however, still clearly indicates that the macrocycle is capable of linear endotopic coordination of an Ag(I) metal.

Interestingly, **[MC2·AgPF$_6$]** also exhibits considerable disorder. As can be seen in Figure 4.12, the disorder is related to the way the macrocycle itself is orientated within the crystal lattice. As determined by the refined occupancy level of the methylene-oxygens and surrounding carbons, the macrocycle is in the same orientation 90% of the time, however, it also appears to be present with the oxygens 'flipped' to the other side approximately 10% of the time. This type of disorder has not been observed for any of the other crystal structures presented in this chapter. Again, all measurements presented in Table 4.1 are based on the atoms with the highest occupancy levels.

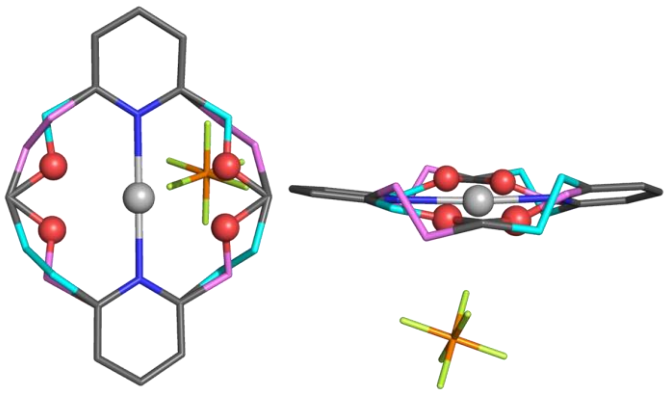


*Figure 4.12. **[MC1·AgPF$_6$]** with modelled disorder. The disordered alkyl chain with the higher occupancy is coloured in cyan and the lower occupancy atoms are coloured in pink. Hydrogens have been removed for clarity. Showing one complex from two different angles.*

Selected distances and angles for **[MC1·AgPF$_6$]**, **[MC2·AgPF$_6$]**, and **[MC3·AgPF$_6$]** are listed in Table 4.1. N1 denotes the nitrogen closest to the methylene-oxygen for **MC1** and **MC2**

(Figure 4.13). This notation will be used throughout to chapter to distinguish the two nitrogen donors.

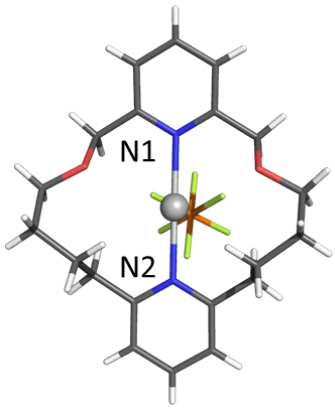



*Figure 4.13. Structure of general $X^+$ MC complex with two distinct nitrogen donors N1 and N2*

*Table 4.1. Selected distances and angles calculated from the solid-state structures using PLATON. Values in angstroms or degrees. Standard uncertainties (±) are in parentheses.*

| | **Distance $Ag^+\cdots N1$ (Å)** | **Distance $Ag^+\cdots N2$ (Å)** | **Angle $N1\cdots Ag^+\cdots N2$ (°)** | **Dihedral Angle Py···Py (°)** |
|---|---|---|---|---|
| **[MC1·AgPF$_6$]** | 2.188(3) | 2.183(3) | 179.56(9) | 3.69(11) |
| **[MC2·AgPF$_6$]** | 2.232(4) | 2.181(4) | 176.73(13) | 15.0(2) |
| **[MC3·AgPF$_6$]** | 2.113(11) | 2.235(6) | 172.1(4) | 6.3(5) |

In general, almost linear coordination of the Ag(I) cation by the pyridine ligands can be observed for all three complexes with all three $N1\cdots Ag^+\cdots N2$ angles being close to 180°.

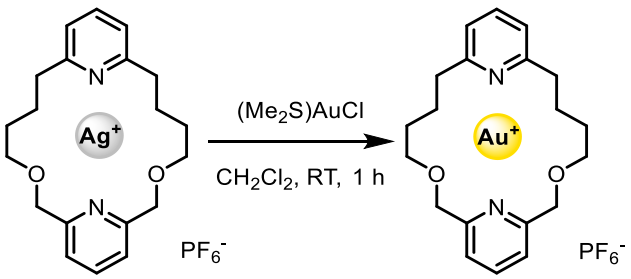
As expected, the $N1\cdots X^+\cdots N2$ bonds of **[MC1·AgPF$_6$]** are the most symmetric and the complex shows the highest degree of linearity. In comparison to the **MC1** complex, the **[MC2·AgPF$_6$]** and **[MC3·AgPF$_6$]** complex shows a much greater level of asymmetry in the

N1···$Ag^+$···N2 bond distances; however, it is unclear how much of it can be attributed to their respective disorders present within the solid-state structure.

It is notable that short $Ag^+$···O distances can also be observed for **[MC2·AgPF$_6$]**, with both oxygens pointing towards the Ag(I) centre (Figure 4.9). The **[MC2·AgPF$_6$]** complex furthermore shows less co-planarity between the pyridine units, which are slightly twisted with respect to one another resulting in a dihedral angle of 15.0(2)° (Table 4.1). The dihedral angles for both **[MC1·AgPF$_6$]** and **[MC3·AgPF$_6$]** are smaller with the pyridine units for **[MC1·AgPF$_6$]** being very close to co-planarity (Table 4.1).

### 4.5.3 Au(I) Complex Formation

The Au(I) coordination chemistry of the different macrocycles was also investigated *via* transmetallation reactions with the corresponding isolated Ag(I) macrocycle complexes. To this end, $CH_2Cl_2$ solutions of **[MC1·AgPF$_6$]**, **[MC2·AgPF$_6$]**, **[MC3·AgPF$_6$]** and **[MC4·AgPF$_6$]** respectively were treated with a stoichiometric quantity of chloro(dimethylsulfide)gold(I), immediately inducing the precipitation of AgCl and Au(I) complexation (Scheme 4.7).[50]




*Scheme 4.7. Formation of **[MC1·AuPF$_6$]***

### 4.5.4 Au(I) Complex Solid-State Characterisation

Solid state structural determination of the resultant **[MC1·AuPF$_6$]**, **[MC2·AuPF$_6$]**, and **[MC3·AuPF$_6$]** complexes confirmed the formation of a linear bis-pyridine-type metal complex (Figure 4.14).

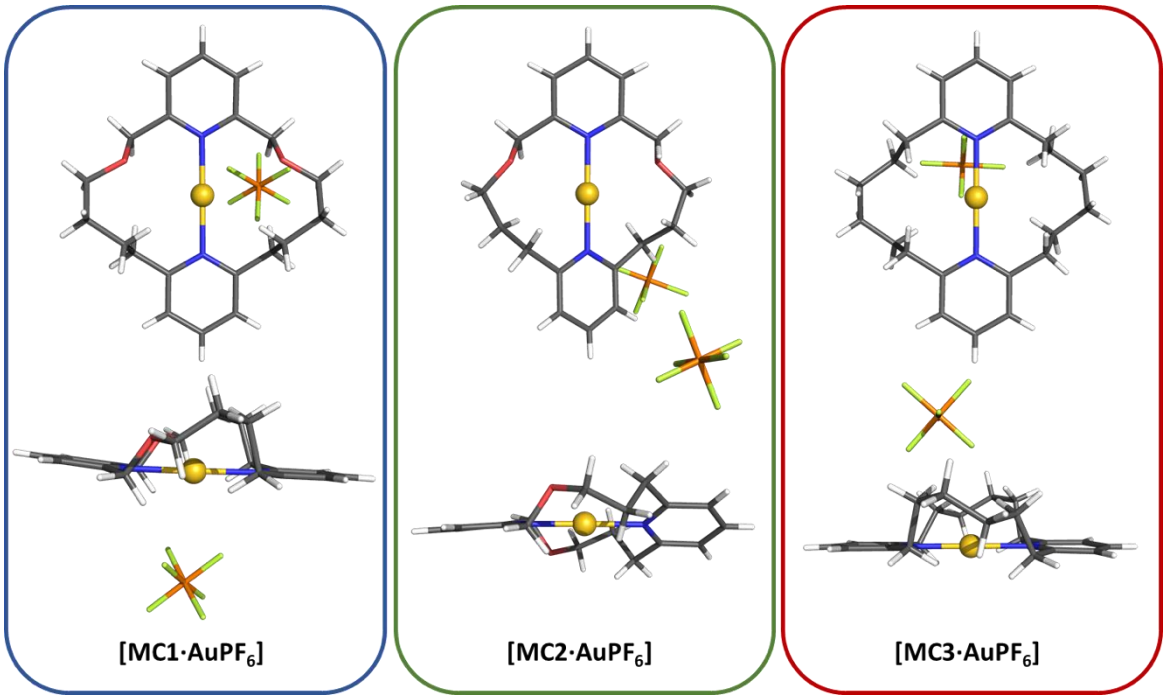



*Figure 4.14. X-ray single crystal structure of **[MC1·AuPF$_6$]**, **[MC2·AuPF$_6$]** and **[MC3·AuPF$_6$]**. Each showing one complex from two different angles.*

Selected distances and angles for **[MC1·AuPF$_6$]**, **[MC2·AuPF$_6$]**, and **[MC3·AuPF$_6$]** are listed in Table 4.2.

Relative to the Ag(I) structures, the Au(I) complexes exhibit a stricter preference for linearity with the measured N···Au$^+$···N angles being consistently within one degree of 180° as listed in Table 4.2. All three complexes are furthermore symmetric with regards to the N1···Au$^+$···N2 bond distances.

*Table 4.2. Selected distances and angles calculated from the solid-state structures using PLATON. Values in angstroms or degrees. Standard uncertainties (±) are in parentheses.*

| | **Distance $Au^{+}\cdots N1$ (Å)** | **Distance $Au^{+}\cdots N2$ (Å)** | **Angle $N1\cdots Au^{+}\cdots N2$ (°)** | **Dihedral Angle Py···Py (°)** |
|---|---|---|---|---|
| **[MC1·AuPF$_6$]** | 2.079(4) | 2.074(4) | 178.94(14) | 5.3(2) |
| **[MC2·AuPF$_6$]** | 2.030(2) | 2.027(7) | 179.51(8) | 22.43(12) |
| **[MC3·AuPF$_6$]** | 2.055(2) | 2.060(2) | 179.90(10) | 3.96(16) |

The longest $Au^{+}\cdots N$ bond distances are observed for the **[MC1·AuPF$_6$]** complex with **[MC3·AuPF$_6$]** exhibiting bond lengths which are on average 0.02 Å shorter. The shortest $Au^{+}\cdots N$ bond distances of approximately 2.03 Å correspond to the complexation by the smallest macrocycle **MC2** (Table 4.2). Overall, the macrocycle asymmetry of **MC1** and **MC2** does not seem to affect the metal-coordinated interaction geometries.

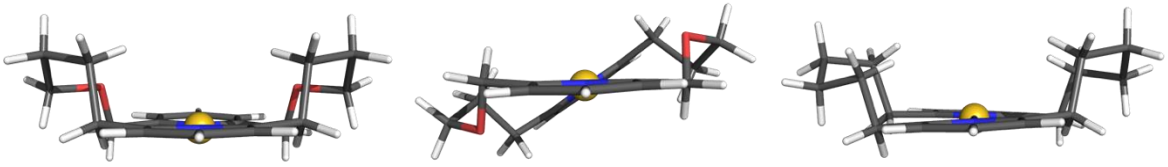



*Figure 4.15. Comparison of **[MC1·AuPF$_6$]**, **[MC2·AuPF$_6$]** and **[MC2·AuPF$_6$]** with view along $N\cdots Au^{+}\cdots N$ bonds.*

Interestingly, the **[MC2·AuPF$_6$]** complex exhibits a much more macrocycle twisted structure with regards to the pyridine planes (Figure 4.15). The dihedral angle is 33.43(12)° in comparison to the small dihedral angles of 5.3(2)° for **[MC1·AuPF$_6$]** and 3.96(16)° for **[MC3·AuPF$_6$]** respectively (Table 4.2). Figure 4.15 also highlights that the deviation from co-planarity of the

pyridine motifs for the **MC2** complexes is accompanied by the alkyl chains pointing in opposite directions rather than being an approximate mirror image of each other, as can be observed for the **MC1** and **MC3** complexes.

As discussed in Section 4.5.2, the pyridine units in the **[MC2·AgPF$_6$]** complex are also not co-planar, however, the twisting is more pronounced for **[MC2·AuPF$_6$]**. However, the structure of the **[MC2·AgPF$_6$]** complex is dominated by short $Ag^+\cdots O$ contacts, which are not observed in the same manner for the analogous gold complex **[MC2·AuPF$_6$]**. These interactions of the Ag(I) with the methylene oxygens therefore mean the Ag(I) and Au(I) $d^{10}$ metals interact slightly differently with **MC2** and the resulting complexes are no longer analogous in their solid-state structure arrangement.

### 4.5.5 Conclusions

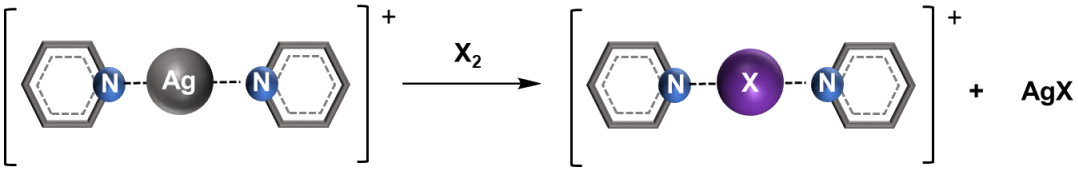
In summary, the three different bis-pyridine containing macrocycles **MC1**, **MC2** and **MC3** proved capable of forming Ag(I) and Au(I) complexes. Their solid-state structures were successfully determined and direct comparisons between the complexes revealed all of them to exhibit linear, endotopic complexation of the $d^{10}$ metal cations.

## 4.6 Formation of Halonium Complexes

### 4.6.1 Iodonium

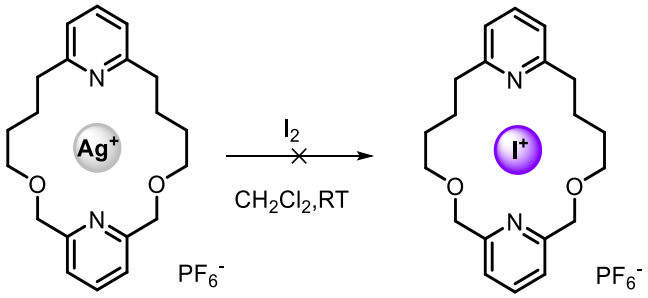
With the ability of the macrocycles to linearly coordinate $d^{10}$ transition metals firmly established, the macrocycles' ability to complex halonium ions was subsequently investigated. The generation of a halonium complex is typically achieved by treatment of a Ag(I) complex

precursor with a source of the elemental halogen, in which a disproportionation reaction occurs, precipitating the corresponding silver halide (Scheme 4.8).[30, 33, 51]




*Scheme 4.8. Formation of a halonium species via silver cation exchange*

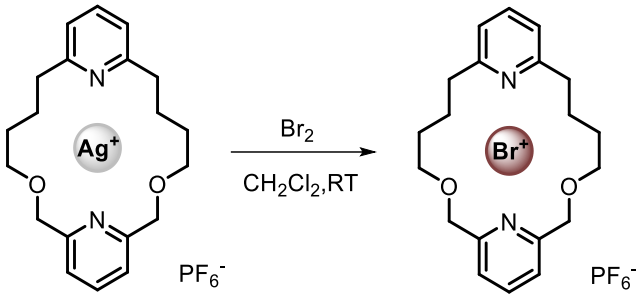
To this end, a $^1$H NMR titration experiment, in which a $CD_2Cl_2$ solution of the Ag(I) macrocycle complex **[MC1·AgPF$_6$]** was treated with $I_2$ at room temperature, was undertaken (Scheme 4.9). Surprisingly, the persistent purple colour of elemental iodine remained and no perturbation by $^1$H NMR was observed even after several days. This suggested that the combination of bis-pyridine coordination and potential additional Ag(I)···O interactions kinetically stabilises Ag(I) from reacting with iodine. Indeed, moderate heating of the reaction mixture resulted in $I_2$ vaporisation and no observable reaction.




*Scheme 4.9. Attempted formation of **[MC1·IPF$_6$]***

### 4.6.2 Bromonium

Despite the lack of reaction with $I_2$, ambitiously a more reactive halogen was selected as the partner for the disproportionation reaction *i.e.*, bromine. Pleasingly, addition of a $CH_2Cl_2$ solution of $Br_2$ to **[MC1·AgPF$_6$]** resulted in the immediate precipitation of AgBr (Scheme 4.10).




*Scheme 4.10. Formation of* ***[MC1·BrPF$_6$]***

The $^1$H-NMR spectrum of the remaining solution revealed the formation of a new species, notably distinct from the free macrocycle or silver(I) complex (Figure 4.16).

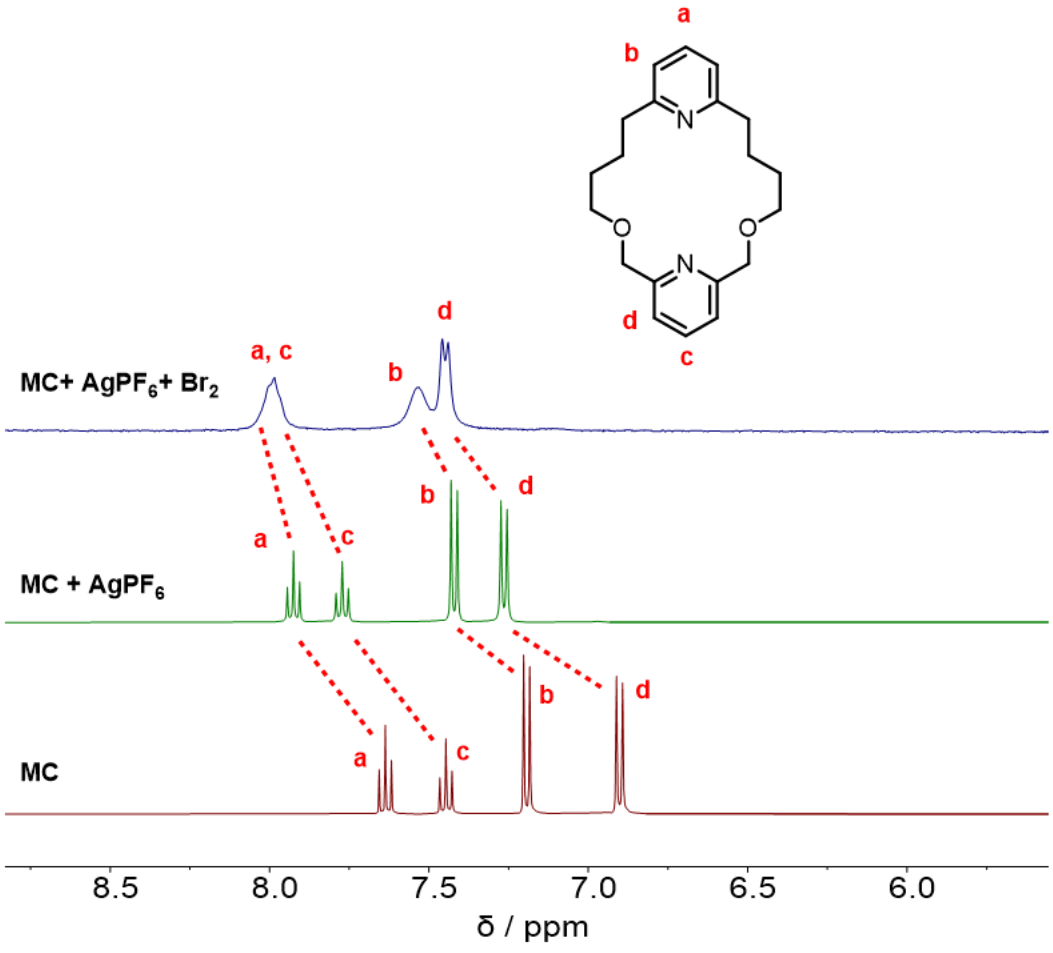



*Figure 4.16. $^1$H-NMR spectra of MC-2 (bottom),* ***[MC1·AgPF$_6$]*** *(middle), and* ***[MC1·BrPF$_6$]*** *(top). ($CD_2Cl_2$, 400 MHz, 298 K).*

Single crystals suitable for X-ray diffraction were obtained for the Br(I) complex by slow evaporation of the $CH_2Cl_2$ solution, protected from moisture, which revealed the linear endotopic coordination of the bromonium cation in the macrocycle cavity (Figure 4.17).

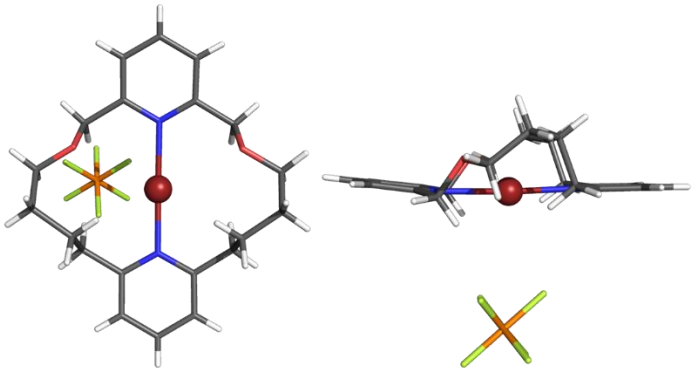


*Figure 4.17. X-ray single crystal structure of **[MC1·BrPF$_6$]**. Showing one complex from two different angles.*

When comparing the bromonium complex to its analogous Ag(I) and Au(I) complexes (Table 4.3), it is noteworthy that Br(I) demonstrated asymmetry in the N···Br$^+$···N bond distances in contrast to the highly symmetric Au(I) and Ag(I) complexes.

*Table 4.3. Selected distances and angles calculated from the solid-state structures using PLATON. Values in angstroms or degrees. Standard uncertainties (±) are in parentheses.*

| | **Distance X$^+$···N1 (Å)** | **Distance X$^+$···N2 (Å)** | **Angle N1···X$^+$···N2 (°)** | **Dihedral Angle Py···Py (°)** |
|---|---|---|---|---|
| **[MC1·BrPF$_6$]** | 2.234(3) | 2.099(3) | 177.18(10) | 7.83(16) |
| **[MC1·AgPF$_6$]** | 2.186(3) | 2.183(3) | 179.55(11) | 3.62(14) |
| **[MC1·AuPF$_6$]** | 2.069(4) | 2.076(4) | 178.90(16) | 5.2(3) |

For the Br(I) complex, the distance to N1 is longer than N2, indicating that the halonium XB is very sensitive to the electronic environment of the ligand. The complex, however, still shows

a strong directionality of the XB interaction and a clear preference for linear bond formation (Table 4.3).

## 4.7 Further Investigation of **MC1** as a Macrocyclic Ligand for Br(I) Stabilisation

To investigate the possible role of the counter-anion in the complexation behaviour of **MC1**, analogous complexation procedures with alternative silver(I) salts, specifically $AgBF_4$ and $AgNO_3$ were undertaken (Scheme 4.6, Scheme 4.7, Scheme 4.10).

Single crystals suitable for X-ray diffraction were obtained for **[MC1·BrBF$_4$]**, **[MC1·AgBF$_4$]**, **[MC1·AuBF$_4$]**, **[MC1·BrNO$_3$]**, **[MC1·AgNO$_3$]** and **[MC1·AuNO$_3$]** complexes by slow evaporation (Figure 4.18).

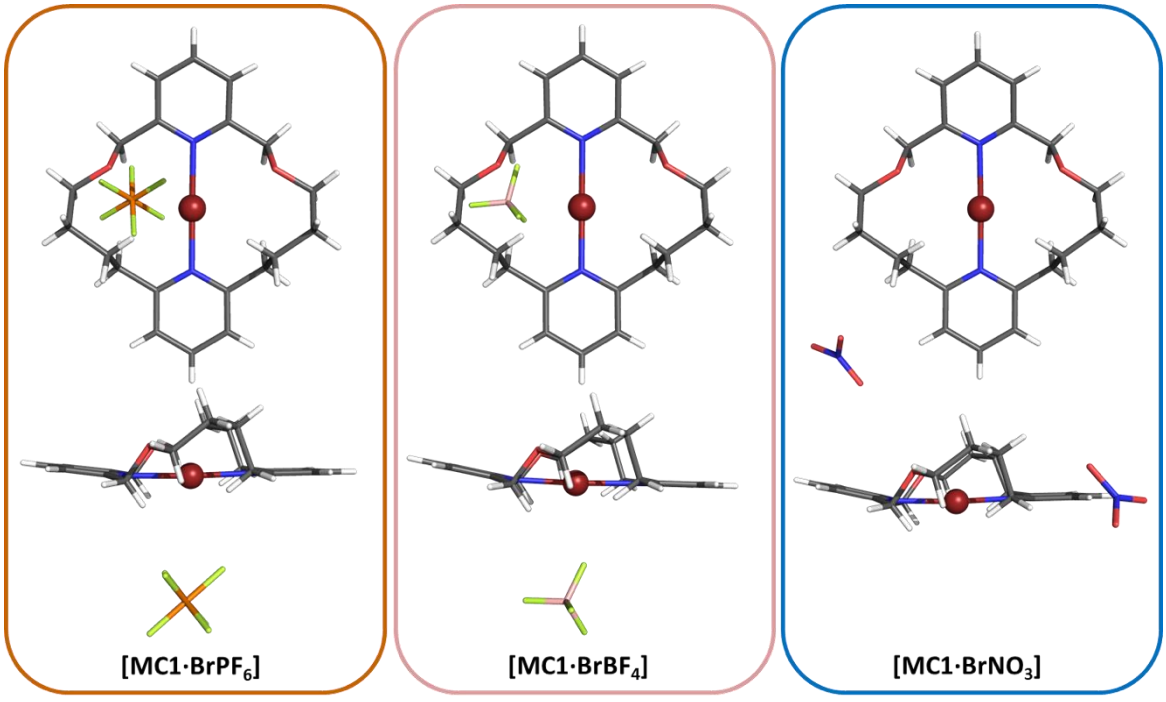



*Figure 4.18. X-ray single crystal structure of **[MC1·BrPF$_6$]**, **[MC1·BrBF$_4$]** and **[MC1·BrNO$_3$]**. Each showing one complex from two different angles.*

For the purpose of comparison, structural data for all 9 complexes are listed in Table 4.4 and Table 4.5. It is noteworthy that **[MC1·AgNO$_3$]** has three symmetrically unrelated molecules in the asymmetric unit, giving rise to the three sets of distances listed for this particular complex.

*Table 4.4. N···X$^+$···N distances calculated from the solid-state structures using PLATON. All values in angstroms. Standard uncertainties (±) are in parentheses.*

| | **Distance (Å)** | | | | | |
|---|---|---|---|---|---|---|
| **X$^+$ =** | **Br(I)** | | **Ag(I)** | | **Au(I)** | |
| **Counter Anion** | **X$^+$···N1** | **X$^+$···N2** | **X$^+$···N1** | **X$^+$···N2** | **X$^+$···N1** | **X$^+$···N2** |
| **$PF_6^-$** | 2.234(3) | 2.099(3) | 2.186(3) | 2.183(3) | 2.069(4) | 2.076(4) |
| **$BF_4^-$** | 2.243(5) | 2.096(5) | 2.195(2) | 2.193(2) | 2.066(3) | 2.068(3) |
| **$NO_3^-$** | 2.227(2) | 2.090(2) | 2.238(1) | 2.224(1) | 2.089(4) | 2.078(4) |
| | | | 2.260(1) | 2.234(1) | | |
| | | | 2.243(1) | 2.233(1) | | |

In contrast to the highly symmetric Au(I) and Ag(I) complexes, Br(I) demonstrated asymmetry in the N···Br$^+$···N bond distances (Table 4.4). For all three Br(I) complexes, the N1···Br(I) distance is consistently longer suggesting that the presence of the Lewis basic oxygens serves to 'repel' the Br(I) cation. Whilst the exact origin of this effect, whether it is repulsion from the methylene oxygens or the reduced basicity of the pyridine nitrogen by the electron withdrawing methylene oxygens, is unclear, the N1···Br$^+$···N2 bond asymmetry of 6-7% is evident and it is believed not to be solely due to crystal packing.

However, previously reported Br(I) complexes have also shown an asymmetry in the N···Br(I)···N bond distances despite containing two chemically identical ligands.[37, 38] It therefore remains unclear how much of the asymmetry can be attributed to the local electronic environment and how much might be an inherent asymmetry observed for certain Br(I) based XB complexes in the solid state.

The strong directionality of the XB interaction and preference for a linear bond formation was observed in all three bromonium complexes. The N···$X^+$···N angles are all close to 180 degrees as listed in Table 4.5.

*Table 4.5. N···$X^+$···N angles calculated from the solid-state structures using PLATON. All values in angstroms. Standard uncertainties (±) are in parentheses.*

| | **Angle (Å)** | | |
|---|---|---|---|
| **$X^+$ =** | **Br(I)** | **Ag(I)** | **Au(I)** |
| **Counter Anion** | **N1···$X^+$···N2** | **N1···$X^+$···N2** | **N1···$X^+$···N2** |
| **$PF_6^-$** | 177.18(10) | 179.55(11) | 178.90(16) |
| **$BF_4^-$** | 177.16(16) | 177.52(6) | 178.69(11) |
| **$NO_3^-$** | 175.79(8) | 169.29(5) | 177.17(16) |
| | | 167.29(5) | |
| | | 169.05(5) | |

The notable difference in the angle of the three symmetrically unrelated molecules in the asymmetric unit of **[MC1·AgNO$_3$]** arises from the coordination of the $NO_3^-$ counter anion to the Ag(I) centre (Figure 4.19). This difference in the coordination of the nitrate anion by Ag(I) reflects one of the most fundamental differences between halonium and transition metal coordination.[52, 53] Unlike its transition metal counterpart, the halonium cation is inert to coordination by additional Lewis bases in the form of the counter anion as previously discussed by Erdélyi,[52, 53] where the Br(I) complexes all remain comparable despite the change in the coordinating ability of the counter anion.

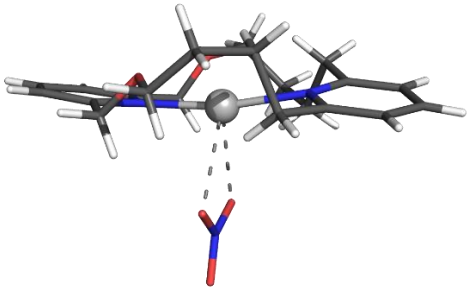


*Figure 4.19. X-ray single crystal structure of **MC1** $AgNO_3$*

*Table 4.6. Ag(I)···O distances calculated from the solid-state structures using PLATON. All values in angstroms. Standard uncertainties (±) are in parentheses. VdW contractions determined using values from[54] shown in %.*

| **X$^+$ =** | **Ag(I)** | | | |
|---|---|---|---|---|
| **Counter Anion** | **Distance Ag(I)···O (Å)** | **%VdW Contraction** | **Distance Ag(I)···O (Å)** | **%VdW Contraction** |
| **$NO_3^-$** | 2.664(2) | 66% | 2.800(2) | 69% |
| | 2.611(2) | 65% | 2.7630(2) | 69% |
| | 2.654(2) | 66% | 2.831(2) | 70% |

The close contacts between the oxygens on the counter anion $NO_3^-$ and the Ag(I) cation are listed in Table 4.6 with all contacts displaying van der Waals (VdW) contractions of 70% or less.[54]

Apart from **[MC1·AgNO$_3$]** and **[MC1·AgPF$_6$]**, all 7 other complexes have crystallised in the monoclinic space group P 21/n with similar unit cell dimensions of a≈11 Å, b≈9 Å, c≈20 Å and β angles ranging from 95° to 98° creating a unit cell with a volume of approximately 2000 Å$^3$ (see SI for more detailed unit cell measurements). As previously discussed in Section 4.5.2, **[MC1·AgPF$_6$]** displays a higher symmetry with the asymmetric unit only containing "half" of the complex, with the two sides of the macrocycle being related by a mirror plane. None of the 9 complexes crystallised with solvent.

### 4.7.1 Solid-State Structures of Protonated Macrocycle Side Products

It is noteworthy, that attempts to crystallise samples of the bromonium complexes were not always successful and unless effective measures were taken to avoid contact with moisture a frequently encountered additional crystalline species observed in the crystallisation sample corresponded to variously protonated forms of the macrocycle. Solid-state structures for bis- and mono-protonated macrocycle complexes could therefore be obtained (Figure 4.20, Figure 4.21).

The solid-state structure of a doubly protonated **MC1** crystallised together with two $BF_4^-$ counter anions was determined.

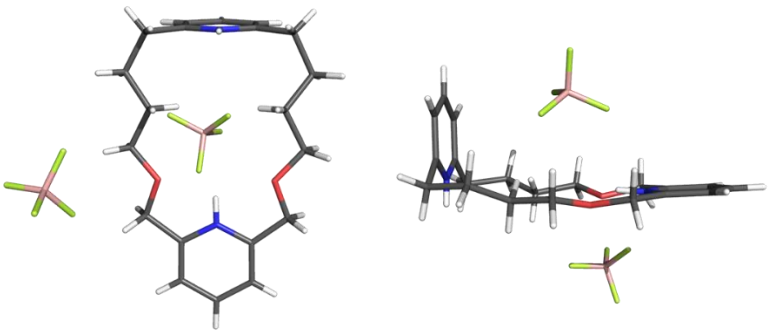


*Figure 4.20. X-ray single crystal structure of **[MC1·2(HBF$_4$)]**. Showing one molecular unit from two different angles.*

The XRD experiments revealed that the conformation of the pyridine units in the macrocycle drastically changes upon protonation with the pyridiniums exhibiting a dihedral angle of 89.15(8)° for the doubly protonated **MC1** (Figure 4.20).

The structure of a mono protonated **[MC1·HPF$_6$.H$_2$O]** complex could furthermore be elucidated (Figure 4.21).

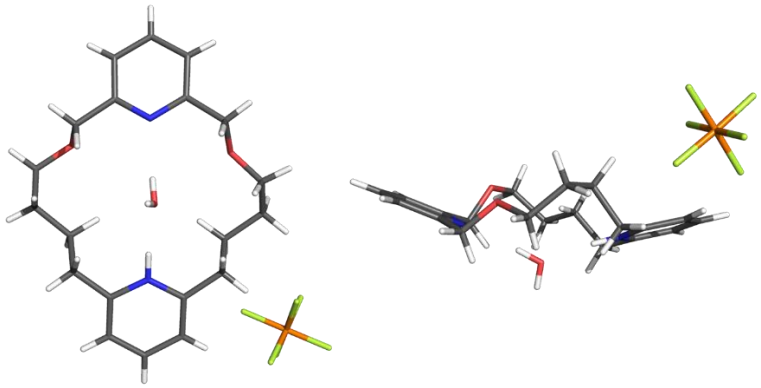


*Figure 4.21. X-ray single crystal structure of **[MC1·HPF$_6$.H$_2$O]**. Showing one molecular unit from two different angles*

The solid-state structure shows the protonated **MC1** crystallising together with $PF_6^-$ and revealing the binding of water within the macrocycle cavity, with evidence of hydrogen bonding occurring to the pyridinium and pyridine unit. Here, N2 is selectively protonated over N1, showing that N1 is a relatively weaker Lewis base due to its proximity to the electron withdrawing methylene-oxygens. The strict linearity observed with XB can no longer be

observed with HB, as shown in Figure 4.21 with an N1···O···N2 angle of 135.98(7)° (Table 4.7). HB distances are listed in Table 4.7.

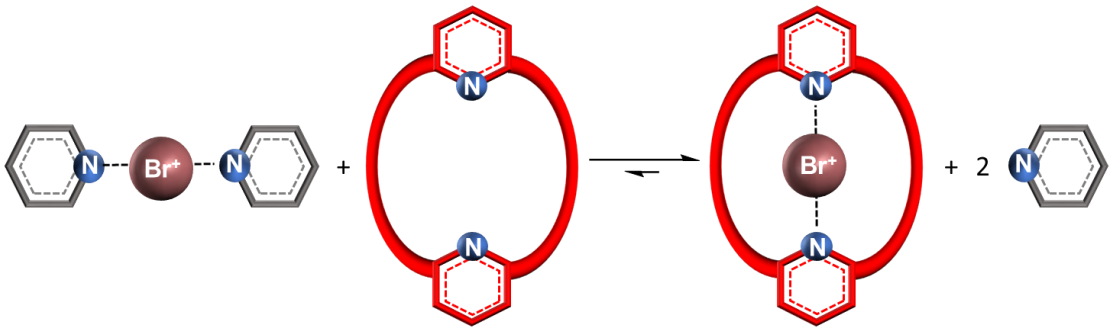
It should be noted that all protonated structures showed much weaker diffraction than their metal or halonium complexed counterparts. However, these structures indicate the versatility of **MC1** with it being able to facilitate both XB and HB.

*Table 4.7. Distances and angles calculated from the **[MC1·HPF$_6$·H$_2$O]** solid-state structure using PLATON. All values in angstroms. Standard uncertainties (±) are in parentheses.*

| **MC1·HPF$_6$·H$_2$O** | | |
|---|---|---|
| **Distance N1···H-OH (Å)** | **Distance N2-H···OH$_2$ (Å)** | **Angle N1···O···N2 (°)** |
| 1.84(3) | 2.06(3) | 135.98(7) |

## 4.7.2 Preliminary Investigation of a Halonium Cation Macrocyclic Effect

Having obtained solid-state crystallographic evidence for the formation of **MC1** bromonium complexes displaying linear endotopic coordination, attention turned to investigate and determine evidence of a potential macrocyclic effect stabilisation of the halonium cation with the cyclic **MC1** ligand. It was postulated that the macrocyclic nature of **MC1** would translate into enhanced bromonium cation complexed thermodynamic stability relative to a simple acyclic bis-pyridine bromonium cation complex species (Scheme 4.11).



*Scheme 4.11. Proposed exchange reaction into the study of a macrocyclic effect of bromonium*

It was anticipated that the Ag(I) cation would also interact with **MC1** according to the conventional macrocyclic effect.

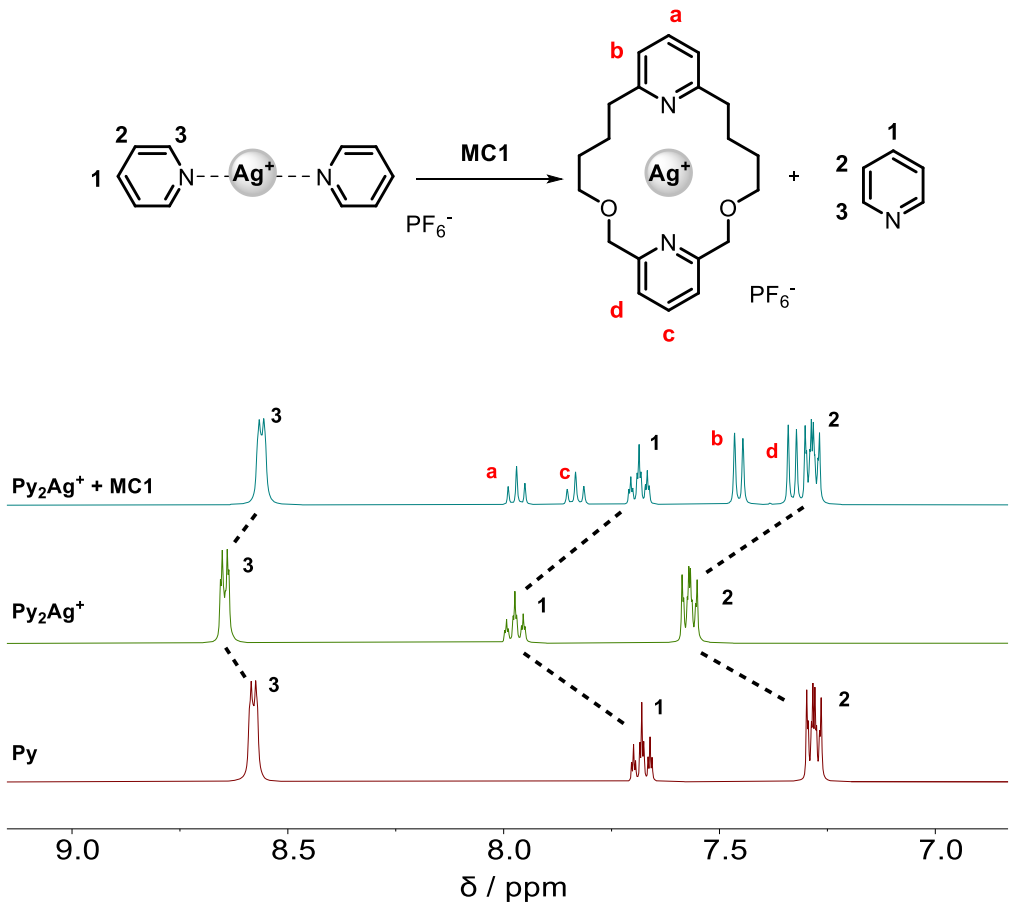



*Figure 4.22. $^{1}$H-NMR Ag(I) exchange experiments of **MC1** and bis-pyridine Ag(I) ($CD_2Cl_2$, 400 MHz, 298 K).*

Therefore, an exchange reaction was conducted in which a pre-formed bis-pyridine Ag(I) complex was mixed with an equimolar amount of the uncomplexed macrocycle **MC1** (Scheme 4.11). The reaction was monitored by $^{1}$H NMR in $CD_2Cl_2$ and, as anticipated, revealed evidence for a metal cation exchange reaction wherein the silver cation is preferentially complexed by **MC1** and pyridine is liberated (Figure 4.22).

With this NMR evidence for the enhanced stability of the Ag(I) **MC1** complex relative to the acyclic analogue (Figure 4.22), an analogous experiment was performed with an *in situ* generated bis-pyridine Br(I) complex (Figure 4.23).

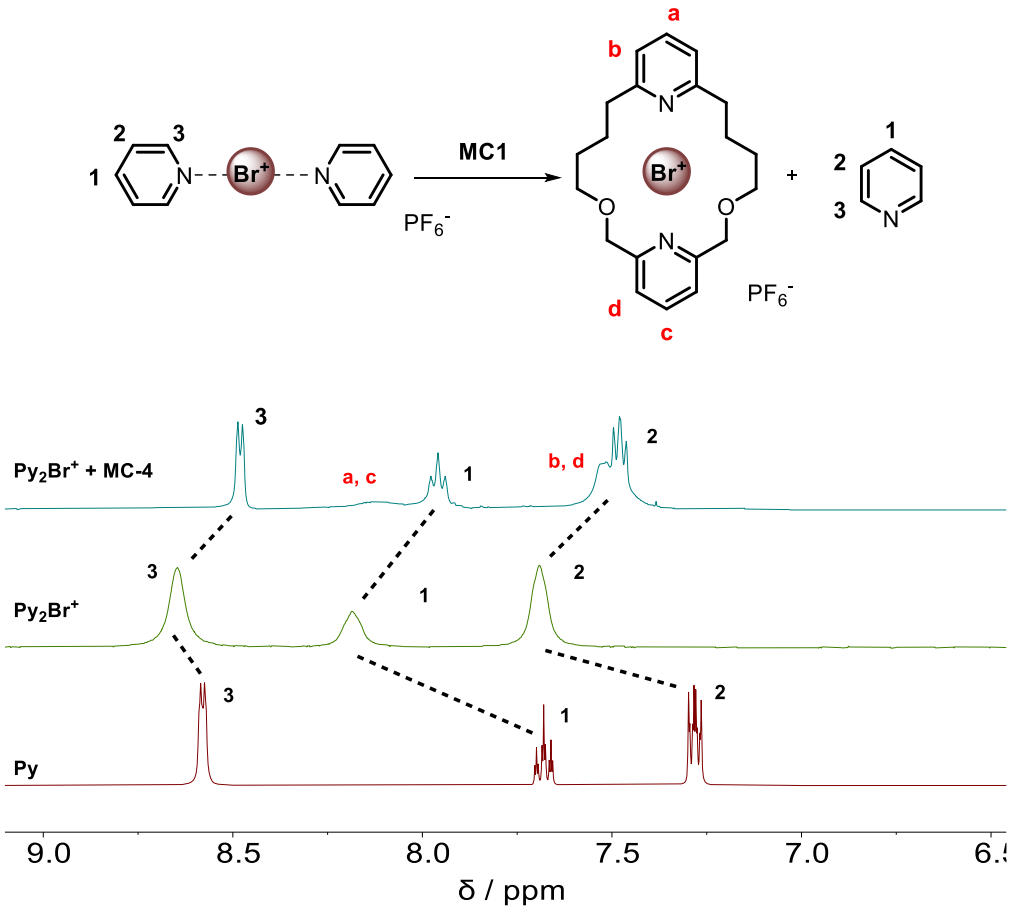



*Figure 4.23. $^{1}$H-NMR Br(I) exchange experiments of **MC1** and bis-pyridine Br(I) ($CD_2Cl_2$, 400 MHz, 298 K).*

Similar perturbations were observed wherein the $^{1}$H-NMR spectrum of the resultant mixture demonstrated evidence for the liberation of pyridine, and concomitant formation of the **MC1**

bromonium complex, providing, to the best of our knowledge, unprecedented evidence of a macrocyclic effect for halonium cations (Figure 4.23).

## 4.8 Conclusion and Future Work

Overall, the synthesis of four different bis-pyridine containing macrocycles was successfully achieved. These included two symmetric and two asymmetric macrocycles with macrocycle ring size variation as well as variation in the Lewis basicity of the pyridine ligands through the incorporation of oxygen atoms into the linker alkyl chain.

Solid state structural characterisation of the Ag(I) and Au(I) complexes of **MC1**, **MC2** and **MC3** revealed symmetric, linear, endotopic complexation of the $d^{10}$ metals. Contrary to Au(I) complexes containing two pyridine based ligands being somewhat rare, due to reported instability[55] as rationalised by the incompatibility of the hard nitrogen donors and soft metal centre,[56] all the Au(I) macrocyclic complexes are stable under atmospheric aerobic conditions and no special measures were needed to be taken in order to avoid decomposition.

The synthesis and solid-state structural characterisation of 9 **MC1** complexes with Ag(I), Au(I) or Br(I) bound endotopically within the cavity was achieved. It is noteworthy, that to the best of our knowledge, only acyclic bromonium cations stabilised by nitrogen-based ligands have been fully structurally characterised previously.[37-43] Furthermore, the bromonium cation has never been isolated before with a counter anion as coordinating as nitrate. The three bromonium complexes reported here also displayed remarkable stability when handled at room temperature under aerobic atmospheric conditions. Previous reports typically describe crystal decomposition when handling crystals of the Br(I) complex or during XRD experiments, which was not observed for the Br(I) **MC1** complexes.[37, 38]

Preliminary solution phase $^{1}$H-NMR exchange experiments revealed unprecedented evidence for a macrocyclic effect for the bromonium cation with **MC1,** which is responsible for its unusual observed enhanced stability. The well-defined cavity size of **MC1** may explain the macrocycle's selectivity for bromonium cation complex formation, while the usually more stable complexed iodonium species could not be formed and isolated with **MC1**.

Future work will focus on a study of halonium complexation with **MC2**, **MC3** and **MC4**, the results of which will determine the effects of macrocycle cavity size as well as the electronic properties of the pyridine ligands have on halonium complex formation and stability.

## 4.9 References


1. I. Roberts and G. E. Kimball, *Journal of the American Chemical Society*, 1937, **59**, 947-948.
2. A. Karim, M. Reitti, A.-C. C. Carlsson, J. Gräfenstein and M. Erdélyi, *Chemical Science*, 2014, **5**, 3226-3233.
3. M. D. Struble, M. T. Scerba, M. Siegler and T. Lectka, *Science*, 2013, **340**, 57-60.
4. V. V. Grushin, *Chemical Society Reviews*, 2000, **29**, 315-324.
5. E. A. Merritt and B. Olofsson, *Angewandte Chemie International Edition*, 2009, **48**, 9052-9070.
6. E. S. Stoyanov, I. V. Stoyanova, F. S. Tham and C. A. Reed, *Journal of the American Chemical Society*, 2010, **132**, 4062-4063.
7. M. D. Struble, M. G. Holl, M. T. Scerba, M. A. Siegler and T. Lectka, *Journal of the American Chemical Society*, 2015, **137**, 11476-11490.
8. C. R. Pitts, M. G. Holl and T. Lectka, *Angewandte Chemie International Edition*, 2018, **57**, 1924-1927.
9. K. F. Hoffmann, A. Wiesner, C. Müller, S. Steinhauer, H. Beckers, M. Kazim, C. R. Pitts, T. Lectka and S. Riedel, *Nature Communications*, 2021, **12**, 5275.

10. L. Turunen and M. Erdélyi, *Chemical Society Reviews*, 2020, **49**, 2688-2700.

11. A.-C. C. Carlsson, K. Mehmeti, M. Uhrbom, A. Karim, M. Bedin, R. Puttreddy, R. Kleinmaier, A. A. Neverov, B. Nekoueishahraki, J. Gräfenstein, K. Rissanen and M. Erdélyi, *Journal of the American Chemical Society*, 2016, **138**, 9853-9863.

12. G. M. De Oliveira, E. Faoro and E. S. Lang, *Inorganic Chemistry*, 2009, **48**, 4607-4609.

13. L. Koskinen, P. Hirva, E. Kalenius, S. Jääskeläinen, K. Rissanen and M. Haukka, *CrystEngComm*, 2015, **17**, 1231-1236.

14. E. Seppälä, F. Ruthe, J. Jeske, W.-W. Du Mont and P. G. Jones, *Chemical Communications*, 1999, 1471-1472.

15. S. Lindblad, F. B. Németh, T. Földes, A. Vanderkooy, I. Pápai and M. Erdélyi, *Chemical Communications*, 2020, **56**, 9671-9674.

16. K. Muñiz, B. García, C. Martínez and A. Piccinelli, *Chemistry - A European Journal*, 2017, **23**, 1539-1545.

17. S. Huber, *Halogen bonding in solution*, Wiley-VCH, Weinheim, 1st edn., 2020.

18. A.-C. C. Carlsson, J. Gräfenstein, A. Budnjo, J. L. Laurila, J. Bergquist, A. Karim, R. Kleinmaier, U. Brath and M. Erdélyi, *Journal of the American Chemical Society*, 2012, **134**, 5706-5715.

19. A.-C. C. Carlsson, J. Gräfenstein, J. L. Laurila, J. Bergquist and M. Erdélyi, *Chemical Communications*, 2012, **48**, 1458-1460.

20. T. Okitsu, S. Yumitate, K. Sato, Y. In and A. Wada, *Chemistry - A European Journal*, 2013, **19**, 4992-4996.

21. Y. Kim, E. J. McKinley, K. E. Christensen, N. H. Rees and A. L. Thompson, *Crystal Growth & Design*, 2014, **14**, 6294-6301.

22. S. B. Hakkert and M. Erdélyi, *Journal of Physical Organic Chemistry*, 2015, **28**, 226-233.

23. D. Sethio, G. Raggi, R. Lindh and M. Erdélyi, *Journal of Chemical Theory and Computation*, 2020, **16**, 7690-7701.

24. M. Erdélyi, *Chemical Society Reviews*, 2012, **41**, 3547.

25. J. Barluenga, *Pure and applied chemistry*, 1999, **71**, 431-436.

26. J. Barluenga, F. González-Bobes, M. C. Murguía, S. R. Ananthoju and J. M. González, *Chemistry - A European Journal*, 2004, **10**, 4206-4213.

27. G. Rousseau and S. Robin, *Tetrahedron Letters*, 2000, **41**, 8881-8885.

28. K. Murai, K. Tateishi and A. Saito, *Organic & Biomolecular Chemistry*, 2016, **14**, 10352-10356.

29. L. Turunen, U. Warzok, R. Puttreddy, N. K. Beyeh, C. A. Schalley and K. Rissanen, *Angewandte Chemie International Edition*, 2016, **55**, 14033-14036.

30. L. Turunen, A. Peuronen, S. Forsblom, E. Kalenius, M. Lahtinen and K. Rissanen, *Chemistry - A European Journal*, 2017, **23**, 11714-11718.

31. L. Turunen, U. Warzok, C. A. Schalley and K. Rissanen, *Chem*, 2017, **3**, 861-869.

32. U. Warzok, M. Marianski, W. Hoffmann, L. Turunen, K. Rissanen, K. Pagel and C. A. Schalley, *Chemical Science*, 2018, **9**, 8343-8351.

33. A. Vanderkooy, A. K. Gupta, T. Földes, S. Lindblad, A. Orthaber, I. Pápai and M. Erdélyi, *Angewandte Chemie*, 2019, **131**, 9110-9114.

34. A. C. Reiersølmoen, S. Battaglia, S. Øien-Ødegaard, A. K. Gupta, A. Fiksdahl, R. Lindh and M. Erdélyi, *Chemical Science*, 2020, **11**, 7979-7990.

35. M. Kandrnálová, Z. Kokan, V. Havel, M. Nečas and V. Šindelář, *Angewandte Chemie International Edition*, 2019, **58**, 18182-18185.

36. A. Del Mauro, Z. Kokan and V. Šindelář, *Chemical Communications*, 2022, **58**, 3815-3818.

37. N. W. Alcock and G. B. Robertson, *Journal of the Chemical Society, Dalton Transactions*, 1975, 2483.

38. L. K. Blair, K. D. Parris, P. S. Hii and C. P. Brock, *Journal of the American Chemical Society*, 1983, **105**, 3649-3653.

39. A. A. Neverov, H. X. Feng, K. Hamilton and R. S. Brown, *The Journal of Organic Chemistry*, 2003, **68**, 3802-3810.

40. L. C. F. Morgan, Y. Kim, J. N. Blandy, C. A. Murray, K. E. Christensen and A. L. Thompson, *Chemical Communications*, 2018, **54**, 9849-9852.

41. Y.-M. Wang, J. Wu, C. Hoong, V. Rauniyar and F. D. Toste, *Journal of the American Chemical Society*, 2012, **134**, 12928-12931.

42. C. Weinberger, R. Hines, M. Zeller and S. V. Rosokha, *Chemical Communications*, 2018, **54**, 8060-8063.

43. M. Elding, A. K. Larsson, G. Svensson, J. Albertsson and L. Eberson, *Acta Crystallographica Section C Crystal Structure Communications*, 1992, **48**, 2078-2080.

44. M. Elding, J. Albertsson, G. Svensson and L. Eberson, *Acta Chemica Scandinavica*, 1990, **44**, 135-138.

45. F. P. Hinz and D. W. Margerum, *Journal of the American Chemical Society*, 1974, **96**, 4993-4994.

46. Y. Suzaki, T. Saito, T. Ide and K. Osakada, *Dalton Trans.*, 2014, **43**, 6643-6649.

47. P. D. Zeits, G. P. Rachiero, F. Hampel, J. H. Reibenspies and J. A. Gladysz, *Organometallics*, 2012, **31**, 2854-2877.

48. M. Newcomb, G. W. Gokel and D. J. Cram, *Journal of the American Chemical Society*, 1974, **96**, 6810-6811.

49. L. Turunen, *Chem*, 2017, **3**, 715-716.

50. T. J. Siciliano, M. C. Deblock, K. M. Hindi, S. Durmus, M. J. Panzner, C. A. Tessier and W. J. Youngs, *Journal of Organometallic Chemistry*, 2011, **696**, 1066-1071.

51. E. Taipale, J. S. Ward, G. Fiorini, D. L. Stares, C. A. Schalley and K. Rissanen, *Inorganic Chemistry Frontiers*, 2022, **9**, 2231-2239.

52. M. Bedin, A. Karim, M. Reitti, A.-C. C. Carlsson, F. Topić, M. Cetina, F. Pan, V. Havel, F. Al-Ameri, V. Sindelar, K. Rissanen, J. Gräfenstein and M. Erdélyi, *Chemical Science*, 2015, **6**, 3746-3756.

53. L. Turunen, F. B. Németh, D. A. Decato, I. Pápai, O. B. Berryman and M. Erdélyi, *Bulletin of the Chemical Society of Japan*, 2021, **94**, 191-196.

54. S. Alvarez, *Dalton Transactions*, 2013, **42**, 8617.

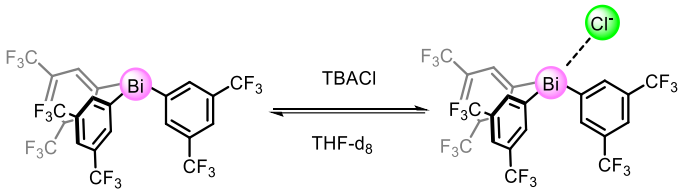
55. J. C. Y. Lin, S. S. Tang, C. S. Vasam, W. C. You, T. W. Ho, C. H. Huang, B. J. Sun, C. Y. Huang, C. S. Lee, W. S. Hwang, A. H. H. Chang and I. J. B. Lin, *Inorganic Chemistry*, 2008, **47**, 2543-2551.

56. B. Ahrens, P. G. Jones and A. K. Fischer, *European Journal of Inorganic Chemistry*, 1999, **1999**, 1103-1110.

# 5 Summary and Conclusions

The work presented in this thesis aims to highlight the strength and versatility of both halogen and pnictogen bonding interactions when employed in anion host-guest chemistry, as well as the stabilisation of reactive halonium cations using macrocyclic ligands.

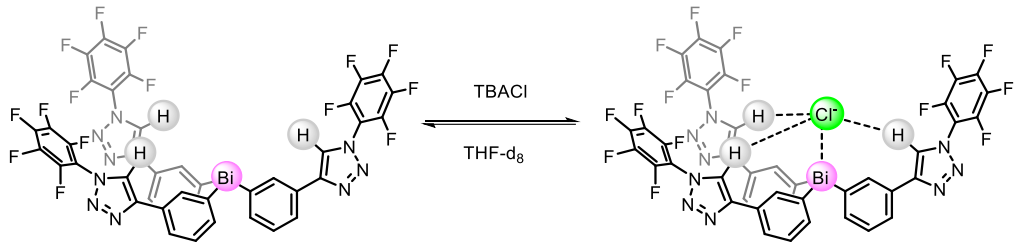
The theme of **Chapter 2** was to gain important insights into the properties of the underexplored pnictogen bonding (PnB) interaction for anion recognition. This was achieved by the synthesis of a series of tripodal antimony(III) and bismuth(III) based triaryl receptors with systematically varied electron withdrawing aryl substituents. Extensive $^{1}$H NMR anion titration experiments in THF-$d_8$ revealed receptor potency is directly influenced by the electronic nature of the substituents, as well as by the nature of the PnB donor. Receptor potency was found to increase significantly through the introduction of electron withdrawing groups such as trifluoromethyl ($CF_3$) as well as incorporating the more potent PnB donor Bi(III) over Sb(III) ( Scheme 5.1).




*Scheme 5.1. Chloride binding with TBACl in THF-$d_8$ for the triaryl bismuth(III) receptor*

The determined anion selectivity profiles highlighted that the PnB receptors displayed notable chloride selectivity over more basic oxoanion guest species, which is in line with observations noted for other XB and ChB sigma(σ)-hole receptors and is in stark contrast to HB based receptors where the opposite anion selectivity trend is commonly encountered. Furthermore, the chapter explored the synthesis of four novel tripodal PnB receptors containing both a central PnB donor as well as HB donor triazole motifs, showing that pnictogens can be successfully utilised as receptor scaffolds for multidentate receptors. $^{1}$H NMR anion titration

experiments revealed cooperative XB-HB binding of anions, and corroborating the observations made for the triaryl PnB receptors, the most potent tripodal anion receptor was the Bi(III) PnB motif appended with strongly electron withdrawing perfluorophenyl units (Scheme 5.2).

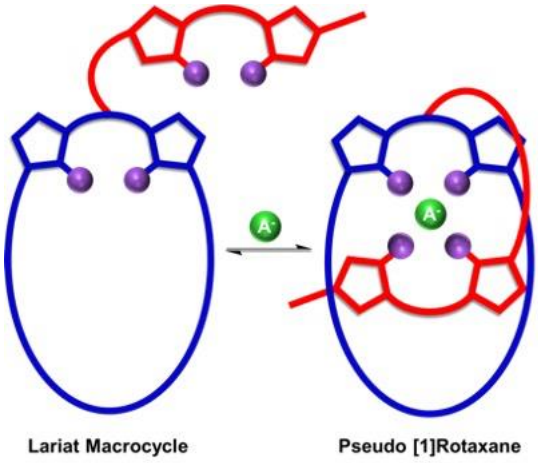



*Scheme 5.2. Chloride binding with TBACl in THF-$d_8$ for the tripodal bismuth(III) receptor*

The chapter furthermore presented the successful synthesis of four novel stibanotriazole based receptors. However, receptor decomposition occurred upon chloride binding for host systems with electron withdrawing substituents. Hence a compromise between receptor stability and polarisation of the central Pn donor must be considered in future effective anion receptor design. This could be potentially achieved through the incorporation of Pn(III) centres into preorganised cage-like scaffolds with well-defined cavities for PnB mediated anion binding. Future work could furthermore include the systematic study of Pn(V) based receptors for the determination of the electronic and structural factors governing the anion binding properties of these higher oxidation state Pn-based receptors. This would be of particular interested due to Sb(V) systems potentially showing enhanced Lewis acidity over Sb(III) analogues.

The aim of **Chapter 3** was to explore synthetic routes towards the construction of a functional [1]rotaxane, which is capable of anion recognition *via* halogen bonding (XB). To this end, the synthesis of a series of lariat macrocycles (LM) was presented. The novel LM designs were initially based upon a previously reported XB [2]rotaxane, which exploits the ambidentate nature of a secondary amine bis-iodotriazole motif incorporated into the macrocycle and axle

components and is capable of both Zn(II) cation recognition when neutral and $Cl^-$ anion recognition in its doubly protonated state. The target lariat macrocycles were appended with an appropriate iodotriazole functionalised lariat arm to facilitate charged guest template directed binding assembly of a pseudo[1]rotaxane *via* an intramolecular self-threading event (Scheme 5.3).




*Scheme 5.3. Schematic representation of an anion template directed binding assembly of a pseudo[1]rotaxane via an intramolecular self-threading event*

Despite employing a variety of XB iodotriazole lariat arm design iterations, chloride anion template $^1$H NMR titration studies with the doubly protonated lariat macrocycles indicated halide binding was indeed occurring *via* cooperative XB and secondary ammonium HB interactions. However, 2D $^1$H NMR ROESY spectral analysis suggested an exotopic coordination mode for chloride complexation (Figure 3.6), instead of the desired endodentate mode of binding required for pseudo[1]rotaxane formation. Despite this, further efforts were made to isolate a [1]rotaxane *via* a metal cation template approach using a Zn(II) cation. This included the synthesis of modified azide appended lariat macrocycles for attempting [1]rotaxane preparation *via* zinc(II) template stoppering reactions and pyridyl lariat macrocycles for active metal templation. Although these numerous attempts failed to isolate a [1]rotaxane product, the novel synthons and strategies undertaken have given valuable insights towards future molecular design strategies for functional [1]rotaxane construction incorporating XB motifs.

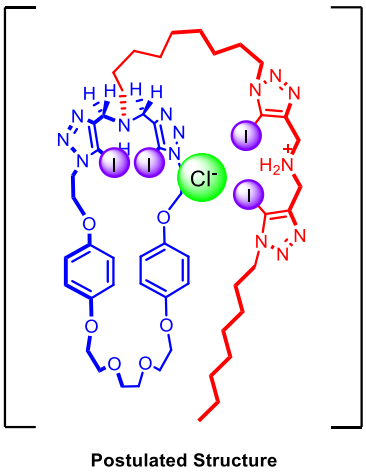



*Figure 5.1. Postulated exotopic binding mode*

Future work will focus on the introduction of new design ideas, such as post-functionalised pillar[5]arene lariat macrocycles, to move towards a molecular lasso-type XB [1]rotaxane, which is capable of anion recognition and contains multiple binding sites for dynamic molecular motion.

The aim of **Chapter 4** was to explore whether the traditionally defined kinetic and thermodynamic factors that contribute to the macrocycle effect translate to the coordination chemistry of halonium species. To this end, the synthesis of a series of pyridine containing macrocycles was described, which included both symmetric and asymmetric ligand systems with two different linker sizes as well as variation in the Lewis basicity of the pyridine ligands through the incorporation of oxygen atoms into the cyclic linker alkyl chain. Single crystal X-ray diffraction experiments revealed symmetric, linear, endotopic coordination of Ag(I) and Au(I) $d^{10}$ metals by the macrocycles (Figure 5.2 a, b). The Ag(I) macrocyclic complexes (Figure 5.2 a) were then used for the successful formation of novel macrocyclic bromonium Br(I) complexes *via* a cation exchange reaction (Figure 5.2 c). The macrocycle **MC1** used for this complex formation is asymmetric and contains two methylene oxygens within its alkyl chain (Figure 5.2).

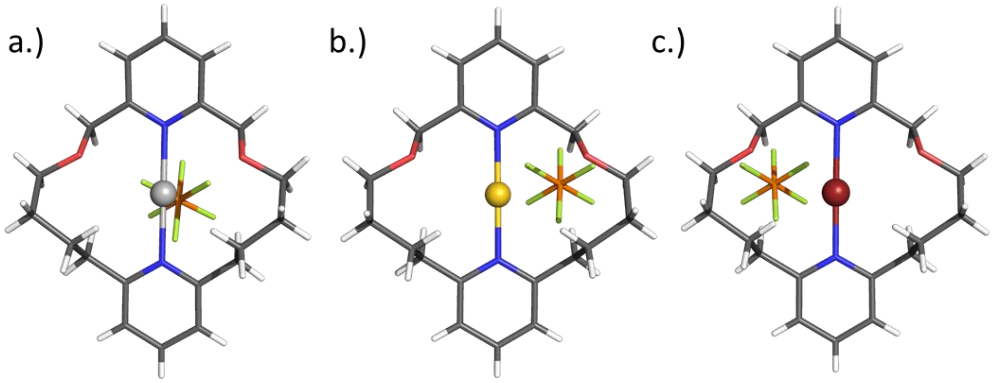
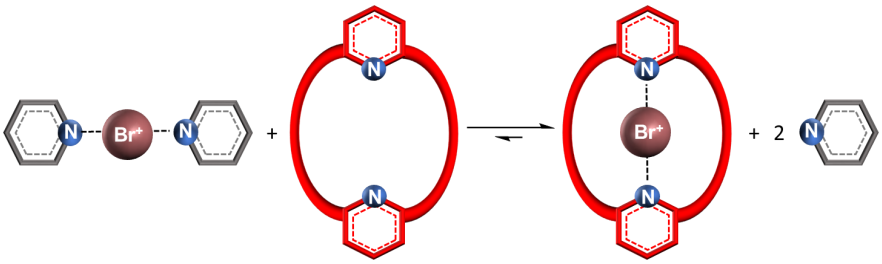



*Figure 5.2. Single crystal solid state structures of a.) Ag(I), b.) Au(I) and c.) Br(I) macrocyclic complexes crystallised with $PF_6^-$*

In contrast to the successful exchange reaction between the **MC1** Ag(I) complex and bromine to form the Br(I) complex, the analogous reaction with elemental iodine failed to produce the corresponding iodonium macrocyclic complexed product. This may be explained by the kinetic stabilisation of the **MC1** Ag(I) complex through secondary Ag(I)···O interactions together with strong coordination of Ag(I) by the pyridine units making it inert for reaction with the less reactive iodine resulting in the surprising inability to form the usually more stable iodonium complex.

With solid state crystallographic evidence for the formation of the macrocyclic bromonium complexes revealing linear endotopic coordination established, a solution phase $^1$H NMR exchange reaction was performed to obtain evidence for the existence of a macrocyclic effect for halonium cations. Here, Br(I) was complexed with two pyridine ligands, to which **MC1** was added. Evidence for a ligand exchange reaction was observed by $^1$H NMR, in which the more stable **MC1** bromonium complex was formed (Scheme 5.4), indicating that the macrocyclic nature of the ligand tested translates into enhanced bromonium cation complexed thermodynamic stability.




*Scheme 5.4. Schematic representation of the exchange reaction into the study of a macrocyclic effect of bromonium*

This work is therefore an unprecedented example of a macrocyclic effect for the stabilisation of halonium cations. Overall, this study reports the first examples of macrocyclic bromonium complexes and importantly reveals how the stabilisation of this reactive species can be achieved *via* application of the macrocyclic effect. Future work includes the full structural characterisation of halonium complexes with the other macrocycles **MC2**, **MC3** and **MC4** to investigate the effects that variation in macrocycle size as well as variation in the Lewis basicity of the pyridine ligands have on the halonium complex formation and stability. Future work will then also include more investigations into the macrocyclic effect observed.

In summary, the results of the research projects presented in this thesis have sought and given new insights into supramolecular host-guest systems stabilised through σ-hole interactions. The synthetic versatility of XB donor iodotriazole motifs is highlighted as well as the underexplored potential of PnB in anion recognition. The results have demonstrated σ-hole interactions to have unique electronic and geometric recognition features that can potentially be exploited in the future design of selective anion receptors. In particular, the study presented concerning the recognition and stabilisation of bromonium species has furthermore expanded our understanding of the stabilisation of these reactive species for future supramolecular chemistry applications.

# 6 Experimental

## 6.1 General Considerations

### 6.1.1 Materials, Methods and Instrumentation for Synthesis and Characterisation

Solvents and reagents were purchased from commercial suppliers and used as received. Dry solvents were obtained by purging with nitrogen and passing through a MBraun MPSP-800 column. $H_2O$ was de-ionized and micro filtered using a Milli-Q® Millipore machine. Experiments were conducted at room temperature unless stated otherwise. Merck silica gel 60 was used for flash column chromatography. Preparative TLC was performed on 20×20 cm plates, with a silica layer of 1 mm thickness. Ratios for solvent mixtures are reported by volume.

Mass spectra were recorded on Waters Micromass LCT and Bruker microTOF spectrometers. NMR spectra were either recorded on a Bruker Avance III HD Nanobay NMR equipped with a 9.4T magnet or a Bruker NEO 600 with broadband helium cryoprobe. Chemical shifts are quoted in parts per million relative to the residual solvent peak with signal splitting denoted as singlet (s), doublet (d), double of doublet (dd), triplet (t), doublet of triplets (dt), pentet (p) and multiplet (m).

CHN elemental analyses were performed in duplicate by the London Metropolitan University Elemental Analysis service using a Thermo Scientific Flash 2000 CHNS/O analyser.

### 6.1.2 Instrumentation and Methods for Single-Crystal XRD

Single crystals suitable for X-ray analysis were each coated with Paratone-N oil, mounted on a 200 μm MiTeGen loop and placed in a cold nitrogen stream (150 K) on an Oxford Diffraction

Supernova X-ray diffractometer. Diffraction intensities were measured using monochromated Cu Kα diffraction.[1] Data collection, indexing, initial cell refinements, frame integration, final cell refinements and absorption corrections were performed using CrysAlisPro. All structures were solved with the CRYSTALS suite using direct methods and refined against $F^2$.[2,3] Hydrogen atoms were included into the model at geometrically calculated positions and refined using a riding model. Figures of the crystal structures were created using the open-source PyMOL Molecular Graphics System (version 2.4.0a0. Schrödinger LLC.). PLATON SQUEEZE was used for the refinement of selected structures in order to include diffuse electron density arising from disordered solvent molecules, which could not be modelled in a sensible manner.[4,5]

### 6.1.3 General Procedures for $^1$H NMR Studies

$^1$H-NMR were recorded on a Bruker Avance III NMR equipped with a 11.75 T magnet. Chemical shifts are quoted in parts per million relative to the residual solvent peak. Commercially available tetrabutylammonium (TBA) salts were used as purchased after being dried under high-vacuum and stored in vacuum desiccators at room temperature.

#### 6.1.3.1 $^1$H NMR Anion Titrations

The $^1$H-NMR anion titrations were performed in THF-$d_8$ at 298 K. Aliquots of the respective anion were added to a solution of the receptor, such that the receptor solution concentration remained constant. Spectra were therefore recorded at 0.00, 0.20, 0.39, 0.59, 0.78, 0.96, 1.15, 1.33, 1.50, 1.68, 1.85, 2.27, 2.68, 3.45, 4.17, 5.47, 7.14 and 9.38 equivalents.

For TBACl and TBABr $^1$H-NMR titrations, the host concentration was 1 mM with a TBACl or TBABr concentration of 25 mM. All other $^1$H-NMR titrations were performed at host

concentrations of 0.5 mM with TBA salt concentrations of 12.5 mM. Titration isotherms were analysed using BindFit.[6, 7]

#### 6.1.3.2 $^1$H-NMR Pseudo [1]Rotaxane Assembly Investigations via Anion Templation

The $^1$H-NMR experiments were performed at 298 K in either acetone-$d_6$ or $CD_2Cl_2$. The respective lariat macrocycle was dissolved in the respective deuterated solvent and a spectrum was recorded before addition of a solution containing 1 eq. of tetrafluoroboric acid diethyl ether complex per amine site. A spectrum of the protonated receptor was then recorded before the addition of aliquots of TBACl with spectra recorded at 0.50 and 1.00 equivalents of TBACl. The host concentration was 1mM with a TBACl concentration of 25 mM.

## 6.2 Experimental Information Related to Chapter 2

### 6.2.1 General Synthetic Procedures

**General Procedure 2.1** (procedure adapted from[8])

Magnesium turnings (3 eq.) with $I_2$ (cat.) were heated with a heat gun briefly until sublimation of the iodine was observed to coat the magnesium turnings evenly. Once cooled, dry THF was added. Aryl bromide (3 eq.) was added dropwise either neat or as a concentrated THF solution over half an hour. The mixture was left to stir for approximately 1 h until the Grignard was fully activated as determined by the disappearance of the solid magnesium turnings and colour change of the solution to grey. A solution of either $SbCl_3$ (1 eq.) or $BiCl_3$ (1 eq.) in THF was added slowly at 0 °C. The mixture was left to stir at room temperature for 1 h and then heated at 60 °C for 1 h. After cooling to room temperature, the mixture was diluted with brine and extracted with EtOAc. The combined organic phases were dried over $MgSO_4$, filtered, and

concentrated under reduced pressure. The crude products were purified using silica gel flash column chromatography.

**General Procedure 2.2** (procedure adapted from[9])

Dry, degassed THF (5.5 mL) was added to a flask containing magnesium turnings (0.27 g, 11.06 mmol, 1.4 eq.) and iodine (cat.). 2-(3-bromophenyl)ethynyltrimethylsilane (2.00 g, 7.90 mmol, 1 eq.) was added dropwise over 3h using a syringe pump. Once the Grignard was fully activated as determined by the disappearance of the solid magnesium turnings and colour change of the solution to grey, a solution of the pnictogen(III) trichloride (2.63 mmol, 1/3 eq.) in THF (5 mL) was added slowly. The resulting reaction mixture was left to stir at room temperature overnight, before being quenched with MeOH (3 mL). The solvents were evaporated under reduced pressure. The crude was dissolved in EtOAc and washed with brine. The organic layer was dried over $MgSO_4$, filtered and concentrated. The product was purified using silica gel flash column chromatography.

**General Procedure 2.3**

The TMS protected triaryl pnictogen (1 eq.) was dissolved in a 1:1 mixture of MeOH and $CHCl_3$ with a few drops of $H_2O$. $K_2CO_3$ (15 eq.) was added and the mixture stirred at room temperature for approximately 5 h, until the reaction reached completion, as determined by TLC (5% DCM in Hexane) The solvent was removed under reduced pressure and the crude mixture dissolved in $CHCl_3$ and washed with brine. The organic layer was dried over $MgSO_4$, filtered and concentrated. The deprotected products were used without further purification.

**General Procedure 2.4**

$[Cu(MeCN)_4]PF_6$ (32 mg, 0.087 mmol, 0.3 eq.) and TBTA (46 mg, 0.087 mmol, 0.3 eq.) were complexed by being stirred in dry, degassed DCM (3 mL) for 30 minutes. The respective

pnictogen(III) triaryl alkyne was added (0.29 mmol, 1 eq.) in dry, degassed DCM (2 mL) before the addition of either perfluorophenyl azide (0.20 g, 0.95 mmol, 3.3 eq.) or benzyl azide (0.13 g, 0.95 mmol, 3.3 eq.). The resulting mixture was stirred at room temperature overnight. The crude was diluted with DCM and washed with an EDTA/$NH_4OH_{(aq)}$ solution followed by brine before drying the organic layer over $MgSO_4$, filtering and concentrating under reduced pressure. Products were purified using silica gel flash column chromatography.

**General Procedure 2.5**

The respective azide (4.13 mmol, 3.5 eq.) was dissolved in a 1:1 mixture of dry, degassed THF and acetonitrile (7.5 mL) . NaI (1.77 g, 11.8 mmol, 10 eq.) and copper(II) perchlorate hexahydrate (2.19 g, 5.9 mmol, 5 eq.) were added and the resulting mixture stirred for 5 minutes in the dark. TBTA (0.031 g, 0.059 mmol, 0.05 eq.) and DBU (0.54 g, 3.54 mmol, 3 eq.) were added to the mixture followed by a solution of Sb(III) alkyne **4** (0.50 g, 1.18 mmol, 1 eq.) in a 1:1 mixture of dry, degassed THF and acetonitrile (2.5 mL). The resulting mixture was left to stir at room temperature overnight, while in the dark, and under an inert nitrogen atmosphere. The solvent was then evaporated under reduced pressure and the crude was dissolved in DCM and washed with an EDTA/$NH_4OH_{(aq)}$ solution followed by brine. The organic phase was dried over $MgSO_4$, filtered, and concentrated under reduced pressure. The crude products were purified using silica gel flash column chromatography.

**General procedure 2.6** (procedure adapted from[10])

Triphenylantimony(III) (0.445 g, 1.26 mmol, 2 eq.) and antimony(III) bromide (0.228 g, 0.63 mmol, 1 eq.) were mixed neat and heated at 100 °C for 2 h. The respective phenylacetylene (1.26 mmol, 2 eq.) was dissolved in dry and degassed diethyl ether (2 mL) and cooled to -78 °C. *n*-BuLi (2.5 M in hexanes, 0.6 mL, 1.51 mmol, 2.4 eq.) was added dropwise, the resulting mixture stirred at -78 °C for 0.5 h before warming up to 0 °C. The redistribution product of

triphenylantimony(III) and antimony(III) bromide was added slowly as a suspension in dry and degassed diethyl ether (3 mL) at 0 °C. The mixture was stirred for 2 h while slowly warming to room temperature. After diluting with DCM, the crude was washed with brine, dried over $MgSO_4$, filtered, and concentrated under reduced pressure. The crude antimony alkyne product was used immediately without further purification.

A solution of the antimony alkyne (assume 1.26 mmol, 1 eq.) in dry and degassed THF (10 mL) was added to CuBr (9 mg, 0.063 mmol, 5 mol%) under an inert atmosphere. Perfluorophenyl azide (0.263 g, 1.26 mmol, 1 eq.) was added and the reaction mixture was heated at 60 °C for 5 h. Once cooled, the mixture was diluted with DCM and washed with an EDTA/$NH_4OH_{(aq)}$ solution followed by brine. The organic phase was dried over $MgSO_4$, filtered, and concentrated under reduced pressure. The crude products were purified using silica gel flash column chromatography.

**General procedure 2.7** (adapted from[10])

Either triphenylantimony(III) (8/3 eq.) or tri-*p*-fluorophenylstibine(III)[5] (8/3 eq.) were mixed neat with antimony(III) bromide (4/3 eq.) respectively and the mixtures heated at 100 °C for 2 h. 1,3-Diethynylbenzene (1 eq.) was dissolved in dry and degassed diethyl ether (0.21 M wrt diethynylbenzene) and cooled to -78 °C. *n*-BuLi (2.5 M in Hexanes, 2.2 eq.) was added dropwise at the resulting mixture stirred at -78 °C for 0.5 h before warming up to 0 °C. The previously prepared redistribution product was suspended in dry, degassed diethyl ether (0.75 M wrt redistribution product) and added slowly to the mixture at 0 °C. The mixture was stirred for 2 h while slowly warming to room temperature. After diluting with DCM, the crude was washed with brine, dried over $MgSO_4$, filtered, and concentrated under reduced pressure. The crude antimony alkyne product was used immediately without further purification.

A solution of the antimony alkyne (assume quantitative, 1 eq.) in dry and degassed THF (0.13 M wrt antimony alkyne) was added to CuBr (10 mol%) in dry, degassed THF (0.06 M wrt CuBr) under an inert atmosphere. Benzyl azide (2 eq.) was added and the reaction mixture was stirred overnight. The mixture was then diluted with DCM and washed with an EDTA/$NH_4OH_{(aq)}$ solution followed by brine. The organic phase was dried over $MgSO_4$, filtered, and concentrated under reduced pressure. The crude products were purified using silica gel flash column chromatography.

## 6.2.2 Synthesis and Characterisation

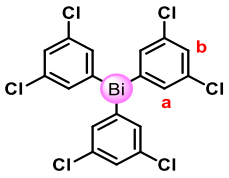
### 6.2.2.1 Synthesis of Triaryl Pnictogens

Compounds **1·Bi$^{CN}$**, **1·Bi$^{NO2}$**, **1·Sb$^{CN}$** and **1·Sb$^{NO2}$** were prepared according to literature procedures.[11, 12]

Compounds **1·Bi$^{2F}$**, **1·Bi$^{3F}$**, **1·Sb$^{3F}$**, **1·Sb$^{2Cl}$** and **1·Sb$^{2CF3}$** were all prepared according to general procedure 2.1.

Spectroscopic data of **1·Bi$^{CN}$**,[12] **1·Bi$^{NO2}$**,[12] **1·Bi$^{2F}$**,[8] **1·Bi$^{3F}$**,[13] **1·Sb$^{CN}$**,[11] **1·Sb$^{NO2}$**,[11] **1·Sb$^{3F}$**,[13] **1·Sb$^{2Cl}$**,[14] **1·Sb$^{2CF3}$**,[15] were consistent with those reported in the literature.

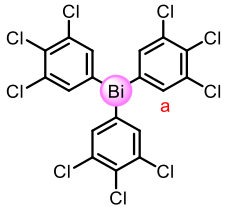
**Compound 1·Bi$^{2Cl}$**




The compound was synthesised according to general procedure 2.1 from $BiCl_3$ (1 eq.) and 1-bromo-3,5-dichlorobenzene (3 eq.) and purified using silica gel flash column chromatography

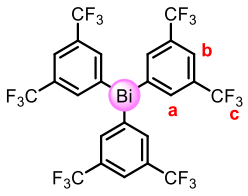
(95:5 Hexane:EtOAc) to afford a white solid in 38% yield. **$^{1}$H NMR** (400 MHz, Acetone-$d_6$) δ 7.84 (d, J = 1.9 Hz, 6H), 7.45 (t, J = 1.9 Hz, 3H). **$^{13}$C NMR-{$^{1}$H}** (101 MHz, Acetone-$d_6$) δ 165.98, 138.90, 136.45, 128.95. The compound was further characterised by XRD and CHN analysis.

**Compound 1·Bi$^{3Cl}$**




The compound was synthesised according to general procedure 2.1 from $BiCl_3$ (1 eq.) and 5-bromo-1,2,3-trichlorobenzene (3 eq.) and purified using silica gel flash column chromatography (95:5 Hexane:EtOAc) to afford a white solid in 32% yield. **$^{1}$H NMR** (600 MHz, Acetone-$d_6$) δ 8.05 (s, 6H, $H_a$). **$^{13}$C NMR-{$^{1}$H}** (151 MHz, Acetone-$d_6$) δ 137.61, 136.79, 130.34. The limited solubility of the compound combined with relaxation effects resulted in the inability to observe the peak corresponding to the carbon adjacent to the central Bi atom. The compound was further characterised by XRD and CHN analysis.

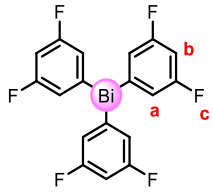
**Compound 1·Bi$^{2CF3}$**




The compound was synthesised according to general procedure 2.1 from $BiCl_3$ (1 eq.) and 1,3-bis(trifluoromethyl)-5-bromobenzene (3 eq.) and purified using silica gel flash column chromatography (95:5 Hexane:EtOAc) to afford a yellow oil which was recrystalised from hexane to afford the product as a pale-yellow solid in 35% yield. **$^{1}$H NMR** (600 MHz, Acetone-

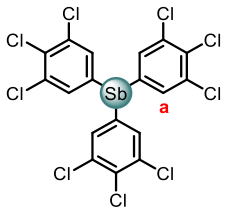
$d_6$) δ 8.55 (s, 6H, $H_a$), 8.02 (s, 3H, $H_b$). **$^{13}$C NMR-{$^1$H}** (151 MHz, Acetone-$d_6$) δ 167.25, 139.20 (d, *J* = 3.8 Hz), 133.57 (q, *J* = 32.6 Hz), 124.98 (q, *J* = 272.5 Hz), 122.79 (hept, *J* = 4.1 Hz). **$^{19}$F NMR** (377 MHz, Acetone-$d_6$) δ -63.46. The compound was further characterised by XRD and CHN analysis.

**Compound 1·Sb$^{2F}$**




The compound was synthesised according to general procedure 2.1 from $BiCl_3$ (1 eq.) and 1-bromo-3,5-difluorobenzene (3 eq.) and purified using silica gel flash column chromatography (9:1 Hexane:EtOAc) to afford a white solid in 48% yield. **$^1$H NMR** (400 MHz, Acetone-$d_6$) δ 7.20 – 7.11 (m, 6H, $H_a$), 7.07 (tt, J = 9.3, 2.3 Hz, 3H, $H_b$). **$^{13}$C NMR-{$^1$H}** (101 MHz, Acetone-$d_6$) δ 164.35 (dd, *J* = 253.3, 10.4 Hz), 143.57 (t, *J* = 4.2 Hz), 119.47 (dd, *J* = 14.7, 5.7 Hz), 105.71 (t, *J* = 25.5 Hz). **$^{19}$F NMR** (377 MHz, Acetone-$d_6$) δ -110.34 – -110.39 (m). The compound was further characterised by CHN analysis.

**1·Sb$^{3Cl}$**




The compound was synthesised according to general procedure 2.1 from $SbCl_3$ (1 eq.) and 5-bromo-1,2,3-trichlorobenzene (3 eq.) and purified using silica gel flash column chromatography (9:1 Hexane:EtOAc) to afford a white solid in 34% yield. **$^1$H NMR** (600 MHz, Acetone-$d_6$) δ

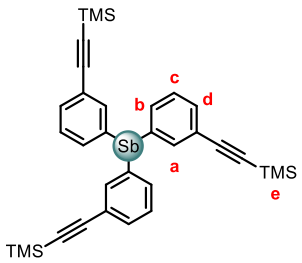
7.72 (s, 6H). **$^{13}$C NMR-{$^{1}$H}** (151 MHz, Acetone-$d_6$) δ 140.97, 137.04, 135.51, 132.74. The compound was further characterised by XRD and CHN analysis.

### 6.2.2.2 Synthesis of Pnictogen Tripods

2-(3-Bromophenyl)ethynyltrimethylsilane[16] and perfluorophenyl azide[17] were prepared according to literature procedures and spectroscopic data were consistent with those reported.

Benzyl azide was prepared according to a modified literature procedure.[18] Benzyl bromide (15 g, 87.7 mmol, 1 eq.) was dissolved in DMSO and sodium azide (6.8 g, 65.02 mmol, 1.2 eq.) was added. The mixture was stirred at room temperature overnight before diluting it with water and extracting the product with diethyl ether. The ethereal layer was dried over $MgSO_4$ and concentrated to afford benzyl azide as a clear liquid in quantitative yield. Spectroscopic data were consistent with those reported.[18]

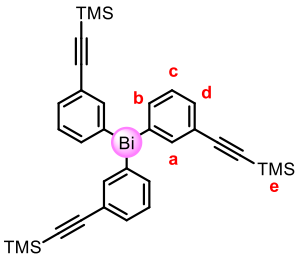
**Compound 2**




Prepared according to general procedure 2.2 with $SbCl_3$ (2.63 mmol, 1/3 eq.) and purified using silica gel flash column chromatography (95:5 Hexane:DCM). When required, the product could be further be purified by dissolving it in minimal amounts of EtOAc and then adding MeOH, causing the pure product to precipitate out, which could then be isolated by vacuum filtration as a white solid (0.51 g, 0.79 mmol, 10 %). **$^{1}$H NMR** (600 MHz, Acetone-$d_6$) δ 7.57 (q, J = 1.1

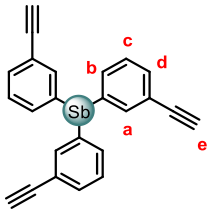
Hz, 1H, $H_a$), 7.51 – 7.35 (m, 3H, $H_{b-d}$), 0.20 (s, 9H, $H_e$). **$^{13}$C NMR-{$^1$H}** (151 MHz, Acetone-$d_6$) δ 140.11, 139.59, 137.26, 133.34, 130.11, 125.07, 105.86, 95.65, 0.13.

**Compound 3**



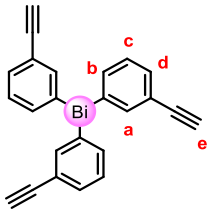

Prepared according to general procedure 2.2 with $BiCl_3$ (2.63 mmol, 1/3 eq.) and purified using silica gel flash column chromatography (95:5 Hexane:DCM). When required, the product could further be purified by dissolving it in minimal amounts of EtOAc and then adding MeOH, causing the pure product to precipitate out, which could then be isolated by vacuum filtration as a white solid (0.86 g, 1.19 mmol, 15 %). **$^1$H NMR** (400 MHz, Acetone-$d_6$) δ 7.92 – 7.91 (m, 1H, $H_a$), 7.79 – 7.76 (m, 1H, $H_b$), 7.49 – 7.38 (m, 2H, $H_{c,d}$), 0.19 (s, 9H, $H_e$). **$^{13}$C NMR-{$^1$H}** (101 MHz, Acetone-$d_6$) δ 158.45, 141.58, 138.76, 132.22, 131.45, 126.52, 106.39, 95.28, 0.17.

**Compound 4**



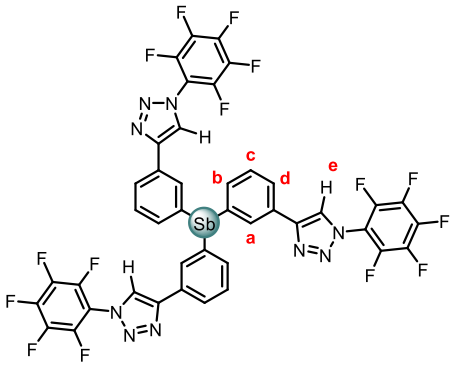

Prepared according to general procedure 2.3 from **2** (0.16 mmol, 1 eq.) to afford a white solid (0.07 g, 0.16 mmol, quantitative). **$^1$H NMR** (400 MHz, Acetone-$d_6$) δ 7.58 (t, J = 1.6 Hz, 1H, $H_a$), 7.53 – 7.48 (m, 2H, $H_{b,d}$), 7.42 (t, J = 7.5 Hz, 1H, $H_c$), 3.66 (s, 1H, $H_e$).**$^{13}$C NMR-{$^1$H}** (151 MHz, Acetone-$d_6$) δ 140.16, 139.52, 137.31, 133.40, 130.05, 124.24, 84.02, 80.11.

**Compound 5**



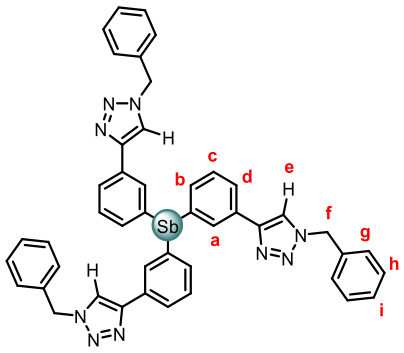

Prepared according to general procedure 2.3 from **3** (3.37 mmol, 1 eq.) to afford a white solid (1.59 g, 3.12 mmol, 93 %). **$^{1}$H NMR** (400 MHz, Acetone-$d_6$) δ 7.94 (broad s, 1H, $H_a$), 7.81 (dt, J = 7.0, 1.4 Hz, 1H, $H_b$), 7.50 – 7.40 (m, 2H, $H_{c,d}$), 3.62 (s, 1H, $H_e$). **$^{13}$C NMR-{$^{1}$H}** (101 MHz, Acetone-$d_6$) δ 158.46, 141.74, 138.75, 132.34, 131.39, 125.81, 84.53, 79.89.

**Compound 2·Sb$^{PFP}$**



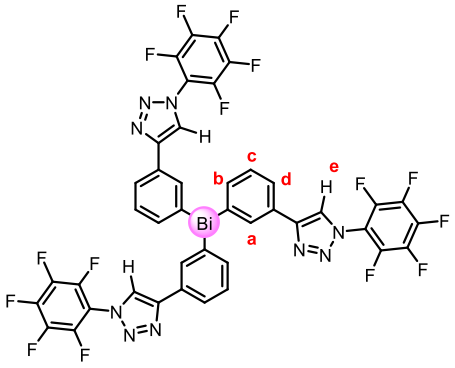

**2·Sb$^{PFP}$** was prepared according to general procedure 2.4 from **4** (0.29 mmol, 1 eq.) and perfluorophenyl azide (0.95 mmol, 3.3 eq.) and purified in DCM to yield a white solid (0.087 g, 0.083 mmol, 29 %). **$^{1}$H NMR** (400 MHz, Acetone-$d_6$) δ 8.83 (s, 3H, $H_e$), 8.32 (t, J = 1.6 Hz, 3H, $H_a$), 8.01 (dt, J = 7.5, 1.6 Hz, 3H, $H_d$), 7.62 – 7.49 (m, 6H, $H_{b,c}$). **$^{13}$C NMR-{$^{1}$H, $^{19}$F}** (126 MHz, Acetone-$d_6$) δ 148.43, 143.74, 143.38, 140.36, 139.18, 137.28, 134.46, 131.51, 130.66, 127.43, 124.67, 114.21. **$^{19}$F NMR** (377 MHz, Acetone-$d_6$) δ -148.28 – -148.43 (m), -153.58 (t, J = 21.1 Hz), -162.93 – -163.13 (m). **HRESI-MS** (pos.) m/z 1074.0112, 1076.0121, 1077.0148 [MNa$^+$] calc. for [$C_{42}H_{15}F_{15}N_9Sb{\cdot}Na^+$] 1074.0165, 1076.0177, 1077.0202.

**Compound 2·Sb$^{Bz}$**




**2·Sb$^{Bz}$** was prepared according to general procedure 2.4 from **4** (0.29 mmol, 1 eq.) and benzyl azide (0.95 mmol, 3.3 eq.) and purified using silica gel flash column chromatography (9:1 DCM:EtOAc) to yield a pale-yellow solid (0.139 g, 0.17 mmol, 58 %). **$^{1}$H NMR** (400 MHz, Acetone-$d_6$) δ 8.34 (s, 3H, $H_e$), 8.17 – 8.12 (m, 3H, $H_a$), 7.88 – 7.86 (m, 3H, $H_d$), 7.44 – 7.28 (m, 21H, $H_{b,c,g,h,i}$), 5.63 (s, 6H, $H_f$). **$^{13}$C NMR-{$^{1}$H}** (151 MHz, $CDCl_3$) δ 148.07, 138.91, 136.01, 134.79, 133.65, 131.16, 129.52, 129.27, 128.90, 128.23, 126.35, 119.99, 54.35. **HRESI-MS** (pos.) m/z 824.2200, 826.2205, 827.2237, 826.2271 [$MH^+$] calc. for [$C_{45}H_{36}N_9Sb{\cdot}H^+$] 824.2205, 826.2216, 827.2242, 828.2270.

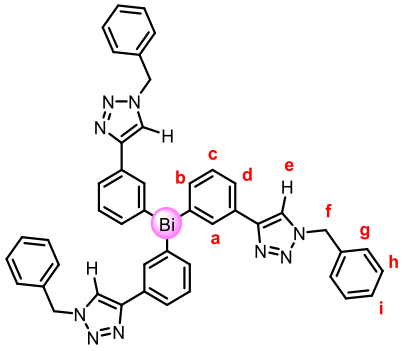
**Compound 2·Bi$^{PFP}$**




**2·Bi$^{PFP}$** was prepared according to general procedure 2.4 from **5** (0.29 mmol, 1 eq.) and perfluorophenyl azide (0.95 mmol, 3.3 eq.) and purified using silica gel flash column chromatography (DCM) to yield a white solid (0.046 g, 0.040 mmol, 14 %). **$^{1}$H NMR** (400 MHz, Acetone-$d_6$) δ 8.80 (s, 3H, $H_e$), 8.63 (t, J = 1.4 Hz, 3H, $H_a$), 7.97 – 7.91 (m, 6H, $H_{b,d}$), 7.56

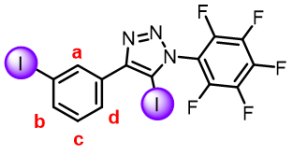
(t, J = 7.6 Hz, 3H, $H_c$). **$^{13}$C NMR-{$^{1}$H, $^{19}$F}** (126 MHz, $CDCl_3$) δ 156.33, 148.52, 142.57, 142.45, 138.27, 138.22, 134.97, 131.62, 131.34, 126.06, 122.52, 113.09. **$^{19}$F NMR** (377 MHz, Acetone-$d_6$) δ -148.28 – -148.43 (m), -153.66 (t, J = 21.1 Hz), -162.96 – -163.16 (m). **HRESI-MS** (pos.) m/z 1140.1079, 1141.1108, 1142.1140 [$MH^+$] calc. for [$C_{42}H_{15}F_{15}N_9Bi{\cdot}H^+$] 1140.1087, 1141.117, 1142.1147.

**Compound 2·Bi$^{Bz}$**



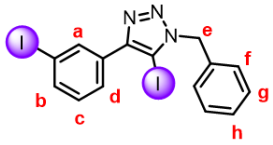

**2·Bi$^{Bz}$** was prepared according to general procedure 2.4 from **5** (0.29 mmol, 1 eq.) and benzyl azide (0.95 mmol, 3.3 eq.) and purified using silica gel flash column chromatography (gradient 9:1 to 8:2 DCM:EtOAc) to yield a white solid (0.16 g, 0.18 mmol, 61 %). **$^{1}$H NMR** (400 MHz, Acetone) δ 8.44 (t, J = 1.4 Hz, 3H, $H_a$), 8.31 (s, 3H, $H_e$), 7.82 (dt, J = 7.8, 1.5 Hz, 3H, $H_d$), 7.75 (dt, J = 7.4, 1.2 Hz, 3H, $H_b$), 7.43 (t, J = 7.5 Hz, 3H, $H_c$), 7.38 – 7.28 (m, 15H, $H_{g\text{-}i}$), 5.63 (s, 6H, $H_f$). **$^{13}$C NMR-{$^{1}$H}** (101 MHz, CDCl3) δ 155.97, 148.30, 137.51, 134.81, 134.72, 132.56, 131.14, 129.22, 128.84, 128.20, 125.45, 120.03, 54.29. **HRESI-MS** (pos.) m/z 912.2953, 913.2988, 144.3031 [$MH^+$] calc. for [$C_{45}H_{36}N_9Bi{\cdot}H^+$] 912.2970, 913.3000, 914.3031.

**Decomposition Product PFP**



The product was prepared according to general procedure 2.5 from **4** (1.18 mmol, 1 eq.) and perfluorophenyl azide (4.13 mmol, 3.5 eq.) and purified using silica gel flash column chromatography (DCM) to yield an off-white solid (0.059 g, 0.10 mmol, 9%). **$^{1}$H NMR** (400 MHz, Acetone-$d_6$) δ 8.45 (t, J = 1.7 Hz, 1H, $H_a$), 8.12 (ddd, J = 7.8, 1.7, 1.0 Hz, 1H, $H_d$), 7.89 (ddd, J = 7.9, 1.8, 1.0 Hz, 1H, $H_b$), 7.40 (t, J = 7.9 Hz, 1H, $H_c$). **$^{13}$C NMR-{$^{1}$H, $^{19}$F}** (126 MHz, $CDCl_3$) δ 148.62, 143.77, 143.63, 138.38, 137.96, 135.91, 131.91, 130.80, 126.54, 112.21, 93.86, 83.03.**$^{19}$F NMR** (377 MHz, Acetone-$d_6$) -145.67 – -146.23 (m), -150.07 (tt, J = 20.8, 3.5 Hz), -161.56 – -162.10 (m). **HRESI-MS** (pos.) m/z 563.8478 [$MH^+$] calc. for [$C_{14}H_4F_5I_2N_3 \cdot H^+$] 563.8488.

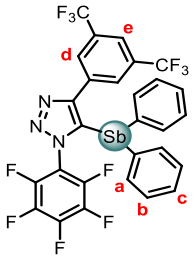
**Decomposition Product Bz**




The product was prepared according to general procedure 2.5 from **4** (1.18 mmol, 1 eq.) and benzyl azide (4.13 mmol, 3.5 eq.) and purified using silica gel flash column chromatography (9:1 DCM:EtOAc) to yield an off-white solid (0.030 g, 0.062 mmol, 5%). **$^{1}$H NMR** (400 MHz, Acetone-$d_6$) δ 8.37 (t, J = 1.7 Hz, 1H, $H_a$), 8.02 (ddd, J = 7.8, 1.7, 1.0 Hz, 1H, $H_d$), 7.80 (ddd, J = 7.9, 1.8, 1.0 Hz, 1H, $H_b$), 7.47 – 7.24 (m, 7H, $H_{c,f-h}$), 5.79 (s, 2H, $H_e$). **$^{13}$C NMR-{$^{1}$H}** (101 MHz, $CDCl_3$) δ 148.75, 137.63, 136.34, 134.27, 132.38, 130.30, 129.09, 128.72, 127.94, 126.63, 94.41, 54.61.

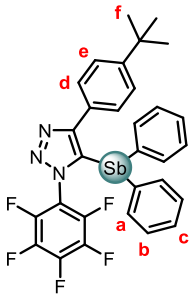
### 6.2.2.3 Synthesis of Mono Stibanotriazoles

**Compound 3·Sb$^{2CF3}$**




The compound was synthesised according to general procedure 2.6 with 1-ethynyl-3,5-bis(trifluoromethyl)benzene (1.26 mmol, 2 eq.) and purified using silica gel flash column chromatography (97:3 Hexane:Acetone) to afford a white solid (0.14 g, 0.19 mmol, 30%). **$^{1}$H NMR** (400 MHz, Acetone-d$_6$) δ 8.17 (s, 2H, H$_d$), 7.93 (s, 1H, H$_e$), 7.50 – 7.43 (m, 4H, H$_a$), 7.38 – 7.24 (m, 6H H$_{b,c}$).**$^{13}$C NMR-{$^{1}$H, $^{19}$F}** (126 MHz, Acetone-d$_6$) 153.26, 144.21, 143.63, 138.55, 137.09, 135.28, 135.19, 133.99, 132.47, 132.22, 130.62, 130.14, 129.76, 122.82, 114.78.**$^{19}$F NMR** (377 MHz, Acetone-d$_6$) δ -63.48, -144.99 – -146.59 (m), -152.23 (tt, J = 21.4, 3.2 Hz), -161.05 – -163.09 (m) **HRESI-MS** (pos.) m/z 722.0045, 724.0047, 725.0085 [MH$^+$] calc. for [$C_{28}H_{13}N_3F_{11}Sb_1$·H$^+$] 722.0045, 724.0052, 725.0082.

**Compound 3·Sb$^{tBu}$**



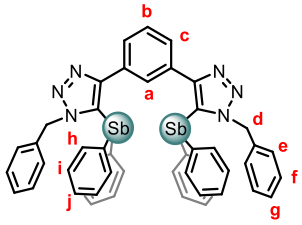

The compound was synthesised according to general procedure 2.6 with 4-*tert*-butylphenylacetylene (1.26 mmol, 2 eq.) and purified using silica gel flash column chromatography (1:1 DCM:Hexane) to afford a pale-yellow solid (0.10 g, 0.16 mmol, 25%). **$^{1}$H NMR** (400 MHz, Acetone-d$_6$) 7.67 – 7.58 (m, 2H, H$_d$), 7.46 – 7.28 (m, 12H, H$_{a-c,e}$), 1.31 (s, 9H,

$H_f$). **$^{13}$C NMR-{$^{1}$H, $^{19}$F}** (126 MHz, Acetone-$d_6$) δ 156.60, 152.55, 144.29, 143.32, 138.27, 137.05, 135.82, 130.37, 130.31, 130.11, 129.59, 129.18, 126.51, 115.06, 35.35, 31.64. **$^{19}$F NMR** (471 MHz, Acetone-$d_6$) δ -145.63 – -146.31 (m), -151.17 – -154.24 (m), -161.24 – -163.79 (m) **HRESI-MS** (pos.) m/z 642.0919, 644.0925, 645.0958 [$MH^+$] calc. for [$C_{30}H_{23}N_3F_5Sb_1 \cdot H^+$] 642.0923, 645.0960, 645.0960.

### 6.2.2.4 Synthesis of Bis Stibanotriazoles

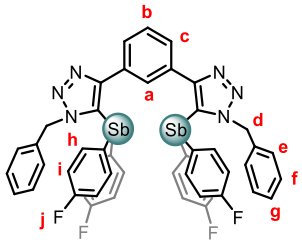
Tri-*p*-fluorophenylstibine(III) was prepared according to a literature procedure and spectroscopic data were consistent with those reported.[19]

**Compound 4·Sb$^{Bz}$**




Compound was prepared according to general procedure 2.7 with triphenylantimony (6.80 mmol, 8/3 eq.) on a 2.55 mmol (1 eq.) scale with respect to the antimony alkyne and purified using silica gel flash column chromatography (9:1 DCM:EtOAc) to afford a white solid (0.26 g, 0.28 mmol, 11%). **$^{1}$H NMR** (500 MHz, Acetone-$d_6$) δ 7.81 (t, J = 1.8 Hz, 1H, $H_a$), 7.41 – 7.17 (m, 28H, $H_{c,f-j}$), 7.03 (t, J = 7.7 Hz, 1H, $H_b$), 6.86 – 6.78 (m, 4H, $H_e$), 5.40 (s, 4H, $H_d$). **$^{13}$C NMR-{$^{1}$H}** (126 MHz, Acetone-$d_6$) δ 156.57, 137.43, 136.98, 136.11, 133.51, 130.42, 130.21, 130.14, 129.44, 129.28, 128.68, 128.65, 128.12, 128.10, 54.68. **HRESI-MS** (pos.) m/z 914.1298, 943.1306, 945.1321, 946.1345, 947.1377 [$MH^+$] calc. for [$C_{48}H_{38}N_6Sb_2 \cdot H^+$] 941.1307, 943.1316, 944.1344, 946.1353, 947.1381.

**Compound 4·Sb$^{1F}$**




Compound was prepared according to general procedure 2.7 with tri-p-fluorophenylstibine (1.68 mmol, 8/3 eq.) on a 0.63 mmol (1 eq.) scale with respect to the antimony alkyne and purified using silica gel flash column chromatography (9:1 DCM:EtOAc) to afford a white solid (0.124 g, 0.122 mmol, 19%). **$^{1}$H NMR** (500 MHz, Acetone-$d_6$) δ 7.66 (t, J = 1.7 Hz, 1H, $H_a$), 7.39 – 7.32 (m, 8H, $H_i$), 7.29 – 7.20 (m, 8H, $H_{c,f,g}$), 7.05 – 6.94 (m, 9H, $H_{b,b}$), 6.88 – 6.80 (m, 4H, $H_e$), 5.48 (s, 4H, $H_d$). **$^{13}$C NMR-{$^{1}$H}** (126 MHz, Acetone-$d_6$) δ 164.63 (d, J = 247.2 Hz), 156.42, 139.03 (d, J = 7.6 Hz), 137.42, 133.34, 131.26 (d, J = 3.8 Hz), 130.48, 129.53, 129.25, 128.75, 128.60, 128.24, 127.88, 117.15 (d, J = 20.5 Hz), 54.76. **$^{19}$F NMR** (377 MHz, Acetone-$d_6$) δ -112.89. **HRESI-MS** (pos.) m/z 1013.0924, 1015.0930, 1016.0961, 1018.0970, 1019.0998 [$MH^+$] calc. for [$C_{48}H_{34}N_6F_4Sb_2 \cdot H^+$] 1013.0930, 1015.0939, 1016.0967, 1018.0975, 1019.1004.

### 6.2.3 CHN Elemental Analysis for Triaryl Pnictogens

*Table 6.1. Summarised CHN analysis for **1·Sb$^{R}$** receptor series*

| **Analysis - 1·Sb$^{2F}$** | | | |
|---|---|---|---|
| **Element** | **Expected %** | **Found (1)** | **Found (2)** |
| **Carbon** | 46.90 | 47.18 | 47.23 |
| **Hydrogen** | 1.97 | 1.73 | 1.72 |
| **Nitrogen** | 0 | 0 | 0 |
| **Analysis - 1·Sb$^{3F}$** | | | |
| **Element** | **Expected %** | **Found (1)** | **Found (2)** |
| **Carbon** | 41.98 | 42.18 | 42.22 |
| **Hydrogen** | 1.17 | 0.95 | 0.94 |
| **Nitrogen** | 0 | 0 | 0 |
| **Analysis - 1·Sb$^{2Cl}$** | | | |
| **Element** | **Expected %** | **Found (1)** | **Found (2)** |
| **Carbon** | 38.63 | 38.84 | 38.83 |
| **Hydrogen** | 1.62 | 1.44 | 1.51 |
| **Nitrogen** | 0 | 0 | 0 |
| **Analysis - 1·Sb$^{3F}$** | | | |
| **Element** | **Expected %** | **Found (1)** | **Found (2)** |
| **Carbon** | 32.61 | 33.72 | 33.65 |
| **Hydrogen** | 0.91 | 0.93 | 1.15 |
| **Nitrogen** | 0 | 0 | 0 |
| **Analysis - 1·Sb$^{2CF3}$** | | | |
| **Element** | **Expected %** | **Found (1)** | **Found (2)** |
| **Carbon** | 37.88 | 38.14 | 38.11 |
| **Hydrogen** | 1.19 | 1.06 | 1.08 |
| **Nitrogen** | 0 | 0 | 0 |
| **Analysis - 1·Sb$^{NO2}$** | | | |
| **Element** | **Expected %** | **Found (1)** | **Found (2)** |
| **Carbon** | 44.30 | 44.74 | 44.81 |
| **Hydrogen** | 2.48 | 2.35 | 2.30 |
| **Nitrogen** | 8.61 | 8.41 | 8.42 |
| **Analysis - 1·Sb$^{CN}$** | | | |
| **Element** | **Expected %** | **Found (1)** | **Found (2)** |
| **Carbon** | 58.92 | 59.49 | 59.48 |
| **Hydrogen** | 2.83 | 2.76 | 2.68 |
| **Nitrogen** | 9.82 | 9.35 | 9.45 |

*Table 6.2. Summarised CHN analysis for **1·Bi$^{R}$** receptor series.*

| **Analysis - 1·Bi$^{2F}$** | | | |
|---|---|---|---|
| **Element** | **Expected %** | **Found (1)** | **Found (2)** |
| **Carbon** | 39.43 | 39.65 | 39.64 |
| **Hydrogen** | 1.65 | 1.44 | 1.44 |
| **Nitrogen** | 0 | 0 | 0 |
| **Analysis - 1·Bi$^{3F}$** | | | |
| **Element** | **Expected %** | **Found (1)** | **Found (2)** |
| **Carbon** | 35.90 | 36.38 | 36.84 |
| **Hydrogen** | 1.00 | 0.80 | 0.68 |
| **Nitrogen** | 0 | 0 | 0 |
| **Analysis - 1·Bi$^{2Cl}$** | | | |
| **Element** | **Expected %** | **Found (1)** | **Found (2)** |
| **Carbon** | 33.42 | 34.62 | 34.56 |
| **Hydrogen** | 1.40 | 1.46 | 1.42 |
| **Nitrogen** | 0 | 0 | 0 |
| **Analysis - 1·Bi$^{3Cl}$** | | | |
| **Element** | **Expected %** | **Found (1)** | **Found (2)** |
| **Carbon** | 28.82 | 29.20 | 29.22 |
| **Hydrogen** | 0.81 | 0.80 | 0.71 |
| **Nitrogen** | 0 | 0 | 0 |
| **Analysis - 1·Bi$^{2CF3}$** | | | |
| **Element** | **Expected %** | **Found (1)** | **Found (2)** |
| **Carbon** | 33.98 | 34.21 | 34.27 |
| **Hydrogen** | 1.07 | 1.01 | 0.90 |
| **Nitrogen** | 0 | 0 | 0 |
| **Analysis - 1·Bi$^{NO2}$** | | | |
| **Element** | **Expected %** | **Found (1)** | **Found (2)** |
| **Carbon** | 37.58 | -[a] | -[a] |
| **Hydrogen** | 2.10 | -[a] | -[a] |
| **Nitrogen** | 7.30 | -[a] | -[a] |
| **Analysis - 1·Bi$^{CN}$** | | | |
| **Element** | **Expected %** | **Found (1)** | **Found (2)** |
| **Carbon** | 48.95 | 49.03 | 49.98 |
| **Hydrogen** | 2.35 | 2.19 | 2.35 |
| **Nitrogen** | 8.15 | 8.00 | 8.09 |

[a] Reliable data could not be obtained

### 6.2.4 Single Crystal X-Ray Diffraction Data

PLATON SQUEEZE was used for the refinement of **2·Sb$^{PFP}$** in order to include diffuse electron density arising from disordered solvent molecules, which could not be modelled in a sensible manner.[4, 5] Selected Crystallographic and Refinement Data for X-ray crystal structures can be found in Table 6.3, Table 6.4 and Table 6.5.

*Table 6.3.Selected Crystallographic and Refinement Data for **1·Sb$^{2Cl}$**, **1·Sb$^{3Cl}$** and **1·Sb$^{2CF3}$***

| **Compound** | **1·Sb$^{2Cl}$** | **1·Sb$^{3Cl}$** | **1·Sb$^{2CF3}$** |
|---|---|---|---|
| **Formula** | $C_{18}$ $H_9$ $Cl_6$ Sb | $C_{18}$ $H_6$ $Cl_9$ Sb, 0.5($C_6$ $H_{14}$) | $C_{24}$ $H_9$ $F_{18}$ Sb |
| **Formula Weight** | 559.74 | 706.16 | 761.05 |
| **a (Å)** | 8.6154(1) | 8.4843(2) | 9.9974(3) |
| **b (Å)** | 12.5670(1) | 11.9393(3) | 12.0314(3) |
| **c (Å)** | 18.5000(2) | 13.5494(3) | 12.6972(3) |
| **$\alpha$ (°)** | 90 | 76.9563(19) | 112.999(2) |
| **$\beta$ (°)** | 91.6678(10) | 72.2091(19) | 104.312(2) |
| **$\gamma$ (°)** | 90 | 78.8859(19) | 101.518(2) |
| **Unit cell volume (Å$^3$)** | 2002.14(4) | 1261.76(5) | 1284.88(7) |
| **Crystal system** | Monoclinic | Triclinic | Triclinic |
| **Space group** | P 21/c | P -1 | P -1 |
| **Z** | 4 | 2 | 2 |
| **Temperature (K)** | 150 K | 150 K | 150 K |
| **Radiation Type** | Copper | Copper | Copper |
| **λ (Å)** | 1.54180 | 1.54180 | 1.54184 |
| **Reflections (all)** | 22200 | 26629 | 27155 |
| **Reflections (unique)** | 4156 | 5216 | 5337 |
| **$R_{int}$** | 0.034 | 0.039 | 0.043 |
| **R[I > 2σ(*I*)]** | 0.0227 | 0.0245 | 0.0300 |
| **wR($F^2$) (all)** | 0.0592 | 0.0706 | 0.0428 |
| **S** | 1.015 | 1.010 | 1.026 |

*Table 6.4. Selected Crystallographic and Refinement Data for **1·Bi$^{2Cl}$**, **1·Bi$^{3Cl}$** and **1·Bi$^{2CF3}$***

| **Compound** | **1·Bi$^{2Cl}$** | **1·Bi$^{3Cl}$** | **1·Bi$^{2CF3}$** |
|---|---|---|---|
| **Formula** | $C_{18}$ $H_9$ Bi $Cl_6$ | $C_{18}$ $H_6$ Bi $Cl_9$ | $C_{24}$ $H_9$ $F_{18}$ Sb |
| **Formula Weight** | 646.97 | 750.30 | 761.05 |
| **a (Å)** | 8.5197(1) | 6.9673(1) | 9.9974(3) |
| **b (Å)** | 12.7341(1) | 13.4206(1) | 12.0314(3) |
| **c (Å)** | 18.5881(1) | 23.0043(2) | 12.6972(3) |
| **$\alpha$ (°)** | 90 | 90 | 112.999(2) |
| **$\beta$ (°)** | 92.2603(5) | 92.4046(8) | 104.312(2) |
| **$\gamma$ (°)** | 90 | 90 | 101.518(2) |
| **Unit cell volume (Å$^3$)** | 2015.07(3) | 2149.13(4) | 1284.88(7) |
| **Crystal system** | Monoclinic | Monoclinic | Triclinic |
| **Space group** | P 21/c | P 21/n | P -1 |
| **Z** | 4 | 4 | 2 |
| **Temperature (K)** | 150 K | 150 K | 150 K |
| **Radiation Type** | Copper | Copper | Copper |
| **λ (Å)** | 1.54184 | 1.54184 | 1.54184 |
| **Reflections (all)** | 48850 | 11233 | 27155 |
| **Reflections (unique)** | 4196 | 4433 | 5337 |
| **$R_{int}$** | 0.040 | 0.035 | 0.043 |
| **R[I > 2σ(*I*)]** | 0.0196 | 0.0287 | 0.0300 |
| **wR($F^2$) (all)** | 0.0502 | 0.0816 | 0.0428 |
| **S** | 1.071 | 0.979 | 1.026 |

*Table 6.5. Selected Crystallographic and Refinement Data for **2·Bi$^{PFP}$** and **2·Sb$^{PFP}$***

| **Compound** | **2·Sb$^{PFP}$** | **2·Bi$^{PFP}$** |
|---|---|---|
| **Formula** | $C_{42}$ $H_{15}$ $F_{15}$ $N_9$ Sb | $C_{42}$ $H_{15}$ Bi $F_{15}$ $N_9$, C H $Cl_3$ |
| **Formula Weight** | 1052.36 | 1258.96 |
| **a (Å)** | 12.6562(3) | 23.5794(4) |
| **b (Å)** | 13.8093(4) | 10.0950(2) |
| **c (Å)** | 14.3601(4) | 18.7203(3) |
| **$\alpha$ (°)** | 104.779(2) | 90 |
| **$\beta$ (°)** | 111.288(3) | 106.246(2) |
| **$\gamma$ (°)** | 97.967(2) | 90 |
| **Unit cell volume (Å$^3$)** | 2185.42(12) | 4278.14(14) |
| **Crystal system** | triclinic | monoclinic |
| **Space group** | P -1 | P 21/c |
| **Z** | 2 | 4 |
| **Temperature (K)** | 150 K | 150 K |
| **Radiation Type** | Copper | Copper |
| **λ (Å)** | 1.54184 | 1.54180 |
| **Reflections (all)** | 34742 | 103371 |
| **Reflections (unique)** | 9040 | 8905 |
| **$R_{int}$** | 0.113 | 0.064 |
| **R[I > 2σ(*I*)]** | 0.0803 | 0.0298 |
| **wR($F^2$) (all)** | 0.2232 | 0.0790 |
| **S** | 1.011 | 0.990 |

## 6.2.5 $^{1}$H NMR Titration Data

### 6.2.5.1 Bismuth(III) Triaryl Compounds

*Table 6.6. Chloride anion association constants for **1·Bi$^{R}$** receptor series. $K_a$($M^{-1}$) values calculated using BindFit software using a 1:1 stoichiometric host-guest binding model. Errors (±) are in parentheses. Solvent = THF-$d_8$. T = 298 K.*

| Receptor | $K_a$ / $M^{-1}$ |
|---|---|
| **1·Bi$^{CN}$** | 76(1) |
| **1·Bi$^{2F}$** | 152(2) |
| **1·Bi$^{2Cl}$** | 213(1) |
| **1·Bi$^{NO2}$** | 227(3) |
| **1·Bi$^{3F}$** | 580(7) |
| **1·Bi$^{3Cl}$** | 716(8) |

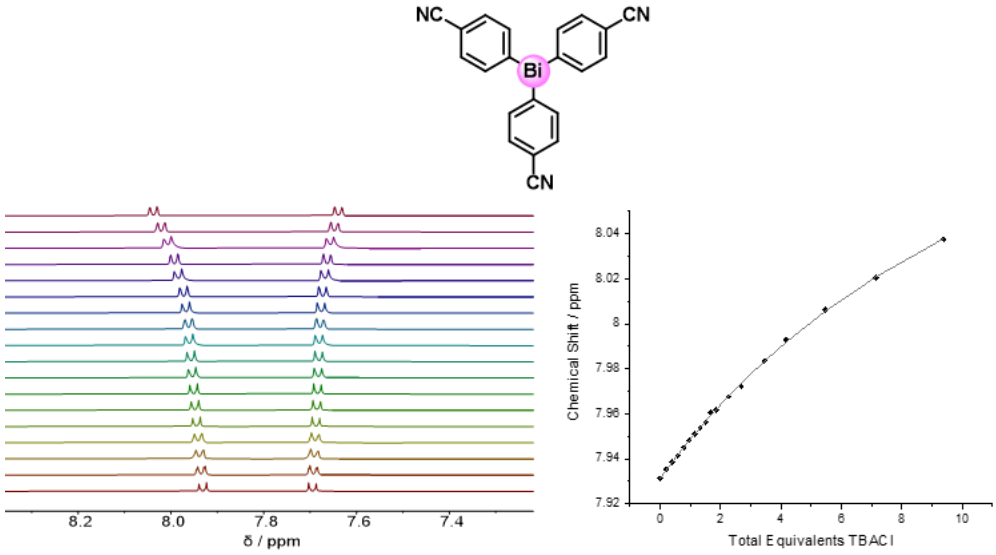



*Figure 6.1. Stacked $^{1}$H-NMR TBACl titration (left) and chloride binding isotherm with dots representing experimental data and solid lines representing the fitted binding isotherm (right) for **1·Bi$^{CN}$**. Solvent = THF-$d_8$. T = 298 K.*

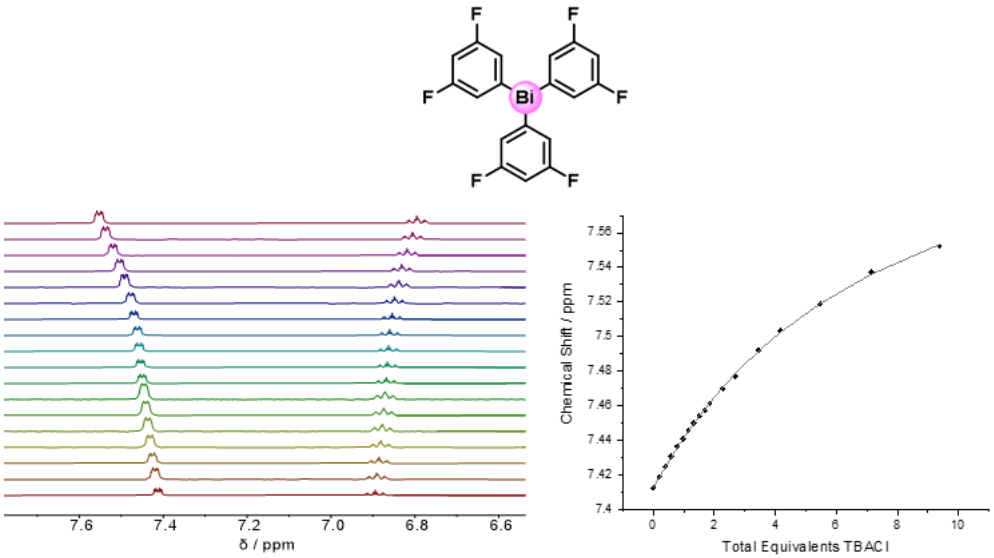



*Figure 6.2. Stacked $^{1}$H-NMR TBACl titration (left) and chloride binding isotherm with dots representing experimental data and solid lines representing the fitted binding isotherm (right) for* ***1·Bi$^{2F}$****. Solvent = THF-$d_8$. T = 298 K.*

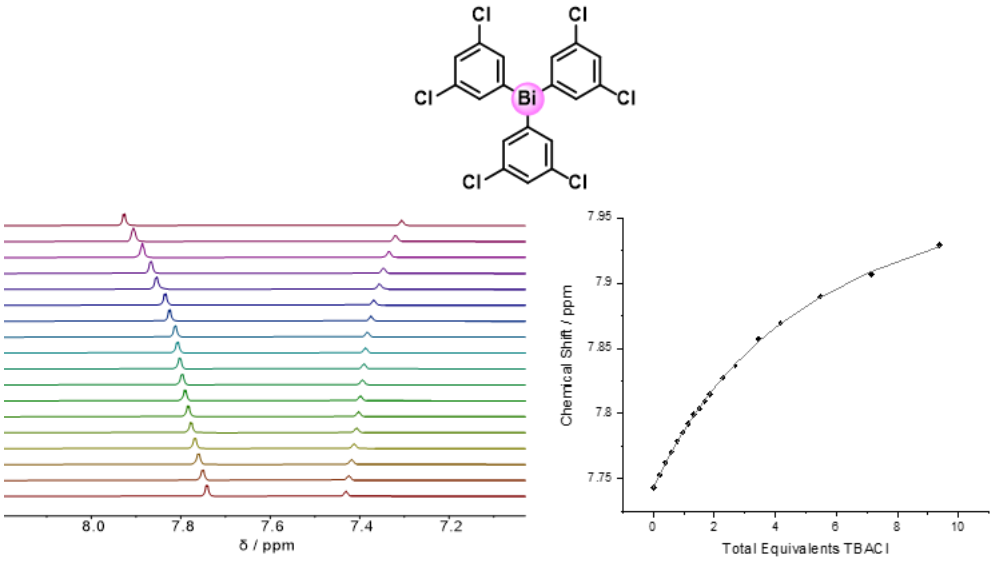



*Figure 6.3. Stacked $^{1}$H-NMR TBACl titration (left) and chloride binding isotherm with dots representing experimental data and solid lines representing the fitted binding isotherm (right) for* ***1·Bi$^{2Cl}$****. Solvent = THF-$d_8$. T = 298 K.*

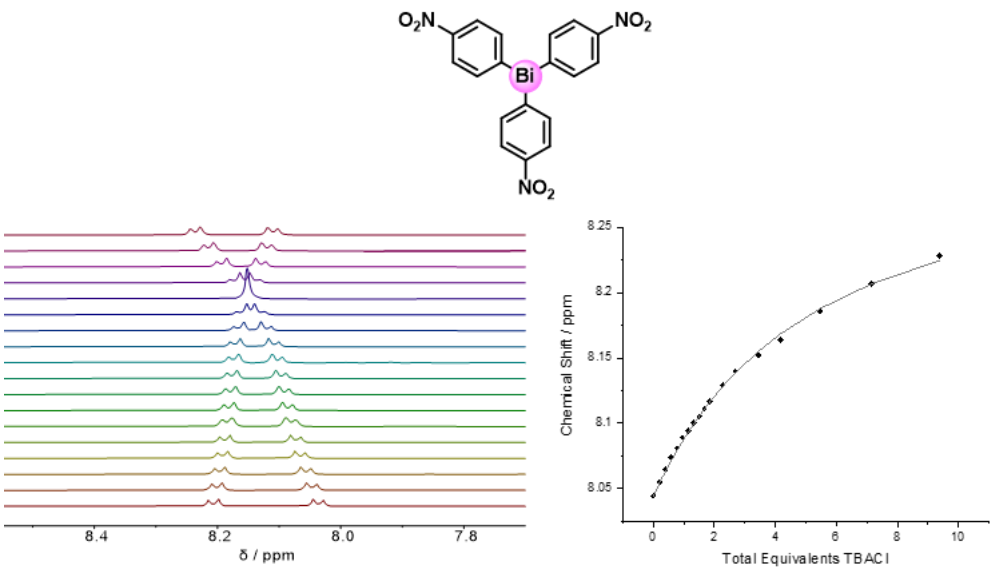



*Figure 6.4. Stacked $^{1}$H-NMR TBACl titration (left) and chloride binding isotherm with dots representing experimental data and solid lines representing the fitted binding isotherm (right) for* ***1·Bi$^{NO2}$****. Solvent = THF-$d_8$. T = 298 K.*

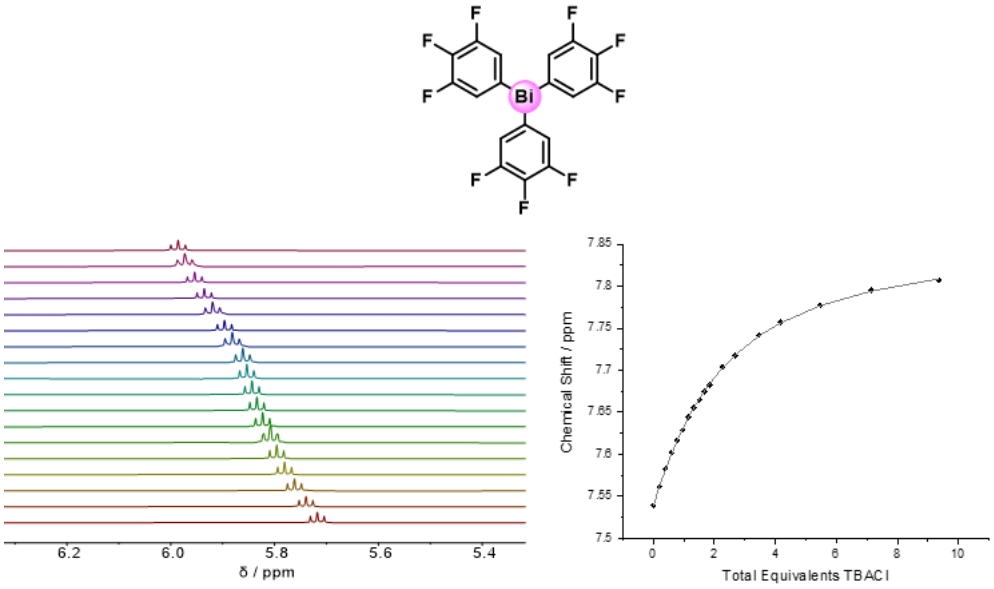



*Figure 6.5. Stacked $^{1}$H-NMR TBACl titration (left) and chloride binding isotherm with dots representing experimental data and solid lines representing the fitted binding isotherm (right) for* ***1·Bi$^{3F}$****. Solvent = THF-$d_8$. T = 298 K.*

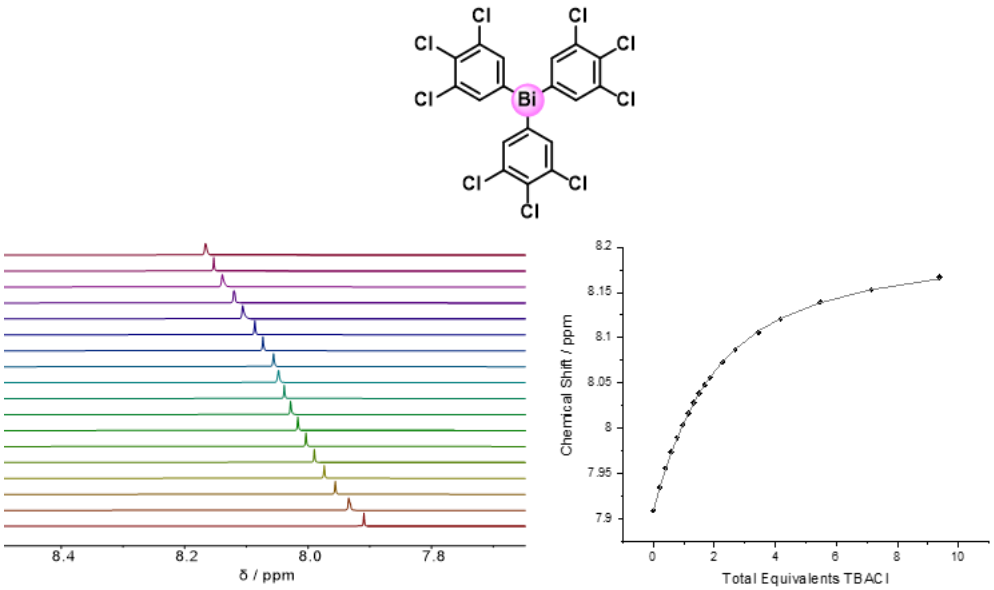



*Figure 6.6. Stacked $^{1}$H-NMR TBACl titration (left) and chloride binding isotherm with dots representing experimental data and solid lines representing the fitted binding isotherm (right) for* ***1·Bi$^{3Cl}$****. Solvent = THF-$d_8$. T = 298 K.*

*Table 6.7. Anion association constants for* ***1·Bi$^{2CF3}$*** *receptor. Ka($M^{-1}$) values calculated using BindFit software using a 1:1 stoichiometric host-guest binding model. All using TBA salts. Errors (±) are in parentheses. Solvent = THF-d8. T = 298 K*

| **1·Bi$^{2CF3}$** | **$K_a$ / $M^{-1}$** |
|---|---|
| $Cl^-$ | 1300(43) |
| $Br^-$ | 432(8) |
| $I^-$ | 192(2) |
| $OCN^-$ | 344(12) |
| $NO_2^-$ | 332(6) |
| $NO_3^-$ | 124(4) |

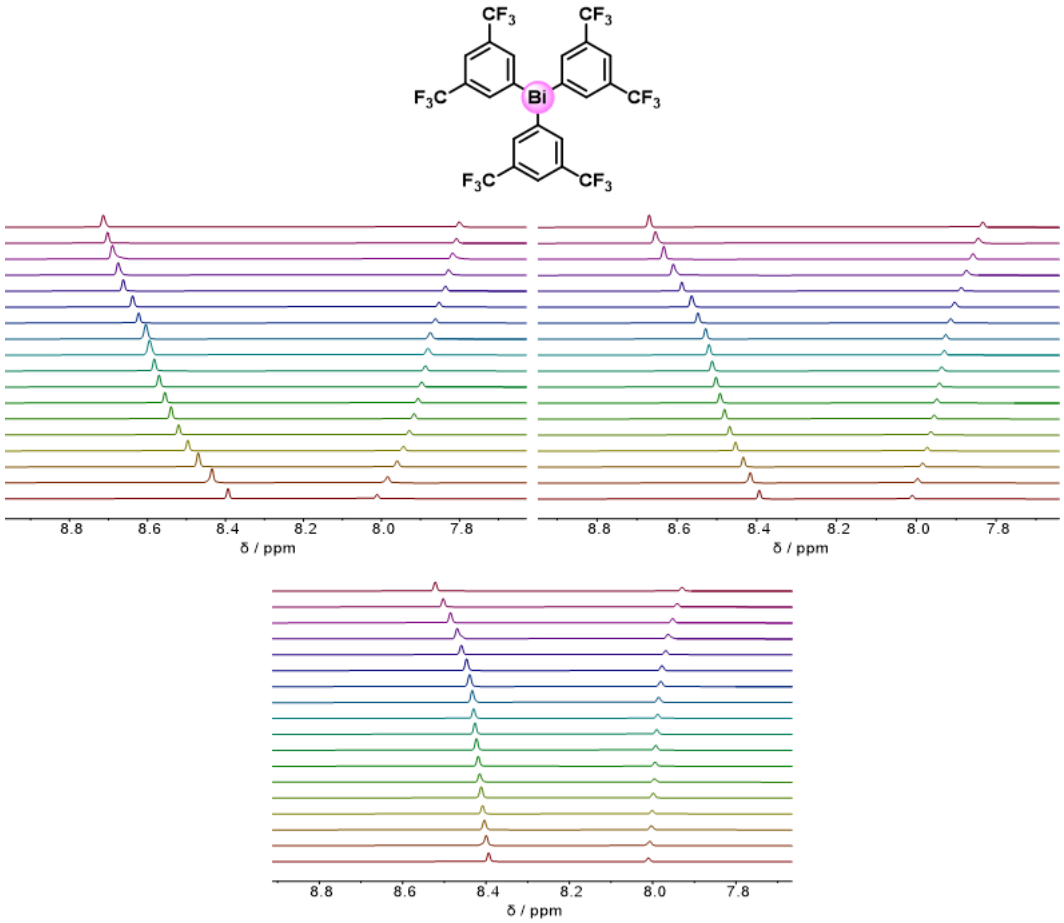



*Figure 6.7. Stacked $^{1}$H-NMR titrations for TBACl (top left), TBABr (top right) and TBAI (bottom) for* ***1·Bi$^{2CF3}$****. Solvent = THF-$d_8$. T = 298 K.*

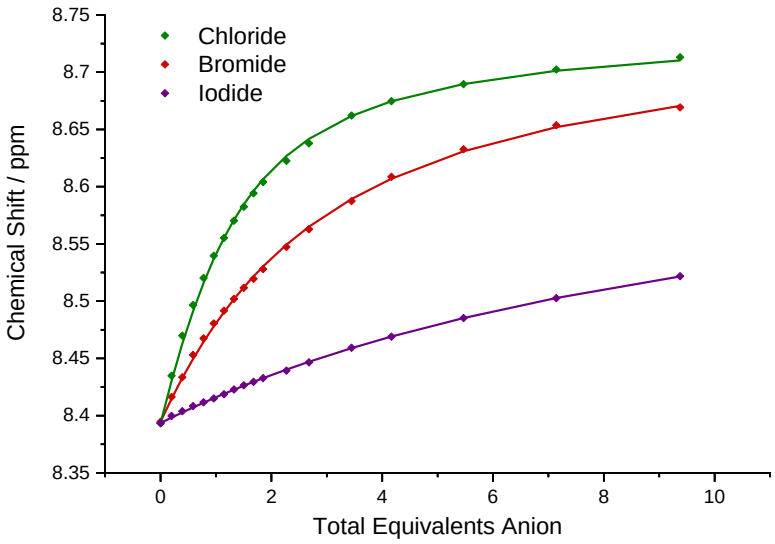



*Figure 6.8. Binding isotherms for halide anions with dots representing experimental data and solid lines representing the fitted binding isotherm for* ***1·Bi$^{2CF3}$***

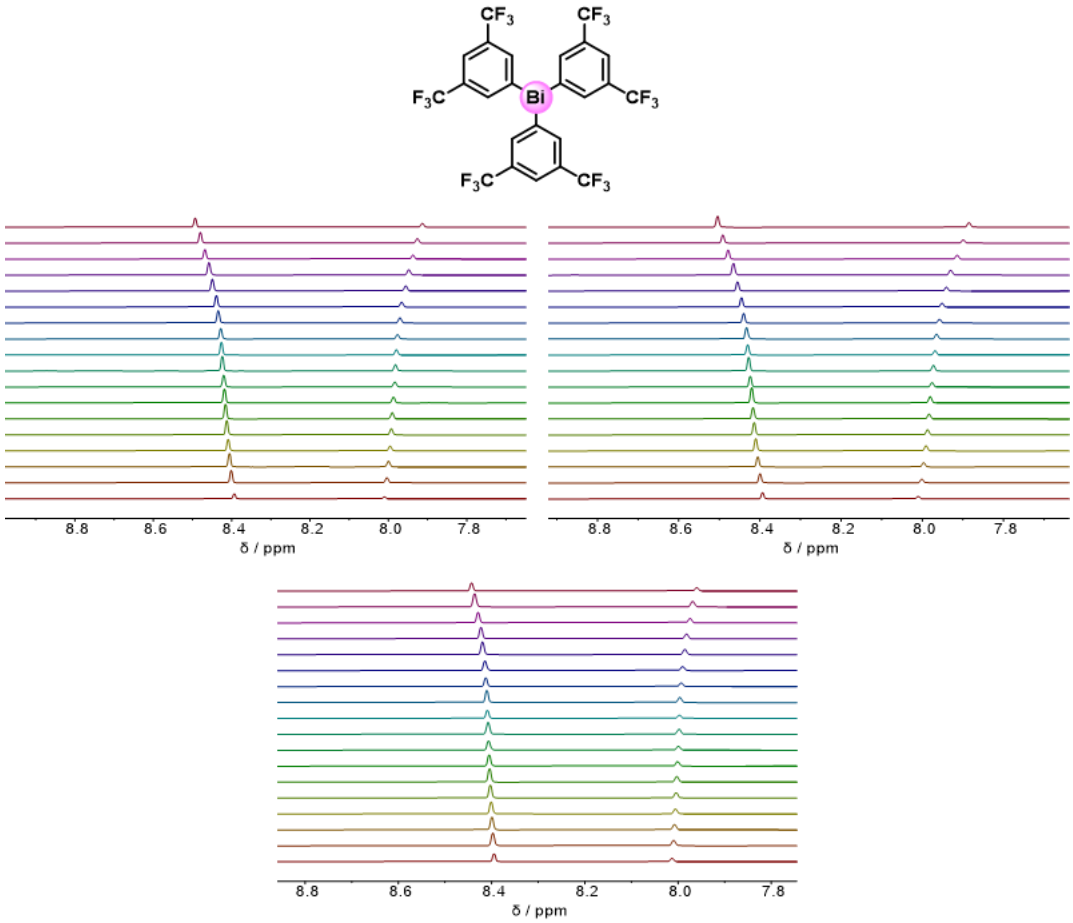



*Figure 6.9. Stacked $^{1}$H-NMR titrations for TBAOCN (top left), $TBANO_2$ (top right) and $TBANO_3$ (bottom) for **1·Bi$^{2CF3}$**. Solvent = THF-$d_8$. T = 298 K.*

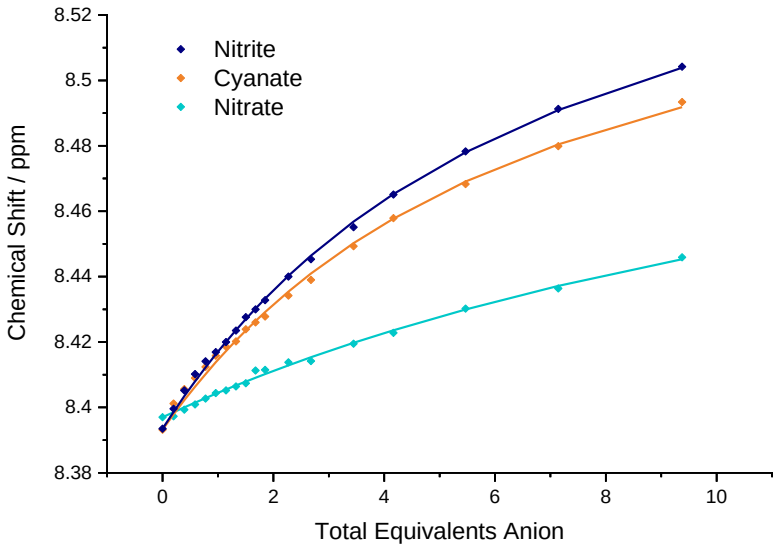



*Figure 6.10. Binding isotherms for oxo-anions with dots representing experimental data and solid lines representing the fitted binding isotherm for **1·Bi$^{2CF3}$***

### 6.2.5.2 Antimony(III) Triaryl Compounds

*Table 6.8. Chloride anion association constants for **1·Sb$^{R}$** receptor series. $K_a$($M^{-1}$) values calculated using BindFit software using a 1:1 stoichiometric host-guest binding model. Errors (±) are in parentheses. Solvent = THF-d8. T = 298 K.*

| Receptor | $K_a$ / $M^{-1}$ |
|---|---|
| **1·Sb$^{CN}$** | 36(2) |
| **1·Sb$^{2F}$** | 61(2) |
| **1·Sb$^{2Cl}$** | 52(1) |
| **1·Sb$^{NO2}$** | 94(2) |
| **1·Sb$^{3F}$** | 253(3) |
| **1·Sb$^{3Cl}$** | 341(6) |

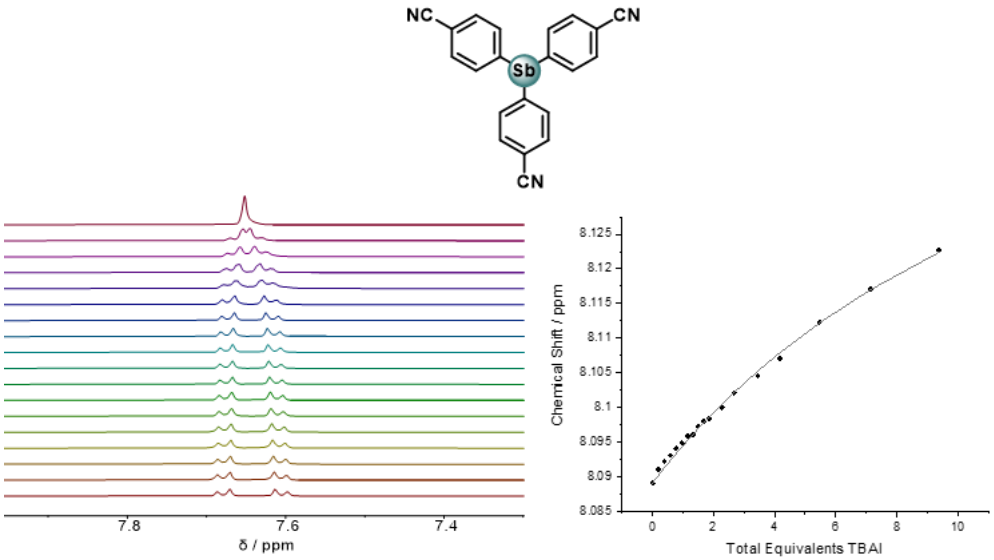



*Figure 6.11. Stacked $^{1}$H-NMR TBACl titration (left) and chloride binding isotherm with dots representing experimental data and solid lines representing the fitted binding isotherm (right) for **1·Sb$^{CN}$**. Solvent = THF-$d_8$. T = 298 K.*

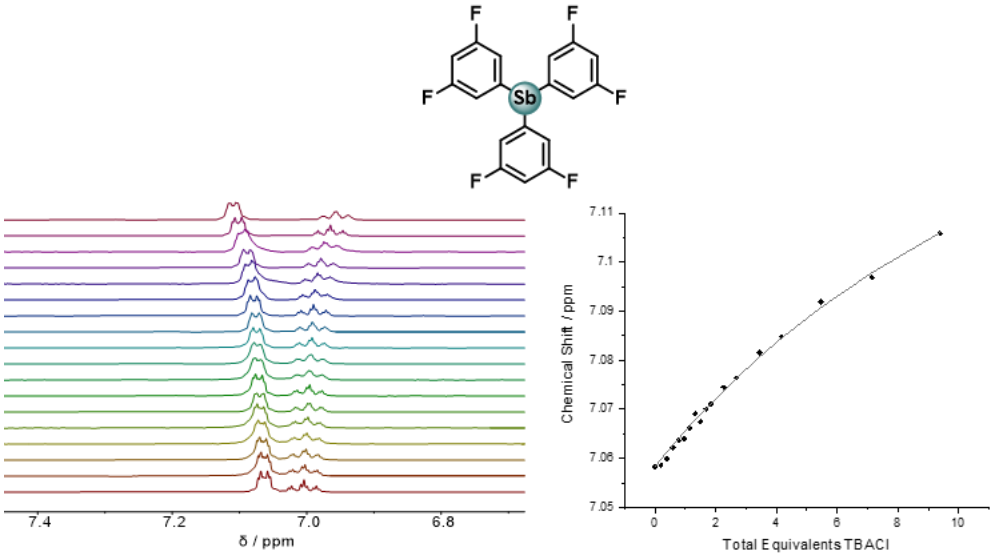



*Figure 6.12. Stacked $^{1}$H-NMR TBACl titration (left) and chloride binding isotherm with dots representing experimental data and solid lines representing the fitted binding isotherm (right) for* ***1·Sb$^{2F}$****. Solvent = THF-$d_8$. T = 298 K.*

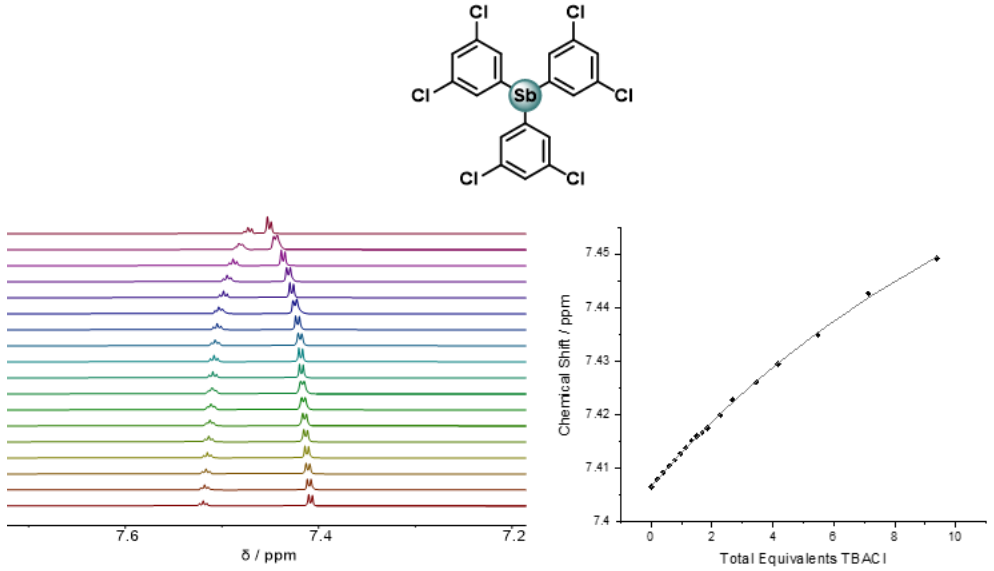



*Figure 6.13. Stacked $^{1}$H-NMR TBACl titration (left) and chloride binding isotherm with dots representing experimental data and solid lines representing the fitted binding isotherm (right) for* ***1·Sb$^{2Cl}$****. Solvent = THF-$d_8$. T = 298 K.*

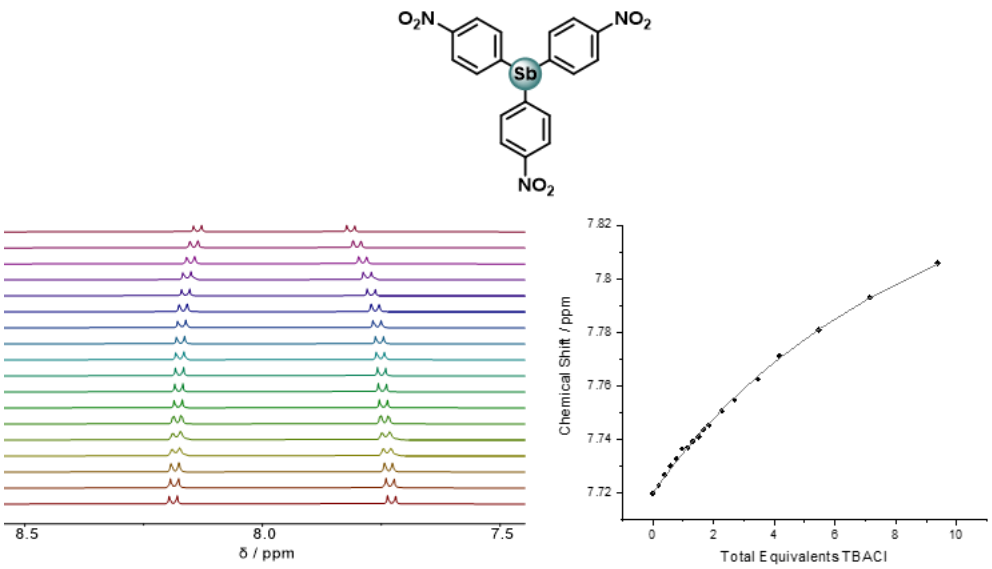



*Figure 6.14. Stacked $^{1}$H-NMR TBACl titration (left) and chloride binding isotherm with dots representing experimental data and solid lines representing the fitted binding isotherm (right) for* ***1·Sb$^{NO2}$****. Solvent = THF-$d_8$. T = 298 K.*

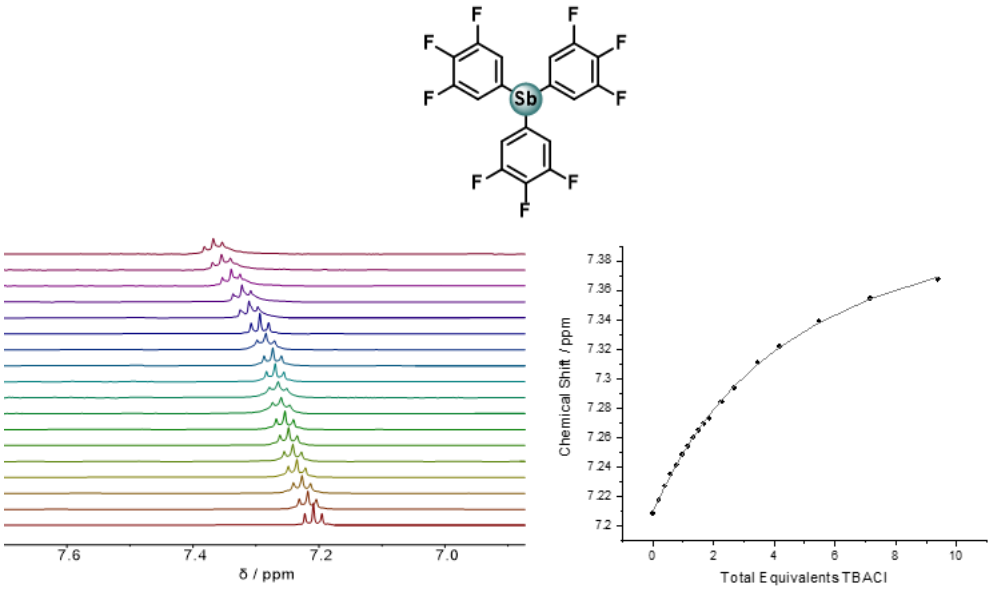



*Figure 6.15. Stacked $^{1}$H-NMR TBACl titration (left) and chloride binding isotherm with dots representing experimental data and solid lines representing the fitted binding isotherm (right) for* ***1·Sb$^{3F}$****. Solvent = THF-$d_8$. T = 298 K.*

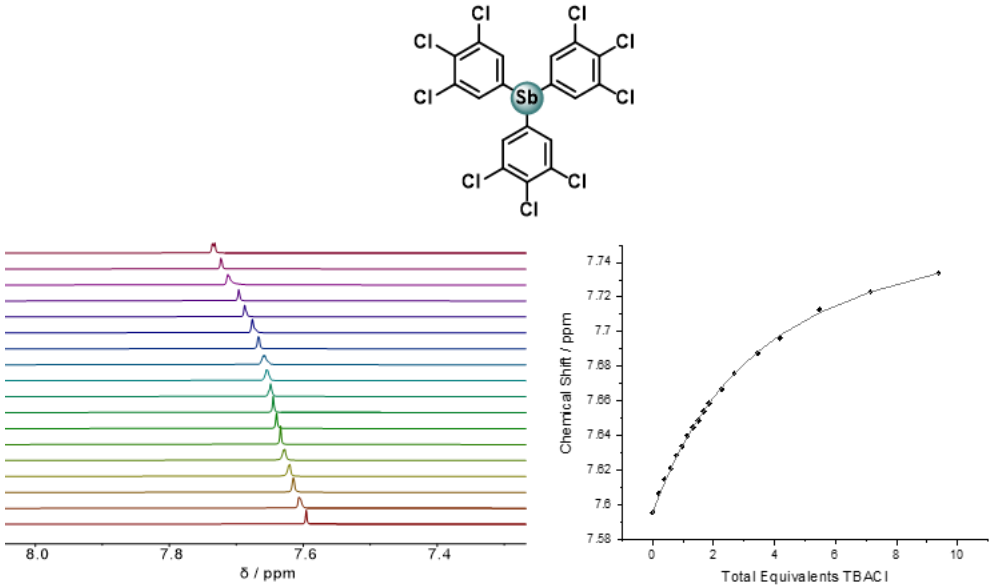



*Figure 6.16. Stacked $^{1}$H-NMR TBACl titration (left) and chloride binding isotherm with dots representing experimental data and solid lines representing the fitted binding isotherm (right) for* ***1·Sb$^{3Cl}$****. Solvent = THF-$d_8$. T = 298 K.*

*Table 6.9. Anion association constants for* ***1·Sb$^{2CF3}$*** *receptor. $K_a$($M^{-1}$) values calculated using BindFit software using a 1:1 stoichiometric host-guest binding model. All using TBA salts. Errors (±) are in parentheses. Solvent = THF-$d_8$. T = 298 K*

| **1·Sb$^{2CF3}$** | ***$K_a$* / $M^{-1}$** |
|---|---|
| $Cl^-$ | 702(16) |
| $Br^-$ | 207(3) |
| $I^-$ | 147(4) |
| $CH_3OCO^-$ | 268(15) |
| $OCN^-$ | 263(11) |
| $NO_2^-$ | 125(4) |
| $NO_3^-$ | 79(3) |

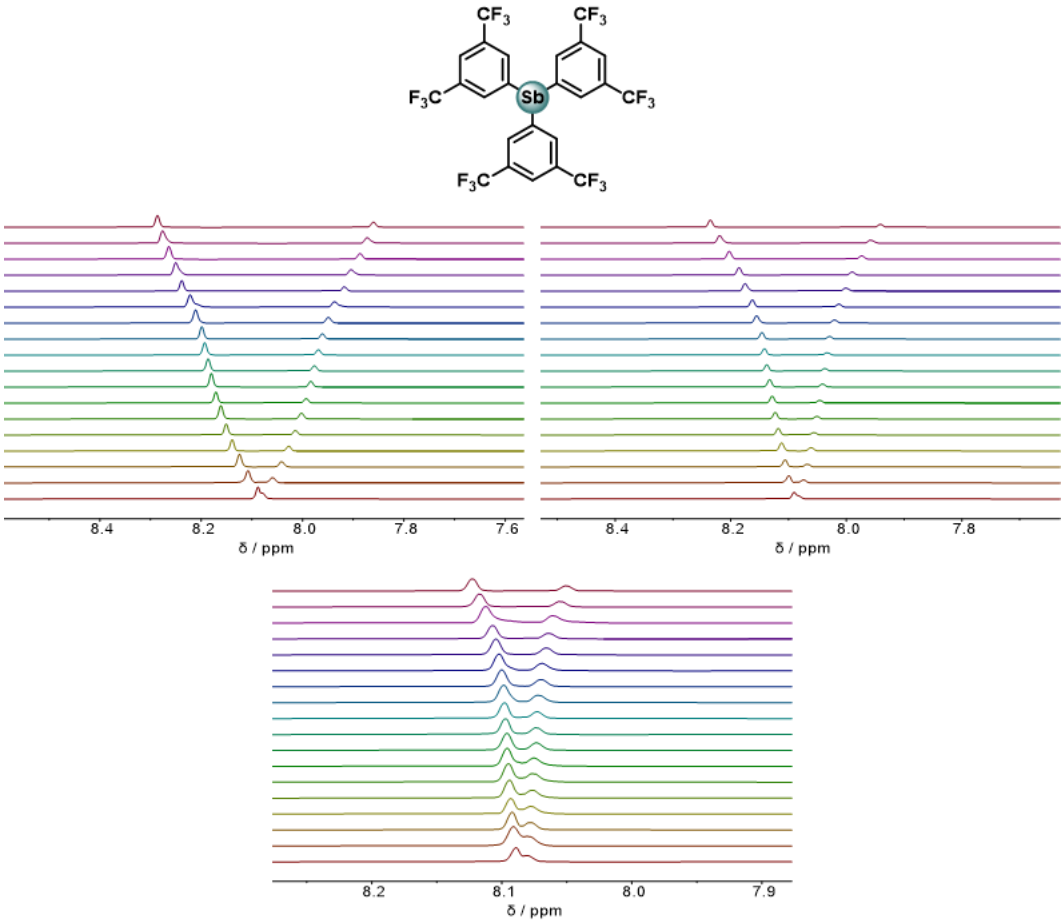



*Figure 6.17. Stacked $^{1}$H-NMR titrations for TBACl (top left), TBABr (top right) and TBAI (bottom) for* ***1·Sb$^{2CF3}$****. Solvent = THF-$d_8$. T = 298 K.*

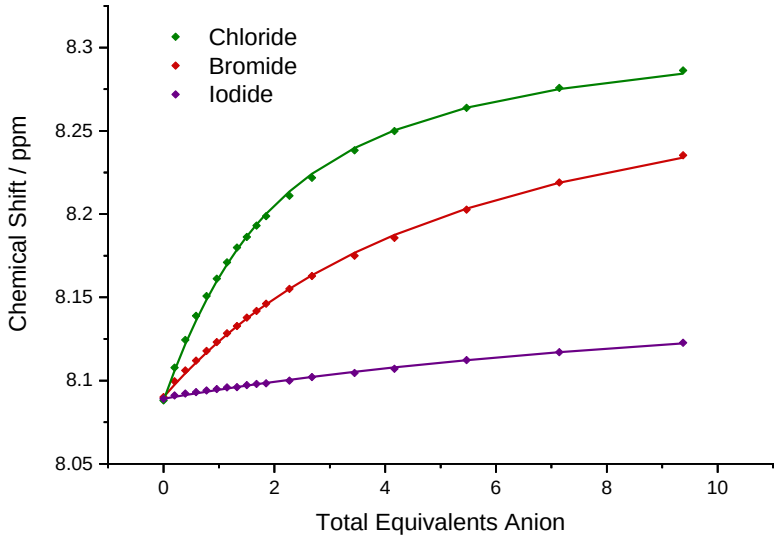



*Figure 6.18. Binding isotherms for halide anions with dots representing experimental data and solid lines representing the fitted binding isotherm for* ***1·Sb$^{2CF3}$****. Solvent = THF-$d_8$. T = 298 K.*

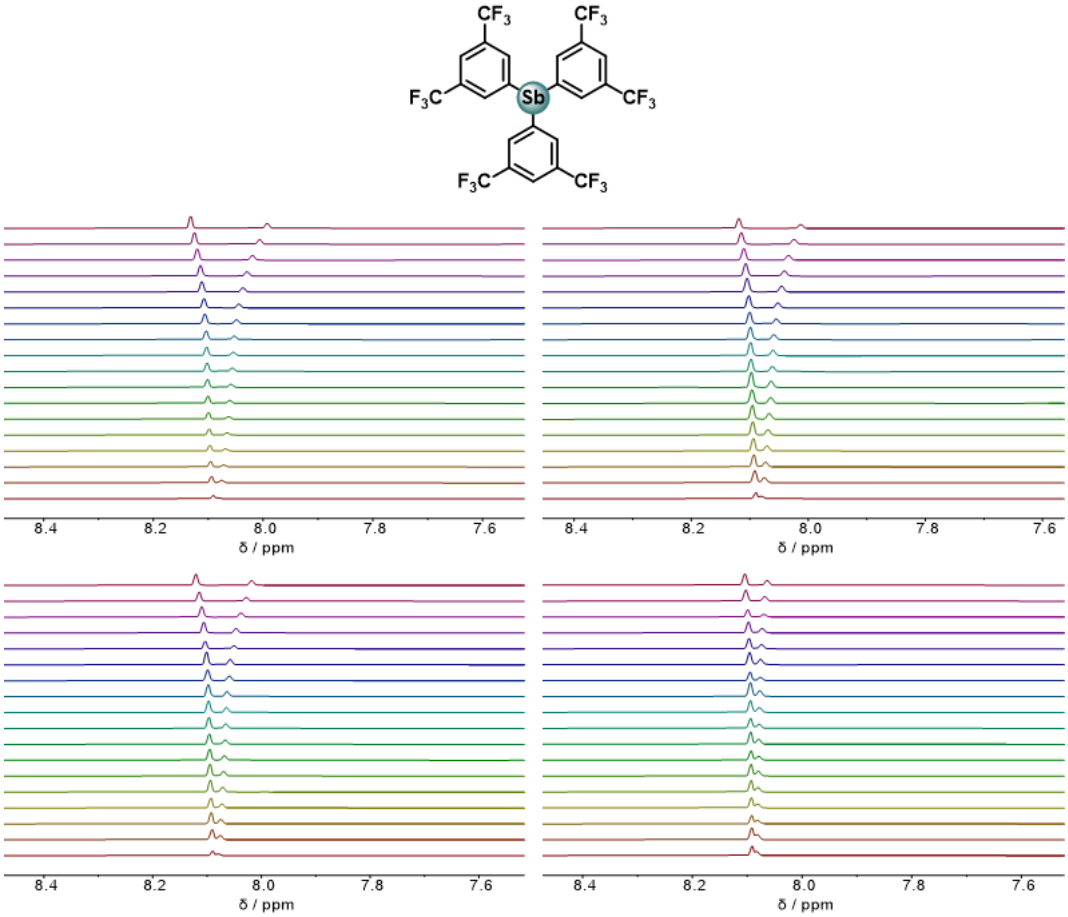



*Figure 6.19. Stacked $^{1}$H-NMR titrations for $TBAOCOCH_3$ (top left), TBAOCN (top right), $TBANO_2$ (bottom left) and $TBANO_3$ (bottom right) for **1·Sb$^{2CF3}$**. Solvent = THF-$d_8$. T = 298 K.*

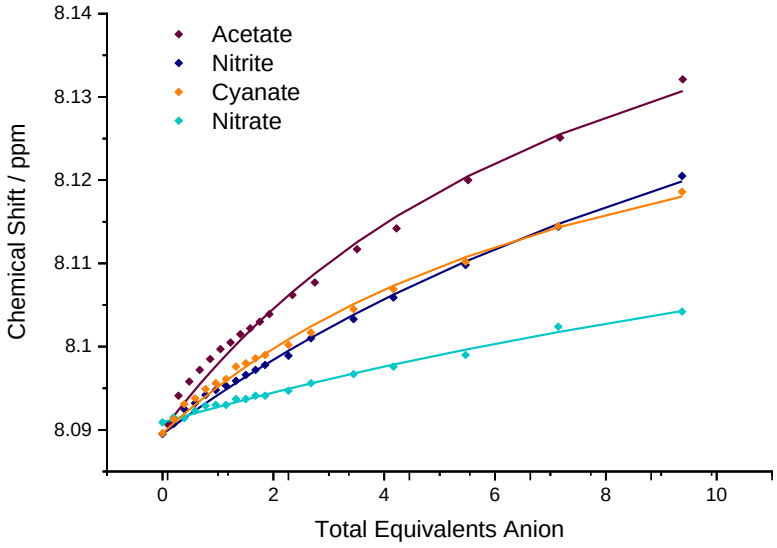



*Figure 6.20. Binding isotherms for oxo-anions with dots representing experimental data and solid lines representing the fitted binding isotherm for **1·Sb$^{2CF3}$***

### 6.2.5.3 Pnictogen Tripods

*Table 6.10. Chloride anion association constants for tripodal receptors. $K_a(M^{-1})$ values calculated using BindFit software using a 1:1 stoichiometric host-guest binding model. Errors (±) are in parentheses. Solvent = THF-$d_8$. T = 298 K.*

| Receptors | $K_a$ / $M^{-1}$ |
|---|---|
| **2·Bi$^{Bz}$** | 63(1) |
| **2·Bi$^{PFP}$** | 115(1) |
| **2·Sb$^{Bz}$** | 25(1) |
| **2·Sb$^{PFP}$** | 58(1) |

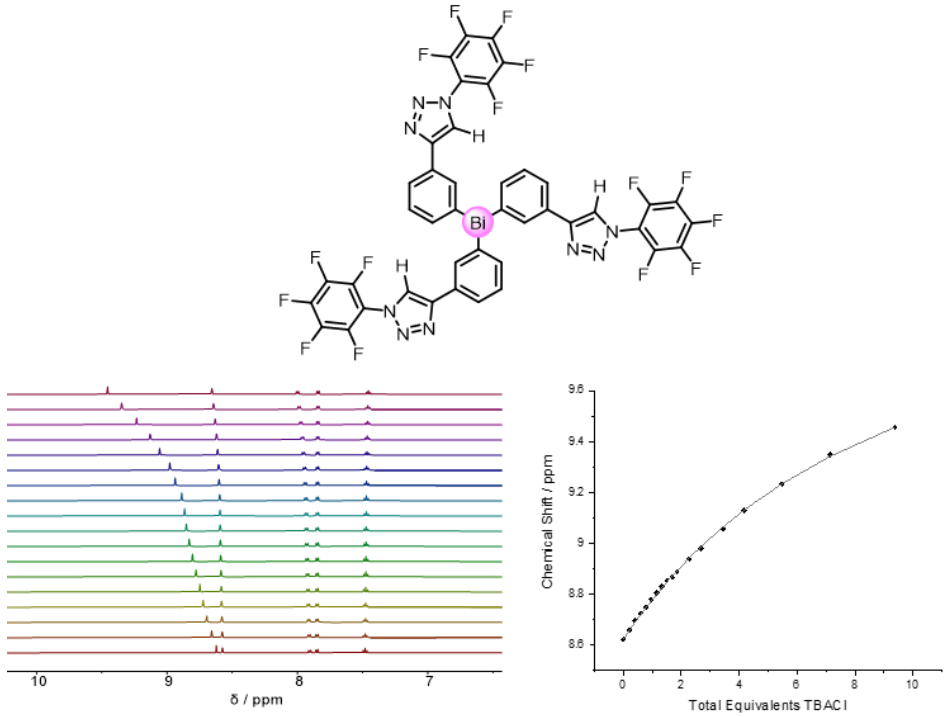



*Figure 6.21. Stacked $^1$H-NMR TBACl titration (left) and chloride binding isotherm with dots representing experimental data and solid lines representing the fitted binding isotherm (right) for **2·Bi$^{PNP}$**. Solvent = THF-$d_8$. T = 298 K.*

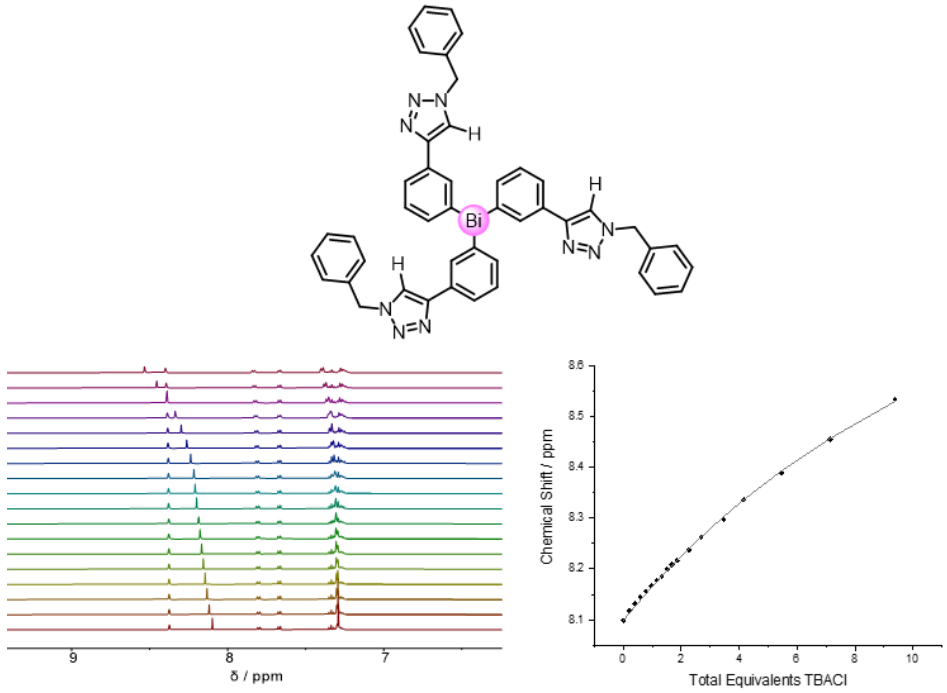



*Figure 6.22. Stacked $^{1}$H-NMR TBACl titration (left) and chloride binding isotherm with dots representing experimental data and solid lines representing the fitted binding isotherm (right) for* ***2·Bi$^{Bz}$****. Solvent = THF-$d_8$. T = 298 K.*

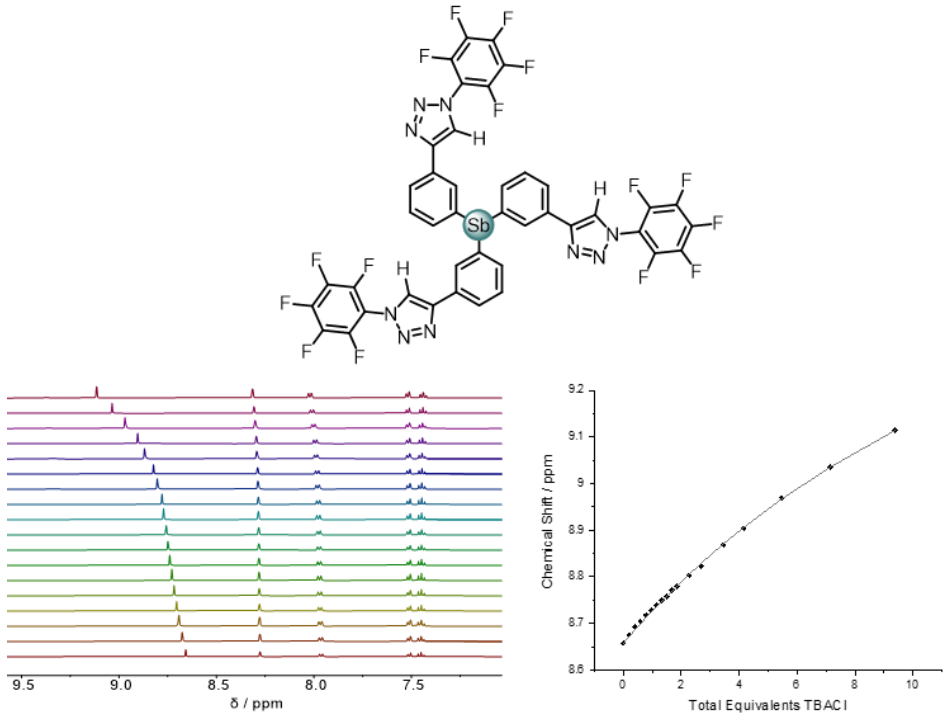



*Figure 6.23. Stacked $^{1}$H-NMR TBACl titration (left) and chloride binding isotherm with dots representing experimental data and solid lines representing the fitted binding isotherm (right) for* ***2·Sb$^{PFP}$****. Solvent = THF-$d_8$. T = 298 K.*

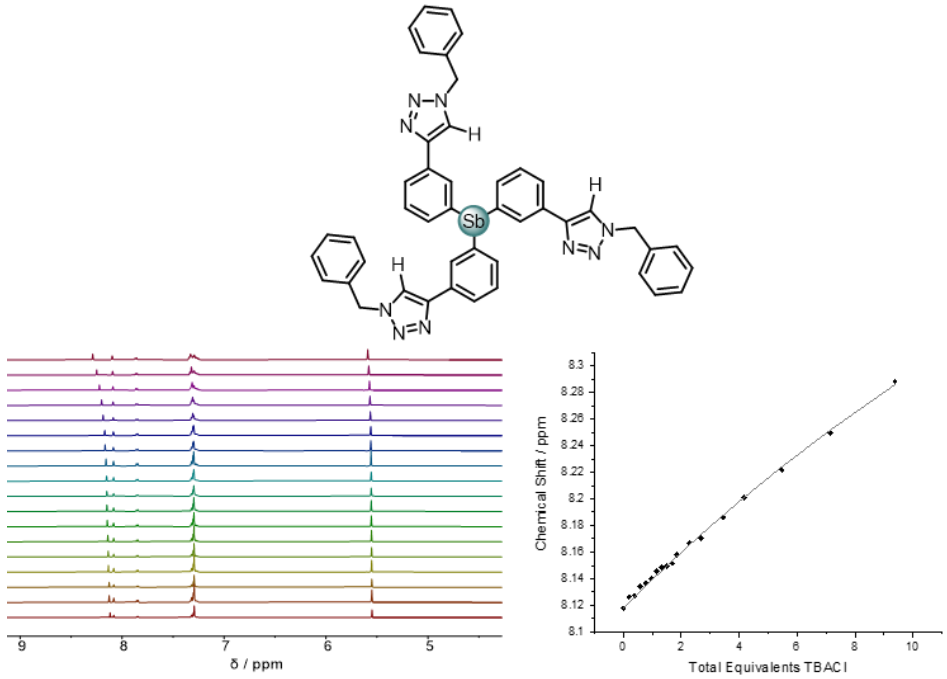



*Figure 6.24. Stacked $^{1}$H-NMR TBACl titration (left) and chloride binding isotherm with dots representing experimental data and solid lines representing the fitted binding isotherm (right) for* ***2·Sb$^{Bz}$****. Solvent = THF-$d_8$. T = 298 K.*

### 6.2.5.4 Stibanotriazoles

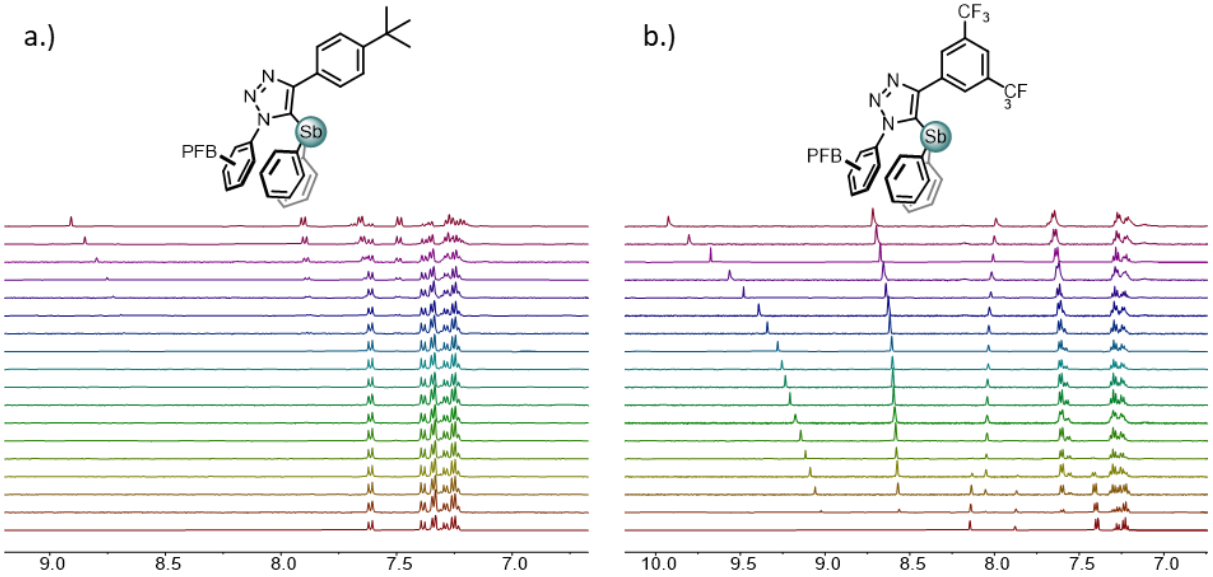



*Figure 6.25. Stacked $^{1}$H-NMR titrations for TBACl for a.)* ***3·Sb$^{2CF3}$*** *and b.)* ***3·Sb$^{tBu}$****. Solvent = THF-$d_8$. T = 298 K.*

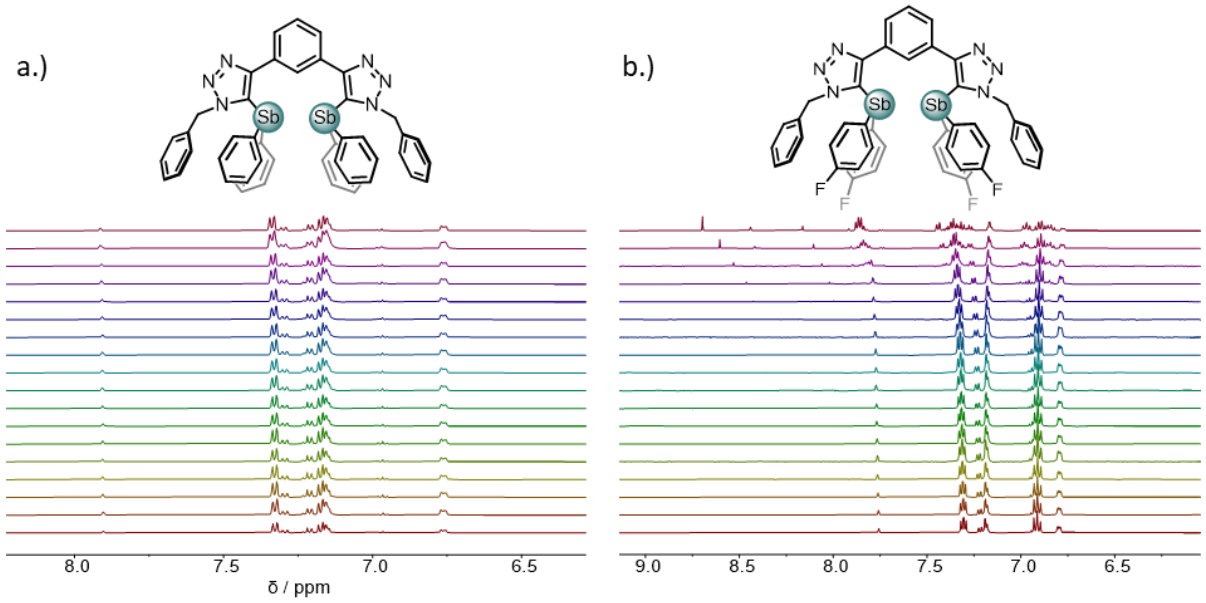



*Figure 6.26. Stacked $^{1}$H-NMR titrations for TBACl for a.) **4·Sb$^{Bz}$** and b.) **4·Sb$^{1F}$**. Solvent = THF-$d_8$. T = 298 K.*

## 6.3 Experimental Information Related to Chapter 3

### 6.3.1 General Synthetic Procedures

**General Procedure 3.1**

CuI (5 eq.) and TBTA (5 eq.) were stirred together in dry, degassed THF (0.1 M wrt CuI) for 15 minutes before the bis-iodoalkyne (5 eq.) was added. The respective organic azide (1 eq.) was dissolved in dry, degassed THF (0.04 M wrt organic azide) and added over 5 h using a syringe pump, while the mixture was kept in the dark. The resulting mixture was stirred overnight under a nitrogen atmosphere, in the dark. The solvent was removed under reduced pressure and the crude product dissolved in DCM before being washed with an EDTA/$NH_4OH_{(aq)}$ solution followed by brine. The organic layer was dried over $MgSO_4$, filtered and concentrated. The product was purified using silica gel flash column chromatography.

**General Procedure 3.2**

CuI (0.6 eq.) and TBTA (0.4 eq.) were stirred together in dry, degassed THF (3.7 mM wrt CuI) for 15 minutes before 1-azidooctane (1.2 eq.) was added. A solution of the previously prepared mono-click product (1 eq.) in dry, degassed THF (0.06 M wrt mono-click product) was furthermore added and the resulting mixture was stirred under a nitrogen atmosphere, in the dark, overnight. The solvent was removed under reduced pressure and the crude dissolved in DCM. An aqueous workup was performed by washing the organic layer with an EDTA/$NH_4OH_{(aq)}$ solution followed by brine. The organic layer was dried over $MgSO_4$, filtered and concentrated. The product was purified using silica gel flash column chromatography.

**General Procedure 3.3**

The alcohol functionalised precursor (1 eq.) was dissolved together with triethylamine (2.1 eq.) in dry, degassed DCM (0.01 M wrt alcohol). The resulting mixture was stirred at 0 °C for 5 minutes. Methane sulfonyl chloride (2 eq.) was dissolved in dry, degassed DCM (0.02 M wrt MsCl) and added dropwise to the cooled mixture. The reaction mixture was allowed to warm to room temperature and stirred for 3 h before washing it with water, 1 M HCl and brine. The organic layer was dried over $MgSO_4$, filtered, and concentrated.

**General Procedure 3.4**

The secondary amine containing macrocycle (1 eq.), the mesylated compound (1.5 eq.), $K_2CO_3$ (5 eq.) and KI (cat.) were dissolved in dry, degassed acetonitrile (0.014 M wrt secondary amine) and a small amount of dry, degassed DCM (0.032 M wrt secondary amine) was added to aid solubility. The reaction mixture was heated at 70 °C for 2 days under a nitrogen atmosphere. The crude reaction mixture diluted with DCM and washed with brine before the organic layer was dried over $MgSO_4$, filtered, and concentrated.

**General Procedure 3.5**

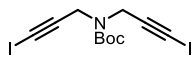
The Boc protected compound (1 eq.) was dissolved in DCM (8 mM wrt Boc protected compound). Trifluoroacetic acid (100 eq.) was added and the reaction mixture stirred overnight. The mixture was diluted with DCM and washed with $NaHCO_3$ and water. The organic layer was dried over $MgSO_4$, filtered and concentrated.

**General Procedure 3.6**

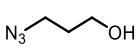
The lariat arm (1 eq.) was dissolved in dry, degassed DCM (0.022 M wrt lariat arm) and $[Cu(CH_3CN)_4]PF_6$ (0.95 eq.) was added. The mixture was left to complex for 30 minutes under a nitrogen atmosphere before the addition of a solution of the stopper (1.1 eq.) in dry, degassed DCM (0.020 M wrt stopper). After stirring overnight under a nitrogen atmosphere, further DCM was added before being washed with an $EDTA/NH_4OH_{(aq)}$ solution followed by brine. The organic layer was dried over $MgSO_4$ and concentrated under reduced pressure. The crude product was purified by silica gel flash column chromatography.

## 6.3.2 Synthesis and Characterisations

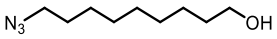
### 6.3.2.1 Synthesis of **LM1** and **LM2**



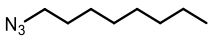

Bis-iodo alkyne **2** was prepared according to a literature procedure and spectroscopic data were consistent with those reported.[20]




3-Azidopropan-1-ol was prepared according to a literature procedure[21] and spectroscopic data[22] were consistent with those reported.

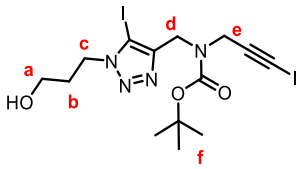


9-Azidononan-1-ol was prepared according to a modified literature procedure.[21] 9-bromononan-1-ol (1.00 g, 4.48 mmol, 1 eq.) was dissolved in DMSO (15 mL) and $NaN_3$ was added. The mixture was heated at 90 °C for 1 day before being cooled to room temperature and diluted with water. The product was extracted into diethyl ether and the organic layer washed with brine, dried over $MgSO_4$, filtered, and concentrated to afford a colourless oil (0.82 g, 4.43 mmol, 99%). Spectroscopic data were consistent with those reported.[22]



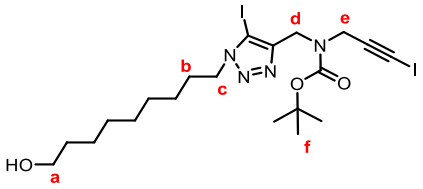
1-Azidooctane was prepared according to a literature procedure[23] and spectroscopic data[24] were consistent with those reported.

**Compound 3a**



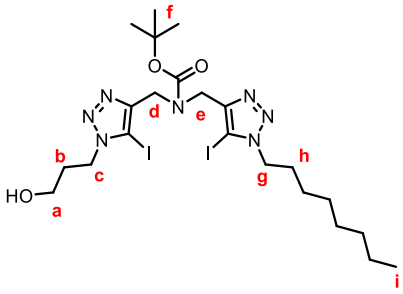

Prepared according to general procedure 3.1 from 3-azidopropan-1-ol (0.45 mmol, 1 eq.) and **2** (2.25 mmol, 5 eq.) and purified in a 7:3 mixture of DCM:EtOAc to afford a pale-yellow solid (0.17 g, 0.31 mmol, 69%). **$^1$H NMR** (400 MHz, $CDCl_3$) δ 4.64 (s, 2H, $H_d$), 4.54 (t, J = 6.8 Hz, 2H, $H_c$), 4.34 – 4.06 (broad m, 2H, $H_e$), 3.67 (broad t, 2H, $H_a$), 2.14 (p, J = 6.3 Hz, 2H, $H_b$), 1.49 (s, 9H, $H_f$). **$^{13}$C NMR-{$^1$H}** (101 MHz, $CDCl_3$) δ 154.60, 147.62, 89.77, 81.04, 79.28, 58.83, 47.80, 38.81, 32.30, 29.72, 28.49, 1.07. **HRESI-MS** (pos.) m/z 546.96943 [$MH^+$] calc. for [$C_{12}H_{20}I_2N_4O_3 \cdot H^+$] 546.96975.

**Compound 3b**




Prepared according to general procedure 3.1 from 9-azidononan-1-ol (0.45 mmol, 1 eq.) and **2** (2.25 mmol, 5 eq.) and purified chromatographically in an 85:15 mixture of DCM:EtOAc to afford a pale-yellow solid (0.22 g, 0.34 mmol, 76%). **$^{1}$H NMR** (400 MHz, $CDCl_3$) δ 4.63 (s, 2H, $H_d$), 4.35 (t, J = 7.4 Hz, 2H, $H_e$), 4.30 – 4.13 (broad m, 2H, $H_e$), 3.64 (broad t, 2H, $H_a$), 1.96 – 1.84 (m, 2H, $H_b$), 1.49 (s, 9H, $H_f$), 1.40 – 1.22 (m, 12H, $H_{alkyl\ chain}$). **$^{13}$C NMR-{$^{1}$H}** (101 MHz, $CDCl_3$) δ 154.68, 147.60, 81.04, 63.07, 50.86, 41.18, 37.87, 32.83, 29.98, 29.40, 29.34, 28.97, 28.55, 28.40, 26.42, 25.78. **HRESI-MS** (pos.) m/z 631.06347 [$MH^+$] calc. for [$C_{20}H_{32}I_2N_4O_3 \cdot H^+$] 631.06365.

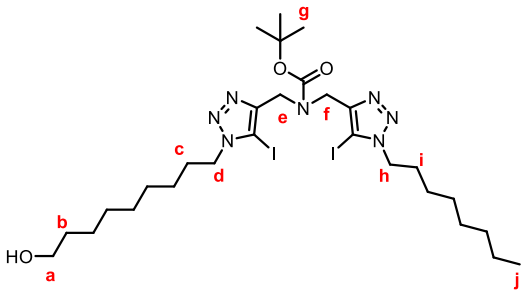
**Compound 4a**




Prepared according to general procedure 3.2 from **3a** (0.309 mmol, 1 eq.) and 1-azidooctane (0.371 mmol, 1.2 eq.) and purified using silica gel flash column chromatography in a 40:60 mixture of DCM:EtOAc to afford a pale-yellow solid (0.167 g, 0.238 mmol, 77%). **$^{1}$H NMR** (400 MHz, $CDCl_3$) δ 4.66 – 4.52 (m, 4H, $H_{d,e}$), 4.49 (t, J = 6.8 Hz, 2H, $H_c$), 4.31 (t, J = 7.4 Hz, 2H, $H_g$), 3.65 – 3.62 (m, 2H, $H_a$), 2.62 (broad s, 1H, $H_{OH}$), 2.16 – 2.06 (m, 2H, $H_b$), 1.86 (t, J = 7.3 Hz, 2H, $H_h$), 1.44 (s, 9H, $H_f$), 1.34 – 1.21 (m, 10H, $H_{alkyl\ chain}$), 0.89 – 0.79 (m, 3H, $H_i$). **$^{13}$C NMR-{$^{1}$H}** (126 MHz, $CDCl_3$) 155.20, 148.02, 147.88, 80.61, 58.83, 50.77, 47.61, 42.15, 41.75,

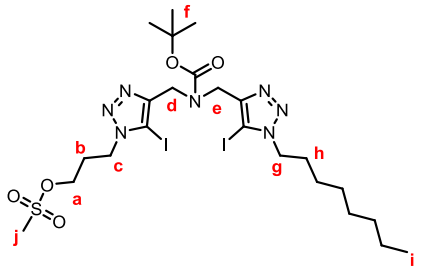
32.23, 31.80, 29.99, 29.14, 29.04, 28.63, 26.47, 22.69, 14.18. **HRESI-MS** (pos.) m/z 702.11220 [$MH^+$] calc. for [$C_{22}H_{37}I_2N_7O_3 \cdot H^+$] 702.11220.

**Compound 4b**




Synthesised according to general procedure 3.2 from **3b** (0.343 mmol, 1 eq.) and 1-azidooctane (0.412 mmol, 1.2 eq.) and purified using silica gel flash column chromatography in a 7:3 mixture of DCM:EtOAc to afford a pale-yellow solid (0.143 g, 0.182 mmol, 53%). **$^1$H NMR** (400 MHz, $CDCl_3$) δ 4.67 – 4.50 (m, 4H, $H_{e,f}$), 4.31 (t, J = 7.3 Hz, 4H, $H_{d,h}$), 3.60 (t, J = 6.6 Hz, 2H, $H_a$), 1.86 (t, J = 7.3 Hz, 4H, $H_{c,i}$), 1.56 – 1.48 (m, 2H, $H_b$), 1.43 (s, 9H, $H_g$), 1.35 – 1.20 (m, 20H, $H_{alkyl\ chain}$), 0.88 – 0.81 (m, 3H, $H_j$). **$^{13}$C NMR-{$^1$H}** (101 MHz, $CDCl_3$) δ 155.19, 147.92, 80.51, 62.93, 50.73, 50.68, 42.09, 41.76, 32.79, 31.78, 29.98, 29.90, 29.34, 29.28, 29.12, 29.03, 28.90, 28.60, 26.45, 26.35, 25.74, 22.68, 14.16. **HRESI-MS** (pos.) m/z 786.20520 [$MH^+$] calc. for [$C_{28}H_{49}I_2N_7O_3 \cdot H^+$] 786.20590.

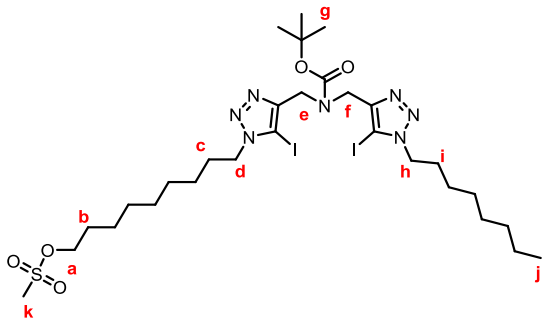
**Compound 5a**



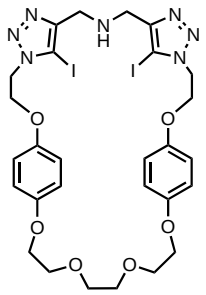

Prepared according to general procedure 3.3 from **4a** (0.073 mmol, 1 eq.) to afford an off-white solid (0.057 g, 0.073 mmol, quantitative). **$^1$H NMR** (400 MHz, $CDCl_3$) δ 4.61 (d, J = 17.5 Hz,

4H, $H_{d,e}$), 4.52 (t, J = 6.6 Hz, 2H, $H_c$), 4.35 – 4.32 (m, 2H, $H_g$), 4.26 (t, J = 5.8 Hz, 2H, $H_a$), 3.07 (s, 3H, $H_j$), 2.38 (p, J = 6.2 Hz, 2H, $H_b$), 1.88 (t, J = 7.3 Hz, 2H, $H_h$), 1.47 (s, 9H, $H_f$), 1.37 – 1.19 (m, 10H, $H_{alkyl\ chain}$), 0.90 – 0.85 (m, 3H, $H_i$). **$^{13}$C NMR-{$^1$H}** (126 MHz, $CDCl_3$) δ 155.07, 148.35, 147.83, 80.56, 66.10, 54.82, 50.69, 46.64, 37.51, 31.72, 29.92, 29.70, 29.20, 29.06, 28.96, 28.54, 26.40, 22.61, 14.08. **HRESI-MS** (pos.) m/z 780.08894 [$MH^+$] calc. for [$C_{23}H_{39}I_2N_7O_5S_1 \cdot H^+$] 780.08955.

**Compound 5b**

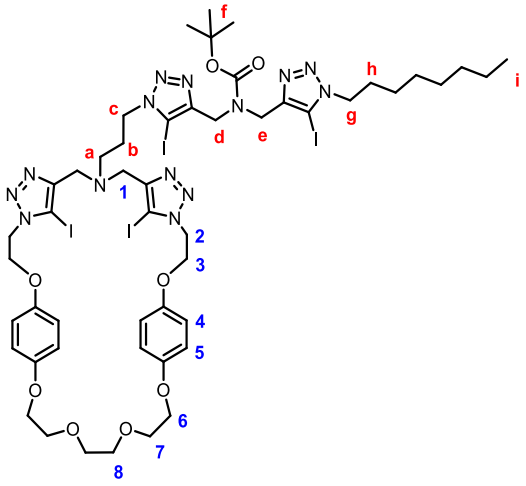



Synthesised according to general procedure 3.3 from **4b** (0.182 mmol, 1 eq.). An off-white solid was afforded (0.154 g, 0.178 mmol, 98%). **$^1$H NMR** (400 MHz, $CDCl_3$) δ 4.68 – 4.49 (m, 4H, $H_{e,f}$), 4.32 (t, J = 7.3 Hz, 4H, $H_{d,h}$), 4.19 (t, J = 6.5 Hz, 2H, $H_a$), 2.98 (s, 3H, $H_k$), 1.86 (p, J = 7.1 Hz, 4H, $H_{c,i}$), 1.77 – 1.66 (m, 2H, $H_b$), 1.44 (s, 9H, $H_f$), 1.35 – 1.21 (m, 20H, $H_{alkyl\ chain}$), 0.88 – 0.82 (m, 3H, $H_j$). **$^{13}$C NMR-{$^1$H}** (101 MHz, $CDCl_3$) δ 155.12, 147.88, 80.39, 70.16, 50.66, 50.57, 41.78, 37.40, 31.72, 29.91, 29.83, 29.69, 29.14, 29.10, 29.05, 28.96, 28.85, 28.82, 28.55, 26.39, 26.29, 25.37, 22.69, 22.61, 14.09. **HRESI-MS** (pos.) m/z 864.18281 [$MH^+$] calc. for [$C_{29}H_{51}I_2N_7O_5S_1 \cdot H^+$] 864.18345.



**MC-1** was prepared according to a literature procedure and spectroscopic data were consistent with those reported.[20]

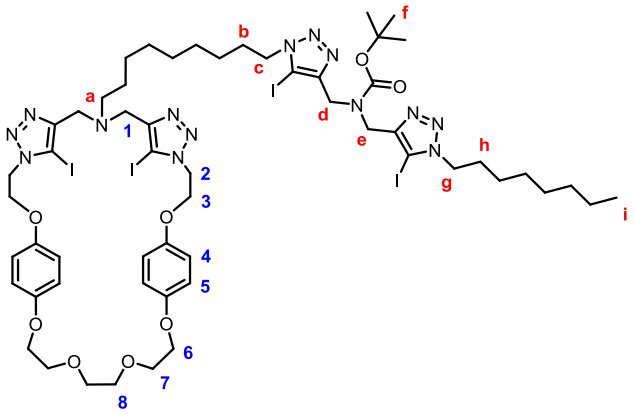
**Compound LM-1-Boc**




Prepared according to general procedure 3.4 from **MC-1** (0.095 mmol, 1 eq.) and **5a** (0.142 mmol, 1.5 eq.) and purified by silica gel flash column chromatography in 3% MeOH in DCM to afford an off-white solid (0.024 g, 0.016 mmol, 17%). **$^1$H NMR** (400 MHz, $CDCl_3$) δ 6.85 – 6.77 (m, 4H, $H_4$), 6.75 – 6.66 (m, 4H, $H_5$), 4.70 (t, J = 5.3 Hz, 4H, $H_3$), 4.63 – 4.49 (m, 4H, $H_{d,e}$), 4.38 – 4.28 (m, 6H, $H_{2,e}$), 4.21 (t, J = 7.8 Hz, 2H, $H_g$), 4.04 (t, J = 4.8 Hz, 4H, $H_6$), 3.84 – 3.76 (m, 4H, $H_7$), 3.70 (s, 8H, $H_{1,8}$), 2.73 (t, J = 6.3 Hz, 2H, $H_a$), 2.16 – 2.09 (m, 2H, $H_b$), 1.87 (m, 2H, $H_h$), 1.45 (s, 9H, $H_f$), 1.35 – 1.22 (m, 10H, $H_{alkyl\ chain}$), 0.87 (t, J = 6.5 Hz, 3H, $H_i$). **$^{13}$C NMR-{$^1$H}** (101 MHz, $CDCl_3$) δ 155.24, 153.83, 152.10, 148.82, 147.78, 116.28, 115.70, 82.87, 80.55, 71.14, 69.91, 68.51, 67.21, 50.79, 50.68, 49.86, 49.23, 49.04, 31.85, 30.05, 29.83, 29.19, 29.09,

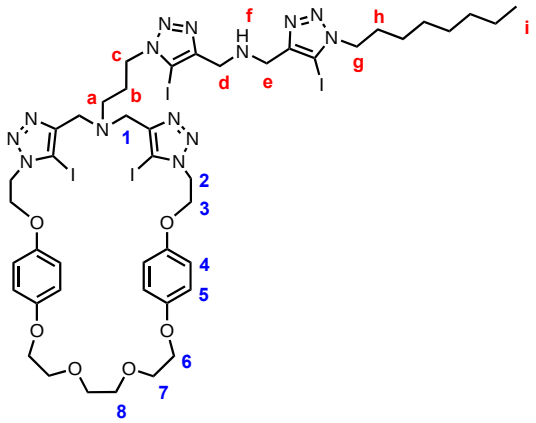
28.68, 27.84, 26.53, 22.74, 14.22. **HRESI-MS** (pos.) m/z 1501.15615 [$MH^+$] calc. for [$C_{50}H_{68}I_4N_{14}O_8 \cdot H^+$] 1501.15960.

**Compound LM-2-Boc**



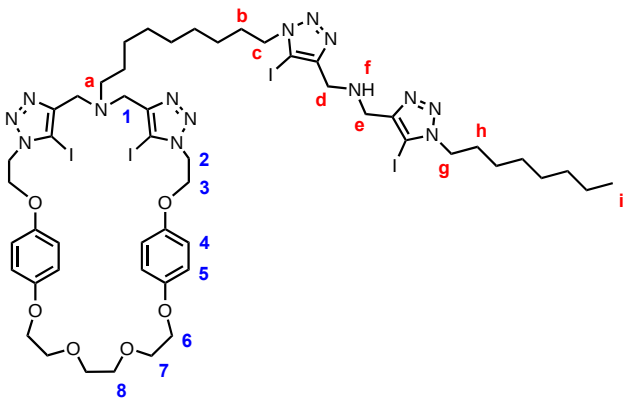

Synthesised according to general procedure 3.4 with **MC-1** (0.117 mmol, 1 eq.) and **5b** (0.175 mmol, 1.5 eq.) and purified by silica gel flash column chromatography in 1% MeOH in DCM to afford an off-white solid (0.107 g, 0.068 mmol, 58%).**$^1$H NMR** (400 MHz, $CDCl_3$) δ 6.86 – 6.80 (m, 4H, $H_4$), 6.76 – 6.71 (m, 4H, $H_5$), 4.68 (t, J = 5.4 Hz, 4H, $H_3$), 4.58 (broad s, 4H, $H_{d,e}$), 4.33 (t, J = 5.1 Hz, 8H, $H_{2,c,g}$), 4.05 (dd, J = 5.7, 3.8 Hz, 4H, $H_6$), 3.82 (dd, J = 5.7, 3.8 Hz, $H_7$), 3.71 (s, 4H, $H_8$), 3.65 (s, 4H, $H_1$), 2.57 (t, J = 7.2 Hz, 2H, $H_a$), 1.88 (q, J = 7.2 Hz, 4H, $H_{b,h}$), 1.46 (s, 9H, $H_j$), 1.36 – 1.16 (m, 22H, $H_{alkyl\ chain}$), 0.90 – 0.85 (m, 3H, $H_i$). **$^{13}$C NMR-{$^1$H}** (101 MHz, $CDCl_3$) δ 155.21, 153.79, 152.13, 149.21, 147.96, 116.19, 115.69, 82.34, 80.49, 76.84, 71.09, 69.88, 68.45, 67.10, 53.96, 50.74, 49.70, 48.78, 41.82, 32.02, 31.81, 30.01, 29.95, 29.79, 29.45, 29.41, 29.30, 29.15, 29.06, 29.00, 28.64, 27.30, 26.97, 26.49, 26.40, 22.71, 14.19. **HRESI-MS** (pos.) m/z 1585.24675 [$MH^+$] calc. for [$C_{56}H_{80}I_4N_{14}O_8 \cdot H^+$] 1585.25350.

**Compound LM-1**



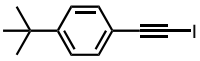
Prepared according to general procedure 3.5 from **LM-1-Boc** (0.015 mmol, 1 eq.). The crude mixture was purified by preparative TLC (3% MeOH in DCM) to afford a pale-yellow solid (0.014 mmol, 0.010 mmol, 65%). **$^1$H NMR** (400 MHz, $CDCl_3$) δ 6.81 (d, J = 8.9 Hz, 4H, $H_4$), 6.74 – 6.68 (m, 4H, $H_5$), 4.70 (t, J = 5.3 Hz, 4H, $H_3$), 4.36 – 4.31 (m, 6H, $H_{2,c}$), 4.22 (t, J = 7.7 Hz, 2H, $H_g$), 4.06 – 4.03 (m, 4H, $H_6$), 3.88 – 3.77 (m, 8H, $H_{7,d,e}$), 3.71 – 3.70 (m, 8H, $H_{1,8}$), 2.73 (t, J = 6.3 Hz, 2H, $H_a$), 2.13 – 2.10 (m, 2H, $H_b$), 1.89 – 1.86 (m, 2H, $H_h$), 0.92 – 0.80 (m, 10H, $H_{alkyl\ chain}$), 0.75 – 0.69 (m, 3H, $H_i$). **$^{13}$C NMR-{$^1$H}** (126 MHz, $CDCl_3$) δ 153.82, 152.15, 148.84, 116.30, 115.72, 82.95, 71.16, 69.94, 68.54, 67.23, 50.88, 50.71, 49.88, 49.17, 44.19, 33.85, 33.55, 32.88, 32.07, 30.31, 30.09, 29.20, 29.11, 27.95, 26.85, 26.55, 23.32, 22.84, 14.24. **HRESI-MS** (pos.) m/z 1401.10229 [$MH^+$] calc. for [$C_{45}H_{60}I_4N_{14}O_6 \cdot H^+$] 1401.10717.

**Compound LM-2**



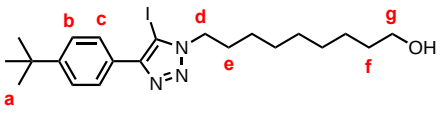
Synthesised according to general procedure 3.5 from **LM-2-Boc** (0.068 mmol, 1 eq.). The pale-yellow solid product was pure without further purification (0.099 g, 0.067 mmol, 98%). **$^1$H NMR** (400 MHz, $CDCl_3$) δ 6.83 (d, J = 9.0 Hz, 4H, $H_4$), 6.73 (d, J = 9.0 Hz, 4H, $H_5$), 4.68 (t, J = 5.4 Hz, 4H, $H_3$), 4.36 – 4.31 (m, 8H, $H_{2,c,g}$), 4.05 (t, J = 4.8 Hz, 4H, $H_6$), 3.89 (s, 4H, $H_1$), 3.81 (t, J = 4.8 Hz, 4H, $H_7$), 3.71 (s, 4H, $H_8$), 3.64 (s, 4H, $H_{d,e}$), 2.57 (t, J = 7.4 Hz, 2H, $H_a$), 1.89 – 1.85 (m, 4H, $H_{b,b}$), 1.32 – 1.19 (m, 22H, $H_{alkyl\ chain}$), 0.90 – 0.83 (m, 3H, $H_i$). **$^{13}$C NMR-{$^1$H}** (101 MHz, $CDCl_3$) δ 153.85, 152.18, 149.62, 149.21, 116.24, 115.75, 82.33, 71.13, 69.92, 68.51, 67.15, 54.01, 50.83, 50.78, 49.73, 48.83, 44.26, 33.84, 32.04, 30.27, 30.04, 29.97, 29.47, 29.39, 29.29, 29.15, 29.07, 28.99, 27.31, 26.99, 26.83, 26.51, 26.40, 22.80, 14.19. **HRESI-MS** (pos.) m/z 1485.19483 [$MH^+$] calc. for [$C_{51}H_{72}I_4N_{14}O_6 \cdot H^+$] 1485.20107.

### 6.3.2.2 Synthesis of **LM-3**



1-(*tert*-Butyl)-4-(iodoethynyl)benzene **6** was prepared according to a literature procedure and spectroscopic data were consistent with those reported.[25]

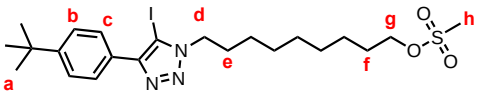
**Compound 7**




$[Cu(CH_3CN)_4]PF_6$ (0.041 g, 0.11 mmol, 0.1 eq.) and TBTA (0.058 g, 0.11 mmol, 0.1 eq.) were stirred together in dry, degassed THF (2 mL) for 20 minutes. A solution of 9-azidononan-1-ol (0.196 g, 1.06 mmol, 1 eq.) and 1-(*tert*-Butyl)-4-(iodoethynyl)benzene (0.301 g, 1.06 mmol, 1 eq.) in dry, degassed THF (8 mL) was added and the mixture stirred overnight, in the dark and under a $N_2$ atmosphere. The solvent was removed under reduced pressure and the crude dissolved in DCM. The organic layer was washed with an EDTA/$NH_4OH_{(aq)}$ solution followed by brine.

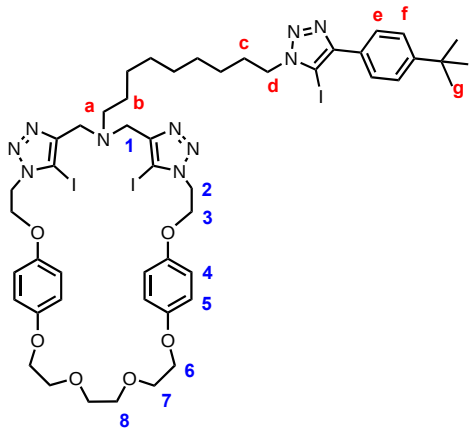
The organic layer was dried over $MgSO_4$, filtered and concentrated. The product was purified using silica gel flash column chromatography (9:1 DCM:EtOAc) to afford a pale-yellow solid (0.31 g, 0.66 mmol, 62%). **$^1$H NMR** (500 MHz, $CDCl_3$) δ 7.93 – 7.81 (m, 2H, $H_c$), 7.53 – 7.42 (m, 2H, $H_b$), 4.48 – 4.35 (m, 2H, $H_d$), 3.63 (t, J = 6.6 Hz, 2H, $H_g$), 1.97 – 1.91 (m, 2H, $H_e$), 1.61 – 1.51 (m, 2H, $H_f$), 1.35 (s, 19H, $H_{a,alkyl\ chain}$). **$^{13}$C NMR-{$^1$H}** (126 MHz, $CDCl_3$) δ 151.64, 149.68, 127.50, 127.17, 125.61, 75.89, 63.14, 51.01, 34.85, 32.84, 31.41, 30.02, 29.44, 29.36, 29.01, 26.46, 25.78. **HRESI-MS** (pos.) m/z 470.16599 [$MH^+$] calc. for [$C_{21}H_{32}I_1N_3O_1 \cdot H^+$] 470.16628.

**Compound 8**



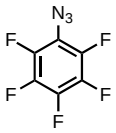

Synthesised according to general procedure 3.3 from **7** (0.32 mmol, 1 eq.). A white solid was afforded (0.17 g, 0.31 mmol, 98%). **$^1$H NMR** (400 MHz, $CDCl_3$) δ 7.91 – 7.86 (m, 2H, $H_c$), 7.52 – 7.47 (m, 2H, $H_b$), 4.47 – 4.40 (m, 2H, $H_d$), 4.22 (t, J = 6.5 Hz, 2H, $H_g$), 3.00 (s, 3H, $H_h$), 1.99 – 1.94 (m, 2H, $H_e$), 1.78 – 1.71 (m, 2H, $H_f$), 1.36 (s, 19H, $H_{a,alkyl\ chain}$). **$^{13}$C NMR-{$^1$H}** (126 MHz, $CDCl_3$) δ 151.69, 149.73, 127.57, 127.20, 125.60, 75.80, 70.25, 50.98, 37.52, 34.86, 31.43, 29.98, 29.84, 29.28, 29.22, 28.98, 26.44, 25.49. **HRESI-MS** (pos.) m/z 548.14320 [$MH^+$] calc. for [$C_{22}H_{34}I_1N_3O_3S_1 \cdot H^+$] 548.14383.

**Compound LM-3**



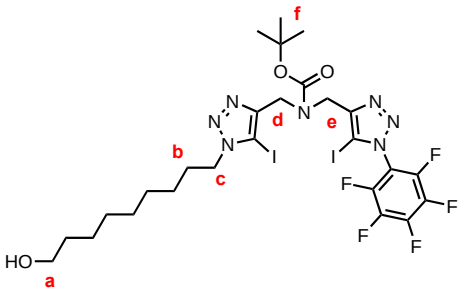

Synthesised according to general procedure 3.4 from **MC-1** (0.121 mmol, 1 eq.) and **8** (0.182 mmol, 1.5 eq.) and purified by silica gel flash column chromatography with a gradient of 1 – 1.5% MeOH in DCM to afford a white solid (0.028 g, 0.022 mmol, 18%). **$^{1}$H NMR** (400 MHz, $CDCl_3$) δ 7.91 – 7.86 (m, 2H, $H_e$), 7.51 – 7.45 (m, 2H, $H_f$), 6.86 – 6.79 (m, 4H, $H_4$), 6.76 – 6.69 (m, 4H, $H_5$), 4.67 (t, J = 5.4 Hz, 4H, $H_3$), 4.41 (t, J = 7.4 Hz, 2H, $H_d$), 4.32 (t, J = 5.4 Hz, 4H, $H_2$), 4.05 – 4.03 (m, 4H, $H_6$), 3.84 – 3.78 (m, 4H, $H_7$), 3.71 (s, 4H, $H_8$), 3.65 (s, 4H, $H_1$), 2.57 (t, J = 7.2 Hz, 2H, $H_a$), 1.93 (p, J = 7.3 Hz, 2H, $H_c$), 1.53 – 1.51 (m, 2H, $H_b$), 1.35 (s, 9H, $H_g$), 1.31 – 1.13 (m, 10H, $H_{alkyl\ chain}$). **$^{13}$C NMR-{$^{1}$H}** (126 MHz, $CDCl_3$) δ 153.84, 152.16, 151.65, 149.68, 149.25, 127.61, 127.22, 125.59, 116.22, 115.73, 82.38, 76.01, 71.13, 69.92, 68.48, 67.13, 54.01, 51.02, 49.76, 48.82, 34.86, 31.43, 30.01, 29.44, 29.31, 29.05, 27.32, 27.00, 26.46. **HRESI-MS** (pos.) m/z 1269.2083 [$MH^+$] calc. for [$C_{49}H_{63}I_3N_{10}O_6 \cdot H^+$] 1269.2139.

### 6.3.2.3 Synthesis of **LM-4**



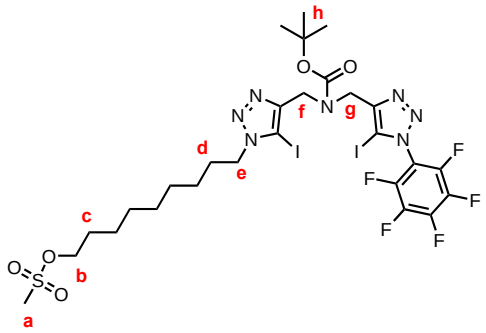

Perfluorophenyl azide was prepared according to a literature procedure and spectroscopic data were consistent with those reported.[17]

**Compound 9**



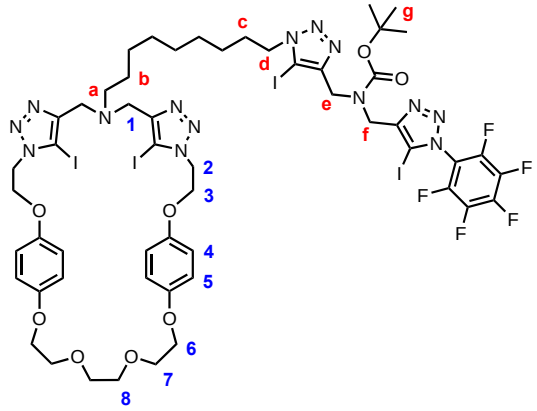

$[Cu(CH_3CN)_4]PF_6$ (0.009 g, 0.023 mmol, 0.1 eq.) and TBTA (0.012 g, 0.023 mmol, 0.1 eq.) were stirred together in dry, degassed DCM (2 mL) for 20 minutes. Mono-click product **3b** (0.145 g, 0.230 mmol, 1 eq.) was added in dry, degassed DCM (5 mL) followed by perfluorophenyl azide (0.072 g, 0.345 mmol, 1.5 eq.) and the mixture stirred overnight, in the dark and under a $N_2$ atmosphere. The mixture was diluted with DCM and the organic layer washed with an $EDTA/NH_4OH_{(aq)}$ solution followed by brine. The organic layer was dried over $MgSO_4$, filtered and concentrated. The product was purified using silica gel flash column chromatography (20% EtOAc in DCM) to afford a pale-yellow solid (0.121 g, 0.144 mmol, 62%). **$^1$H NMR** (400 MHz, $CDCl_3$) δ 4.83 – 4.57 (m, 4H, $H_{d,e}$), 4.35 (t, J = 7.3 Hz, 2H, $H_c$), 3.63 (t, J = 6.6 Hz, 2H, $H_a$), 1.90 (t, J = 7.2 Hz, 2H, $H_b$), 1.69 – 1.18 (m, 21H, $H_{f,alkyl\ chain}$). **$^{13}$C NMR-{$^1$H, $^{19}$F}** (126 MHz, $CDCl_3$) δ 155.17, 149.61, 147.92, 144.66, 142.71, 142.61, 139.09, 137.13, 137.03, 112.38, 80.92, 63.14, 50.84, 42.41, 32.87, 29.98, 29.42, 29.36, 28.99, 28.62, 26.44, 25.80. **$^{19}$F NMR** (376 MHz, $CDCl_3$) δ -150.62 – -152.88 (m), -158.69 – -160.65 (m), -160.78 – -162.31 (m). **HRESI-MS** (pos.) m/z 840.0636 $[MH^+]$ calc. for $[C_{26}H_{32}F_5I_2N_7O_3 \cdot H^+]$ 840.0649.

**Compound 10**



Experiment conducted according to general procedure 3.3 from **9** (0.078 mmol, 1 eq.) to afford an off-white solid (0.051 g, 0.056 mmol, 72%). The mesylation of the product was confirmed by $^{1}$H NMR but some unknown impurities were also detected. Due to concerns over instability, the product was used without further purification. **$^{1}$H NMR** (400 MHz, $CDCl_3$) δ 4.83 – 4.57 (m, 4H, $H_{f,g}$), 4.34 (t, J = 7.3 Hz, 2H, $H_e$), 4.20 (t, J = 6.5 Hz, 2H, $H_b$), 2.99 (s, 3H, $H_a$), 1.88 (m, 2H, $H_d$), 1.78 – 1.64 (m, 2H, $H_c$), 1.54 – 1.18 (m, 19H, $H_{b,alkyl\ chain}$).

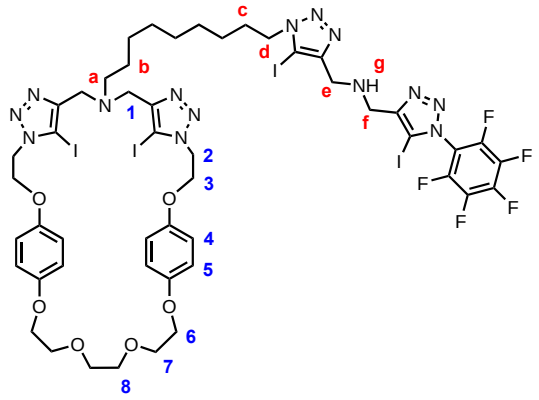
**Compound LM-4-Boc**



Synthesis conducted according to general procedure 3.4 from **MC-1** (0.037 mmol, 1 eq.) and **10** (0.056 mmol, 1.5 eq.). Purified by preparative TLC (6:4 $CHCl_3$:EtOAc) to afford a pale-yellow solid (0.024 g, 0.015 mmol, 41%). **$^{1}$H NMR** (400 MHz, $CDCl_3$) δ 6.87 – 6.77 (m, 4H, $H_4$), 6.76 – 6.68 (m, 4H, $H_5$), 4.67 (q, J = 8.4 Hz, 8H, $H_{3,e,f}$), 4.40 – 4.26 (m, 6H, $H_{2,d}$), 4.05 – 4.03 (m, 4H, $H_6$), 3.88 – 3.77 (m, 4H, $H_7$), 3.71 (s, 4H, $H_8$), 3.64 (s, 4H, $H_1$), 2.57 (t, J = 7.3 Hz, 2H, $H_a$), 1.89 – 1.84 (m, 2H, $H_c$), 1.57 – 1.52 (m, 2H, $H_b$), 1.37 – 1.11 (m, 19H, $H_{g,alkyl\ chain}$). **$^{13}$C NMR-{$^{1}$H, $^{19}$F}**

(126 MHz, $CDCl_3$) δ 155.17, 153.84, 152.16, 149.24, 147.89, 145.78, 143.70 (m), 138.05 (m), 130.50 (m), 128.87, 127.77, 127.07, 116.23, 115.73, 82.38, 80.89, 71.13, 69.92, 68.49, 67.14, 54.00, 50.83, 49.74, 48.80, 42.42, 29.98, 29.50, 29.44, 29.33, 29.03, 28.62, 27.34, 26.97, 26.43. **$^{19}$F NMR** (376 MHz, $CDCl_3$) δ -141.89 – -142.89 (m), -147.18 – -147.95 (m), -158.90 – -159.56 (m). **HRESI-MS** (pos.) m/z 820.05932 [M2H$^+$] calc. for [$C_{54}H_{63}F_5I_4N_{14}O_8$·2H$^+$] 820.05868.

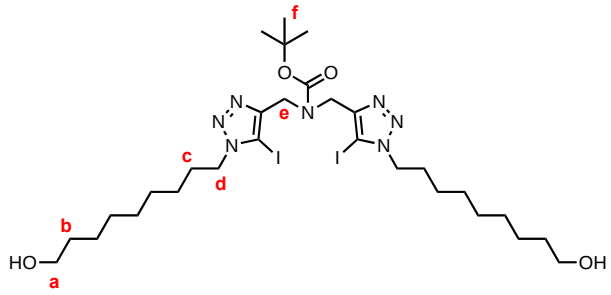
**Compound LM-4**




Prepared according to general procedure 3.5 from **LM-4-Boc** (0.014 mmol, 1 eq.). Purified by preparative TLC (75:25 $CHCl_3$:EtOAc) to afford an off-white solid (0.013 g, 0.008 mmol, 56%). **$^1$H NMR** (400 MHz, $CDCl_3$) δ 6.87 – 6.78 (m, 4H, $H_4$), 6.76 – 6.68 (m, 4H, $H_5$), 4.68 (t, J = 5.4 Hz, 4H, $H_3$), 4.36 – 4.31 (m, $H_{2,d}$), 4.05 – 4.03 (m, 4H, $H_6$), 4.00 (s, 2H, $H_f$), 3.94 (s, 2H, $H_e$), 3.82 – 3.80 (m, 4H, $H_7$), 3.71 (s, 4H, $H_8$), 3.64 (s, 4H, $H_1$), 2.56 (t, J = 7.3 Hz, 2H, $H_a$), 1.95 – 1.80 (m, 6H, $H_c$), 1.25 (broad s, 12H, $H_{alkyl\ chain}$). **$^{13}$C NMR-{$^1$H, $^{19}$F}** (126 MHz, $CDCl_3$) δ 153.88, 152.20, 150.90, 149.28, 147.12, 143.06, 135.16, 116.26, 115.77, 88.97, 83.11, 82.35, 71.15, 69.94, 68.52, 67.16, 54.02, 50.85, 49.75, 48.83, 44.17, 32.07, 30.00, 29.85, 29.41, 29.31, 29.01, 27.33, 26.99, 26.42, 22.84. **$^{19}$F NMR** (376 MHz, $CDCl_3$) δ -142.40 (dt, J = 19.3, 4.0 Hz), -147.55 (tt, J = 21.6, 3.3 Hz), -157.37 – -162.08 (m). **HRESI-MS** (pos.) m/z 1539.06067 [MH$^+$] calc. for [$C_{49}H_{55}F_5I_4N_{14}O_6$·H$^+$] 1539.06006.

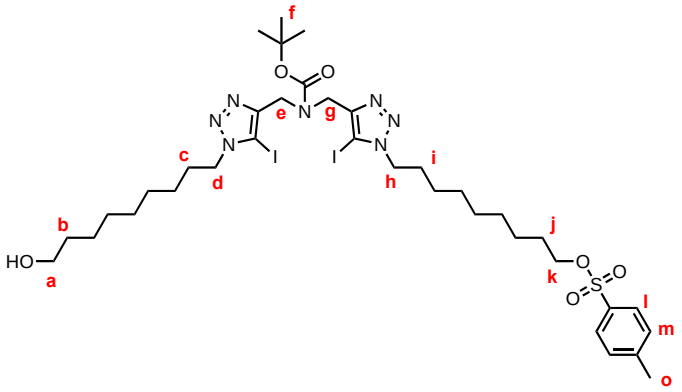
### 6.3.2.4 Synthesis of **LM-5** and **LM-6**

**Compound 11**



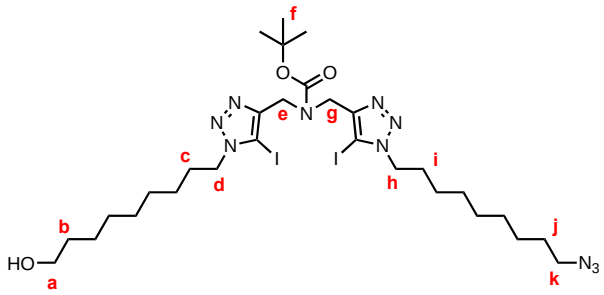

$[Cu(CH_3CN)_4]PF_6$ (0.134 g, 0.359 mmol, 0.8 eq.) and TBTA (0.212 g, 0.180 mmol, 0.4 eq.) were stirred together in dry, degassed THF (5 mL) for 15 minutes. 9-azidononan-1-ol (0.200 g, 1.080 mmol, 2.4 eq.) and bis-iodo-alkyne **2** (0.200 g, 0.449 mmol, 1 eq.) were added and the whole mixture degassed before being stirred for two days, in the dark, under a $N_2$ atmosphere. The solvent was removed under reduced pressure and the mixture dissolved in DCM. The organic layer was washed with an EDTA/$NH_4OH_{(aq)}$ solution followed by brine. The organic layer was dried over $MgSO_4$, filtered and concentrated. The product was purified using silica gel flash column chromatography (1:1 EtOAc:DCM) to afford an off-white solid (0.314 g, 0.385 mmol, 86%). **$^1$H NMR** (400 MHz, $CDCl_3$) δ 4.74 – 4.51 (m, 4H, $H_e$), 4.34 (t, J = 7.3 Hz, 4H, $H_d$), 3.63 (t, J = 6.6 Hz, 4H, $H_a$), 1.89 (t, J = 7.3 Hz, 4H, $H_c$), 1.67 – 1.51 (m, 4H, $H_b$), 1.46 (s, 9H, $H_f$), 1.40 – 1.22 (m, 20H, $H_{alkyl\ chain}$). **$^{13}$C NMR-{$^1$H}** (101 MHz, $CDCl_3$) δ 155.14, 147.82, 80.47, 62.75, 50.62, 42.00, 32.70, 29.82, 29.67, 29.27, 29.23, 28.83, 28.54, 26.28, 25.70. **HRESI-MS** (pos.) m/z 816.21594 [$MH^+$] calc. for [$C_{29}H_{51}I_2N_7O_4 \cdot H^+$] 816.21647.

**Compound 12-1**



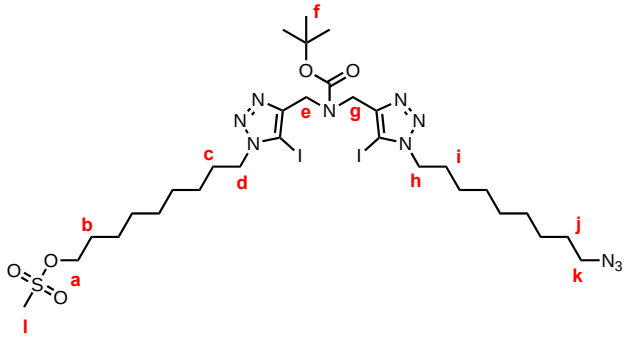

**Compound 11** (0.491 g, 0.602 mmol, 1.5 eq.), triethylamine (0.061 g, 0.602 mmol, 1.5 eq.) and DMAP (cat.) were dissolved in dry, degassed THF (3 mL). *p*-Toluenesulfonyl chloride (0.076 g, 0.401 mmol, 1 eq.) was dissolved in dry, degassed THF (1.5 mL) and added dropwise to the solution. The resulting mixture was stirred for 2 days after which the mixture was diluted with DCM and washed with brine. The organic layer was dried over $MgSO_4$, filtered, and concentrated and the crude purified by silica gel flash column chromatography (gradient 3:7 to 1:1 EtOAc:DCM) to afford the mono-tosylated product (0.254 g, 0.262 mmol, 65%). **$^1$H NMR** (400 MHz, $CDCl_3$) δ 7.81 – 7.75 (m, 2H, $H_{l}$), 7.34 (d, J = 8.0 Hz, 2H, $H_{m}$), 4.70 – 4.51 (m, 4H, $H_{e,g}$), 4.34 (td, J = 7.3, 4.5 Hz, 4H, $H_{d,h}$), 4.01 (t, J = 6.5 Hz, 2H, $H_{k}$), 3.63 (t, J = 6.6 Hz, 2H, $H_{a}$), 2.45 (s, 3H, $H_{o}$), 1.91 – 1.85 (m, 4H, $H_{c,i}$), 1.67 – 1.51 (m, 4H, $H_{b,j}$), 1.46 (s, 9H, $H_{f}$), 1.39 – 1.19 (m, 20H, $H_{alkyl\ chain}$). **$^{13}$C NMR-{$^1$H}** (176 MHz, $CDCl_3$) δ 155.14, 147.87, 144.63, 133.24, 129.80, 127.88, 80.44, 70.62, 62.99, 50.61, 41.79, 32.74, 29.85, 29.27, 29.21, 29.12, 28.84, 28.82, 28.80, 28.54, 26.29, 25.67, 25.30, 21.64. **HRESI-MS** (pos.) m/z 970.22394 [$MH^+$] calc. for [$C_{36}H_{57}I_2N_7O_6S_1 \cdot H^+$] 970.22532.

**Compound 12-2**




The mono tosylate precursor (0.246 g, 0.254 mmol, 1 eq.) was dissolved in DMF (2mL) before sodium azide (0.025 g, 0.381 mmol, 1.5 eq.) was added and the resulting mixture stirred at room temperature overnight. The solvent was removed under reduced pressure and the crude then dissolved in chloroform before being washed with water and brine. The organic layer was dried over $MgSO_4$ and concentrated to afford the product as a white solid (0.186 g, 0.221 mmol, 87 %). **$^1$H NMR** (400 MHz, $CDCl_3$) δ 4.70 – 4.51 (m, 4H, $H_{e,g}$), 4.34 (t, J = 7.3 Hz, 4H, $H_{d,h}$), 3.63 (t, J = 6.6 Hz, 2H, $H_a$), 3.25 (t, J = 6.9 Hz, 2H, $H_k$), 1.92 – 1.85 (m, 4H, $H_{c,i}$), 1.63 – 1.52 (m, 4H, $H_{b,j}$), 1.46 (s, 9H, $H_f$), 1.41 – 1.28 (m, 20H, $H_{alkyl\ chain}$). **$^{13}$C NMR-{$^1$H}** (126 MHz, $CDCl_3$) δ 155.26, 148.03, 80.59, 63.11, 51.58, 50.75, 42.16, 41.76, 32.87, 30.00, 29.97, 29.84, 29.40, 29.36, 29.34, 29.14, 29.01, 28.97, 28.94, 28.67, 26.79, 26.46, 26.42, 25.79. **HRESI-MS** (pos.) m/z 841.22269 [$MH^+$] calc. for [$C_{29}H_{50}I_2N_{10}O_3 \cdot H^+$] 841.22295.

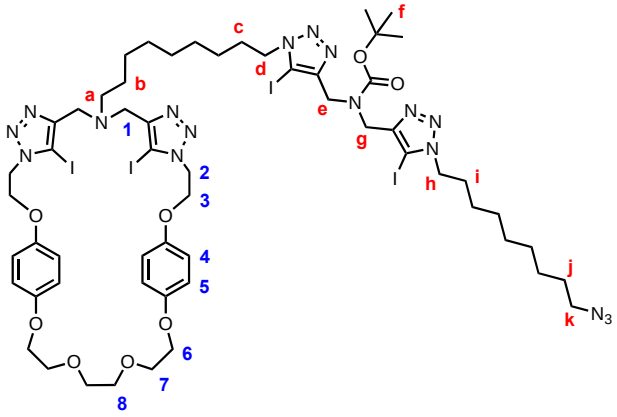
**Compound 13**




Synthesised according to general procedure 3.3 from **12-2** (0.207 mmol, 1 eq.) and purified by silica-gel flash column chromatography in an 8:2 mixture of DCM:EtOAc to afford a pale-

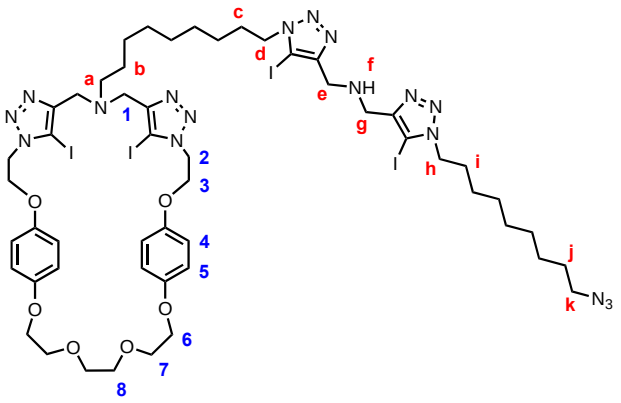
yellow solid (0.093 g, 0.101 mmol, 49 %). **$^{1}$H NMR** (500 MHz, $CDCl_3$) δ 4.69 – 4.51 (m, 4H, $H_{e,g}$), 4.34 (t, J = 7.4 Hz, 4H, $H_{d,h}$), 4.21 (t, J = 6.5 Hz, 2H, $H_a$), 3.25 (t, J = 6.9 Hz, 2H, $H_k$), 3.00 (s, 3H, $H_l$), 1.94 – 1.83 (m, 4H, $H_{c,i}$), 1.79 – 1.69 (m, 2H, $H_b$), 1.62 – 1.54 (m, 2H, $H_j$), 1.46 (s, 9H, $H_f$), 1.42 – 1.23 (m, 20H, $H_{alkyl\ chain}$). **$^{13}$C NMR-{$^{1}$H}** (126 MHz, $CDCl_3$) δ 155.25, 148.03, 80.59, 70.24, 51.58, 50.74, 50.72, 42.16, 41.75, 37.52, 30.00, 29.97, 29.36, 29.28, 29.22, 29.14, 29.01, 29.00, 28.96, 28.94, 28.67, 26.79, 26.46, 26.42, 25.50. **HRESI-MS** (pos.) m/z 919.1990 [$MH^+$] calc. for [$C_{30}H_{52}I_2N_{10}O_5S_1 \cdot H^+$] 919.2005.

**Compound LM-5-Boc**

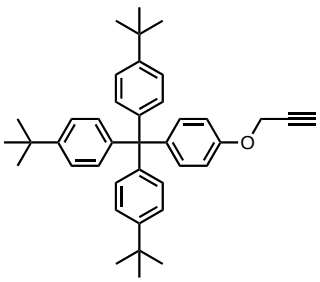



Synthesised according to general procedure 3.3 from **MC-1** (0.056 mmol, 1 eq.) and **13** (0.084, 1.5 eq.) and purified using preparative thin layer chromatography in DCM with 1.5% MeOH to afford a pale-yellow solid (0.066 g, 0.040 mmol, 71 %). **$^{1}$H NMR** (400 MHz, $CDCl_3$) δ 6.89 – 6.78 (m, 4H, $H_4$), 6.77 – 6.68 (m, 4H, $H_5$), 4.73 – 4.53 (m, 8H, $H_{3,e,g}$), 4.38 – 4.27 (m, 8H, $H_{2,d,h}$), 4.09 – 4.00 (m, 4H, $H_6$), 3.85 – 3.77 (m, 4H, $H_7$), 3.71 (s, 4H, $H_8$), 3.64 (s, 4H, $H_1$), 3.25 (t, J = 6.9 Hz, 2H, $H_k$), 2.57 (t, J = 7.3 Hz, 2H, $H_a$), 1.94 – 1.81 (m, 4H, $H_{c,i}$), 1.61 – 1.54 (m, 4H, $H_{j,b}$), 1.46 (s, 9H, $H_f$), 1.40 – 1.16 (m, 20H, $H_{alkyl\ chain}$). **$^{13}$C NMR-{$^{1}$H}** (126 MHz, $CDCl_3$) δ 155.26, 153.84, 152.17, 149.26, 148.03, 116.24, 115.74, 82.37, 80.58, 71.14, 69.92, 68.49, 67.14, 63.13, 54.02, 51.59, 50.75, 49.74, 48.81, 42.17, 41.77, 30.01, 29.84, 29.46, 29.36, 29.15, 29.05, 29.02, 28.94, 28.68, 27.36, 27.00, 26.80, 26.47, 26.45. **HRESI-MS** (pos.) m/z 1640.2725 [$MH^+$] calc. for [$C_{57}H_{81}I_4N_{17}O_8 \cdot H^+$] 1640.7206.

**Compound LM-5**

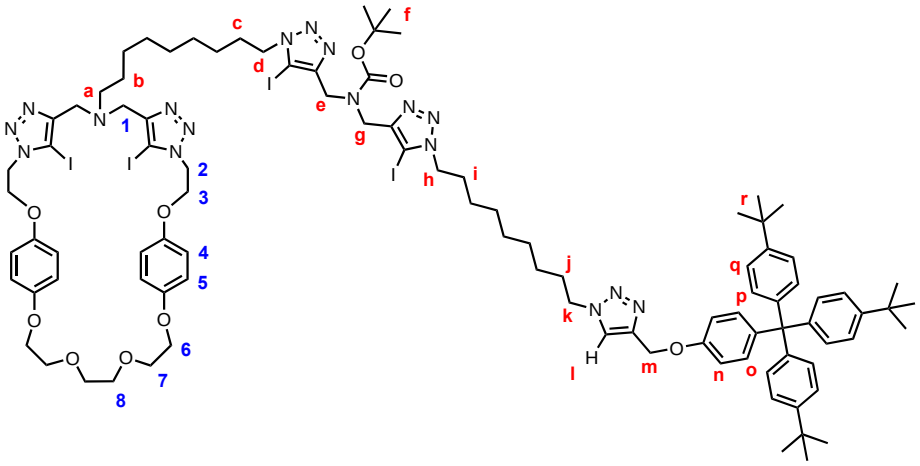


Synthesised according to general procedure 3.5 from **LM-5-Boc** (0.018 mmol, 1 eq.) to afford a pale-yellow solid (0.028 g, 0.018 mmol, quantitative). **$^{1}$H NMR** (500 MHz, $CDCl_3$) δ 6.82 (d, J = 8.9 Hz, 4H, $H_4$), 6.77 – 6.68 (m, 4H, $H_5$), 4.68 (t, J = 5.4 Hz, 4H, $H_3$), 4.40 – 4.25 (m, 8H, $H_{2,d,h}$), 4.04 (t, J = 4.7 Hz, 4H, $H_6$), 3.91 (s, 4H, $H_1$), 3.86 – 3.77 (m, 4H, $H_7$), 3.71 (s, 4H, $H_8$), 3.66 (s, 4H, $H_{e,g}$), 3.25 (t, J = 7.0 Hz, 2H, $H_k$), 2.59 (t, J = 7.2 Hz, 2H, $H_a$), 1.96 – 1.83 (m, 4H, $H_{c,i}$), 1.68 – 1.51 (m, 4H, $H_{b,j}$), 1.40 – 1.08 (m, 20H, $H_{alkyl\ chain}$). **$^{13}$C NMR-{$^{1}$H}** (126 MHz, $CDCl_3$) δ 153.84, 152.17, 149.40, 149.04, 116.23, 115.73, 82.53, 79.13, 79.01, 71.13, 69.92, 68.49, 67.13, 53.98, 51.58, 50.83, 49.77, 48.76, 44.17, 30.01, 29.99, 29.50, 29.40, 29.34, 29.29, 29.13, 29.01, 29.00, 28.94, 27.30, 26.91, 26.78, 26.46, 26.40. **HRESI-MS** (pos.) m/z 1540.2153 [$MH^+$] calc. for [$C_{52}H_{73}I_4N_{17}O_6 \cdot H^+$] 1540.2181.



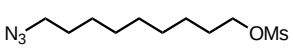
Stopper alkyne **14** was prepared according to a literature procedure and spectroscopic data were consistent with those reported.[26]

**Compound LM-6**

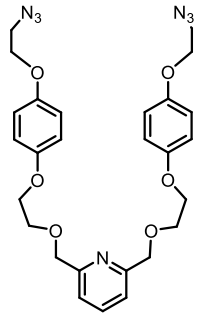


Synthesised according to general procedure 3.6 from **LM-5-Boc** (0.022 mmol, 1 eq.) and stopper alkyne **14** (0.024 mmol, 1.1 eq.) and was purified by column chromatography using 2% MeOH in DCM to afford the product as an off-white solid (0.031 g, 0.014 mmol, 63%). **$^1$H NMR** (400 MHz, $CDCl_3$) δ 7.59 (s, 1H, $H_l$), 7.25 – 7.20 (m, 6H, $H_p$), 7.13 – 7.03 (m, 8H, $H_{o,q}$), 6.89 – 6.79 (m, 6H, $H_{4,n}$), 6.75 – 6.69 (m, 4H, $H_5$), 5.18 (s, 2H, $H_k$), 4.75 – 4.49 (m, 8H, $H_{3,e,g}$), 4.40 – 4.26 (m, 10H, $H_{2,d,b,m}$), 4.09 – 3.99 (m, 4H, $H_6$), 3.85 – 3.78 (m, 4H, $H_7$), 3.71 (s, 4H, $H_8$), 3.64 (s, 4H, $H_1$), 2.57 (t, J = 7.2 Hz, 2H, $H_a$), 1.91 – 1.86 (d, J = 8.7 Hz, 4H, $H_{c,i}$), 1.67 (broad s, 4H, $H_{b,j}$), 1.46 (s, 9H, $H_f$), 1.38 – 1.21 (m, 47H, $H_{r,alkyl\ chain}$). **$^{13}$C NMR-{$^1$H}** (126 MHz, $CDCl_3$) δ 157.34, 156.24, 156.06, 153.82, 152.17, 148.49, 144.18, 140.36, 132.47, 130.85, 129.71, 129.61, 124.18, 122.03, 120.54, 116.40, 116.24, 115.74, 115.52, 113.37, 94.56, 80.79, 71.10, 69.92, 68.49, 67.12, 63.20, 56.10, 50.82, 49.84, 48.80, 34.43, 32.06, 31.52, 30.35, 29.49, 29.41, 29.23, 28.93, 28.67, 26.54, 26.40. **HRESI-MS** (pos.) m/z 2183.62629 [$MH^+$] calc. for [$C_{97}H_{127}I_4N_{17}O_9 \cdot H^+$] 2183.62600.

### 6.3.2.5 Synthesis of **LM-7**

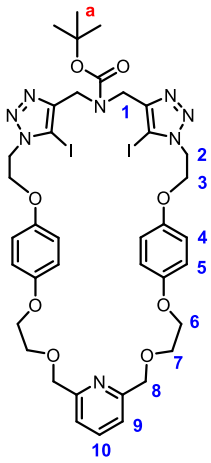



9-Azidononyl methanesulfonate was prepared according to a literature procedure and spectroscopic data were consistent with those reported.[27]



2,6-Bis((2-(4-(2-azidoethoxy)phenoxy)ethoxy)methyl)pyridine **15** was prepared according to a literature procedure and spectroscopic data were consistent with those reported.[28]

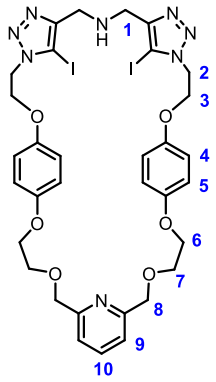
**Compound MC-2-Boc**



Compound **15** (0.37 g, 0.67 mmol, 1 eq.) was added to a mixture of TBTA (0.089 g, 0.17 mmol, 0.25 eq.) and $[Cu(CH_3CN)_4]PF_6$ (0.13 g, 0.34 mmol, 0.5 eq.) in dry, degassed THF (180 mL). A solution of bis-iodoalkyne **2** (0.30 g, 0.67 mmol, 1 eq.) in dry, degassed THF (20 mL) was added and the mixture stirred under a nitrogen atmosphere for 3 days. The solvent was removed under reduced pressure and the crude dissolved in DCM before being washed with an EDTA/$NH_4OH_{(aq)}$ solution followed by brine. The organic layer was dried over $MgSO_4$, filtered and concentrated. The product was purified using silica gel flash column chromatography (gradient EtOAc to EtOAc with 5% MeOH) to afford the product as a white powder (0.26 g, 0.26 mmol, 38%). **$^1$H NMR** (400 MHz, $CDCl_3$) δ 7.58 (t, J = 7.7 Hz, 1H, $H_{10}$), 7.27 (broad s, 2H, $H_9$), 6.81 – 6.64 (m, 8H, $H_{4,5}$), 4.73 – 4.64 (m, 8H, $H_{3,8}$), 4.55 (broad s, 4H, $H_1$), 4.30 (t, J =

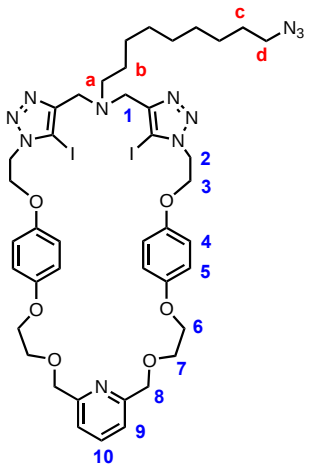
5.4 Hz, 4H, $H_2$), 4.11 – 4.04 (m, 4H, $H_6$), 3.89 – 3.81 (m, 4H, $H_7$), 1.49 (s, 9H, $H_a$). **$^{13}$C NMR-{$^1$H}** (101 MHz, $CDCl_3$) δ 157.64, 155.16, 153.27, 152.18, 147.43, 137.06, 120.44, 115.85, 115.49, 80.42, 80.12, 74.06, 69.25, 68.09, 66.98, 49.62, 41.70, 28.48. **HRESI-MS** (pos.) m/z 995.14381 [$MH^+$] calc. for [$C_{38}H_{44}I_2N_8O_8 \cdot H^+$] 995.14442.

**Compound MC-2**



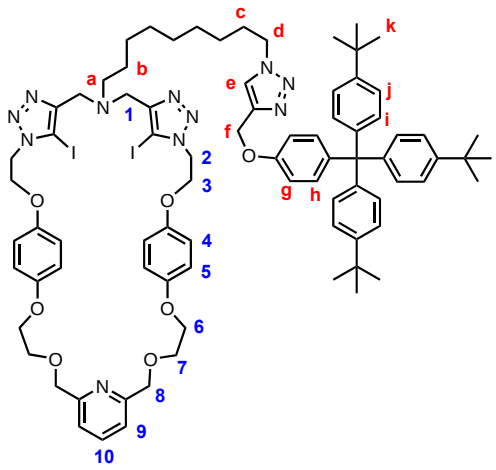

Synthesised according to general procedure 3.5 from **15** (0.26 mmol, 1 eq.) to afford an off-white solid (0.21 g, 0.23 mmol, 89%). **$^1$H NMR** (400 MHz, $CDCl_3$) δ 7.59 (t, J = 7.7 Hz, 1H, $H_{10}$), 7.28 (m, 2H, $H_9$), 6.80 – 6.65 (m, 8H, $H_{4,5}$), 4.72 – 4.64 (m, 8H, $H_{3,8}$), 4.31 (t, J = 5.4 Hz, 4H, $H_2$), 4.13 – 4.03 (m, 4H, $H_6$), 3.86 (m, 8H, $H_{1,7}$). **$^{13}$C NMR-{$^1$H}** (101 MHz, $CDCl_3$) δ 157.62, 153.29, 152.13, 149.46, 137.12, 120.53, 115.80, 115.46, 80.70, 74.09, 69.26, 68.06, 66.90, 49.71, 43.81. **HRESI-MS** (pos.) m/z 895.09163 [$MH^+$] calc. for [$C_{33}H_{36}I_2N_8O_6 \cdot H^+$] 895.09199.

**Compound LM-7**



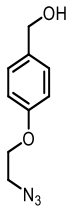

Synthesised according to general procedure 3.4 from **MC-1** (0.060 mmol, 1 eq.) and 9-azidononyl methanesulfonate (0.090 mmol, 1.5 eq.) and purified using preparative thin layer chromatography in a 55:45 mixture of DCM:EtOAc to afford an off-white solid (0.040 g, 0.038 mmol, 63%). **$^{1}$H NMR** (400 MHz, $CDCl_3$) δ 7.60 (t, J = 7.7 Hz, 1H, $H_{10}$), 7.27 – 7.25 (m, 2H, $H_9$), 6.78 – 6.67 (m, 8H $H_{4,5}$), 4.67 (d, J = 2.3 Hz, 8H, $H_{3,8}$), 4.30 (t, J = 5.5 Hz, 4H, $H_2$), 4.11 – 4.02 (m, 4H, $H_6$), 3.89 – 3.81 (m, 4H, $H_7$), 3.65 (s, 4H, $H_1$), 3.23 (t, J = 7.0 Hz, 2H, $H_d$), 2.54 (t, J = 7.2 Hz, 2H, $H_a$), 1.62 – 1.47 (m, 4H, $H_{b,c}$), 1.38 – 1.11 (m, 10H, $H_{alkyl\ chain}$). **$^{13}$C NMR-{$^{1}$H}** (126 MHz, $CDCl_3$) δ 157.82, 153.57, 152.21, 149.14, 137.27, 120.90, 116.00, 115.71, 82.07, 74.26, 69.32, 68.26, 67.08, 53.78, 51.61, 49.75, 48.75, 29.58, 29.42, 29.25, 28.96, 27.38, 27.06, 26.82. **HRESI-MS** (pos.) m/z 1062.23315 [$MH^+$] calc. for [$C_{42}H_{53}I_2N_{11}O_6 \cdot H^+$] 1062.23424.

**Compound LM-8**



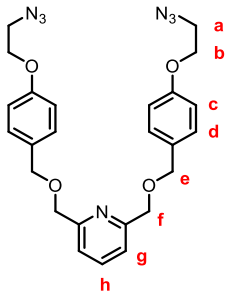
Synthesised according to general procedure 3.6 from **LM-7** (0.038 mmol, 1 eq.) and purified in DCM with 1.5% MeOH to afford the product as an off-white solid (0.055 g, 0.034 mmol, 89%). **$^1$H NMR** (400 MHz, $CDCl_3$) δ 7.63 – 7.57 (m, 2H, $H_{10,e}$), 7.30 – 7.20 (m, 8H, $H_{9,i}$), 7.19 – 7.15 (m, 2H, $H_h$), 7.13 – 7.03 (m, 6H, $H_j$), 6.89 – 6.82 (m, 2H, $H_g$), 6.79 – 6.65 (m, 8H, $H_{4,5}$), 5.17 (s, 2H, $H_d$), 4.68 (s, 8H, $H_{3,8}$), 4.39 – 4.25 (m, 6H, $H_{2,f}$), 4.12 – 4.02 (m, 4H, $H_6$), 3.92 – 3.82 (m, 4H, $H_7$), 3.67 (broad s, 4H, $H_1$), 2.35 (s, 2H, $H_a$), 1.88 (t, J = 7.2 Hz, 2H, $H_c$), 1.37 – 1.07 (m, 39H, $H_{b,k,alkyl\ chain}$). **$^{13}$C NMR-{$^1$H}** (126 MHz, $CDCl_3$) δ 157.79, 156.31, 153.56, 152.21, 148.48, 144.20, 140.29, 132.47, 130.85, 129.17, 128.36, 125.43, 124.19, 122.63, 120.87, 115.99, 115.70, 113.36, 74.23, 69.36, 68.25, 67.00, 63.20, 62.23, 53.64, 50.56, 49.93, 34.94, 34.43, 32.07, 31.77, 31.52, 30.36, 29.84, 29.50, 28.97, 26.52, 21.60. **HRESI-MS** (pos.) m/z 1604.5848 [$MH^+$] calc. for [$C_{82}H_{99}I_2N_{11}O_7 \cdot H^+$] 1604.5891.

### 6.3.2.6 Synthesis of **LM-9** and **LM-10**

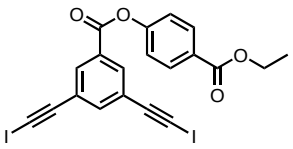


[4-(2-Azidoethoxy)phenyl]methanol **17** was prepared according to a literature procedure and spectroscopic data were consistent with those reported.[29]

**Compound 18**

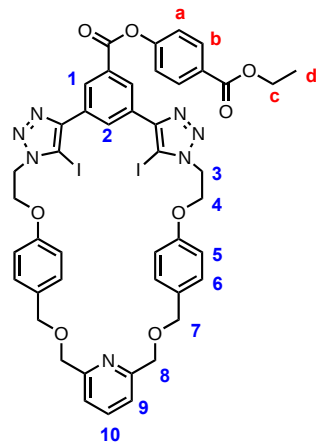



Azide **17** (1.6 g, 8.3 mmol, 2.2 eq.) was dissolved in dry, degassed THF (50 mL) and NaH (0.45 g of 60 % dispersion in mineral oil, 11.3 mmol, 3 eq.) was added portion wise. The mixture was stirred under nitrogen for 20 minutes before 2,6-bis-(bromomethyl)pyridine (1.0 g, 3.8 mmol, 1 eq.) was added and the resulting mixture stirred for 1 h at room temperature before heating to 50 °C for 48 h. The mixture was cooled to 0 °C and quenched with MeOH (5 mL) and the volatiles removed *in vacuo*. The crude mixture was dissolved in DCM and washed with brine before drying the organic layer over $MgSO_4$ and concentrating it *in vacuo*. The residue was purified by silica gel flash column chromatography (1-2% MeOH gradient in DCM) to afford a pale-yellow solid (1.2 g, 2.5 mmol, 66%). **$^1$H NMR** (400 MHz, $CDCl_3$) δ 7.71 (t, J = 7.7 Hz, 1H, $H_h$), 7.38 (d, J = 7.7 Hz, 2H, $H_g$), 7.36 – 7.29 (m, 4H, $H_d$), 6.98 – 6.82 (m, 4H, $H_c$), 4.60 (s, 4H, $H_f$), 4.58 (s, 4H, $H_e$), 4.14 (t, J = 5.0 Hz, 4H, $H_b$), 3.59 (t, J = 5.0 Hz, 4H, $H_a$). **$^{13}$C NMR-{$^1$H}** (126 MHz, $CDCl_3$) δ 158.09, 158.06, 137.39, 131.00, 129.68, 120.14, 114.70, 73.01, 72.65, 67.16, 50.29. **HRESI-MS** (pos.) m/z 490.2192 [$MH^+$] calc. for [$C_{25}H_{27}N_7O_4 \cdot H^+$] 490.2197.



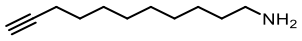
The active ester appended bis-iodo-alkyne **19** was prepared according to a literature procedure and spectroscopic data were consistent with those reported.[30]

**Compound MC-3**



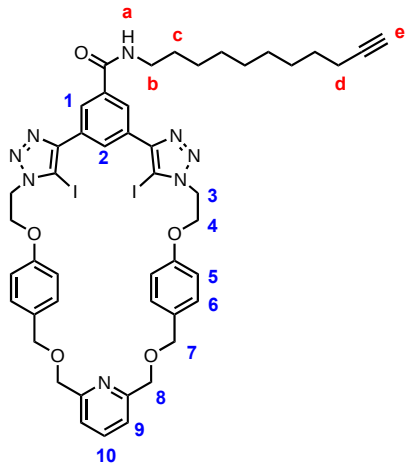

CuI (0.042 g, 0.220 mmol, 0.5 eq.) and TBTA (0.058 g, 0.110 mmol, 0.25 eq.) were stirred together in dry, degassed THF (5 mL) for 20 minutes. Two separate solutions were prepared, one with azide precursor **18** (0.215 g, 0.439 mmol, 1 eq.) and one with bis-iodoalkyne **19** (0.250 g, 0.439 mmol, 1 eq.) in dry, degassed THF (15mL). These solutions were both added and the resulting mixture stirred under a nitrogen atmosphere for 3 days. The solution was concentrated under reduced pressure and the crude dissolved in DCM and washed with an EDTA/$NH_4OH_{(aq)}$ solution followed by brine. The organic layer was dried over $MgSO_4$ and concentrated under reduced pressure. The crude product was purified by silica gel flash column chromatography (60:40 DCM:EtOAC) to afford a pale-yellow solid (0.117 g, 0.110 mmol, 25%). **$^1$H NMR** (400 MHz, $CDCl_3$) δ 8.81 (d, J = 1.7 Hz, 2H, $H_1$), 8.76 (t, J = 1.7 Hz, 1H, $H_2$), 8.19 – 8.11 (m, 2H, $H_b$), 7.66 (t, J = 7.7 Hz, 1H, $H_{10}$), 7.38 – 7.29 (m, 4H, $H_{9,a}$), 7.24 – 7.18 (m, 4H, $H_6$), 6.83 – 6.75 (m, 4H, $H_5$), 4.91 (t, J = 4.8 Hz, 4H, $H_4$), 4.56 (s, 4H, $H_8$), 4.47 (t, J = 4.8 Hz, 4H, $H_3$), 4.40 (d, J = 6.9 Hz, 6H, $H_{c,7}$), 1.41 (t, J = 7.1 Hz, 3H, $H_d$). **$^{13}$C NMR-{$^1$H}** (101 MHz,

$CDCl_3$) δ 165.96, 164.15, 157.79, 157.69, 154.57, 148.73, 137.20, 131.65, 131.58, 131.31, 130.81, 130.20, 129.85, 129.35, 128.32, 121.82, 120.04, 114.53, 79.01, 72.14, 71.69, 66.75, 61.22, 50.17, 14.45. **HRESI-MS** (pos.) m/z 1060.1021 [$MH^+$] calc. for [$C_{45}H_{39}I_2N_7O_8 \cdot H^+$] 1060.1022.



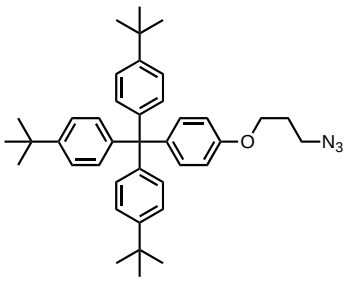

Undec-10-ynyl-1-amine **22** was prepared according to a modified literature procedure.[31] Undec-10-ynyl-1-azide (0.40 g, 2.07 mmol, 1 eq.) was dissolved in diethyl ether (6 mL) and cooled to 0 °C. Triphenyl phosphine (0.60 g, 2.28 mmol, 1.1 eq.) was added and the resulting mixture stirred for 10 minutes at 0 °C before warming to room temperature and stirring overnight. Water (0.07 g, 4.14 mmol, 2 eq.) was added and the mixture stirred for a further 7 h. 4M $HCl_{aq}$ was added and the mixture washed with $Et_2O$. The aqueous layer was basified with 4M $NaOH_{aq}$. The organic layer was dried over $MgSO_4$, filtered, and concentrated and the crude purified by silica gel flash column chromatography (10% MeOH in DCM with 2% triethylamine) to afford the product as a colourless oil that solidified upon standing (0.29 g, 1.74 mmol, 84%). Spectroscopic data were consistent with those reported.[32]

**Compound LM-9**



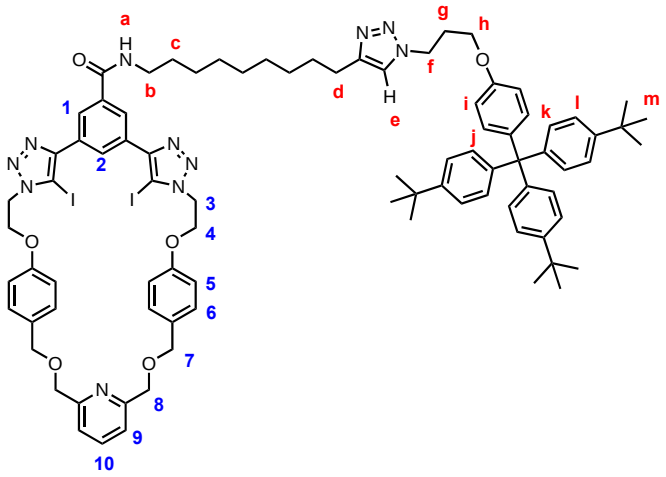

The macrocycle **MC-3** (0.050 g, 0.047 mmol, 1 eq.) and undec-10-ynyl-1-amine **22** (0.016 g, 0.094 mmol, 2 eq.) were dissolved in dry, degassed DCM (5 mL) and stirred under a nitrogen

atmosphere overnight. The crude mixture was diluted with further DCM and washed with brine. The organic layer was dried over $MgSO_4$ and concentrated under reduced pressure. The product was purified by silica gel flash column chromatography (gradient 6:4 to 1:1 DCM:EtOAC) to yield an off-white solid (0.048 g, 0.045 mmol, 96%). **$^1$H NMR** (400 MHz, $CDCl_3$) δ 8.61 (t, J = 1.7 Hz, 1H, $H_{2}$), 8.38 (d, J = 1.7 Hz, 2H, $H_{1}$), 7.65 (t, J = 7.7 Hz, 1H, $H_{10}$), 7.31 (d, J = 7.7 Hz, 2H, $H_{9}$), 7.21 (d, J = 8.6 Hz, 4H, $H_{6}$), 6.79 (d, J = 8.6 Hz, 4H, $H_{5}$), 6.43 – 6.28 (m, 1H, $H_{a}$), 4.90 (t, J = 4.8 Hz, 4H, $H_{4}$), 4.56 (s, 4H, $H_{8}$), 4.50 – 4.43 (m, 4H, $H_{3}$), 4.39 (s, 4H, $H_{7}$), 3.54 – 3.44 (m, 2H, $H_{b}$), 2.18 (td, J = 7.1, 2.6 Hz, 2H, $H_{d}$), 1.93 (t, J = 2.7 Hz, 1H, $H_{e}$), 1.70 – 1.60 (m, 2H, $H_{c}$), 1.45 – 1.18 (m, 12H, $H_{alkyl\ chain}$). **$^{13}$C NMR-{$^1$H}** (101 MHz, $CDCl_3$) δ 166.78, 157.85, 157.75, 149.13, 137.22, 135.92, 131.24, 130.89, 129.91, 129.17, 126.26, 120.07, 114.62, 84.95, 78.78, 72.21, 71.75, 68.22, 66.80, 50.19, 40.40, 29.53, 29.40, 29.17, 28.86, 28.62, 27.15, 18.54. **HRESI-MS** (pos.) m/z 1061.2050 [$MH^+$] calc. for [$C_{47}H_{50}I_2N_8O_5 \cdot H^+$] 1061.2066.




Stopper azide **23** was prepared according to a literature procedure and spectroscopic data were consistent with those reported.[26]

**Compound LM-10**



Synthesis conducted according to general procedure 3.6 from **LM-9** (0.009 mmol, 1 eq.) and stopper azide **23** (0.010 mmol, 1.1 eq.). Purified by preparative TLC (6:4 DCM:EtOAc) to afford a white solid (0.006 g, 0.004 mmol, 43%). **$^{1}$H NMR** (400 MHz, $CDCl_3$) δ 8.60 (t, J = 1.7 Hz, 1H, $H_{2}$), 8.37 (d, J = 1.6 Hz, 2H, $H_{1}$), 7.65 (t, J = 7.8 Hz, 1H, $H_{10}$), 7.31 (d, J = 7.7 Hz, 2H, $H_{9}$), 7.29 – 7.18 (m, 11H, $H_{6,e,k}$), 7.13 – 7.04 (m, 8H, $H_{j,l}$), 6.78 (d, J = 8.7 Hz, 6H, $H_{5,i}$), 6.37 (s, 1H, $H_{a}$), 4.89 (s, 4H, $H_{4}$), 4.56 (s, 6H, $H_{8,b}$), 4.45 (t, J = 4.8 Hz, 4H, $H_{3}$), 4.39 (s, 4H, $H_{7}$), 3.94 (t, J = 5.7 Hz, 2H, $H_{f}$), 3.54 – 3.40 (m, 2H, $H_{h}$), 2.69 (t, J = 7.7 Hz, 2H, $H_{d}$), 2.44 – 2.30 (m, 2H, $H_{g}$), 1.72 – 1.15 (m, 41H, $H_{m,alkyl\ chain}$). **$^{13}$C NMR-{$^{1}$H}** (151 MHz, $CDCl_3$) δ 166.79, 157.75, 156.45, 149.14, 148.52, 144.22, 140.23, 139.43, 135.93, 132.49, 131.24, 130.86, 129.90, 129.19, 126.28, 124.21, 121.21, 120.14, 114.64, 114.21, 113.11, 107.40, 72.23, 66.79, 64.17, 63.21, 50.15, 47.10, 40.38, 37.25, 34.44, 33.86, 33.56, 32.89, 32.08, 31.53, 27.12, 26.86, 25.80, 25.35, 23.32, 22.84. **HRESI-MS** (pos.) m/z 1648.5885 [$MH^+$] calc. for [$C_{87}H_{99}I_2N_{11}O_6 \cdot H^+$] 1648.5942.

## 6.4 Experimental Information Related to Chapter 4

### 6.4.1 General Procedures

**General Procedure 4.1**

2,6-Dibromopyridine (1.00 g, 4.22 mmol, 1 eq.), $Pd(PPh_3)Cl_2$ (296 mg, 0.422 mmol, 0.1 eq.) and CuI (80 mg, 0.422 mmol, 0.1 eq.) were sealed into a microwave vial to which THF (8 ml) and $NEt_3$ (8 ml) were added and the mixture thoroughly sonicated. The appropriate alkyne (21.1 mmol, 5 eq.) was added and the reaction mixture was heated under microwave irradiation at 80°C for 1 hour. The crude mixture was then diluted with $CH_2Cl_2$ (ca. 100 ml) and filtered through celite. The filtrate was concentrated to a residue *in vacuo* and subsequently redissolved in $CH_2Cl_2$ (ca. 300 ml). The organic phase was washed with EDTA/$NH_4OH_{(aq)}$ solution (20 ml), then water (10 ml), dried over $MgSO_4$ and the solvent removed *in vacuo*. The crude residue was purified by silica gel column chromatography (EtOAc/MeOH mixtures) to afford the product.

**General Procedure 4.2**

The appropriate alkyne-diol (4.00 mmol) was dissolved in MeOH (50 ml), to which was carefully added 10% Pd/C (10% w/w), the reaction was then subjected to an atmosphere of hydrogen and the reaction mixtures stirred overnight at room temperature. The mixture was then filtered and concentrated *in vacuo* to afford the appropriate diol.

**General Procedure 4.3**

NaH (60 % /w dispersion) was suspended in anhydrous THF (100 ml) and stirred at 70°C for 30 minutes. Separate solutions of 2,6-bis(bromomethyl)pyridine (1.32 g, 4.98 mmol, 1 eq.) and the appropriate diol (4.98 mmol, 1 eq.), each in THF (50 ml), were added dropwise to the refluxing solution over the course of 3 hours. Once the addition was complete, the mixture was

left to stir overnight at 70°C. After which, the mixture was left to cool to room temperature and was carefully quenched by the addition of MeOH (ca. 50 ml). The resultant mixture was concentrated to dryness *in vacuo* and the crude reaction mixture was partioned between $CH_2Cl_2$ (250 ml) and $H_2O$ (250 ml), the organic phase was collected and washed with $H_2O$ (250 ml) dried over $MgSO_4$ and the solvent removed *in vacuo*. The crude reaction mixture was subjected to silica gel chromatography (3:2:0.3, $CH_2Cl_2$/EtOAc/MeOH) to afford the product.

**General Procedure 4.4**

The respective macrocycle (0.046 mmol, 1 eq.) and the appropriate silver salt (0.046 mmol, 1 eq.) were dissolved in anhydrous $CH_2Cl_2$ (ca. 2 ml) and left to stir for 1 hour. After this the solution was filtered to yield a solution of the silver complex.

**General Procedure 4.5**

The respective macrocycle (0.046 mmol, 1 eq.) and the appropriate silver salt (0.046 mmol, 1 eq.) were dissolved in anhydrous $CH_2Cl_2$ (ca. 2 ml) and left to stir for 1 hour. To this stirred solution was added $(Me_2S)AuCl$ ( 13.5 mg , 0.046 mmol, 1 eq.) after which time AgCl immediately precipitated and left to stir for 30 minutes. After this the solution was filtered to yield a solution of the gold(I) complex.

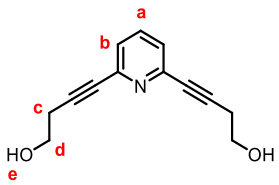
**General Procedure 4.6**

The respective macrocycle (15 mg, 0.046 mmol, 1 eq.) and the appropriate silver salt (0.046 mmol, 1 eq.) were dissolved in anhydrous $CH_2Cl_2$ (ca. 2 ml) and left to stir for 1 hour. An anhydrous 1 M $Br_2$ in $CH_2Cl_2$ solution (0.046 mmol) was added dropwise the stirred solution, after which time AgBr immediately precipitated and left to stir for 30 minutes. After this the solution was filtered to yield a solution of the bromonium complex.

## 6.4.2 Synthesis and Characterisation

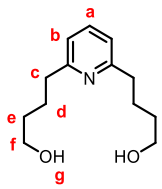
### 6.4.2.1 Synthesis of Macrocycle **MC1**

**Compound 1**



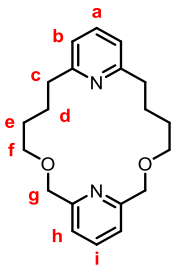

Prepared according to general procedure 4.1 from commercially available 3-butyn-1-ol and 2,6-dibromopyridine and purified by silica gel flash column chromatography (MeOH:EtOAc) to afford the product as a yellow solid in 59% yield. **$^{1}$H NMR** (400 MHz, Acetone-$d_6$) δ 7.71 (t, *J* = 7.8 Hz, 1H, $H_a$), 7.35 (d, *J* = 7.8 Hz, 2H, $H_b$), 4.06 (t, *J* = 6.0 Hz, 2H, $H_e$), 3.75 (td, *J* = 6.8, 6.0 Hz, 4H, $H_d$), 2.63 (t, *J* = 6.8 Hz, 4H, $H_c$). **$^{13}$C NMR-{$^{1}$H}** (101 MHz, Acetone-$d_6$) δ 144.64, 137.57, 126.54, 88.97, 81.70, 61.10, 24.18. **HRESI-MS** (pos.) m/z 216.1017 [$MH^+$] calc. for [$C_{13}H_{13}NO_2 \cdot H^+$] 216.1019.

**Compound 3**




Prepared according to general procedure 4.2 from **1** to afford the product as a colourless oil in 78% yield. **$^{1}$H NMR** (400 MHz, Acetone-$d_6$) δ 7.55 (t, *J* = 7.7 Hz, 1H, $H_a$), 7.02 (d, *J* = 7.7 Hz, 2H, $H_b$), 3.63 (s, 2$H_g$), 3.57 (t, *J* = 6.5 Hz, 4H, $H_f$), 2.91 – 2.59 (m, 4H, $H_c$), 1.89 – 1.68 (m, 4H, $H_e$), 1.66 – 1.44 (m, 4H, $H_d$). **$^{13}$C NMR-{$^{1}$H}** (101 MHz, Acetone-$d_6$) δ 162.30, 137.30, 120.55, 62.25, 38.50, 33.32, 26.92. **HRESI-MS** (pos.) m/z 224.1647 [$MH^+$] calc. for [$C_{13}H_{21}NO_2 \cdot H^+$] 224.1645.

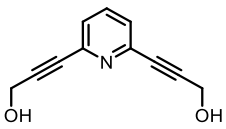
**Compound MC1**




Prepared according to general procedure 4.3 from **3** and 2,6-bis(bromomethyl)pyridine and subjected to silica gel flash column chromatography (3:2:0.3 $CH_2Cl_2$/EtOAc/MeOH) to afford the product as white solid in 42% yield. **$^1$H NMR** (400 MHz, Acetone-$d_6$) δ 7.71 (t, *J* = 7.6 Hz, 1H, $H_i$), 7.50 (t, *J* = 7.6 Hz, 1H, $H_a$), 7.26 (d, *J* = 7.6 Hz, 2H, $H_h$), 6.96 (d, *J* = 7.6 Hz, 2H, $H_b$), 4.45 (s, 4$H_g$), 3.51 (t, *J* = 6.1 Hz, 4$H_c$), 2.67 (t, *J* = 7.4 Hz, 4$H_f$), 1.79 (p, *J* = 7.5 Hz, 4$H_d$), 1.66 – 1.41 (m, 4$H_e$). **$^{13}$C NMR-{$^1$H}** (101 MHz, Acetone-$d_6$) δ 162.09, 159.06, 137.48, 137.07, 122.09, 120.65, 73.54, 70.15, 38.12, 26.69. **HRESI-MS** (pos.) m/z 327.2062 [$MH^+$] calc. for [$C_{20}H_{26}N_2O_2 \cdot H^+$] 327.2067.

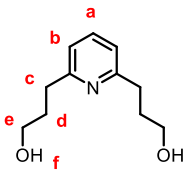
### 6.4.2.2 Synthesis of Macrocycle **MC2**

**Compound 2**



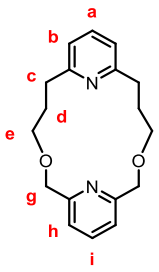

Prepared according to general procedure 4.1 from commercially available propargyl alcohol and 2,6-dibromopyridine, after silica gel flash column chromatography purity approximately 90% subjected to further reaction. $^1$H NMR in accordance with[33]

**Compound 4**




Prepared according to general procedure 4.2 from **2** and isolated as a colourless oil (50% over two steps). **$^1$H NMR** (400 MHz, Acetone-$d_6$) δ 7.58 (t, *J* = 7.7 Hz, 1H$_a$), 7.06 (d, *J* = 7.7 Hz, 2H$_b$), 3.96 (s, 2H$_f$), 3.58 (t, *J* = 6.3 Hz, 4H$_c$), 2.86 – 2.76 (m, 4H$_e$), 1.99 – 1.80 (m, 4H$_d$). **$^{13}$C NMR-{$^1$H}** (101 MHz, Acetone-$d_6$) δ 162.03, 137.66, 120.81, 62.05, 35.44, 33.39. **HRESI-MS** (pos.) m/z 196.1332 [MH$^+$] calc. for [$C_{11}H_{17}NO_2 \cdot H^+$] 196.1333.

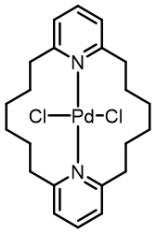
**Compound MC2**




Prepared according to general procedure 4.3 from **4** and 2,6-bis(bromomethyl)pyridine and subjected to silica gel flash column chromatography (3:2:0.3, $CH_2Cl_2$/EtOAc/MeOH) to afford the product as white solid in 63% yield. **$^1$H NMR** (400 MHz, Acetone-$d_6$) δ 7.66 (t, *J* = 7.6 Hz, 1H$_i$), 7.42 (t, *J* = 7.6 Hz, 1H$_a$), 7.24 (d, *J* = 7.6 Hz, 2H$_h$), 6.89 (d, *J* = 7.6 Hz, 2H$_b$), 4.51 (s, 4H$_g$), 3.37 – 3.18 (m, 4H$_c$), 2.71 – 2.62 (m, 4H$_e$), 1.92 – 1.78 (m, 4H$_d$). **$^{13}$C NMR-{$^1$H}** (101 MHz, Acetone-$d_6$) δ 161.40, 158.84, 137.81, 137.24, 123.09, 120.63, 74.55, 69.50, 34.66. **HRESI-MS** (pos.) m/z 299.1753 [MH$^+$] calc. for [$C_{18}H_{22}N_2O_2 \cdot H^+$] 299.1760.

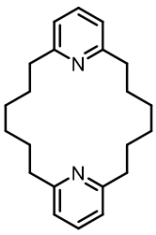
### 6.4.2.3 Synthesis of Macrocycle **MC3**

**Compound [MC3·$PdCl_2$]**




**MC-3** complexed with $PdCl_2$ was prepared according to a literature procedure starting from commercially available 2,6-bis(bromomethyl)pyridine and spectroscopic data were consistent with those reported.[34]

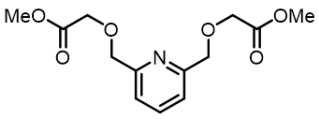
**Compound MC-3**




A solution of the palladium complex **[MC3·$PdCl_2$]** (1 eq.) was dissolved in a 1:1 mixture of $CH_2Cl_2$:MeOH to which was added $NaBH_4$ (5 eq.), after which a precipitation of palladium black was observed. The reaction mixture was left to stir at room temperature for 3 hours and filtered a purified by column chromatography in a $CH_2Cl_2$:EtOAc mixture to afford the macrocycle in 14% yield as a colourless solid. Spectroscopic data of MC-3 was consistent those reported.[35]

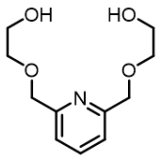
### 6.4.2.4 Synthesis of Macrocycle **MC4**

**Compound 8**



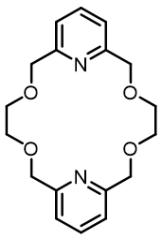

2,6-Bis(methoxycarbonylmethoxy)methyl-pyridine was prepared according to a literature procedure starting from commercially available methyl bromoacetate and 2,6-bis(hydroxymethyl)pyridine.[36] Spectroscopic data were consistent with those reported.[37]

**Compound 9**




2,6-Bis((2-hydroxyethoxy)methyl)pyridine was prepared according to a literature procedure from compound **8**.[36] Spectroscopic data were consistent with those reported.[37]

**Compound MC4**




MC4 was prepared according to general procedure 3 from compound **9** and 2,6-bis(bromomethyl)pyridine. Spectroscopic data was consistent with those reported.[38]

## 6.4.3 Single Crystal X-Ray Diffraction Data

### 6.4.3.1 **MC1** Complexes

*Table 6.11. Selected crystallographic data for **MC1** complexes co-crystallised with $BF_4^-$*

| **Compound** | **MC1·BrBF$_4$** | **MC1·AgBF$_4$** | **MC1·AuBF$_4$** |
|---|---|---|---|
| **Formula** | $C_{20}$ $H_{26}$ Br $N_2$ $O_2$, B $F_4$ | $C_{20}$ $H_{26}$ Ag $N_2$ $O_2$, B $F_4$ | $C_{20}$ $H_{26}$ Au $N_2$ $O_2$, B $F_4$ |
| **Formula Weight** | 493.15 | 521.11 | 610.21 |
| **a (Å)** | 11.2164(3) | 11.0544(1) | 11.2013(2) |
| **b (Å)** | 9.2532(3) | 9.3938(1) | 9.2294(1) |
| **c (Å)** | 20.0349(5) | 19.6489(2) | 19.8827(2) |
| **$\alpha$ (°)** | 90 | 90 | 90 |
| **$\beta$ (°)** | 96.530(2) | 96.9146(8) | 97.6829(13) |
| **$\gamma$ (°)** | 90 | 90 | 90 |
| **Unit cell volume (Å$^3$)** | 2065.88(10) | 2025.56(4) | 2037.05(5) |
| **Crystal system** | Monoclinic | Monoclinic | Monoclinic |
| **Space group** | P 21/n | P 21/n | P 21/n |
| **Z** | 4 | 4 | 4 |
| **Temperature (K)** | 150 K | 150 K | 150 K |
| **Radiation Type** | Copper | Copper | Copper |
| **λ (Å)** | 1.54184 | 1.54180 | 1.54184 |
| **Reflections (all)** | 11192 | 14225 | 10425 |
| **Reflections (unique)** | 4265 | 4189 | 4204 |
| **$R_{int}$** | 0.065 | 0.025 | 0.023 |
| **R[I > 2σ($I$)]** | 0.0778 | 0.0237 | 0.0267 |
| **wR($F^2$) (all)** | 0.1606 | 0.0607 | 0.0710 |
| **S** | 1.074 | 1.028 | 0.999 |

*Table 6.12. Selected crystallographic data for **MC1** complexes co-crystallised with $PF_6^-$*

| Compound | **MC1·BrPF$_6$** | **MC1·AgPF$_6$** | **MC1·AuPF$_6$** |
|---|---|---|---|
| **Formula** | $C_{20}$ $H_{26}$ Br $N_2$ $O_2$, $F_6$ P | $C_{20}$ $H_{26}$ Ag $N_2$ $O_2$, $F_6$ P | $C_{20}$ $H_{26}$ Au $N_2$ $O_2$, $F_6$ P |
| **Formula Weight** | 551.30 | 579.27 | 668.37 |
| **a (Å)** | 11.5204(2) | 9.4670(1) | 11.4974(2) |
| **b (Å)** | 9.4275(2) | 11.4980(1) | 9.3872(2) |
| **c (Å)** | 20.2367(4) | 19.8471(2) | 20.2176(5) |
| **$\alpha$ (°)** | 90 | 90 | 90 |
| **$\beta$ (°)** | 97.6240(18) | 90 | 98.060(2) |
| **$\gamma$ (°)** | 90 | 90 | 90 |
| **Unit cell volume (Å$^3$)** | 2178.45(7) | 2160.39(4) | 2160.50(8) |
| **Crystal system** | Monoclinic | Orthorhombic | Monoclinic |
| **Space group** | P 21/n | P n m a | P 21/n |
| **Z** | 4 | 4 | 4 |
| **Temperature (K)** | 150 K | 150 K | 150 K |
| **Radiation Type** | Copper | Copper | Copper |
| **λ (Å)** | 1.54184 | 1.54184 | 1.54184 |
| **Reflections (all)** | 11115 | 47336 | 10950 |
| **Reflections (unique)** | 4498 | 2386 | 4477 |
| **$R_{int}$** | 0.029 | 0.045 | 0.034 |
| **R[I > 2σ($I$)]** | 0.0437 | 0.0239 | 0.0350 |
| **wR($F^2$) (all)** | 0.1160 | 0.0643 | 0.0940 |
| **S** | 1.023 | 1.003 | 1.013 |

*Table 6.13. Selected crystallographic data for **MC1** complexes co-crystallised with $NO_3^-$*

| **Compound** | **MC1·$BrNO_3$** | **MC1·$AgNO_3$** | **MC1·$AuNO_3$** |
|---|---|---|---|
| **Formula** | $C_{20}$ $H_{26}$ Br $N_2$ $O_2$, N $O_3$ | $C_{20}$ $H_{26}$ Ag $N_2$ $O_2$, N $O_3$ | $C_{20}$ $H_{26}$ Au $N_2$ $O_2$, N $O_3$ |
| **Formula Weight** | 468.35 | 496.31 | 585.41 |
| **a (Å)** | 10.9813(2) | 12.4752(1) | 11.0010(2) |
| **b (Å)** | 9.0131(2) | 17.6251(1) | 9.0134(2) |
| **c (Å)** | 20.1527(4) | 27.6185(1) | 20.0199(4) |
| **$\alpha$ (°)** | 90 | 90 | 90 |
| **$\beta$ (°)** | 94.9674(17) | 90 | 96.5686(17) |
| **$\gamma$ (°)** | 90 | 90 | 90 |
| **Unit cell volume (Å$^3$)** | 1987.13(7) | 6072.66(6) | 1972.07(7) |
| **Crystal system** | Monoclinic | Orthorhombic | Monoclinic |
| **Space group** | P 21/n | P 21 21 21 | P 21/n |
| **Z** | 4 | 12 | 4 |
| **Temperature (K)** | 150 K | 150 K | 150 K |
| **Radiation Type** | Copper | Copper | Copper |
| **λ (Å)** | 1.54184 | 1.54180 | 1.54180 |
| **Reflections (all)** | 10588 | 167574 | 21338 |
| **Reflections (unique)** | 4104 | 12689 | 4088 |
| **$R_{int}$** | 0.030 | 0.036 | 0.054 |
| **R[I > 2σ(*I*)]** | 0.0389 | 0.0185 | 0.0426 |
| **wR($F^2$) (all)** | 0.1108 | 0.0488 | 0.1224 |
| **S** | 1.014 | 1.010 | 1.007 |

*Table 6.14. Selected crystallographic data for protonated **MC1** complexes*

| **Compound** | **MC1·2HBF$_4$** | **MC1·HPF$_6$·H$_2$O** |
|---|---|---|
| **Formula** | $C_{20}$ $H_{28}$ $N_2$ $O_2$, 2(B $F_4$) | $C_{20}$ $H_{27}$ $N_2$ $O_2$, $F_6$ P, $H_2$ O |
| **Formula Weight** | 502.06 | 490.42 |
| **a (Å)** | 10.5402(1) | 12.7520(1) |
| **b (Å)** | 16.5055(2) | 15.5805(1) |
| **c (Å)** | 13.2252(2) | 11.3073(1) |
| **$\alpha$ (°)** | 90 | 90 |
| **$\beta$ (°)** | 92.7601(14) | 102.3491(10) |
| **$\gamma$ (°)** | 90 | 90 |
| **Unit cell volume (Å$^3$)** | 2298.14(5) | 2194.58(3) |
| **Crystal system** | Monoclinic | Monoclinic |
| **Space group** | P 21/c | P 21/c |
| **Z** | 4 | 4 |
| **Temperature (K)** | 150 K | 150 K |
| **Radiation Type** | Copper | Copper |
| **λ (Å)** | 1.54184 | 1.54180 |
| **Reflections (all)** | 11951 | 11862 |
| **Reflections (unique)** | 4764 | 4542 |
| **$R_{int}$** | 0.027 | 0.021 |
| **R[I > 2σ($I$)]** | 0.0412 | 0.0447 |
| **wR($F^2$) (all)** | 0.1140 | 0.1184 |
| **S** | 0.979 | 0.991 |

### 6.4.3.2 **MC2** Complexes

*Table 6.15. Selected crystallographic data for **MC2** complexes co-crystallised with $PF_6^-$*

| **Compound** | **MC2·AgPF$_6$** | **MC2·AuPF$_6$** |
|---|---|---|
| **Formula** | $C_{18}$ $H_{22}$ Ag $N_2$ $O_2$, $F_6$ P | $C_{18}$ $H_{22}$ Au $N_2$ $O_2$, $F_6$ P |
| **Formula Weight** | 551.21 | 640.31 |
| **a (Å)** | 8.6000(6) | 9.9433(2) |
| **b (Å)** | 9.8267(6) | 10.2408(2) |
| **c (Å)** | 13.0181(6) | 11.5754(3) |
| **$\alpha$ (°)** | 79.486(4) | 96.209(2) |
| **$\beta$ (°)** | 76.821(5) | 114.082(2) |
| **$\gamma$ (°)** | 70.533(6) | 106.759(2) |
| **Unit cell volume (Å$^3$)** | 1003.13(11) | 995.43(5) |
| **Crystal system** | Triclinic | Triclinic |
| **Space group** | P -1 | P -1 |
| **Z** | 2 | 2 |
| **Temperature (K)** | 150 K | 150 K |
| **Radiation Type** | Copper | Copper |
| **λ (Å)** | 1.54184 | 1.54184 |
| **Reflections (all)** | 9131 | 20961 |
| **Reflections (unique)** | 4119 | 4115 |
| **$R_{int}$** | 0.019 | 0.031 |
| **R[I > 2σ($I$)]** | 0.0507 | 0.0160 |
| **wR($F^2$) (all)** | 0.1334 | 0.0405 |
| **S** | 1.080 | 1.039 |

### 6.4.3.3 **MC3** Complexes

*Table 6.16. Selected crystallographic data for **MC3** complexes co-crystallised with $PF_6^-$*

| Compound | **MC3·AgPF$_6$** | **MC3·AuPF$_6$** |
|---|---|---|
| **Formula** | $C_{22}$ $H_{30}$ Ag $N_2$, $F_6$ P, C $H_2$ $Cl_2$ | $C_{22}$ $H_{30}$ Au $N_2$, $F_6$ P, C $H_2$ $Cl_2$ |
| **Formula Weight** | 660.25 | 749.35 |
| **a (Å)** | 9.0869(1) | 12.0937(1) |
| **b (Å)** | 19.6623(2) | 10.9701(1) |
| **c (Å)** | 15.4434(1) | 20.5471(2) |
| **$\alpha$ (°)** | 90 | 90 |
| **$\beta$ (°)** | 105.8107(9) | 105.1837(8) |
| **$\gamma$ (°)** | 90 | 90 |
| **Unit cell volume (Å$^3$)** | 2654.87(4) | 2630.80(4) |
| **Crystal system** | Monoclinic | Monoclinic |
| **Space group** | P 21/c | P 21/n |
| **Z** | 4 | 4 |
| **Temperature (K)** | 150 K | 150 K |
| **Radiation Type** | Copper | Copper |
| **λ (Å)** | 1.54184 | 1.54184 |
| **Reflections (all)** | 14931 | 14557 |
| **Reflections (unique)** | 5506 | 5443 |
| **$R_{int}$** | 0.022 | 0.022 |
| **R[I > 2σ(*I*)]** | 0.0286 | 0.0242 |
| **wR($F^2$) (all)** | 0.0713 | 0.0630 |
| **S** | 1.011 | 0.998 |

## 6.5 References


1. J. Cosier and A. M. Glazer, *Journal of Applied Crystallography*, 1986, **19**, 105-107.

2. P. Parois, R. I. Cooper and A. L. Thompson, *Chemistry Central Journal*, 2015, **9**.

3. P. W. Betteridge, J. R. Carruthers, R. I. Cooper, K. Prout and D. J. Watkin, *Journal of Applied Crystallography*, 2003, **36**, 1487-1487.

4. P. V. Van der Sluis and A. L. Spek, *Acta Crystallographica Section A: Foundations of Crystallography*, 1990, **46**, 194-201.

5. A. L. Spek, *Acta Crystallographica Section C Structural Chemistry*, 2015, **71**, 9-18.

6. BindFit v0.5 | Supramolecular, http://app.supramolecular.org/bindfit/).

7. D. Brynn Hibbert and P. Thordarson, *Chemical Communications*, 2016, **52**, 12792-12805.

8. P. Petiot, J. Dansereau and A. Gagnon, *RSC Advances*, 2014, **4**, 22255-22259.

9. I. S. Makarov, C. E. Brocklehurst, K. Karaghiosoff, G. Koch and P. Knochel, *Angewandte Chemie International Edition*, 2017, **56**, 12774-12777.

10. M. Yamada, M. Matsumura, Y. Uchida, M. Kawahata, Y. Murata, N. Kakusawa, K. Yamaguchi and S. Yasuike, *Beilstein Journal of Organic Chemistry*, 2016, **12**, 1309-1313.

11. A. F. M. M. Rahman, T. Murafuji, M. Ishibashi, Y. Miyoshi and Y. Sugihara, *Journal of Organometallic Chemistry*, 2005, **690**, 4280-4284.

12. T. Murafuji, K. Nishio, M. Nagasue, A. Tanabe, M. Aono and Y. Sugihara, *Synthesis*, 2000, **2000**, 1208-1210.

13. A. Gini, M. Paraja, B. Galmés, C. Besnard, A. I. Poblador-Bahamonde, N. Sakai, A. Frontera and S. Matile, *Chemical Science*, 2020, **11**, 7086-7091.

14. S. Yasuike, K. Nakata, W. Qin, M. Matsumura, N. Kakusawa and J. Kurita, *Journal of Organometallic Chemistry*, 2015, **788**, 9-16.

15. M. Yang, D. Tofan, C. H. Chen, K. M. Jack and F. P. Gabbaï, *Angewandte Chemie International Edition*, 2018, **57**, 13868-13872.

16. J. C. Burnett, C. Lim, B. D. Peyser, L. P. Samankumara, M. Kovaliov, R. Colombo, S. L. Bulfer, M. G. Laporte, A. R. Hermone, C. F. McGrath, M. R. Arkin, R. Gussio, D. M. Huryn and P. Wipf, *Organic & Biomolecular Chemistry*, 2017, **15**, 4096-4114.

17. L.-M. Jin, X. Xu, H. Lu, X. Cui, L. Wojtas and X. P. Zhang, *Angewandte Chemie International Edition*, 2013, **52**, 5309-5313.

18. L. S. Campbell-Verduyn, L. Mirfeizi, R. A. Dierckx, P. H. Elsinga and B. L. Feringa, *Chemical Communications*, 2009, 2139-2141.

19. Q. Simpson, M. J. G. Sinclair, D. W. Lupton, A. B. Chaplin and J. F. Hooper, *Organic Letters*, 2018, **20**, 5537-5540.

20. X. Li, J. Y. C. Lim and P. D. Beer, *Chemistry - A European Journal*, 2018, **24**, 17788-17795.

21. J. Yuan, X. Fang, L. Zhang, G. Hong, Y. Lin, Q. Zheng, Y. Xu, Y. Ruan, W. Weng, H. Xia and G. Chen, *Journal of Materials Chemistry*, 2012, **22**, 11515.

22. N. Wolf, L. Kersting, C. Herok, C. Mihm and J. Seibel, *The Journal of Organic Chemistry*, 2020, **85**, 9751-9760.

23. C. Ghosh, M. M. Konai, P. Sarkar, S. Samaddar and J. Haldar, *ChemMedChem*, 2016, **11**, 2367-2371.

24. M. R. Maddani, S. K. Moorthy and K. R. Prabhu, *Tetrahedron*, 2010, **66**, 329-333.

25. P. Liu, X. Liu, G. Chen and C. Li, *Synlett*, 2018, **29**, 2051-2055.

26. V. Aucagne, K. D. Hänni, D. A. Leigh, P. J. Lusby and D. B. Walker, *Journal of the American Chemical Society*, 2006, **128**, 2186-2187.

27. F. F. Hilário, R. C. De Paula, M. L. T. Silveira, G. H. R. Viana, R. B. Alves, J. R. C. S. Pereira, L. M. Silva, R. P. De Freitas and F. De Pilla Varotti, *Chemical Biology & Drug Design*, 2011, **78**, 477-482.

28. A. Brown, T. Lang, K. M. Mullen and P. D. Beer, *Organic & Biomolecular Chemistry*, 2017, **15**, 4587-4594.

29. Y. Tian, J. Jin, C. Wang, W. Lv, X. Li, X. Che, Y. Gong, Y. Li, Q. Li, J. Hou, P. G. Wang and J. Shen, *Bioorganic & Medicinal Chemistry Letters*, 2016, **26**, 2434-2437.

30. A. Docker, J. G. Stevens and P. D. Beer, *Chemistry – A European Journal*, 2021, **27**, 14600-14604.

31. N. Kojima, Y. Suga, T. Matsumoto, T. Tanaka, A. Akatsuka, T. Yamori, S. Dan, H. Iwasaki and M. Yamashita, *Bioorganic & Medicinal Chemistry*, 2015, **23**, 1276-1283.

32. T. Utsumi, K. Noda, D. Kawauchi, H. Ueda and H. Tokuyama, *Advanced Synthesis & Catalysis*, 2020, **362**, 3583-3588.

33. N. Miyagawa, M. Watanabe, T. Matsuyama, Y. Koyama, T. Moriuchi, T. Hirao, Y. Furusho and T. Takata, *Chemical Communications*, 2010, **46**, 1920-1922.

34. P. D. Zeits, G. P. Rachiero, F. Hampel, J. H. Reibenspies and J. A. Gladysz, *Organometallics*, 2012, **31**, 2854-2877.

35. B. B. Smith, D. E. Hill, T. A. Cropp, R. D. Walsh, D. Cartrette, S. Hipps, A. M. Shachter, W. T. Pennington and W. R. Kwochka, *The Journal of Organic Chemistry*, 2002, **67**, 5333-5337.

36. R. R. Whitney and D. A. Jaeger, *Journal of Heterocyclic Chemistry*, 1980, **17**, 1093-1095.

37. A. M. Costero, M. J. Bañuls, M. J. Aurell, L. E. Ochando and A. Doménech, *Tetrahedron*, 2005, **61**, 10309-10320.

38. M. Newcomb, G. W. Gokel and D. J. Cram, *Journal of the American Chemical Society*, 1974, **96**, 6810-6811.